UCRL-17406

Cy. 2

University of California

Ernest O. Lawrence Radiation Laboratory

MAGNETIC RESONANCE SPECTRA OF VCl_4 AND OTHER PARAMAGNETIC SPECIES

TWO-WEEK LOAN COPY

This is a Library Circulating Copy which may be borrowed for two weeks. For a personal retention copy, call Tech. Info. Division, Ext. 5545

RECEIVED
LAWRENCE
RADIATION LABORATORY
JUL 25 1967
LIBRARY AND
DOCUMENTS SECTION

Berkeley, California

DISCLAIMER

This document was prepared as an account of work sponsored by the United States Government. While this document is believed to contain correct information, neither the United States Government nor any agency thereof, nor the Regents of the University of California, nor any of their employees, makes any warranty, express or implied, or assumes any legal responsibility for the accuracy, completeness, or usefulness of any information, apparatus, product, or process disclosed, or represents that its use would not infringe privately owned rights. Reference herein to any specific commercial product, process, or service by its trade name, trademark, manufacturer, or otherwise, does not necessarily constitute or imply its endorsement, recommendation, or favoring by the United States Government or any agency thereof, or the Regents of the University of California. The views and opinions of authors expressed herein do not necessarily state or reflect those of the United States Government or any agency thereof or the Regents of the University of California.

Research and Development

UCRL-17406

UNIVERSITY OF CALIFORNIA

Lawrence Radiation Laboratory
Berkeley, California

AEC Contract No. W-7405-eng-48

MAGNETIC RESONANCE SPECTRA OF VCl_4 AND OTHER PARAMAGNETIC SPECIES

David Wixon Pratt

(Ph. D. Thesis)

April 1967

TABLE OF CONTENTS

Abstract

I. INTRODUCTION. 1

II. SURVEY OF PREVIOUS WORK 10

A. $V(CO)_6$. 10

B. VCl_4. 22

1. Synthesis and Properties. 22

2. Structure and Bonding 24

3. Optical, Infrared and Raman Spectra 27

4. Theoretical Work. 32

5. Related Magnetic Resonance Results. 36

C. Sulfur-Nitrogen Radicals. 46

III. EXPERIMENTAL TECHNIQUES 58

A. ESR Experiments in the Temperature Range 90-500°K 58

1. The Spectrometer. 58

2. Sample Preparation. 59

3. Temperature Control and Measurement 61

B. ESR Experiments at Liquid Helium Temperatures 62

1. The X-Band Spectrometer 62

2. The K-Band Spectrometer 66

3. Liquid Helium Cryostat and Vacuum System. 69

4. Sample Preparation. 74

5. ESR Spectra of DPPH 77

6. Apparatus for Determining T_1 in VCl_4. 80

C. NMR 83

1. Experimental Apparatus. 83

2. Sample Preparation. 84

3. Temperature Control and Measurement 88

4. Signal Display and Measurement. 89

IV. RESULTS AND DISCUSSION. 93

A. ESR of $V(CO)_6$ at Liquid Helium Temperatures 93

1. Assignment of the Spectra 93

2. Lineshapes and the Exchange Interaction 106

3. Effect of Power Saturation in Exchanged Systems 111
4. Calculation of g-Values 117
5. Discussion of g-Values. 130
B. ESR of VCl_4 at Liquid Helium Temperatures 141
1. Assignment of the Spectra 141
2. Temperature Dependence of the Spectra 169
3. Enhancement Phenomena and T_1 Measurements 176
4. Discussion. 200
C. NMR of VCl_4 and $TiCl_4$ 214
1. Assignment of the Spectra 214
2. ^{35}Cl A-Value in VCl_4. 218
3. Temperature Dependence of the Linewidths. 228
4. Relaxation Effects in VCl_4 and $TiCl_4$. 231
D. ESR of Sulfur-Nitrogen Radicals 242
1. Assignment of the Spectra 242
2. Discussion. 246

Acknowledgments 259

Appendix I. ESR Linewidth of $Gd(H_2O)_9^{3}$ as a Function of Temperature. 260

MAGNETIC RESONANCE SPECTRA OF VCl_4 AND OTHER PARAMAGNETIC SPECIES

David Wixon Pratt

Inorganic Materials Research Division, Lawrence Radiation Laboratory,
Department of Chemistry, University of California
Berkeley, California

April 1967

ABSTRACT

Techniques for performing electron spin resonance studies of paramagnetic species in glasses or polycrystalline matrices at temperatures below the λ-point of liquid helium have been developed and the experimental procedures have been described in detail. These methods have been applied in the investigation of the transition metal compounds VCl_4 and $V(CO)_6$.

The ESR spectrum of VCl_4 at liquid helium temperatures has been studied in the pure compound and in the following solvents: n-heptane, mineral oil, CCl_4, $SiCl_4$, $TiCl_4$ and $SnCl_4$. The spin Hamiltonian parameters for pure VCl_4 and VCl_4 in n-heptane and mineral oil have been obtained. These have provided significant evidence for the presence of a Jahn-Teller effect in this molecule at low temperatures. The spectra in the remaining solvents are quite complex but a partial assignment of these has been made. The effect of both static and dynamic Jahn-Teller distortions on the ESR spectra of VCl_4 in these solvents has been discussed in detail.

The relaxation times for the unpaired electron in VCl_4 have been measured over a wide temperature range using a variety of techniques including pulse experiments. These results have been discussed in terms

of the existing theories for spin relaxation in solids at low temperatures and a model for relaxation in VCl_4 in the temperature range 1-50°K has been proposed. In addition, an unusual self-enhancement behavior of the ESR spectrum of VCl_4 has been discovered and interpreted in terms of the above model.

^{35}Cl NMR experiments have been performed on pure VCl_4 and solutions of VCl_4 in $TiCl_4$ at room temperature and above. The temperature dependence of the chemical shift in VCl_4 has made possible the measurement of the ^{35}Cl hyperfine coupling constant in this molecule. The NMR linewidths in both VCl_4 and $TiCl_4$ have been studied as a function of temperature and the data interpreted on the basis of quadrupolar and scalar relaxation theories. Evidence is presented for the existence of chemical exchange in solutions of VCl_4 in $TiCl_4$.

The ESR spectrum of $V(CO)_6$ at liquid helium temperatures has been observed in the pure material and in benzene and n-heptane glasses. Because of an unusual power dependence of the spectrum in n-pentane, both the isotropic and anisotropic g-values have been measured directly. These are compared with theoretical expressions for g for both trigonal and tetragonal distortions of the octahedron derived in this thesis. The presence of a tetragonal distortion in $V(CO)_6$ is shown to be consistent with a molecular orbital description of the bonding. Evidence for the presence of back-bonding is also presented.

Radicals produced by the chemical and electrolytic reduction of S_4N_4 and S_4N_3Cl have been studied by ESR and the spin Hamiltonian parameters have been obtained. The radical anion of S_4N_4 has been prepared. Finally, the ESR linewidth of $Gd(H_2O)_9^{+3}$ has been studied as a function of temperature in the range 20-260°C.

I. INTRODUCTION

The field of magnetic resonance spectroscopy has proven to be of great importance in the elucidation of molecular structure, despite its relatively short history. Although the splitting of the sodium D line into multiplets in a magnetic field was discovered by Zeeman in 1863, it was not until 1925 when Goudsmit and Uhlenbeck postulated the existence of an electron spin that the Zeeman effect was understood. These early experiments formed the basis of the modern techniques of magnetic resonance, but it was not until the development of suitable energy sources in the radiofrequency region of the electromagnetic spectrum that these techniques became possible.

The first successful nuclear magnetic resonance experiments using bulk material were carried out independently at the end of 1945 by Purcell, et al.[1] on protons in solid paraffin and by Bloch, et al.[2] on protons in water doped with copper sulfate. At about the same time, Zavoisky[3] first observed laboratory-induced transitions between the Zeeman levels of electrons in paramagnetic materials, thus discovering the field of electron paramagnetic (or spin) resonance. Both of these techniques depend on the existence of a magnetic moment in the nucleus, atom or molecule under study. Since this magnetic moment is proportional to the total angular momentum $\underline{J}$, the coupling of the moment with an externally-applied magnetic field produces 2J+1 energy levels whose splitting in a given field depends on the molecular interactions present in the system in question.

Magnetic resonance is the phenomenon of inducing transitions among these 2J+1 levels. Typically, the magnetic moment of an electron is

larger than that of a nucleus by the inverse ratio of their masses, so the frequency of these transitions is roughly three orders of magnitude higher for ESR than for NMR in a given field. Nonetheless, at the magnetic field strengths normally attainable in the laboratory, these transitions occur in the radiofrequency range of the spectrum for both types of magnetic resonance. Thus the energy level splittings which are observed are very small when viewed on the scale of normal molecular interactions.

It is just this fact that makes magnetic resonance a versatile technique for the chemical physicist. For when radiofrequency transitions are induced in a molecule, the structure of the molecule remains essentially unperturbed and thus the parameters obtained from a magnetic resonance experiment are true probes of molecular structure. Further, many intramolecular interactions can be thought of as producing internal magnetic fields which may add to or subtract from the external field, thus providing additional structural information.

In the study of transition metal ions by electron spin resonance, as well as many other systems, it is usually assumed that the complete Hamiltonian for the problem can be written as

$$\mathcal{H} = \mathcal{H}_o + \mathcal{H}'$$

where $\mathcal{H}_o$ contains all the kinetic and electrostatic energy terms and $\mathcal{H}'$ contains all other terms involving the electron and nuclear spins. Treating $\mathcal{H}'$ as a perturbation, Abragam and Pryce[4] showed that it was possible to derive an operator called the spin Hamiltonian, $\mathcal{H}_S$, which expresses the interactions pertinent to the magnetic resonance experiment. Although the coefficients of the operators appearing in $\mathcal{H}_S$ contain contributions from

orbital as well as spin angular momentum, the operators themselves are spin operators and hence $\mathcal{H}_S$ operates only in the space of the electronic and nuclear spin coordinates. Thus the spin Hamiltonian expresses interactions involving the effective spins $\underline{S}$ and $\underline{I}$.

The usual spin Hamiltonian is of the form

$$\mathcal{H}_S = \beta \underline{H} \cdot \underset{\sim}{g} \cdot \underline{S} + \underline{I} \cdot \underset{\sim}{A} \cdot \underline{S} + \underline{S} \cdot \underset{\sim}{D} \cdot \underline{S} + \underline{I} \cdot \underset{\sim}{P} \cdot \underline{I} - g_I \mu_N \underline{H} \cdot \underline{I}$$

where $\underset{\sim}{g}$, $\underset{\sim}{A}$, $\underset{\sim}{D}$ and $\underset{\sim}{P}$ are all second-rank tensors. The term involving $\underline{H}$ and $\underline{S}$ represents the Zeeman interaction of the electronic magnetic moment with the applied magnetic field. The hyperfine term, $\underline{I} \cdot \underset{\sim}{A} \cdot \underline{S}$, results from the coupling of the electron spin with the nuclear spin by two mechanisms - the Fermi contact interaction and the magnetic dipole-dipole interaction between the two spins. The term $\underline{S} \cdot \underset{\sim}{D} \cdot \underline{S}$, called the fine structure term, expresses the zero-field splitting in the absence of a magnetic field and results from the second-order effects of the crystal field exerted through the spin-orbit coupling as well as the dipole-dipole interaction between two or more electron spins. It is usually assumed to be zero for $S = 1/2$, which is the case of primary interest in this thesis. The last two terms are purely nuclear terms which arise from the coupling of two nuclei by a quadrupole interaction and the Zeeman interaction of the external field with the nuclear magnetic moment. These terms are usually ignored in an ESR experiment because of their small contribution to the energy of an unpaired electron in a magnetic field. The nuclear spin Hamiltonian is analogous to that shown above except that the terms not involving $\underline{I}$ do not contribute to the splitting of the nuclear levels.

For an effective spin of 1/2 the spin Hamiltonian is therefore

$$\mathcal{H}_S = \beta \underline{H} \cdot \underset{\sim}{g} \cdot \underline{S} + \underline{I} \cdot \underset{\sim}{A} \cdot \underline{S}$$

In ESR experiments at X- and K-band, this expression is usually treated in the Paschen-Back representation; that is, the coupling between the electron spin and the magnetic field is assumed to be the dominant interaction. Therefore, the axis of quantization for both the nuclear and electronic spins is assumed to be defined as the direction of the externally-applied field and is taken as the z-axis. In this coordinate system, $\mathcal{H}_S$ becomes

$$\mathcal{H}_S = \beta(g_{xx}H_xS_x + g_{yy}H_yS_y + g_{zz}H_zS_z) + A_{xx}I_xS_x + A_{yy}I_yS_y + A_{zz}I_zS_z$$

So far, we have assumed that the axis of the crystal field lies along the z-axis. In general this is not the case. Since the contributions from orbital angular momentum produced by spin-orbit coupling depend on the orientation of the spin with respect to the axis of the crystal field and since, as noted above, these contributions occur in $\underset{\sim}{g}$ and not in $\underline{S}$, $\underset{\sim}{g}$ depends on the orientation of the crystal with respect to the magnetic field. In other words, it is anisotropic. This argument also applies to $\underset{\sim}{A}$ and it is customary to express these facts in the spin Hamiltonian by writing

$$\mathcal{H}_S = g\beta H_zS_z + AI_zS_z$$

where g and A are now given by

$$g^2 = g_z^2\cos^2\theta + g_x^2\sin^2\theta\cos^2\phi + g_y^2\sin^2\theta\sin^2\phi$$

$$(gA)^2 = A_z^2g_z^2\cos^2\theta + A_x^2g_x^2\sin^2\theta\cos^2\phi + A_y^2g_y^2\sin^2\theta\sin^2\phi$$

In these expressions, g_x, g_y, g_z and A_x, A_y, A_z are the principal values of the $\underset{\sim}{g}$ and $\underset{\sim}{A}$ tensors, respectively, and θ and ϕ are the angles which describe the orientation of the crystal field with respect to the magnetic field. Physically, these expressions mean that when a single crystal is oriented with its principal axis parallel to the magnetic field, a signal is observed with a g-value equal to g_z, etc. In a field of axial symmetry, $g_x = g_y$ and $A_x = A_y$ and the expressions for g and A reduce to

$$g^2 = g_{\parallel}^2 \cos^2\theta + g_{\perp}^2 \sin^2\theta$$

$$(gA)^2 = A_{\parallel}^2 g_{\parallel}^2 \cos^2\theta + A_{\perp}^2 g_{\perp}^2 \sin^2\theta$$

with $g_{\parallel} = g_z$, $g_{\perp} = g_x = g_y$, etc. In an octahedral (or cubic) field, $g_{\parallel} = g_{\perp}$ and $A_{\parallel} = A_{\perp}$ and the ESR spectrum is said to be isotropic.

This approach using an effective spin Hamiltonian proved to be quite useful in the extensive studies of the ESR spectra of paramagnetic transition metal compounds by Bleaney and others at the Clarendon laboratories. This early work, which was performed mostly on single crystals, has been reviewed in the literature.[5] In addition, the concept of a spin Hamiltonian provided a basis for the understanding of other ESR problems. For example, in the gas phase or in solution, where there is rapid tumbling of the paramagnetic species, one sees only the average values of the spin Hamiltonian parameters such as

$$g = 1/3\ (g_x + g_y + g_z), \quad A = 1/3\ (A_x + A_y + A_z)$$

A second kind of averaging that can occur in an ESR spectrum is of particular interest in this thesis. This is a spatial average rather than

a temporal one and is observed for polycrystalline or glass samples in which the sample containing the paramagnetic species has simultaneously all possible relative orientations of crystal field and magnetic field axes. Ignoring for the moment the hyperfine term and assuming axial symmetry, the g-values for this case are

$$g^2 = g_{\parallel}^2 \cos^2\theta + g_{\perp}^2 \sin^2\theta$$

However, since we have a sample with all possible values of the angle θ, the spectrum will consist of a superposition of a large number of lines, each with a different g-value. Thus the absorption spectrum, if $\underline{g}$ is anisotropic, is spread over a wide range of magnetic fields and is describable by two extreme values of g. One is for those molecules with $\cos\theta = 1$ and is $g_{\parallel}$; it is the g-value for those molecules whose principal axis is parallel to the magnetic field. At the other extreme, $g=g_{\perp}$ and the spectrum is due to those molecules perpendicularly oriented. Thus, in a derivative spectrum, one observes (for example) the onset of absorption at $g_{\parallel}$ which terminates abruptly at $g_{\perp}$. In favorable cases, the g-values (and A-values for $A \neq 0$) one obtains from these band edges are as accurately determined as they would be in a single crystal.

The field of NMR has perhaps received more attention in the literature in recent years primarily because most molecules of chemical interest possess nuclei with magnetic moments, whereas there are relatively few molecules which have magnetic moments due to unpaired electrons. Further restricting the number of species subject to study by the ESR technique is the fact that many molecules and ions which are paramagnetic possess very short electron relaxation times, even at very low temperatures. This causes the ESR spectrum to be composed of very broad

lines which are frequently unobservable. Such observations are especially true for species which have orbital degeneracy.

There has been a great deal of interest in such relaxation effects in the recent literature. One important question which has not yet been resolved is what the role of the Jahn-Teller effect[6] is in such systems, if any. This celebrated theorem states that when the orbital state of a molecule or ion is degenerate for symmetry reasons, the ligands will experience forces distorting the nuclear framework until the molecule assumes a configuration of both lower symmetry and lower energy, thereby resolving the degeneracy. The distortion can of course be static or dynamic with respect to the time scale of the experiment and in either case could have a significant effect on the ESR spectrum. Further, it could be possible that, in cases of strong electron-nuclear coupling, the dynamic Jahn-Teller effect contributes to electron spin relaxation. Also, since the theorem is a purely group-theoretical result, very little is understood about the mechanisms by which these distortions occur.

A major portion of this thesis is devoted to a number of experimental approaches to this problem. In particular, we have studied the ESR spectrum of VCl_4 in various glasses at liquid helium temperatures and found significant evidence for the existence of a dynamic Jahn-Teller effect under some experimental conditions. The electron spin-lattice relaxation time has also been measured and the temperature dependence of the spectrum has been studied. It is believed that valuable new information on relaxation mechanisms has been obtained. We have, in addition, studied the ESR spectra of other paramagnetic systems and, for example, characterized the ESR spectrum of $V(CO)_6$ for the first time. Before describing the techniques used in these experiments (Chapter III), we

first present in Chapter II a survey of the previous work on the molecular systems which we have investigated. The basic approach is from the point of view of an ESR spectroscopist, but NMR techniques have been utilized where possible to study nuclear transitions in a paramagnetic molecule. This combination of magnetic resonance techniques has been particularly fruitful for measuring the ^{35}Cl hyperfine coupling constant in VCl_4 and for the determination of relaxation times. In Chapter IV the results obtained from these experiments are presented and then used as a basis for the discussion of the structure and bonding in these systems.

I. REFERENCES

1. E. M. Purcell, H. C. Torrey and R. V. Pound, Phys. Rev. 69, 37 (1946).
2. F. Bloch, W. W. Hansen and M. E. Packard, Phys. Rev. 69, 127 (1946).
3. E. Zavoisky, J. Phys. USSR 9, 211, 245 (1945).
4. M. H. L. Pryce, Proc. Phys. Soc. (London) A63, 25 (1950); A. Abragam and M. H. L. Pryce, Proc. Roy. Soc. (London) A205, 135 (1951).
5. B. Bleaney and K. W. H. Stevens, Repts. Progr. Phys. 16, 108 (1953); K. D. Bowers and J. Owen, ibid. 18, 304 (1955); J. W. Orton, ibid. 22, 204 (1959).
6. H. A. Jahn and E. Teller, Proc. Roy. Soc. (London) A161, 220 (1937).

II. SURVEY OF PREVIOUS WORK

A. $V(CO)_6$

The synthesis of vanadium hexacarbonyl was first reported in 1959 by Natta, et al.[1] $V(CO)_6$ was found to be a volatile, air-sensitive, blue-green solid which decomposes at 60-70°C. It is slightly soluble in hydrocarbon solvents, yielding yellow solutions which are sensitive to light and of low stability. The molecular weight and structure of $V(CO)_6$ were determined by Natta, et al. in these and subsequent experiments[2] using X-ray techniques. From this work it was concluded that $V(CO)_6$ is monomeric in the solid state and crystallizes in the orthorhombic system, space group P_{nma} (a = 11.97, b = 11.28, c = 6.47Å; z = 4), the unit cell being analogous to that of $Mo(CO)_6$. The X-ray powder spectrum of $V(CO)_6$ was practically the same as that for $Cr(CO)_6$, which is known to be monomeric.[3] (Both the chromium and molybdenum carbonyls have octahedral structures, with metal-to-carbon bond distances of 1.92 Å and 2.08 Å, respectively.[4]) Natta, et al.[1] also measured the magnetic susceptibility of the solid $V(CO)_6$ and found it to be paramagnetic with one unpaired electron (μ_{eff} = 1.73 BM).

The nature of $V(CO)_6$ in solution is not as well understood. At about the same time as the synthesis of $V(CO)_6$ was first reported, Pruett and Wyman[5] prepared a vanadium carbonyl from ditoluene vanadium which they characterized as the dimer, $V_2(CO)_{12}$. This compound had the same physical properties as that reported by Natta, et al.[1] The bases for their assignment of the dimeric formula to this molecule were molecular weight determinations and magnetic resonance experiments which were performed, in the main, on hydrocarbon solutions of the material. From the latter, which gave sharp proton lines for the benzene solution NMR spectrum and a negative result for the ESR spectrum, they concluded that the compound

was diamagnetic. Pruett, in a comment following ref. 2, suggests that these results could be explained if a change from the monomeric state in crystalline form to a dimeric state in solution occurred. Molecular weight measurements on hydrocarbon solutions performed by Calderazzo, et al.[2] were inconclusive.

Magnetic susceptibility measurements subsequently showed that benzene and toluene solutions of $V(CO)_6$ were paramagnetic with about one unpaired electron per molecule (μ_{eff} = 1.81±0.04 BM).[6] From this result, Calderazzo concluded that vanadium hexacarbonyl is monomeric in solution as well as in the solid state, although no explanation was given for the anomalous cryoscopic behavior. (Similar behavior has been observed for solutions of $Cr(CO)_6$ and $Mo(CO)_6$.)[2] In addition, some NMR measurements of proton relaxation times in benzene solutions of $V(CO)_6$ have been reported.[7] The results confirmed the paramagnetism of $V(CO)_6$ and showed that it does not dimerize in solution.

Metal carbonyls such as $V(CO)_6$ may be regarded as coordination complexes formed between zerovalent transition metals and electron-donor carbon monoxide ligands. The nature of the metal-CO bond in this class of compounds has been the subject of a review article[8] and is also discussed at some length in standard texts.[9,10] Because it will be useful in the discussion of the ESR results to be presented later, we shall review here briefly the electronic structure of the metal carbonyls in general, and $V(CO)_6$ in particular. The reader is referred to the above-mentioned references for a more complete discussion.

Ignoring the possibility of π-bonding for the moment, Fig. 1 shows a qualitative molecular orbital energy level diagram which is appropriate for an octahedral complex between a metal ion of the first transition

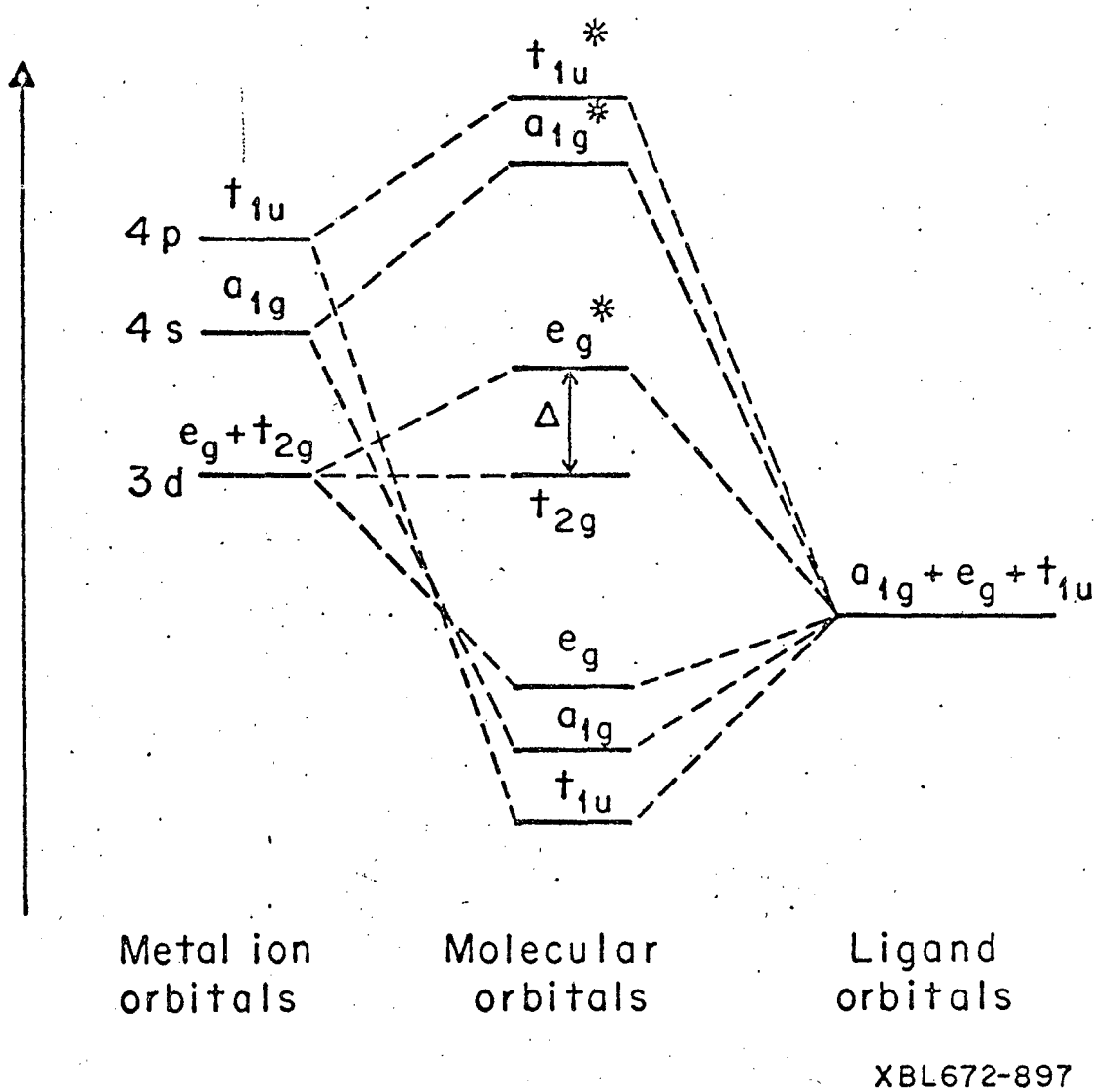

XBL672-897

Fig. 1. Qualitative molecular orbital energy level diagram for octahedral $V(CO)_6$ assuming no π-bonding.[11]

series and six ligands.[11] The t_{1u}, a_{1g}, and e_g molecular orbitals, which are primarily ligand in character, are formed from the proper linear combinations of σ-orbitals of the ligands (one from each) and the d_{z^2}, $d_{x^2-y^2}$, 4s, and three 4p orbitals of the metal ion. These metal orbitals are primarily directed along the metal-ligand bond axes and are therefore suitable for σ-bonding. Next are the t_{2g} molecular orbitals; these are, in this diagram, composed entirely of the three metal orbitals d_{xy}, d_{yz}, and d_{zx} and are therefore non-bonding because they are not directed toward the ligands. The anti-bonding molecular orbitals e_g^* are next in energy and are primarily of metal ion character. The splitting $E(e_g^*) - E(t_{2g})$ is assigned the parameter Δ.

In $V(CO)_6$, the zerovalent vanadium will be assumed to have the electronic configuration $(Ar)(3d)^5$, where (Ar) represents the completed shell of argon. With each carbonyl group contributing two σ-electrons, we must place 17 electrons in the molecular orbitals shown in Fig. 1. This results in the configuration $(t_{1u})^6(a_{1g})^2(e_g)^4(t_{2g})^5$; $V(CO)_6$ is therefore one electron shy of the closed shell configuration...$(t_{2g})^6$ and can be considered to have a single hole in the t_{2g} shell. The ground state of $V(CO)_6$ is then $^2T_{2g}$ and the single unpaired electron is located in one of the metal t_{2g} orbitals.

Since the t_{2g} molecular orbitals are formed, in this approximation, by a linear combination of the metal ion orbitals, the M-C bonds are essentially formed by the donation of two σ-electrons from each ligand. Thus the M-C bond has a bond order of one when π-bonding is neglected. However, it is generally thought that in the carbonyls the M-C bond has a bond order of about 1.5 and that this partial double bond character is achieved by the utilization of the t_{2g} orbitals of the metal ion in π-bonding with both filled and empty π-orbitals of the ligand.[8] This

has the effect of lowering the C-O bond order from that in free CO. This conception of the bonding in metal carbonyls is supported by the observation that the C-O stretching frequency in most carbonyls is lower than that in free carbon monoxide.[9] Further, the existence and relative stability of the carbonyl and cyanide complexes of the transition metals provides additional evidence that stronger M-C bonds are involved in these compounds than are present, for example, in the metal alkyls.[8]

The effect of π-bonding between the d_{xy}, d_{yz}, and d_{zx} metal orbitals and the π-orbitals of the ligands is shown in Fig. 2, which is taken from Cotton and Wilkinson.[12] From this diagram, it is seen that the splitting Δ in Fig. 1 is modified both by the interaction of the π-orbitals which are of lower energy than the metal t_{2g} orbitals and those which are of higher energy, the π^* ligand orbitals. Further, the unpaired electron has now acquired some ligand character, it being located in the $t_{2g}(\pi)[d_{xz}, d_{yz}, d_{xy}]$ molecular orbital.

A test of these views of the bonding in metal carbonyls could be provided by ESR experiments. For, if there were some participation of the unpaired d-electron(s) of the metal atom in a π-bond with the ligand, the mechanism of spin polarization[13] could give rise to some unpaired electron spin density at the carbon atom. This would result in ^{13}C hyperfine structure in the ESR spectrum of a paramagnetic carbonyl and provide a direct test of the above theories. $V(CO)_6$ is one of the few known paramagnetic metal carbonyls. Yet, to the knowledge of this author, there have been no published reports of the ESR spectrum of $V(CO)_6$.[14,15]

In the likely possibility of considerable overlap between the metal d-orbitals and the π-orbitals of the ligand, the most logical starting point for a discussion of spectral properties of $V(CO)_6$ is the

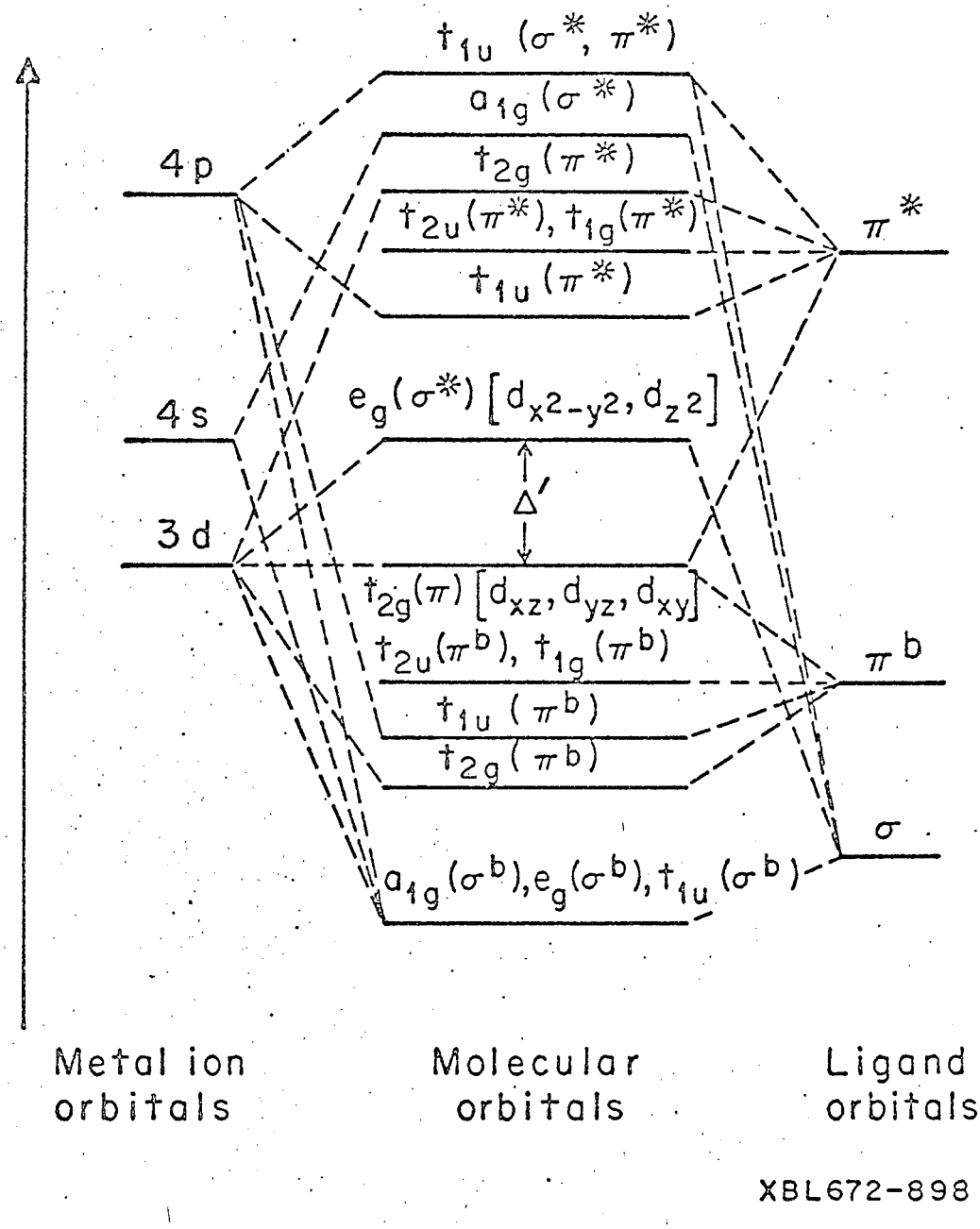

XBL672-898

Fig. 2 Qualitative molecular orbital energy level diagram for octahedral $V(CO)_6$ with both σ- and π-bonding.[12]

molecular orbital theory which has been outlined above. However, because of the lack of spectral information on $V(CO)_6$ (vide infra), the purely electrostatic crystal field theory will be used as a basis for discussion in this paper. In this approach, the ligands serve only to provide a constant electric potential having the symmetry of the arrangement of the ligands around the metal ion, in which the electrons can move. No provision for bonding between metal and ligand is made; however, if there is evidence for covalency in the ESR results, certain parameters can be adjusted empirically to account for this without explicitly introducing covalence into the crystal field theory. In this case, the molecular orbital scheme we have just discussed becomes a useful guide for these adjustments. Such an approach (termed adjusted crystal field theory[17]) has been shown to be useful in the interpretation of the g-values of paramagnetic ions,[18] and this is the application intended here. The techniques of the method have been discussed in a number of important monographs.[18,19]

In the molecular orbital theory without π-bonding, it was shown that the ground state of $V(CO)_6$ was $^2T_{2g}$, with the unpaired electron located in one of the metal t_{2g} orbitals. Figure 3 shows that a similar result is obtained using the crystal field theory. According to this approach, the strong octahedral field of the six CO ligands will remove the fivefold orbital degeneracy of the d-orbitals, yielding two sets of orbitals which differ in energy by the crystal field parameter 10Dq ($\sim \Delta$ of Fig. 1). The lower set of t_{2g} orbitals is threefold degenerate (d_{xy}, d_{yz}, d_{zx}) and the upper set, the e_g orbitals, is doubly-degenerate (d_{z^2}, $d_{x^2-y^2}$). If the parameter 10Dq is large compared to the pairing energy of the electrons, the five 3d electrons of $V(CO)_6$ will enter the

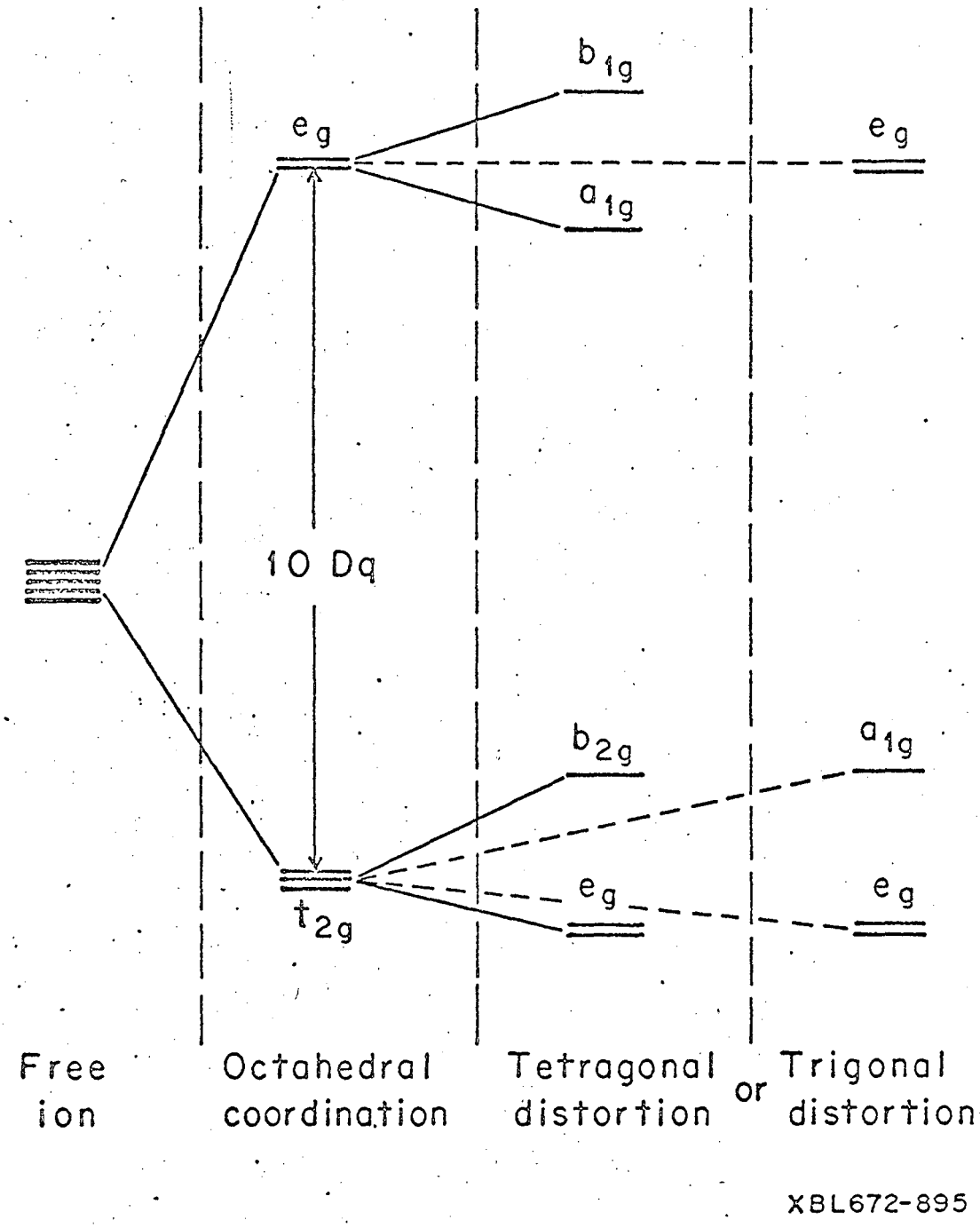

Fig. 3 Crystal field energy level diagram for $V(CO)_6$.

lower t_{2g} shell and the ground state will be $^2T_{2g}$. However, if 10Dq is small, the electronic configuration will be $(t_{2g})^3(e_g)^2$ [in Fig. 1, this would be $(t_{2g})^3(e_g^*)^2$] and the ground state will be $^6A_{1g}$. Since the magnetic susceptibility data mentioned above demonstrate that $V(CO)_6$ has a single unpaired electron, the former filling scheme is necessary and the ground state of octahedral $V(CO)_6$ is $^2T_{2g}$. Thus, in the sense that the unpaired electron occupies one of the non-bonding metal t_{2g} orbitals, the crystal field approach gives the same result as the molecular orbital theory providing there is no π-bonding.

Since the ground state $^2T_{2g}$ possesses a three-fold orbital degeneracy, the molecule should experience a distortion from its assumed octahedral symmetry in compliance with the Jahn-Teller theorem. In the case of a tetragonal distortion, the octahedron would experience an elongation along a C_4 axis and the ground state would be $^2B_{2g}$. In this configuration, there would be four equatorial ligands in a square-planar arrangement with two axial CO's at a greater distance, and $V(CO)_6$ would possess axial symmetry. (A tetragonal compression would give rise to a ^2E_g ground state, which would distort further.) A trigonal distortion along one of the C_3 axes of the octahedron splits the levels in a quite similar way; in this case the configuration would be $(e_g)^4(a_{1g})^1$ and the ground state would be $^2A_{1g}$ with axial symmetry. These alternatives are also shown in Fig. 3. Finally, the axial symmetry could be removed by a further distortion of lower symmetry although this is not required by the Jahn-Teller theorem.

The optical spectrum of $V(CO)_6$ has not been extensively studied. In the only reported work to date, Haas and Sheline[20] showed that some of the bands in the diamagnetic $Cr(CO)_6$ are shifted or split in the corresponding ultraviolet spectrum of $V(CO)_6$ in the gas phase. The (presumably) $\pi \rightarrow \pi^*$ ligand transitions which occur at about 2300 Å in

$Cr(CO)_6$ are shifted to higher wavelength in $V(CO)_6$ and appear to be split. The authors suggest that two weak bands at 3500 - 4000 Å in $V(CO)_6$ are a pair of transitions having mainly d-d character. However, no attempt was made to assign these transitions.

Haas and Sheline also studied the infrared spectrum of $V(CO)_6$ and the corresponding chromium compound. The gaseous $Cr(CO)_6$ shows a C-O stretching band centered at 2000 cm^{-1} in which the P, Q, R branches of the rotational structure are clearly discernable, although not well-resolved. In contrast, the C-O stretch in $V(CO)_6$ is centered at about 1985 cm^{-1} and is half-again as wide. Since only one band is observed, they suggest that in the gas phase $V(CO)_6$ is undergoing a dynamic Jahn-Teller distortion. However, they do not rule out the possibility of two close but overlapping transitions. Pruett and Wyman[21] have investigated the infrared spectrum of $V(CO)_6$ in hydrocarbon solvents and they also observed an unresolved band at 1980 cm^{-1}. The infrared results on gaseous $V(CO)_6$ have been confirmed in independent experiments.[22]

The methods of crystal field theory were first applied to d^5 systems by Van Vleck.[23] He showed that the magnetic susceptibility of covalent complexes of the iron group (e.g., ferricyanide), which corresponded to one unpaired electron, could be explained if the five d-electrons all entered the d-orbital triplet (t_{2g}) present in a strong field of octahedral symmetry. A more detailed treatment of these ideas has been given by Howard.[24] The extension of the theory to complexes of the 4d and 5d group has also appeared.[25] In this work, it was noted that there is good agreement with the theory for all covalent d^5 systems to a first approximation, but that significant discrepancies do exist. For example, the observed g-values of these complexes are slightly smaller than the calculated values. The reasons for these discrepancies were not clear

until an unusual ligand hyperfine structure was found in the complex $IrCl_6^{-2}$, ($5d^5$).[26] This observation led to the conclusion that some of the unpaired spin was shared between the metal ion and the ligands in π-bonds, which explained both the hyperfine structure and the reduction in g-values in such systems.

The theory of the ESR spectra of covalent XY_6 complexes has been developed in a paper by Stevens.[27] His treatment allows for the formation of weak π-bonds between the central ion and the ligands and is most appropriate in a discussion of the hyperfine structure in such compounds, as noted above. Subsequently, Bleaney and his co-workers[28] extended the theory of Stevens for d^5 low-spin complexes with low symmetry. Starting with a crystal field perturbation V that was subject to no symmetry restrictions, they treated the $(t_{2g})^5$ configuration as a single hole in the t_{2g} shell with a negative spin-orbit coupling constant. The results of this calculation were then used to interpret the g-values and susceptibility of $K_3Fe(CN)_6$ and $K_4Mn(CN)_6$. It was found necessary to include an orbital reduction factor k of 0.87 for the ferricyanide and 0.74 for the manganocyanide in order to fit the g-values to the experimental data. These values of k were in basic agreement with the observed hyperfine structure in both cases and are interpreted as resulting from covalency in the M-C bond. In the absence of any ESR data on paramagnetic carbonyls, the results of such studies on cyanide complexes are of particular interest as CO and CN^- are isoelectronic ligands.

More recently, the ESR spectra of $Mn(CN)_5NO^{-2}$ and $Cr(CN)_5NO^{-3}$ in dilute single crystals have been reported.[29] In this work, Fortman and Hayes derived explicit g-value expressions for the case of a $(t_{2g})^5$ configuration in a tetragonal field. In the case of a trigonal distortion,

no analogous calculation has been published. However, the method of Abragam and Pryce[30] for $3d^1$ complexes is directly applicable, since there is in $(t_{2g})^5$ one hole in the t_{2g} subshell and the lowest energy levels are as for $(t_{2g})^1$ except that they are inverted. The results for Ti^{3+}, which is a $3d^1$ ion, in a trigonal field have been reported by Bleaney.[31]

The purpose of the work reported herein was to investigate the ESR spectrum of $V(CO)_6$ at low temperatures. In view of the magnetic susceptibility results on this compound both in the solid state and in solution, it seemed likely that the failure to observe an ESR spectrum at normal temperatures was due to a very short electron spin relaxation time of the unpaired electron in $V(CO)_6$. (Similar behavior has been reported for the ferricyanide, $K_3Fe(CN)_6$, whose spectrum is observable only at liquid hydrogen temperatures and below.[28a]) This would make the ESR spectrum very broad and possibly unobservable even down to 77°K. Further, the proton lines in an NMR spectrum of hydrocarbon solutions of the hexacarbonyl would not be broadened if electron spin relaxation were very rapid.

These qualitative considerations have proven to be correct. The ESR spectrum of $V(CO)_6$ has been observed at temperatures in the range 1.5-4.2°K, both for the pure solid and for dilute solutions in various glasses. Because of an unusual power dependence of the spectrum, both the isotropic and anisotropic spectra are obtained under different experimental conditions. The g-values measured from the anisotropic spectrum are in good agreement with those calculated from crystal field theory if a tetragonal distortion is assumed. This data is used in a discussion of the apparent Jahn-Teller distortion in $V(CO)_6$ as well as the associated optical spectrum.

B. VCl_4

1. Synthesis and Properties

Vanadium tetrachloride is an unusual paramagnetic transition metal compound which is a liquid at room temperature and has an appreciable vapor pressure under normal conditions. The synthesis of VCl_4 was first reported by Roscoe[32] and its physico-chemical properties have been studied by Simons and Powell[33] and others. These properties are listed in Table I. At room temperature (and more rapidly at elevated temperatures) VCl_4 decomposes slowly into VCl_3 and Cl_2; it reacts readily with water to form $VOCl_2$ and HCl, and with oxygen to form $VOCl_3$. Particularly troublesome as an impurity is $VOCl_3$, which has similar physical properties.[34] VCl_4 is soluble in most non-polar solvents such as CCl_4, $CHCl_3$, heptane, hexane, and mineral oil, as well as $TiCl_4$, $SiCl_4$, etc. However, there is some evidence for the formation of eutectics in the binary solutions VCl_4/CCl_4 and $VCl_4/VOCl_3$, but none in the system $VCl_4/TiCl_4$. The specific gravities of the latter system have also been measured over a wide concentration range.[41]

On the basis of cryoscopic measurements, Simons and Powell[33] reported that an equilibrium existed between VCl_4 and V_2Cl_8 in carbon tetrachloride solution. Subsequent experiments by Whittaker and Yost[38] suggested that, because of the formation of a CCl_4/VCl_4 eutectic at -64°C, the results quoted above were invalid and that VCl_4 existed as a monomer in both the pure liquid and CCl_4 solutions. This work was substantiated by magnetic susceptibility measurements on CCl_4 solutions[38] and in later experiments by Grubb, et al.[42] Thus it was concluded that the molecular species present in vapor, liquid and solution is monomer VCl_4.[42]

Table I. Physico-chemical Properties of Pure VCl_4

Property	Values	Reference
Boiling point, °C	154 (760mm), 149.7(731mm)	32,33
Freezing point, °C	-25.7	33,38
Density, ρ(g/cc at 25°C)	1.8159	32,38
Dielectric constant, ϵ(at 25°C)	3.05, 3.11	34,36
Electric moment	~0	34
Molar refraction (CCl_4), cc	40.0	34
Vapor pressure, log p (mm)	-1998/T + 7.581	33,37
Magnetic susceptibility, X_m (25°C) cgs units	1152×10^{-6}	38,39,40
Electrical conductivity	~0	35

2. Structure and Bonding

Formally, the electronic configuration of V^{+4} is $(Ar)(3d)^1$, where (Ar) represents the completed shell of argon. With one unpaired electron per molecule, the molar paramagnetic susceptibility of VCl_4 should be 1247×10^{-6} cgs units at 25°C. With an estimated diamagnetic susceptibility of -98×10^{-6}, the predicted susceptibility of this compound is 1149×10^{-6} cgs units per mole,[38] which is in good agreement with the value quoted in Table I. Other measurements of the susceptibility have given similar results.[39,40] Assuming g = 2, calculation of the magnetic moment from the susceptibility yields μ_{eff} = 1.67 BM over the temperature range -186-45°C.[43]

Electron diffraction studies of pure VCl_4 vapor have shown that the molecule is tetrahedral with a V-Cl distance of 2.03 Å,[44] (Cl-Cl, 3.32 Å). This bond distance is considerably shorter than that found for $TiCl_4$ (Ti-Cl, 2.18 Å)[45] and this "bond-shrinkage" effect has been attributed to ligand-field effects in VCl_4 (vide infra).[46] The effect of molecular vibrations on bond distances obtained by electron diffraction methods has been investigated extensively for VCl_4 and other molecules.[47] Other representative bond distances have been measured in $VOCl_3$ (V-Cl, 2.12 Å),[48] CCl_4 (C-Cl, 1.76 Å),[49] $SiCl_4$ (Si-Cl, 2.00 Å)[49] and $SnCl_4$ (Sn-Cl, 2.30 Å).[49] To the knowledge of the author, no X-ray work on VCl_4, $TiCl_4$, etc. in the solid state has been reported.

In contrast to the situation with $V(CO)_6$, the optical spectrum of VCl_4 has been extensively studied, both in the vapor phase and in condensed media (solutions and pure liquid). Because an understanding of these spectra is important in the interpretation of our magnetic resonance results, we shall discuss this work in some detail here. Further, since the assignment

of optical spectra requires the assumption of a particular electronic configuration for the molecule, some qualitative considerations of the bonding in VCl_4 will be presented. The reader is referred to the literature for a more detailed treatment.[50]

In the LCAO/MO approximation without π-bonding, the electronic configuration of VCl_4 can be represented as shown in Fig. 4.[46] The atomic orbitals taken for the calculation are the 3d, 4s, and 4p for vanadium and the 3s and 3p for chlorine. Employing the usual group-theoretical methods outlined in Ballhausen,[51] ligand σ-orbitals of symmetry a_1 and t_2 are constructed from the chlorine 3s and $3p_z$ orbitals. The metal orbitals of the same symmetry are found in an analogous way and the σ-molecular orbitals are appropriate linear combinations of these two sets of symmetry orbitals. We note here that, because of the absence of a center of symmetry in the tetrahedral molecule, the 3p orbitals and three of the d-orbitals (d_{xy}, d_{yz}, and d_{xz}) of the vanadium ion have the same symmetry (t_2) and therefore mix with one another. Thus the t_2 molecular orbital contains some metal-ion p-character, even in the σ-bonding approximation. With each Cl ligand supplying two σ-electrons, the electronic configuration of VCl_4 is $(a_1)^2\ (t_2)^6\ (e)^1$ and the splitting $[E(t_2^*) - E(e)]$ is assigned the parameter Δ. Thus the ground state is ^2E and the unpaired electron is located in a pure metal (e) orbital. This result is also obtained by the use of a strong crystal field model for a $(3d)^1$ ion in tetrahedral symmetry, so the situation is analogous to that found in $V(CO)_6$; i.e., the same results are obtained in the MO approach with no π-bonding and crystal field theory.

The experiments to be reported herein show conclusively that there is a small (but significant) unpaired electron spin density at the chlorine nuclei in VCl_4. Because the molecular orbital treatment given

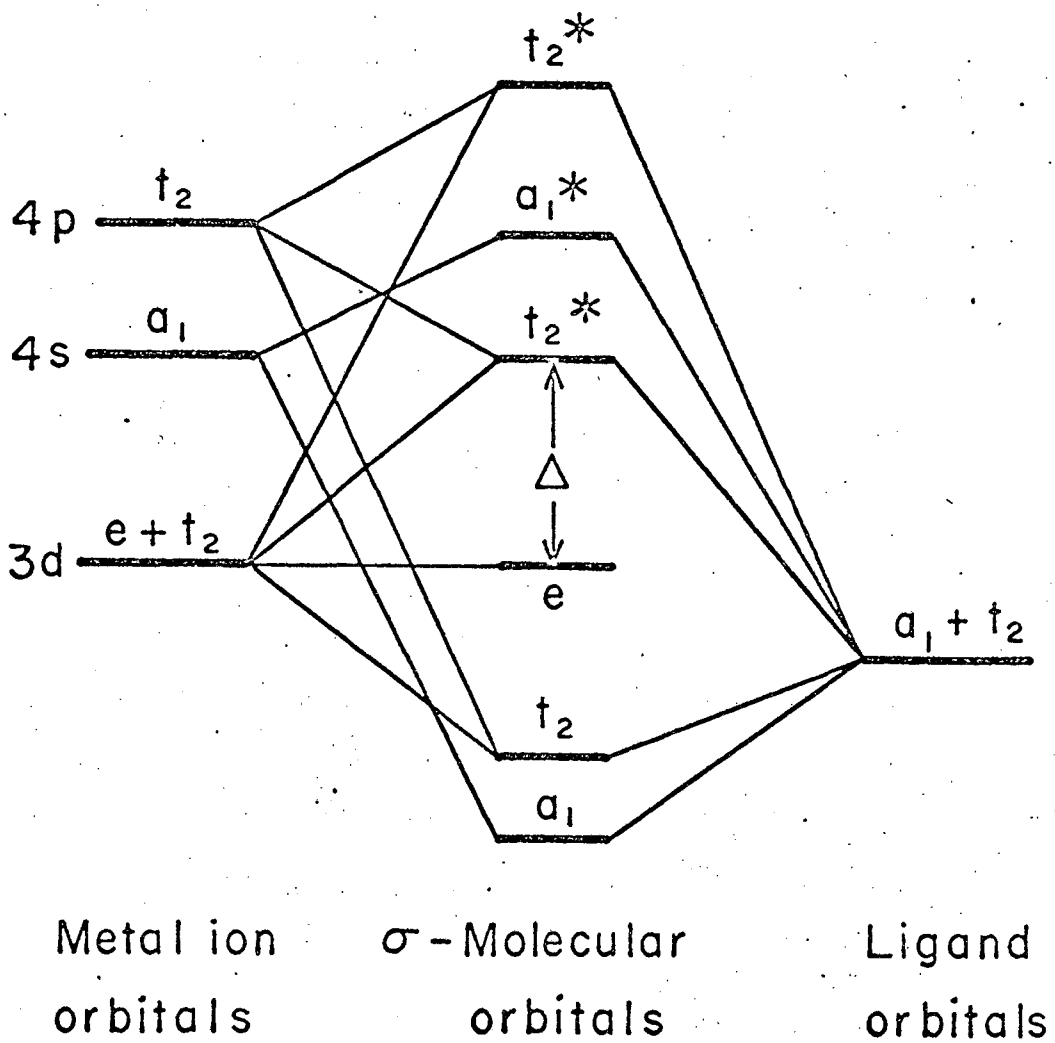

XBL673-2355

Fig. 4. Qualitative molecular orbital energy level diagram for tetrahedral VCl_4 in the σ-bonding approximation.[46]

above predicts that the unpaired electron is located in a pure metal orbital, and therefore does not account for the presence of this additional hyperfine interaction, it will be necessary to include the effects of π-bonding in our molecular orbital description of the bonding in VCl_4. These effects can be considered using methods analogous to those used by several authors[50a,52] for the tetrahedral XO_4^{-n} ions, for the inclusion of π-bonding was found to be necessary in the interpretation of the optical spectra of MnO_4^- and CrO_4^{-2}.

Figure 5 shows a molecular orbital energy level diagram which is appropriate for VCl_4, where both σ- and π-ligand orbitals are included.[53] Again, the molecular orbitals of the molecule may be characterized by the irreducible representations of the tetrahedral symmetry group T_d. The representations of particular interest to us for the interpretation of our magnetic resonance results are the doubly-degenerate $e(\pi^*)[d_{x^2-y^2}, d_{z^2}]$ and the triply-degenerate $t_2(\sigma^*,\pi^*)[d_{xz}, d_{yz}, d_{xy}]$. The inclusion of the 16 π-electrons of the ligands results in the configuration $(a_1)^2(t_2)^6(e)^4(t_2)^6(t_1)^6(e)^1$ for VCl_4. By inspection of Fig. 5, is seen that the e^* orbitals are π-type combinations of $3d_{x^2-y^2}$ and $3d_{z^2}$ metal orbitals with π chlorine orbitals, and that the t_2 orbitals may contain both σ and π admixtures of chlorine orbitals with the metal $3d_{xy}$, $3d_{yz}$, $3d_{xz}$, and 4p orbitals. Thus the ground state of VCl_4 is still ^2E but now the unpaired electron is located in an antibonding orbital which contains some ligand character.

3. Optical, Infrared, and Raman Spectra

Table II summarizes the results obtained by several authors for the optical spectrum of VCl_4. The near-infrared transition at ~9000 cm^{-1} was first observed by Whittaker and Yost[38] in CCl_4 solutions. Orgel[54] assigned

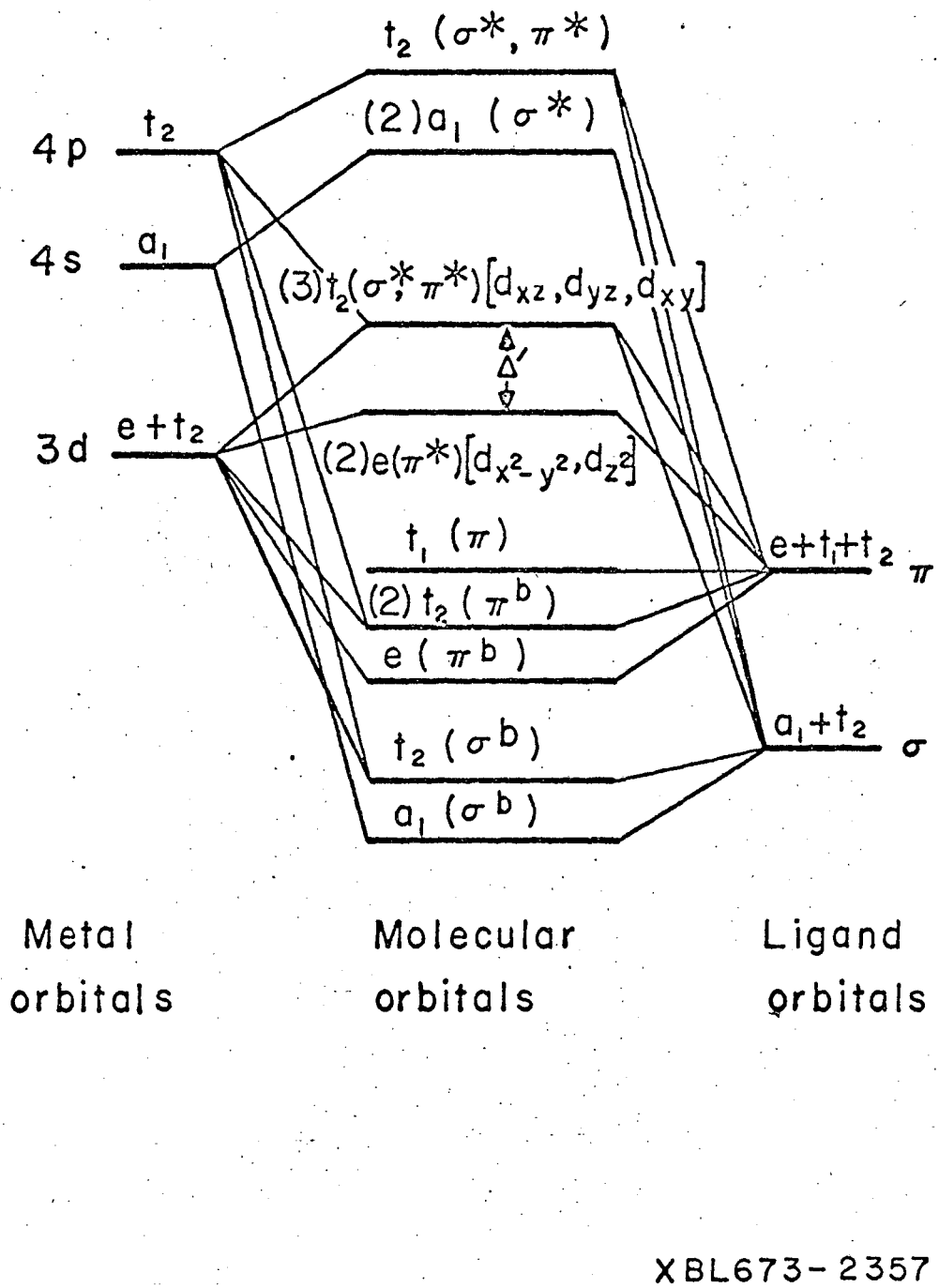

XBL673-2357

Fig. 5. Qualitative molecular orbital energy level diagram for tetrahedral VCl_4 with π-bonding (after Dijkgraff[55]).

Table II. Assignment of Optical Transitions in VCl_4[57]

Transition	ν_{max}, cm^{-1}	Reference
$2e \rightarrow 3t_2$	~9000, CCl_4 soln	38
	9250/7850/6600, vapor	55
	9010/7880/6000, CCl_4 soln	39
	9000(split), cyclohexane soln	53
$t_1 \rightarrow 2e$	24,800, vapor	56
	24,800, vapor	57
	25,000, vapor	58
	24,200, cyclohexane soln	53
$t_1 \rightarrow 3t_2$ (see text)	33,900, vapor	56
	33,900, vapor	57
	34,100, vapor	58
	33,200, cyclohexane soln	53
$2t_2 \rightarrow 3t_2$	>50,000, vapor (calc.~54,000)	57
$2t_2 \rightarrow 2e$	45,400, vapor	57
$2e \rightarrow 2a_1$	17,200, solid at low T	57

this band to the $2e \rightarrow 3t_2$ transition and subsequent workers (see Table II) have agreed with this interpretation. Further, it will be noted that the difference in the $(t_1 \rightarrow 3t_2)$ and $(t_1 \rightarrow 2e)$ splittings is about 9100 cm^{-1}, which is in agreement with the assigned $2e \rightarrow 3t_2$ transition. Grubb, et al.[42] have made a careful study of the 9000 cm^{-1} band (in pure VCl_4 liquid and vapor and in VCl_4/CCl_4 solutions) and found that its integrated intensity was essentially independent of temperature, pressure and physical state in the range 25-70°C. This was taken as good evidence for the lack of dimer formation (vide supra).

The remainder of the assignment given in Table II is based on the interpretation of Pennella and Taylor.[57] It should be noted here that the band at 33,900 cm^{-1} has been assigned to the transition $2t_2 \rightarrow 2e$ by Grubb and Belford[59] but we prefer the assignment given in Table II for reasons stated in the literature.[57] However, because of widely-varying intensities[58] and the possibility of $VOCl_3$ contamination, this assignment must still be considered somewhat tentative.

As is indicated in Table II, the $2e \rightarrow 3t_2$ transition is split into at least three components. This splitting has been attributed[55] to the Jahn-Teller effect. Since this transition corresponds to a promotion of VCl_4 from its ^2E ground state to a $^2T_2$ excited state, the assumed Jahn-Teller splitting could be due to a distortion in either or both of these states as they both are orbitally-degenerate. These effects would, on qualitative grounds, be expected to be greater for the $^2T_2$ state since the unpaired electron is in an antibonding σ-orbital in this state and in a π-orbital in the ^2E state. However, this splitting cannot be taken as proof of the existence of the Jahn-Teller effect in either the ground or excited states, but can only be said to be consistent with this interpretation. A closer analysis of this

splitting will be possible only when the vibrational structure is resolved[60] such as has been done for the absorption bands of V^{+3} in a corundum lattice.[61]

No concrete evidence has been found of any influence by the Jahn-Teller effect on the ground-state vibrational spectra of VCl_4. Early attempts[55] at the assignment of the infrared spectrum of this molecule were complicated by the presence of $VOCl_3$ impurities.[62] However, when care was taken to purify the VCl_4, both infrared and Raman spectra were obtained which were internally consistent. Table III lists the results of these experiments. The frequencies shown in parentheses were not

Table III. Infrared and Raman Spectra of VCl_4 and Related Molecules

	Fundamentals, cm^{-1}				
Sample	$\nu_1(a_1)$	$\nu_2(e)$	$\nu_3(f_2)$	$\nu_4(f_2)$	Reference
VCl_4	R	R	I,R	I,R	
vapor (IR)			490		43
liquid (IR)			475		43
CCl_4 soln (R)	383	128	475	128	43
CCl_4 soln (IR)			482		43
vapor (IR)	(383)		487	(128)	62
CCl_4 soln (IR)		(105)*		129	63
CCl_4 freq.	458	218	776	314	64
$SiCl_4$ freq.	424	150	608	221	64
$TiCl_4$ freq.	386	120	495	141	64

* See text.

observed directly but calculated from combination bands. The assignment of ν_1 and ν_3 is fairly certain but ν_4, and in particular ν_2, are only tentative. Creighton et al.[63] concluded on the basis of their experiments that ν_4 = 129 cm^{-1} and, with the aid of force-field calcuations, showed that ν_2 was probably 105±20 cm^{-1}. This assignment seems reasonable in view of the known fundamental frequencies in CCl_4, etc., shown in Table III. However, ν_2 has not been observed directly in either the Raman or IR spectrum.

Several authors have suggested that the absence of ν_2 in the Raman spectrum of VCl_4 is due to the Jahn-Teller effect,[43,62] for ν_2 is observed for $TiCl_4$, etc. They suggest that this fundamental has the same symmetry as the predicted Jahn-Teller distortion in VCl_4,[46] thus destroying the even spacing of its vibrational levels and making it difficult to observe because of broadening. Similar effects are thought to be important in the vibrational spectra of ReF_6 and OsF_6.[65] However, until a theory of the vibrational spectra of Jahn-Teller molecules is formulated, no conclusions can be drawn from these observations. Some efforts in this direction have been made.[66]

4. Theoretical Work

In addition to the experimental references to the Jahn-Teller effect in VCl_4 which have been discussed above, many workers have treated this problem on a theoretical basis. Because of its inherent simplicity, we shall introduce a crystal-field model here in order to discuss this work. The appropriate diagram in shown in Figure 6. With a single d-electron in a tetrahedral field, the ground state is ^2E and from the optical results, 10 Dq ~9000 cm^{-1} ($\cong\Delta$, Δ' of Figs. 4 and 5). Since a distortion of trigonal symmetry does not split levels of e symmetry (see Fig. 3 of

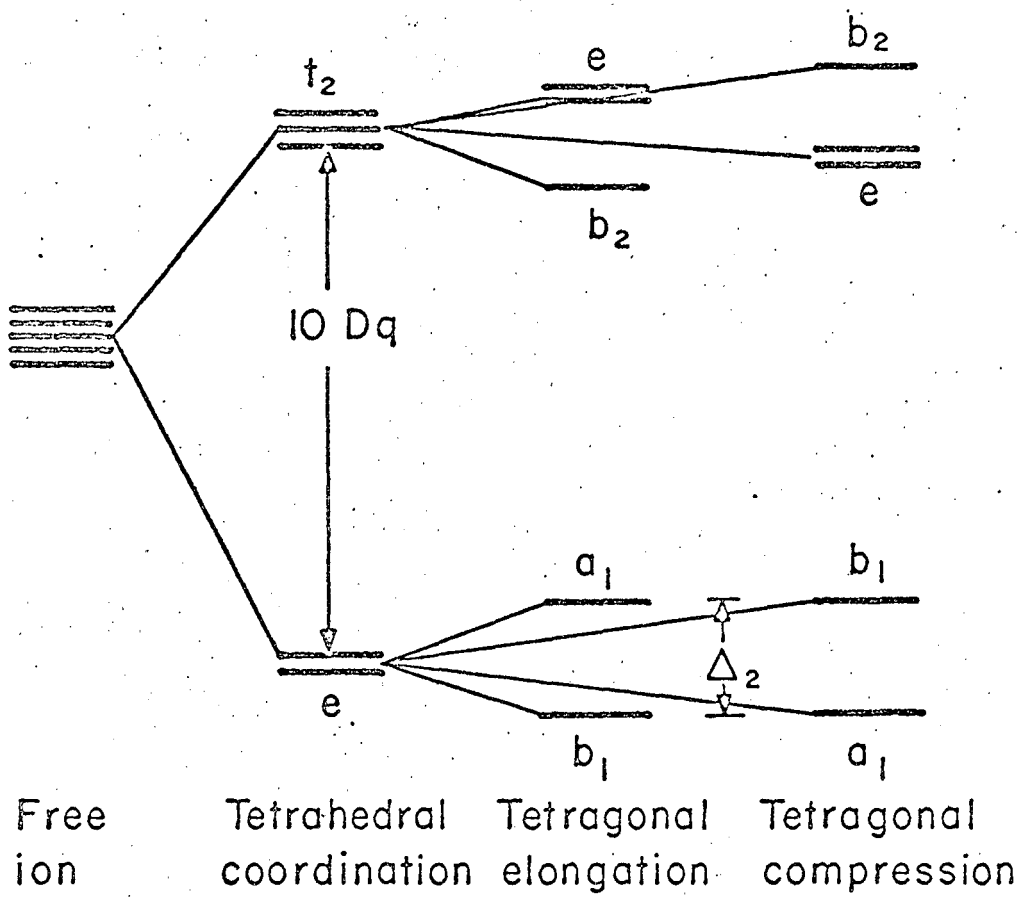

XBL673-2356

Fig. 6. Crystal field energy level diagram for VCl_4.

the previous section), the distortion produced by the Jahn-Teller effect must have tetragonal symmetry or lower. Thus the ground state is $^2B_1$ for an elongated tetrahedron and $^2A_1$ for compressed tetragonal symmetry (so-called bisphenoidal geometry).[50b] The excited e state may also be split by a distortion of lower symmetry.

The first reported theoretical application of the Jahn-Teller theorem to VCl_4 was published by Ballhausen and Liehr.[46] This work, which was an extension of an earlier paper on octahedral complexes,[67] was based on a crystal field model in which the electronic energy was minimized with respect to properly selected symmetry coordinates of the molecule. The authors predicted that VCl_4 would assume a stable elongated structure of symmetry D_{2d} below about 200°K. and suggested that there were three equivalent distortions of this symmetry. Their calculations showed that the three-fold barrier height is of the order of 150 cm^{-1} (the so-called inversion splitting), that the stabilization of the distorted structure relative to the tetrahedral one is about 250 cm^{-1} and that the stable configuration corresponded to a closing of ~6° of two of the tetrahedral angles and an opening of ~3° for each of the four remaining angles. Thus Δ_2 (Fig. 6) was estimated to be ~500 cm^{-1} by this calculation. A later treatment,[55] which was concerned primarily with the distortion of the upper t_2 state, is in basic agreement with this work.

Lohr and Lipscomb[50b] have also performed theoretical calculations on the static Jahn-Teller effect in VCl_4. In this case, the authors used an abbreviated LCAO/MO method suitable for "one-electron" systems in which the bond distances were fixed and the bond angles were used as variational parameters. Either with or without the inclusion of the 4s and 4p orbitals of vanadium, their results indicated that the D_{2d} structure was only

stabilized by ~80 cm^{-1} with respect to the tetrahedral VCl_4. This corresponded to a change in the tetrahedral bond angle of about 1°. Since this splitting is of the order of a zero-point vibrational energy, no static distortion would result except perhaps at very low temperatures. The authors also predicted the absorption bands for the most stable configurations with both compressed and elongated tetragonal geometry and these are in reasonable, although not quantitative, agreement with the observed spectrum. (For example, they predict $b_1 \rightarrow a_1$ at 81, $b_1 \rightarrow b_2$ at 9450, and $b_1 \rightarrow e$ at 10250 cm^{-1} for the elongated molecule.)

These conclusions were generally confirmed in a more complete ligand-field calculation published recently by Ballhausen and de Heer.[68] They expanded the Hamiltonian to second order in the totally-symmetric and doubly degenerate vibrations (ν_1 and ν_2) and used a perturbation approach to estimate the Jahn-Teller splitting. Since the experimental difference between the M-Cl bond length in VCl_4 and $TiCl_4$ is -0.15 Å, the authors assumed that 0.1 Å was a reasonable estimate for the shortening due to q_1. This assumption led to a calculated value of 0.026 Å for the Jahn-Teller amplitude, q_2. Although this predicts an energy stabilization of about 700 cm^{-1}, Ballhausen and de Heer suggest that the static effect in VCl_4 is probably too small to observe since the Jahn-Teller amplitude is about half of the zero-point amplitude for the ν_2 vibration (0.06 Å).[68] They placed an upper limit of 5 cm^{-1} on the barrier height and estimated that ν_2 would be split by about 40 cm^{-1} in the Raman spectrum.

From this review of the experimental and theoretical results on VCl_4, it can be concluded that there is no positive evidence for the presence of a Jahn-Teller effect, either static or dynamic, in this molecule. Further, as Ballhausen[68] has pointed out, it is of interest to note that

the ligand field theory predicts a flattening of the tetrahedron whereas crystal field theory predicts an elongation. Clearly, more work, both experimental and theoretical, is in order. We note finally that there is an interesting series of calculations in the Russian literature in which the inversion splitting in VCl_4 is estimated to be 2.3 cm^{-1}.[69]

5. Related Magnetic Resonance Results

Classically, metallic halides such as VCl_4 and $TiCl_4$ have been regarded as essentially covalent molecules because of their volatility, solubility in non-polar solvents, and lack of conductivity in the pure state and in solution.[70] Such methods of classification have been useful in the past but they are not conducive to quantitative treatment. More recently, two techniques using radiofrequency spectroscopy have been employed to determine degrees of covalency (or ionicity) in such compounds. One method, which applies to paramagnetic molecules only, involves the use of magnetic resonance (ESR and NMR) to measure the hyperfine coupling constants of the ligands (e.g., Cl^-). Since the hyperfine interaction is due to the presence of unpaired electron spin density at the nucleus, this technique provides a direct estimate of the participation of the electrons of the central ion in bonds with the ligands. The second method makes use of the fact that the quadrupole coupling constant eqQ of a nucleus in a molecule is proportional to the electric field gradient q at the nucleus in question. In turn, according to the theory of Townes and Dailey,[71] the magnitude of q depends to a large extent on the way in which the available p-orbitals are occupied by valence electrons surrounding the nucleus. Thus a direct measurement of eqQ (using NQR or microwave techniques) provides an estimate of the covalent character of the bond. Further, the two methods are complementary since magnetic resonance ex-

periments usually reveal s-electron contributions to the wavefunction. Some of the work using radiofrequency techniques is particularly relevant to the VCl_4 problem and will be reviewed here; a comparison of these methods as they have been applied to transition metal chlorides in general has recently been published.[72]

a. ESR

That the mixing of metal and ligand orbitals can be estimated using ESR techniques is well-documented. One procedure uses the fact that the orbital magnetic moment of an unpaired d-electron is reduced if the electron is partially delocalized over the entire molecule, i.e., quenched. This reduction leads to a change in the g-value of the molecule and has been applied by Stevens[27] and Owen[73] to the case of $IrCl_6^{-2}$. However, this method usually requires an accurate estimate of the spin-orbit and crystal-field splittings which are sometimes not available (cf. $V(CO)_6$).

A more direct method for estimating the wavefunctions of unpaired electrons in paramagnetic species utilizes the hyperfine structure which is frequently present in an ESR spectrum. In a now-classic series of papers in which they introduced the concept of a spin Hamiltonian, Abragam and Pryce[30,74] showed that such hyperfine structure could be interpreted using a simple expression involving the components of the nuclear and electronic spin. This model was used to successfully interpret the ESR spectra of hydrated copper and cobalt salts.[75] Their theory was extended by Bleaney[76] who gave general formulae for the allowed transitions in a strong magnetic field, using perturbation theory to second order. That the hyperfine structure in paramagnetic resonance was primarily due to s-electrons was recognized by Abragam, et al.,[77] who suggested that configuration interaction played a significant role in the production of

such effects in the spectra of Mn^{2+}. These early papers were concerned only with the isotropic hyperfine interaction in the central metal ion and a review of the existing experimental data on this effect has recently appeared.[78]

Using the formalism developed by Abragam and Pryce,[74] the extension of these ideas to include ligand hyperfine structure is relatively straightforward. In addition to the Cl hyperfine interaction observed in $IrCl_6^{-2}$,[26] similar effects have been detected in MnF_2[79] and other molecules. The relationship between the spin densities on such ligands and the mixing coefficients of the molecular orbitals has been discussed by Helmholz and others[80] and briefly reviewed by Ballhausen.[51]

The theory of the ESR of $3d^1$ systems such as VCl_4 has received wide attention in the literature because of its applicability to the well-known paramagnetic ions Ti^{3+}, VO^{2+}, and Cu^{2+} ($3d^9$). A recent compilation of ESR data[81] lists well over five hundred references on these ions alone. Therefore, we shall confine ourselves to some qualitative remarks concerning these systems and quote only those references which seem particularly appropriate to VCl_4. Except for VO^{2+}, the free ions each have ^2E or ^2T ground states in fields of octahedral or tetrahedral symmetry. Therefore, they are subject to distortions of lower symmetry of both intra- and intermolecular origin when the ion is placed in a crystal field of arbitrary geometry. Generally speaking, the ESR experiments reported to date have shown that when the local environment surrounding the paramagnetic ion has low symmetry and the molecule is badly distorted, electron spin relaxation is relatively slow and the lines are fairly narrow. Thus the ESR spectrum of VO^{2+} is readily observable at room temperature[82] and this is due to the distortion produced by the strong axial field of the oxygen atom.

Thus the absence of an observable spectrum of a $3d^1$ ($3d^9$) ion at room temperature can be taken as good evidence that the crystal field is (relatively) symmetric, for the presence of low-lying orbital states provides a path for rapid spin relaxation except at the very lowest temperatures. For example, in titanium cesium alum ($TiCs(SO_4)_2 \cdot 12H_2O$), the crystal field is basically octahedral with a small trigonal component. The ESR spectrum is unobservable down to 20°K.[83] Bijl[84] has shown that if the trigonal splitting were of the order of 100 cm^{-1}, this would correspond to a T_1 of about 10^{-12} seconds and make the line observable only at the lowest temperatures. Indeed, he observed a single line when the temperature was reduced to 8°K and below. Bleaney[31] has shown, using Bijl's data, that the observed g-values correspond to a trigonal splitting of 410 cm^{-1}. This distortion has not been observed in optical spectra of the alum, even when it is cooled to liquid nitrogen temperatures.[85] However, a splitting of the crystal field band of $Ti(H_2O)_6^{3+}$ has been observed[86] and attributed in this case to a Jahn-Teller effect in the excited ^2E_g state.[67]

In the molecule $CuSiF_6 \cdot 6H_2O$ (Cu^{2+}), the symmetry of the local crystal field is also essentially octahedral. In this case, the ground state is ^2E_g and therefore subject to Jahn-Teller distortion. That such a distortion exists in this ion is one of the few well-documented demonstrations of this effect. In an early paper, Van Vleck[87] showed that the trigonal configuration is unstable because it does not split the doublet but that there is a whole system of distortions (e.g., tetragonal) which give the same energy. Thus, at high temperatures, the molecule would be expected to interconvert freely between these equivalent configurations. Abragam and Pryce[88] suggested that this would lead to an isotropic g-value even though the g-tensor for a static distortion would be anisotropic. This

interpretation was in accord with the experimental observation[89] that the g-value of $CuSiF_6 \cdot 6H_2O$ was isotropic (=2.24) even at 90°K in dilute single crystals. Subsequent work on this molecule[90] showed that at temperatures between 60 and 20°K, a transition takes place in the ESR spectrum. Instead of a nearly isotropic resonance line, the spectrum becomes anisotropic and is found to consist of three sets of lines, with $g_{\parallel} = 2.46$ and $g_{\perp} = 2.11$. As explained by Griffith[91] and others,[67] this is the expected behavior when the molecule is permanently distorted. In this case, there are three equivalent distortions of tetragonal symmetry and the three sets of lines correspond to molecules located in each of the three potential minima.

A similar situation might be expected to exist in VCl_4 if the inversion barrier were sufficiently high, as has been discussed by Ballhausen and Liehr.[46] However, Chien and Boss[92] detected no ESR absorption in heptane solutions of VCl_4 from 90 to 300°K. They attributed this to a very short relaxation time in this system. The spectrum of VCl_4 in dioxane at room temperature which has been reported[93] is almost certainly that of vanadyl ion. Although there have been some reported attempts to observe the spectrum at liquid helium temperatures,[94,98] no data have been published. The results of some other work on V^{+4} in crystal fields of various symmetry have been published. These include V^{+4} in TiO_2[99,100] and V^{+4} in SnO_2.[101] The spectrum of this ion in TiO_2 was observable at liquid nitrogen temperatures and below and $\underset{\sim}{g}$ was anisotropic ($g_1 = 1.955$, $g_2 = 1.913$, $g_3 = 1.912$). Zverev[100] also measured the temperature dependence of T_1 in the range 4.2-110°K and suggested that above 50°K, spin relaxation proceeded via an excited state which is 650 cm^{-1} above the ground state. This splitting was interpreted as being due to a tetragonal distortion modified by spin-orbit effects.

b. NMR and NQR

Another technique for estimating the "covalent" character of a chemical bond is closely related to the ESR method but has not been as widely applied. This technique depends on the fact that the NMR signal of a ligand nucleus in a paramagnetic molecule can be shifted by the presence of unpaired electron spin density at the nucleus. Thus it is similar in its theoretical aspects to the Knight shift in metals.[102] Shulman and Jaccarino[103] were among the first to demonstrate that experiments of this sort were useful in the determination of mixing coefficients of molecular orbitals. These shifts are usually large compared to the (diamagnetic) chemical shifts normally observed for a given nucleus in different environments; in the ^{19}F experiments on MnF_2[103] they were as large as eight percent of the predicted field for ^{19}F resonance. This large shift was explained[103,104] as being the result of the mixing of the fluorine orbitals with those manganese orbitals which possess some unpaired electron character. This mixing produces, by the mechanism of spin polarization,[13] a slight excess of α (or β) spin in the fluorine orbitals which leads to a net internal field at the ^{19}F nuclei and a shift of the resonance. This shift can then be related directly to the ESR coupling constant for the ^{19}F nuclei in MnF_2. The agreement with the ESR results of Tinkham on MnF_2 is quite good.[79] The theory of NMR in such (paramagnetic) systems is well-understood and is described in standard texts.[105] A review of the existing experimental data on these effects, particularly as they relate to contact interactions and paramagnetic relaxation, has recently appeared.[106]

That the NMR technique has been of only limited use can be understood by a consideration of nuclear relaxation times in paramagnetic systems. This was first discussed by Bloembergen, et al.[107] who showed that, in the

absence of line-narrowing mechanisms, the NMR signal would be broadened by the rapidly-fluctuating dipolar interactions with electron spins and would, in general, be unobservable. However, if electron spin relaxation were very rapid, the nucleus would see only a time-averaged field and not be affected by the electronic motion. Bloembergen also suggested that, in the case of rapid electron spin relaxation, the NMR signal would be shifted by an amount proportional to the contact interaction and that this shift would be inversely proportional to temperature.[108] These proposals formed the theoretical basis for the determination of isotropic coupling constants discussed above and have been widely applied in the determination of proton relaxation times in aqueous solutions of paramagnetic ions.[109] Although the theory was initially devised to explain intermolecular effects, McConnell and Chesnut[110] showed that these ideas were applicable to intramolecular contact interactions as well. They suggested that contact NMR shifts such as have been observed in MnF_2 could only be detected experimentally when the coupling constant, A_N, was much less than the inverse electron spin-lattice relaxation time, T_{1e}^{-1}. The converse is also true, namely that when T_{1e} is relatively long (i.e., $T_{1e}^{-1} << A_N$), the hyperfine splittings should be observable in the ESR spectrum and the corresponding NMR signal is broadened beyond recognition. Thus when an ESR spectrum is not detectable at reasonable temperatures (e.g., liquid nitrogen temperature and above), it is possible that the contact shifts can be determined for the central metal ion or the ligands by performing an NMR experiment on the nucleus in question. These criteria are in some cases subject to qualification; for example, when nuclear relaxation is dominated by the scalar interaction with electrons, the nuclear relaxation time is inversely proportional to the magnitude of the contact interaction as well as to T_{1e}^{-1}.

Pure quadrupole resonance studies have been made for a number of paramagnetic iron-group halides[111] but to the knowledge of this author, there have been no attempts to observe ^{35}Cl NQR transitions in VCl_4. The results for $TiCl_3$, VCl_3, etc., obtained by Barnes and Segel[111] were used to provide an estimate of the covalent character of the metal-halogen bond in these compounds. It is of interest to note that these spectra were observable for essentially the same reason that the ^{19}F contact shift in MnF_2 could be measured using NMR techniques; both the NQR and NMR signals are exchange-narrowed by the exchange field responsible for antiferromagnetic ordering in these substances.[111] Thus the effect of the scalar relaxation of the nuclei is in a sense nullified by the presence of a strong exchange interaction which renders the lines observable at normal temperatures in the pure solid. The ^{35}Cl quadrupole coupling constants have also been measured in $TiCl_4$ and related diamagnetic molecules.[112]

It is also possible to estimate quadrupole coupling constants by performing NMR experiments. For nuclei with $I > 1/2$, the coupling of the nuclear quadrupole moment with the fluctuating electric fields that exist in diamagnetic solutions or pure liquids is almost always the primary relaxation mechanism.[105] Thus one would expect there to be a correlation between nuclear quadrupole coupling constants and NMR linewidth. Such a relation has been shown to exist in the series of liquid chlorine compounds $TiCl_4$, $VOCl_3$, CrO_2Cl_2, and $SiCl_4$.[113] In this work, Masuda showed that the ^{35}Cl NMR linewidths of these molecules were nearly proportional to the square of the quadrupole coupling constants, as measured by Dehmelt.[114] Not only may this relationship be used to predict the eqQ values of nuclei in other molecules, but also, in cases where both the

quadrupole coupling constant and NMR linewidth are known, these data may be used to estimate correlation times for tumbling in solution. This has been demonstrated by Diehl.[115] In addition to the standard reference works on nuclear magnetic resonance,[105] a general review of quadrupole effects in NMR studies of solids has appeared.[116]

Although the previous experimental work on VCl_4 reported in this section has not provided positive evidence for Jahn-Teller distortion in this molecule, there seem to be strong theoretical arguments that such an effect should exist and that evidence of the distortion might be obtained from ESR experiments. Further, the absence of published ESR data on VCl_4 makes such an investigation interesting per se, particularly since the molecule is relatively stable and easy to handle. For these reasons, we have investigated the ESR spectrum of VCl_4 using a specially-designed liquid helium cryostat in which temperatures of the order of 1°K can be obtained. The spectra of VCl_4 in low-temperature matrices of mineral oil, CCl_4, $TiCl_4$ and $SnCl_4$ which will be described herein demonstrate that the molecule is considerably distorted in the temperature range 1.2 - 4.2°K and that this distortion is at least partially due to effects of the surrounding environment. Because the spectra are quite complex, ESR experiments have been performed at both X- and K-band microwave frequencies.

In addition, an unusual power dependence of the ESR spectrum has been discovered and shown to be consistent with a model describing the onset of dynamic Jahn-Teller motion in VCl_4. The measurement of the electron spin-lattice relaxation time T_1 in VCl_4 at 1.5°K has also been accomplished using fast microwave circuitry.

Since the ESR spectrum is broadened beyond recognition at temperatures above about 50°K, T_{1e} is very short at room temperature and above.

This property has made possible the measurement of both the sign and magnitude of the ^{35}Cl coupling constant in VCl_4 using NMR methods analogous to those described in this section. Further, an estimate of T_{1e} at room temperature can be made from the observed ^{35}Cl NMR linewidth. The data obtained from both the ESR and NMR experiments have been used in an analysis of the structure and bonding in VCl_4.

C. Sulfur-Nitrogen Radicals

The existence of the general class of compounds known as sulfur nitrides has been known for some time. As early as 1835, Gregory[117] discovered a sulfur nitride formed by the reaction of S_2Cl_2 and NH_3. This compound proved to be S_4N_4 and today, many sulfur-nitrogen compounds are known which are derived from this nitride. Their chemistry has been thoroughly investigated and reviewed in the literature.[118]

The compounds of particular interest to us, S_4N_4 and S_4N_3Cl, are crystalline solids at room temperature. Tetrasulfur tetranitride, S_4N_4, form orangeyellow crystals which are insoluble in water but soluble in many organic solvents. X-ray diffraction results on the crystal have been reported. Lu and Donohue,[119] and also Clark,[120] have suggested that their results support a cyclic eight-membered ring structure of D_{2d} symmetry, in which the nitrogen atoms are coplanar. Electron diffraction results[121] also indicate that the structure of S_4N_4 has D_{2d} symmetry but these have been interpreted in terms of a tetracyclic ring with bonds between the nitrogen atoms, in which the sulfur atoms are coplanar. This latter model is supported by infrared measurements.[122] The S_4N_3Cl molecule has also been investigated by X-ray diffraction and the $S_4N_3^+$ cation is a planar ring with six nitrogen-sulfur bonds and one sulfur-sulfur bond.[123] This result is supported by the ^{15}N NMR studies of Logan and Jolly[124] who found that two of the three nitrogens are equivalent.

The structure of S_4N_4 first proposed by Lu and Donohue[119] (and subsequently by Sharma and Donohue[125]), having four coplanar nitrogen atoms with two sulfur atoms above and below the plane, has now generally

been accepted. This conclusion was supported by the molecular orbital calculations of Turner and Mortimer.[126] From this work, the authors also concluded that appreciable bonding between sulfur atoms located on the same side of the nitrogen plane was to be expected. This bonding arises mostly by overlap of p orbitals on each of the sulfur atoms, but approximately one-third of it comes from the participation of the d_{xy} orbital on each sulfur. The existence of S-S bonds was also proposed by Braterman to explain the observed optical spectrum.[127] The optical spectra of S_4N_4 and its derivatives produced by chemical reduction have also been studied by Ray.[128]

In the work to be described here, the anion of S_4N_4 and other radicals produced by the reduction of S_4N_4 were studied using electron spin resonance. That negative ions of S_4N_4 should exist and exhibit π-electron delocalization analogous to aromatic systems was suggested by the calculations of Turner and Mortimer.[126] Chapman, et al.[129] were the first to investigate this possibility using ESR techniques. When a solution of S_4N_4 in dimethoxyethane at room temperature is treated with alkali metals, these authors first observed a claret-red solution which appeared to be diamagnetic. Then, on further shaking, the solution became green and gave rise to a weak ESR spectrum consisting of nine lines. From this work, Chapman and Massey[129b] concluded that this spectrum was due to the $S_4N_4^-$ radical anion in which the unpaired electron is delocalized over the entire ring, and ruled out the possibility of ring cleavage.

Using both chemical and electrolytic methods of reduction, we have reinvestigated the S_4N_4 system as well as the radicals derived from S_4N_3Cl. Our results show that the nine-line radical observed by Chapman

and Massey is almost certainly a result of the polymerization of smaller fragments formed from a cleaved S_4N_4 ring and is probably not $S_4N_4^-$. In addition, a new nine-line radical has been discovered by reduction at low temperatures and subsequently identified by others in this laboratory as $S_4N_4^-$. The ESR results for these systems are described in Section D of Chapter IV.

II. REFERENCES

1. G. Natta, R. Ercoli, F. Calderazzo, A. Alberola, P. Corradini and G. Allegra, Rend. Accad. Naz. Lincei 27, 107 (1959); CA 54, 16252 (1960). See also R. Ercoli, F. Calderazzo and A. Alberola, J. Am. Chem. Soc. 82, 2966 (1960) for a summary of this work.
2. F. Calderazzo, R. Cini, P. Corradini, R. Ercoli and G. Natta, Chem. and Ind. 1960, 500.
3. M. Windsor and A. Blanchard, J. Am. Chem. Soc. 56, 823 (1934).
4. W. Rudorf and U. Hofmann, Z. physik. Chem. B28, 351 (1935); L. O. Brockway, R. V. G. Evens and M. W. Lister, Trans. Faraday Soc. 34, 1350 (1938).
5. R. L. Pruett and J. E. Wyman, Chem. and Ind. 1960, 119.
6. (a) F. Calderazzo, R. Cini and R. Ercoli, Chem. and Ind. 1960, 934; (b) F. Calderazzo, private communication, 1966.
7. G. Bonera and A. Rigamonti, Rend. Sez. Ric. Sci. A3, 213 (1963). (CA 59, 13506 (1963)).
8. J. W. Cable and R. K. Sheline, Chem. Revs. 56, 1 (1956).
9. F. A. Cotton and G. Wilkinson, Advanced Inorganic Chemistry, 2nd edition (Interscience, John Wiley and Sons, Inc., New York, 1966), Chapter 27.
10. L. E. Orgel, Introduction to Transition Metal Chemistry (Methuen and Co., Ltd., London, 1960), Chapter 9.
11. Reference 9, Fig. 26-27, p. 705.
12. Reference 9, Fig. 26-30, p. 708.
13. H. M. McConnell, J. Chem. Phys. 24, 632, 764 (1956).
14. As mentioned earlier, Pruett and Wyman (Ref. 5), obtained negative results in their ESR experiments on $V(CO)_6$, which were presumably done at room temperature.

15. In addition, there is an oblique reference to a successful ESR experiment on $V(CO)_6$ in the literature; see H. Haas and R. K. Sheline, J. Am. Chem. Soc. 88, 3219 (1966). Their information was obtained from R. S. Nyholm, private communication, but no details were given.[16]

16. J. P. Hargaden, private communication, 1966.

17. See Ref. 9, Chapter 26.

18. C. J. Ballhausen, Introduction to Ligand Field Theory (McGraw-Hill Book Co., Inc., New York, 1962).

19. T. M. Dunn, D. S. McClure and R. G. Pearson, Some Aspects of Crystal Field Theory (Harper and Row Publishers, Inc., New York, 1965).

20. H. Haas and R. K. Sheline, J. Am. Chem. Soc. 88, 3219 (1966).

21. See Ref. 5; see also the comment following Ref. 2.

22. G. V. Nelson, unpublished results at the University of California at Berkeley, 1966.

23. J. H. Van Vleck, J. Chem. Phys. 3, 807 (1935).

24. J. B. Howard, J. Chem. Phys. 3, 813 (1935).

25. J. H. E. Griffiths, J. Owen and I. M. Ward, Proc. Roy. Soc. (London) A219, 526 (1953).

26. J. Owen and K. W. H. Stevens, Nature 171, 836 (1953).

27. K. W. H. Stevens, Proc. Roy. Soc. (London) A219, 542 (1953).

28. (a) J. M. Baker, B. Bleaney and K. D. Bowers, Proc. Phys. Soc. (London) B69, 1205 (1956); (b) B. Bleaney and M. C. M. O'Brien, ibid., B69, 1216 (1956).

29. J. J. Fortman and R. G. Hayes, J. Chem. Phys. 43, 15 (1965).

30. A. Abragam and M. H. L. Pryce, Proc. Roy. Soc. (London) A205, 135 (1951).

31. B. Bleaney, Proc. Phys. Soc. (London) A63, 407 (1950).

32. H. E. Roscoe, Ann. Chem. Liebigs 7, 70 (1869).

33. J. H. Simons and M. G. Powell, J. Am. Chem. Soc. 67, 75 (1945).

34. C. N. Caughlan and F. Cartan, J. Am. Chem. Soc. 81, 3840 (1959).

35. A. Voigt and W. Biltz, Z. anorg. allgem. Chem. 133, 277 (1924).

36. A. G. Loomis and H. Schlundt, J. Phys. Chem. 19, 734 (1915).

37. S. A. Shchukarev, M. A. Oransyaya, T. A. Tolmacheva and A. K. Yakhkind, Zhur. Neorg. Khim. 1, 30 (1956).

38. A. G. Whittaker and D. M. Yost, J. Chem. Phys. 17, 188 (1949).

39. R. J. H. Clark and D. J. Machen, J. Chem. Soc. 1963, 4430.

40. W. Klemm and E. Hoschek, Z. anorg. Allgem. Chem. 226, 359 (1936).

41. I. S. Morozov and D. Ya. Toptygin, Zhur. Neorg. Khim. 1, 2601 (1956); [Eng. tr. J. Inorg. Chem. (USSR) 1 (11), 174 (1956).]

42. E. L. Grubb, F. A. Blankenship and R. L. Belford, J. Phys. Chem. 67, 1562 (1963).

43. M. F. A. Dove, J. A. Creighton and L. A. Woodward, Spectrochim. Acta 18, 267 (1962).

44. W. N. Lipscomb and A. G. Whittaker, J. Am. Chem. Soc. 67, 2019 (1945).

45. M. W. Lister and L. E. Sutton, Trans. Fara. Soc. 37, 393 (1941).

46. C. J. Ballhausen and A. D. Liehr, Acta. Chem. Scand. 15, 775 (1961).

47. See G. Nagarajan and E. R. Lippincott, J. Chem. Phys. 42, 1809 (1965) and references contained therein.

48. K. J. Palmer, J. Am. Chem. Soc. 60, 2360 (1938).

49. L. O. Brockway and H. O. Jenkins, J. Am. Chem. Soc. 58, 2036 (1936); L. O. Brockway, Rev. Mod. Phys. 8, 231 (1936).

50. See, for example, (a) M. Wolfsberg and L. Helmholz, J. Chem. Phys. 20, 837 (1952); (b) L. L. Lohr and W. N. Lipscomb, Inorg. Chem. 2, 911 (1963) and references contained therein.

51. See Ref. 18, Chapter 7.

52. (a) C. J. Ballhausen and A. D. Liehr, J. Mol. Spectry. 2, 342, (1958); (b) A. Carrington and D. S. Schonland, Mol. Phys. 3, 331 (1960).

53. C. Dijkgraaf, Spectrochim. Acta 21, 769 (1965).

54. L. E. Orgel, J. Chem. Phys. 23, 1004 (1955).

55. F. A. Blankenship and R. L. Belford, J. Chem. Phys. 36, 633 (1962); ibid. 37, 675 (1962).

56. G. L. Carlson, USAEC, TID-12120 (1961).

57. F. Pennella and W. J. Taylor, J. Mol. Spectry. 11, 321 (1963).

58. D. S. Alderdice, J. Mol. Spectry. 15, 509 (1965).

59. E. L. Grubb and R. L. Belford, unpublished results presented at the Symposium on Molecular Structure and Spectroscopy, Columbus, Ohio, 1963. These authors have also observed the transitions at 24,800 and 33,900 cm^{-1} but, as their results were not available to us, they are not included in Table II. See footnote (1) in Ref. 57.

60. W. Moffitt and W. Thorson, Phys. Rev. 108, 1251 (1957).

61. M. H. L. Pryce and W. A. Runciman, Disc. Fara. Soc. 26, 34 (1958).

62. E. L. Grubb and R. L. Belford, J. Chem. Phys. 39, 244 (1963).

63. J. A. Creighton, J. H. S. Green and W. Kynaston, J. Chem. Soc. (A) 1966, 208.

64. G. Herzberg, Infrared and Raman Spectra of Polyatomic Molecules (D. Van Nostrand Co., Inc., Princeton, N. J., 1945), p. 167.

65. B. Weinstock and H. H. Claasen, J. Chem. Phys. 31, 262 (1959). See also B. Weinstock and G. L. Goodman in Advances in Chemical Physics, Vol. IX (Interscience, John Wiley and Sons, Inc., New York, 1965), Ed. I. Prigogine, p. 169.

66. See, for example, M. S. Child and H. C. Longuet-Higgins, Phil. Trans. Roy. Soc. 254, 259 (1961).

67. A. D. Liehr and C. J. Ballhausen, Ann. Phys. (N. Y.) 3, 304 (1958).

68. C. J. Ballhausen and J. de Heer, J. Chem. Phys. 43, 4304 (1965); see also abstracts of papers presented at the 8th European Congress on Molecular Spectroscopy, Copenhagen, 1965, p. 372.

69. I. B. Bersuker, Teor. i Eksperim. Khim., Akad. Nauk Ukr. SSR 1, 5 (1965); CA 63, 6325g (1965). See also Sov. Phys. (JETP) 17, 1060 (1963); Sov. Phys. (Solid State) 5, 1772 (1964).

70. L. Pauling, The Nature of the Chemical Bond (Cornell University Press, Ithaca, N. Y., 1939).

71. C. H. Townes and B. P. Dailey, J. Chem. Phys. 17, 782 (1949).

72. R. Bersohn and R. G. Shulman, J. Chem. Phys. 45, 2298 (1966).

73. J. Owen, Proc. Roy. Soc. (London) A227, 183 (1955).

74. A. Abragam, Phys. Rev. 79, 534 (1950).

75. A. Abragam and M. H. L. Pryce, Proc. Roy. Soc. (London) A206, 164, 173 (1951).

76. B. Bleaney, Phil. Mag. 42, 441 (1951).

77. A. Abragam, J. Horowitz and M. H. L. Pryce, Proc. Roy. Soc. (London) A230, 169 (1955).

78. B. R. McGarvey, J. Phys. Chem. 71, 51 (1967).

79. M. Tinkham, Proc. Roy. Soc. (London) A236, 549 (1956); A. M. Clogston, J. P. Gordon, V. Jaccarino, M. Peter and L. R. Walker, Phys. Rev. 117, 1222 (1960).

80. L. Helmholz, J. Chem. Phys. 31, 172 (1959); R. G. Shulman and S. Sugano, Phys. Rev. 130, 506 (1963).

81. E. König, Magnetic Properties of Coordination and Organo-Metallic Transition Metal Compounds, Vol. 2 of Landolt-Börnstein (New Series) (Springer-Verlag, New York, 1966), Ed. K.-H. Hellwege and A. M. Hellwege.

82. R. N. Rogers and G. E. Pake, J. Chem. Phys. 33, 1107 (1960).

83. D. M. S. Bagguley, B. Bleaney, J. H. E. Griffiths, R. P. Penrose, and B. I. Plumpton, Proc. Phys. Soc. (London) A61, 542 (1948).

84. D. Bijl, Proc. Phys. Soc. (London) A63, 405 (1950).

85. H. Hartmann and H. L. Schläfer, Angew. Chem. 66, 768 (1954).

86. H. Hartman, H. L. Schläfer, and K. H. Hansen, Z. anorg. u. allgem. Chem. 284, 153 (1956).

87. J. H. Van Vleck, J. Chem. Phys. 7, 72 (1939).

88. A. Abragam and M. H. L. Pryce, Proc. Phys. Soc. (London) A63, 409 (1950).

89. B. Bleaney and D. J. E. Ingram, Proc. Phys. Soc. (London) A63, 408 (1950).

90. B. Bleaney and K. D. Bowers, Proc. Phys. Soc. (London) A65, 667 (1952).

91. J. S. Griffith, The Theory of Transition-Metal Ions (Cambridge University Press, London, 1961), p. 343-5.

92. J. C. W. Chien and C. R. Boss, J. Am. Chem. Soc. 83, 3767 (1961).

93. R. H. Sands, ASTM Symposium on Spectroscopy, San Francisco, 1959 (Am. Soc. Test. Matl. Special Technical Publication No. 269), p. 165.

94. There are two references[95,96] in the literature to some unpublished work of R. B. Johannesen at NBS, Washington, D.C. In this work, the author observed a signal in pure VCl_4 at 4°K. (but not at 77°K.). A spectrum was also obtained for dilute solutions of VCl_4 in $TiCl_4$ at 4°K. in which some distortion was present. He also suggests that the signal in $TiCl_4$ solutions seems to become more isotropic at higher temperatures.[97]

95. See Ref. 50b, footnote 37.

96. I. Siegel, Phys. Rev. 134, A193 (1964), footnote 30.

97. H. C. Allen, private communication, 1965.

98. A report of the meeting of the Northwest Section of the American Chemical Society at the University of British Columbia on June 16, 1966 lists the following paper: "Electron Spin Resonance Spectrum of VCl_4 Trapped in Inert Matrices at 4.2°K.", F. G. Herring, H. Nakajima and C. A. McDowell. No details were given.

99. H. J. Gerritsen and H. R. Lewis, Phys. Rev. 119, 1010 (1960); see also P. H. Kasai, Phys. Ltrs. 7, 5 (1963).

100. G. M. Zverev, Sov. Phys. (JETP) 17, 1251 (1963).

101. C. Kikuchi, I. Chen, W. H. From and P. B. Dorain, J. Chem. Phys. 42, 181 (1965).

102. C. P. Slichter, Principles of Magnetic Resonance (Harper and Row, Publishers, New York, 1963), Chapter 4.

103. R. G. Shulman and V. Jaccarino, Phys. Rev. 108, 1219 (1957).

104. F. Keffer, T. Oguchi, W. O'Sullivan and J. Yamashita, Phys. Rev. 115, 1553 (1959).

105. E. R. Andrew, Nuclear Magnetic Resonance (Cambridge University Press, London, 1958); A. Abragam, The Principles of Nuclear Magnetism (Oxford University Press, London, 1961), Chapter 6.

106. D. R. Eaton and W. D. Phillips, Advances in Magnetic Resonance, Vol. 1, Ed. J. S. Waugh (Academic Press, Inc., New York, 1965), p. 103.

107. N. Bloembergen, Physica 16, 95 (1950); N. Bloembergen and J. Poulis, Physica 16, 915 (1951).

108. N. Bloembergen, J. Chem. Phys. 27, 572, 595 (1957).

109. N. Bloembergen and L. O. Morgan, J. Chem. Phys. 34, 842 (1961); R. S. Marianelli, (Ph. D. Thesis) University of California, Berkeley, California, UCRL-17069, 1966.

110. H. M. McConnell and D. B. Chesnut, J. Chem. Phys. 28, 107 (1958).

111. R. G. Barnes and S. L. Segel, Phys. Rev. Ltrs. 3, 462 (1959); J. Chem. Phys. 37, 1895 (1962).

112. A. H. Reddoch, J. Chem. Phys. 35, 1085 (1961).

113. Y. Masuda, J. Phys. Soc. Japan 11, 670 (1956).

114. H. G. Dehmelt, J. Chem. Phys. 21, 380 (1954).

115. P. Diehl, Helv. Phys. Acta 29, 219 (1956).

116. M. H. Cohen and F. Reif, Solid State Physics, Vol. 5 (Academic Press, Inc., New York, 1957), Ed. F. Seitz and D. Turnbull, p. 322.

117. M. Gregory, J. Pharm. 21, 315; 22, 301 (1835).

118. M. Goehring, Quart. Rev. 10, 437 (1956). See also W. L. Jolly, Synthetic Inorganic Chemistry (Prentice-Hall, Inc., Englewood Cliffs, N. J., 1960).

119. C. S. Lu and J. Donohue, J. Am. Chem. Soc. 66, 818 (1944).

120. D. Clark, J. Chem. Soc. (London) 1952, 1615.

121. O. Hassel and H. M. Viervoll, Tidsskr. Kjemi Bergvesen Met. 3, 7 (1943).

122. E. R. Lippincott and M. C. Tobin, J. Chem. Phys. 21, 1559 (1953).

123. A. W. Cordes, R. F. Kruh and E. K. Gordon, Inorg. Chem. 4, 681 (1965).

124. N. Logan and W. L. Jolly, Inorg. Chem. 4, 1508 (1965).

125. B. D. Sharma and J. Donohue, Acta Cryst. 16, 891 (1963).

126. A. G. Turner and F. S. Mortimer, Inorg. Chem. 5, 906 (1966).

127. P. S. Braterman, J. Chem. Soc. (London) 1965, 2297.

128. S. K. Ray, unpublished results at the University of California at Berkeley, 1964.

129. a) D. Chapman, R. M. Golding, A. G. Massey and J. T. Moelwyn-Hughes, Proc. Chem. Soc. (London) 1961, 377; b) D. Chapman and A. G. Massey, Trans. Far. Soc. 58, 1291 (1962). See also D. Chapman and A. G. Massey, Chem. and Ind. 1962, 2088.

III. EXPERIMENTAL TECHNIQUES

A. ESR Experiments in the Temperature Range 90-500°K

1. The Spectrometer

The ESR spectra of the S_4N_4, S_4N_3Cl and Gd^{+3} systems reported herein were obtained with a Varian V-4502 ESR spectrometer operating at X-band (~ 9 GHz). This instrument was used in conjunction with a 100 KHz field modulation and control unit (V-4560) and standard rectangular cavity (V-4531). The Varian V-4500-41A microwave bridge was operated in the high power configuration and all measurements were made at power levels such that there was no detectable power saturation of the signal. The modulation amplitude was always adjusted to a level where broadening was not noticeable.

A nine-inch Varian magnet equipped with a Fieldial unit (V-FR2503) was used for all ESR experiments. The magnet was mounted on a base with wheels which allowed the unit to be moved on a track from the "room-temperature" position to the liquid helium dewar location for low temperature experiments. For absolute field measurements, an external NMR oscillator (Harvey-Wells FC-502) was used and the proton probe was placed as close to the cavity as possible. The frequency for NMR resonance was displayed on an electronic counter (HP 5245L) and converted to a field value using the relationship 10^4 G = 42.577 MHz. Where reported, line-widths are peak-to-peak values for the first derivative lineshape. These correspond to the full width between points of maximum and minimum slope of the corresponding absorption spectra. For g-value measurements, the microwave frequency was measured using a Hewlett-Packard frequency converter (2590A) and the counter. The values of β and h were taken to be 9.2732×10^{-21} erg/gauss and 6.6256×10^{-27} erg sec,[1] respectively.

2. Sample Preparation

a. S_4N_4 and S_4N_3Cl Solutions

The S_4N_4 and S_4N_3Cl used in this work were synthesized by Dr. S. K. Ray employing methods described in the literature.[2] These solids were recrystallized several times from tetrahydrofuran (THF) or other suitable solvents to ensure their purity. Dr. Ray also prepared the solutions of these compounds in THF which were subsequently treated with a reducing agent to produce the desired radicals. These solutions were prepared on a vacuum line. The THF was first dried by refluxing with $LiAlH_4$ and then distilled into an evacuated burette. The S_4N_4 and S_4N_3Cl solutions were then prepared by adding an appropriate amount of the THF to a previously weighed quantity of the solute.

Several techniques were used for the preparation of radicals from these solutions. Two of them employed methods of chemical reduction. In one, a solution of sodium naphthalide was prepared by the reaction of sodium metal with naphthalene in THF. After refluxing for about three hours, the green $(naphthalide)^-$ solution was transferred to a burette and then added as necessary to the sulfur nitride solution. In this way the amount of reducing agent added could be controlled carefully. In other experiments, sodium-potassium alloy was substituted for the naphthalide as a reducing agent. The color changes and radicals observed in this case were the same but the speed of the reaction was much more rapid. The ESR samples in both cases were obtained from the reaction flask using a hypodermic syringe which was inserted into the flask through a serum cap. The solution was then transferred to a quartz sample tube in a dry box which was continuously flushed with argon and the tube was sealed with silicone grease.

In subsequent experiments performed by the author, electrolytic methods of reduction were employed. Such techniques have been developed extensively in this laboratory by D. H. Levy and others and the electrolysis cell used for this work has been described.[3] The solvent used most frequently in these experiments was THF and it was dried by refluxing with sodium chips under a nitrogen atmosphere and then distilled to a second flask containing CaH_2. After several freeze-thaw-pump cycles on the vacuum line, the dry THF was transferred by vacuum distillation to the electrolysis cell. The cell had been cleaned and dried thoroughly and contained both the supporting electrolyte, t-butylammonium perchlorate, and a small amount of S_4N_4. All chemicals used were of reagent grade or higher purity and silicone grease was used on all ground glass joints. The electrolysis was performed, at both room temperature and below, by connecting leads from a voltage source to the anode and cathode of the cell. Typically, currents of the order of 10 μa were obtained with an applied voltage of 10-20 volts. The electrolysis products were continuously monitored over a period of up to three weeks. The results of these experiments are described in Chapter IV, Section D.

b. Gd^{+3} Solutions

Aqueous solutions of $Gd(ClO_4)_3$ were prepared in the following manner. A weighed amount of $GdCl_3 \cdot 6H_2O$ was dissolved in distilled water and added to a solution of Na_2CO_3. The $Gd_2(CO_3)_3$ precipitate was filtered and washed with water. Then a dilute solution of $HClO_4$ was added to the solid carbonate to the point where it dissolved and the solution was heated to drive off the excess water. The resulting $Gd(ClO_4)_3$ was then carefully dried in an oven and used for the preparation of 0.01M aqueous solutions.

The sample tubes used for this work were melting point capillaries which were prepared and sealed following the methods of McCain.[4] Since these were to be heated to approximately 250°C in the ESR experiments, they were first tested by preheating in an oven. The linewidth of the Gd^{+3} ESR signal was then measured as a function of temperature and the results of these experiments are described in Appendix I.

3. Temperature Control and Measurement

Temperatures below room temperature were obtained by passing cold nitrogen gas through an unsilvered quartz dewar which was located in the cavity. The cold gas supply was provided by boiling liquid nitrogen in a storage dewar, the rate of boiling being controlled by the power dissipated in a resistor suspended in the liquid nitrogen. The flow rate could be regulated by adjusting the current through the resistor and, at the highest flow rates, the temperature of the sample in the cavity was approximately 90°K.

For experiments at higher temperatures, dry air flowed through a heater which was attached to the bottom of the quartz cavity dewar. The temperature was regulated by adjusting the flow rate and/or the heater current and was measured using a copper-constantan thermocouple which was glued to the sample tube just at the edge of the cavity. The thermocouple junction was well within the quartz dewar and downstream in the air flow. The reference junction was kept at 0°C and thermocouple voltages were measured with a L&N K-3 potentiometer. The uncertainty in the temperature readings made in this way was estimated to be ±2°C.

B. ESR Experiments at Liquid Helium Temperatures

1. The X-band Spectrometer

The Varian V-4502 ESR spectrometer, with some modifications, was used to obtain the spectra at X-band of $V(CO)_6$ and VCl_4 at liquid helium temperatures. The first modification was necessitated by the fact that the distance from the "room temperature" position to the liquid helium station was about ten feet. Because this gave a long run of waveguide on the cell arm of the bridge, a separate X-band bridge was constructed on a shelf which was built around the helium dewar system. This bridge was of conventional design and is shown in Fig. 7. A waveguide switch (Waveline 678H) was installed below the Varian bridge and attached to a long section of waveguide which led to the helium shelf. This enabled one to convert the room temperature spectrometer to operation at liquid helium temperatures with a minimum of effort. In most experiments, the microwave power level was controlled with attenuator No.2 (0.20 DB) and attenuator No.1 on the Varian bridge was set at 0 DB. However, in order to prevent power saturation of some of the narrower lines, the power was reduced further using attenuator No.1 when necessary. That power saturation was not a factor in these experiments was confirmed by experiments on another instrument employing superheterodyne detection.

For the liquid helium experiments, a modulation frequency of 400 Hz was generally used and this was provided by the V-4250B sweep unit on the spectrometer console. The output of the sweep unit was amplified with a Bogen CHB-10 audio amplifier and applied to modulation coils located on the outside of the cavity. The connection to the coils was made through a ceramic to metal fitting in the top flange of the copper tee of the vacuum system (vide infra). The signal at the detector was phase detected at 400 Hz with the low-frequency phase detector on the console and amplified using the V-4270B output control unit before displaying on the

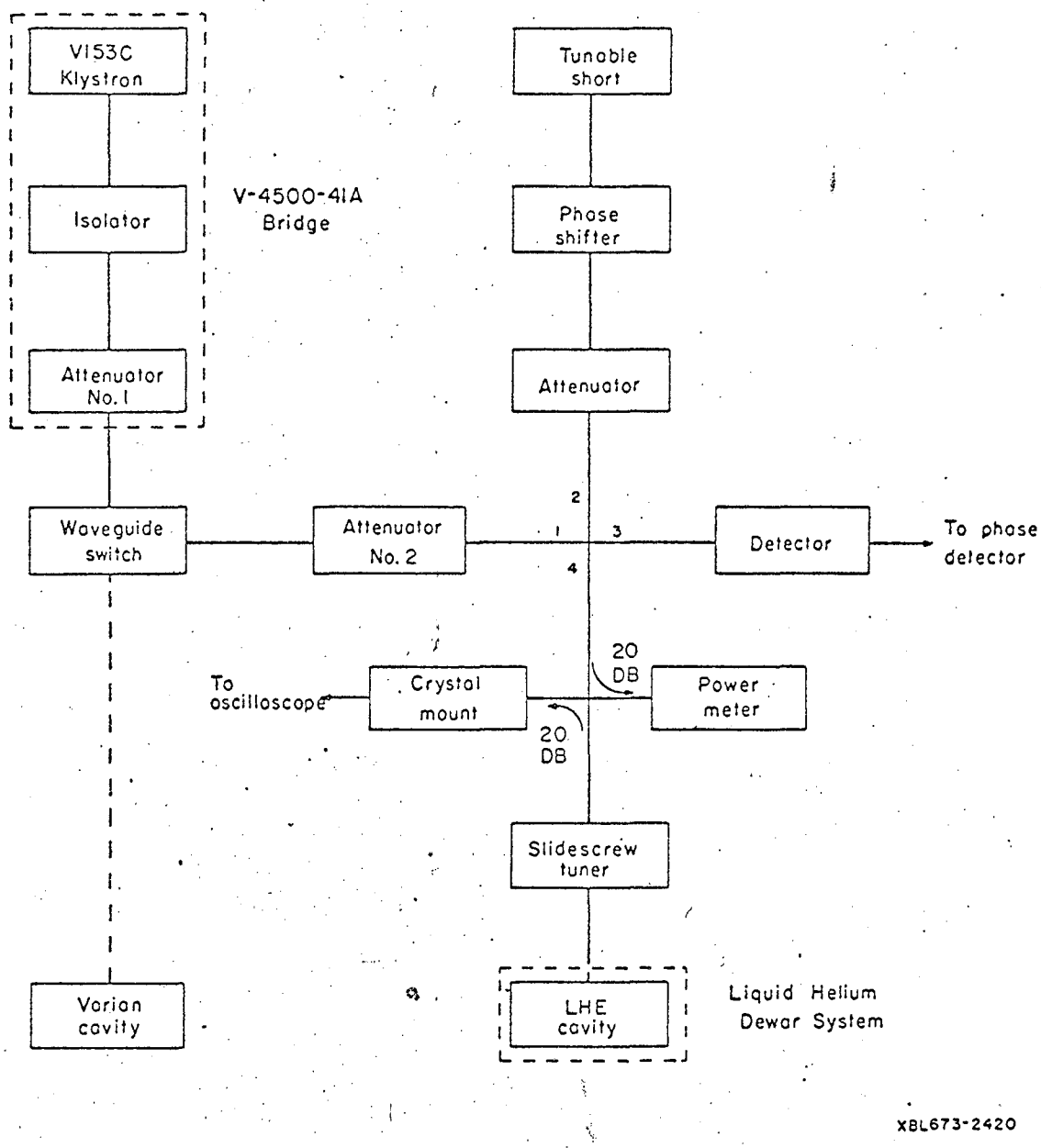

Fig. 7. Block diagram of the microwave bridge used for the X-band ESR experiments at liquid helium temperatures.

recorder. The recorder used in these experiments was an EAI X-Y 1110 Variplotter equipped with a time-base.

The cavity arm of the bridge contained a 20 DB crossguide directional coupler and a slidescrew tuner. The two arms of the crossguide coupler were used for monitoring the resonant frequency of the cavity and the power incident on the cavity. The waveguide then passed through the top flange to which it was hard-soldered. At this point, a section of stainless steel waveguide (0.010" wall) was inserted to reduce the thermal contact between the helium and room temperature. This extended approximately two feet into the dewar where it was connected to a short section of coin silver waveguide (0.050" wall) and thence to the cavity with small brass flanges.

The rectangular microwave cavity used for most experiments was fabricated from standard brass X-band waveguide and is shown in Figure 8. This cavity, when operating in the TE012 mode, has an unloaded resonant frequency of 10.075 GHz and a Q ($f/\Delta f$) of about 2000 at room temperature. When filled with styrofoam, which was used to hold the sample in place, the value of ν_o drops to 9.923 GHz and at liquid helium temperature, the resonant frequency is in the range 9.4-9.7 GHz. As can be seen from Figure 8, the walls of the cavity were milled down to 0.010-0.020" in the sample region to maximize the modulation amplitude at the sample. With an applied 400 Hz voltage of about 10 v, the modulation amplitude was approximately 2 gauss but for most experiments, only 1 or 2 volts was applied to the coils. The inner walls of the cavity were plated with either copper or silver to a thickness of 0.001". The modulation coils were wound from #36 copper wire and each coil consisted of 200-300 turns. They were fastened to the cavity using mylar tape. The coupling windows were fashioned from 10 mil silver sheet and for most samples an aperture of 3/16

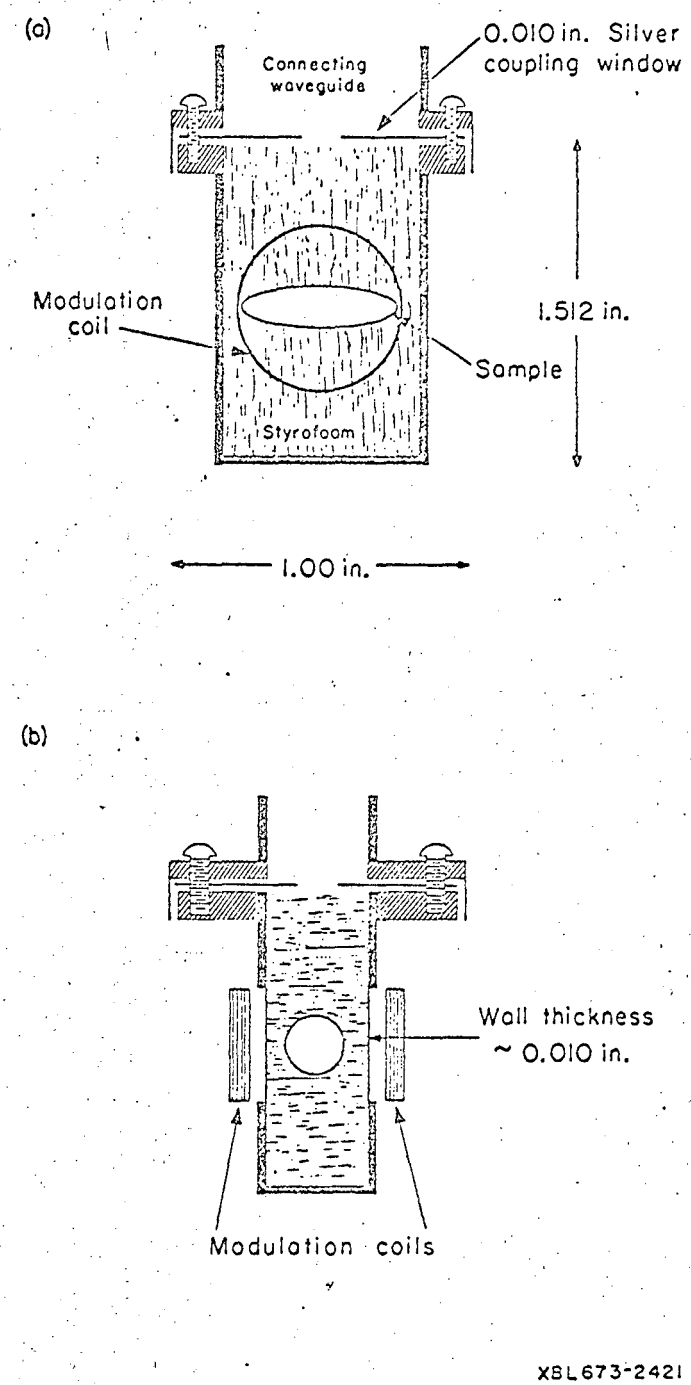

Fig. 8. Rectangular X-band TE012 cavity. a) Broad wall view, b) Narrow wall view.

or 7/32" was sufficient to make the cavity slightly overcoupled. Maximum S/N ratio was obtained when the cavity was coupled in this way. In cases where the cavity was critically coupled, the slidescrew tuner was used to introduce leakage for crystal bias.

2. The K-Band Spectrometer

A K-band (~ 24 GHz) ESR spectrometer was assembled for experiments on VCl_4 at liquid helium temperatures. A schematic drawing of the microwave bridge and associated electronics is shown in Figure 9. The frequency source for these experiments was an OKI 24V10 klystron operating in the range 22-26 GHz with a maximum power output of 250 mw in the center of this range. In order to phase-lock the K-band klystron on the cavity frequency, a 30 MHz difference signal was generated in the Narda 518F mixer by mixing 3 DB of the K-band power with the third or fourth harmonic of a stabilized C-band (4-8 GHz) klystron. A coaxial impedance matching device (FXR-N300A) was employed for maximizing the C-band power input to the mixer. The 30 MHz signal was then amplified and phase detected, and the rectified error voltage was applied to the OKI klystron reflector to adjust the K-band frequency. The C-band source (Polarad 1207) was also phase locked using a Dymec oscillator-synchronizer and harmonics of a 100 MHz fundamental obtained from a Hewlett-Packard 540B transfer oscillator.

In a typical experiment, the cavity frequency was located by sweeping the klystron reflector over a narrow range with a modulation unit in the FXR power supply and monitoring the power reflected from the cavity on an oscilloscope. If necessary, the klystron was tuned manually using the tuning knob on the klystron mount. When the cavity dip appeared on the scope, the reflector and beam voltages were adjusted to maximize the

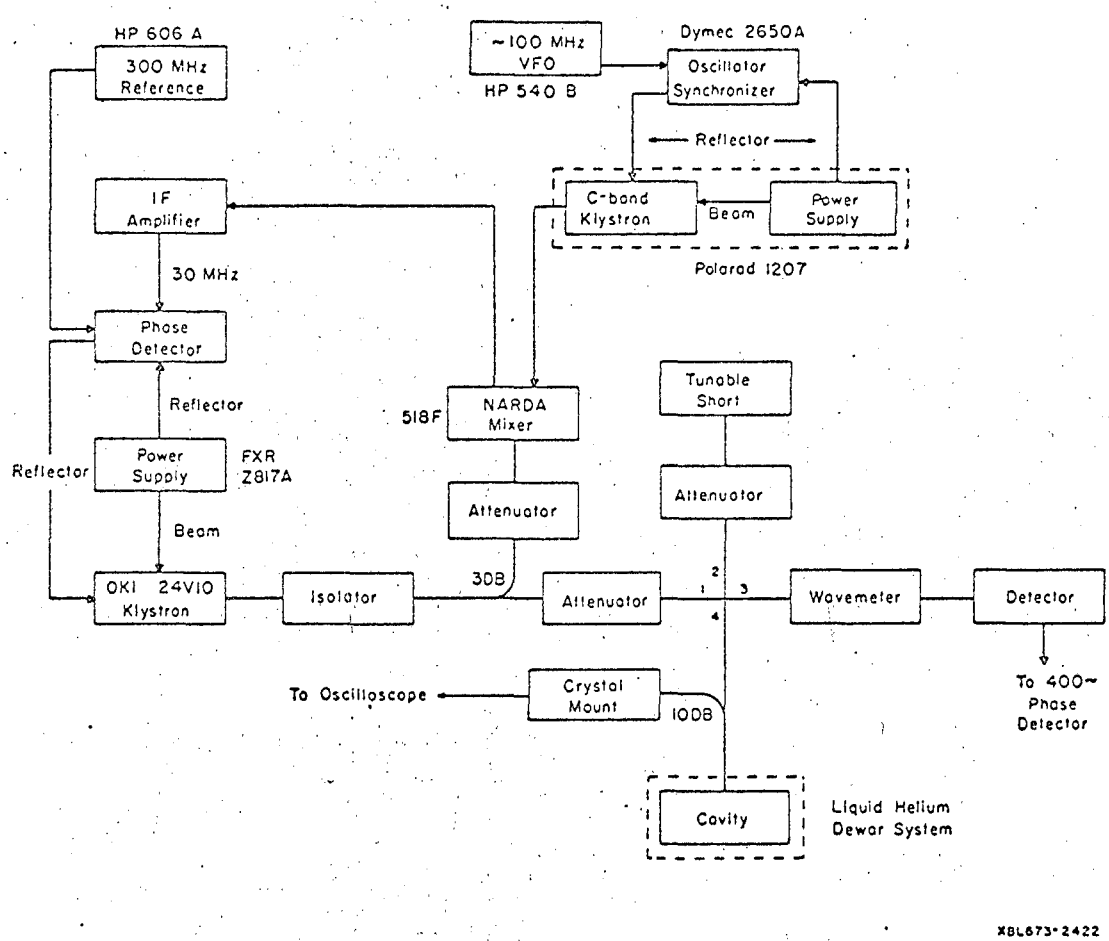

Fig. 9. Block diagram of the K-band bridge and spectrometer used for ESR experiments at liquid helium temperatures.

output and the approximate frequency was determined with the wavemeter. The modulation was then turned off and the C-band klystron tuned until the IF level meter on the phase detector showed a deflection. Then the C-band klystron was locked with the Dymec unit. By monitoring the DC level of the reflected power on the oscilloscope, the K-band frequency could be set to the exact cavity frequency by tuning the HP 540B oscillator carefully until the DC level was at a minimum. This same adjustment could be used for improving the quality of the lock on the phase detector. The operating frequency at ~ 24 GHz was measured accurately by determining the C-band frequency with the frequency converter and counter and using the relation

$$\nu_K = (n\nu_C \pm 30 \text{ MHz})$$

where n = 3 or 4.

Phase detection and amplification of the ESR signal at the detector was accomplished by using the 400 Hz unit on the Varian V-4502 spectrometer. The modulation coils were again placed on the outside of the cavity and the circuit was the same as that used for the X-band experiments. Waveguide connections to the cavity were made through a flange similar to that described earlier and a section of stainless waveguide was used to reduce thermal contact. The rectangular K-band cavity, operating in the TE012 mode, was fabricated from brass waveguide and silver plated. It had a resonant frequency of 24.345 GHz with a Q of about 1000 at room temperature. The cavity was also milled down in the sample region and was 1.176" deep. When loaded with styrofoam and sample at liquid helium temperature, the value of ν_o was in the range 23.3-23.5 GHz. The cavity could be slightly overcoupled using a coupling window

with a hole diameter of about 0.120".

3. Liquid Helium Cryostat and Vacuum System

Figure 10 shows a diagram of the liquid helium cryostat used for the ESR experiments on VCl_4 and $V(CO)_6$. Both the liquid helium and liquid nitrogen dewars were fabricated from large pyrex tubing; the diameters of the large, upper sections of the two dewars were approximately 3 and 5", respectively. The narrow tail sections were designed so that the dewar assembly could be accommodated in the 2.63" pole gap of the Varian magnet. The outer diameter of the nitrogen dewar tail was 60 mm (2.36") and the inner diameter of the helium dewar tail was 36 mm (1.42"). The total capacity of the helium dewar was approximately 2.5 liters. Both dewars were silvered except for narrow stripes running the full length of the cryostat so that the helium level could be monitored during an experiment.

The two dewars were suspended from a 3" (nominal) copper tee as shown in Figure 10. This tee was fitted with 6" brass flanges equipped with Viton O-rings. The helium dewar terminated at the upper end in heavy wall water pipe with a fluted upper end so that it could be held against the lower flange of the tee with an aluminum collar. The top edge of the pipe was grooved so that an O-ring could be placed between it and the flange. Silicone grease was used sparingly on all O-rings. The nitrogen dewar was open to the atmosphere at the top to facilitate filling and was suspended from the tee with braided stainless cable attached with eye bolts to the lower flange of the tee and an aluminum saddle at the neck of the dewar just above the pole pieces.

The diagram also illustrates the positioning of the waveguide and cavity in the dewar. The waveguide was soldered at the upper end to a thin brass plate which was bolted to the upper flange of the copper tee.

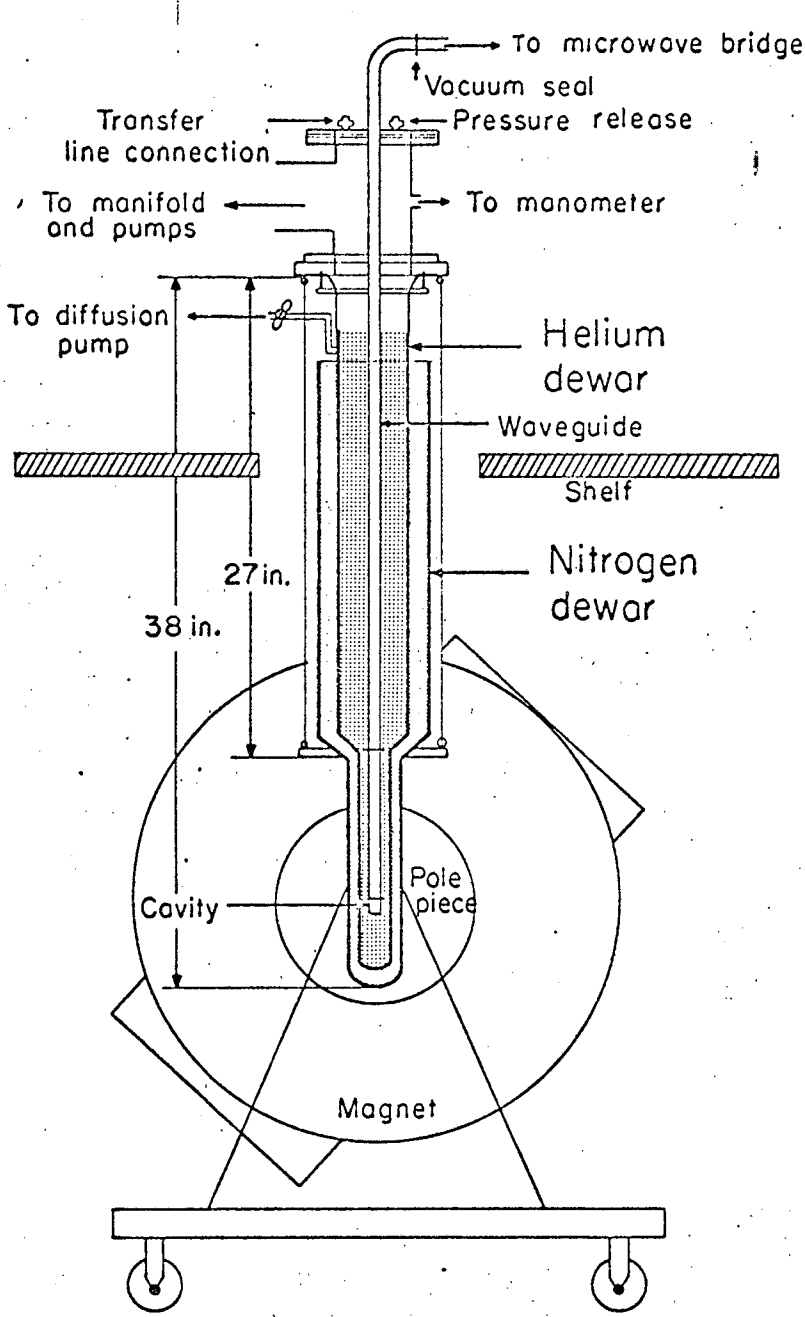

XBL673-2423

Fig. 10. The liquid helium cryostat.

The brass plate was provided with a transfer line connection, a pressure-release valve, and the ceramic-to-metal seal (not shown) with electrical connections for the modulation coils and thermocouple. In order to prevent condensation of air and/or water in the waveguide, a vacuum seal using a mylar window and Apiezon T was installed between two waveguide flanges just outside the cryostat. No vacuum seals were used for the flanges in the cryostat so it was assumed that helium filled the cavity and waveguide up to the liquid level.

The jacket of the helium dewar was evacuated as necessary using a small vacuum line equipped with an oil diffusion pump (NRC H-2-SP), liquid nitrogen trap and mechanical fore pump. Whenever it was necessary to clean the dewars, the jacket and dewar were pumped on continuously during warmup to prevent the buildup of pressure.

The copper tee was connected to a manifold fabricated from 3" copper tubing. This is illustrated in Figure 11. The main valve was a Neptune ball valve with a 2-1/2" port and it was coated inside and out with Columbine high-vacuum leak sealant. The manifold and dewar were evacuated with two Welch 1397B mechanical pumps operated in parallel. In addition to the thermocouple gauge and rough pressure gauge on the low pressure side of the manifold, provision was made for reading the pressure above the liquid helium level via a connection at the tee to a Kinney mercury manometer (Type TDI). This line also contained a rough pressure gauge and a hose barb and needle valve for admitting gaseous helium into the dewar.

In a typical experiment, the top of the tee was closed with a blank flange and the liquid nitrogen dewar was filled. Gaseous helium was admitted into the helium dewar with the large ball valve closed. After

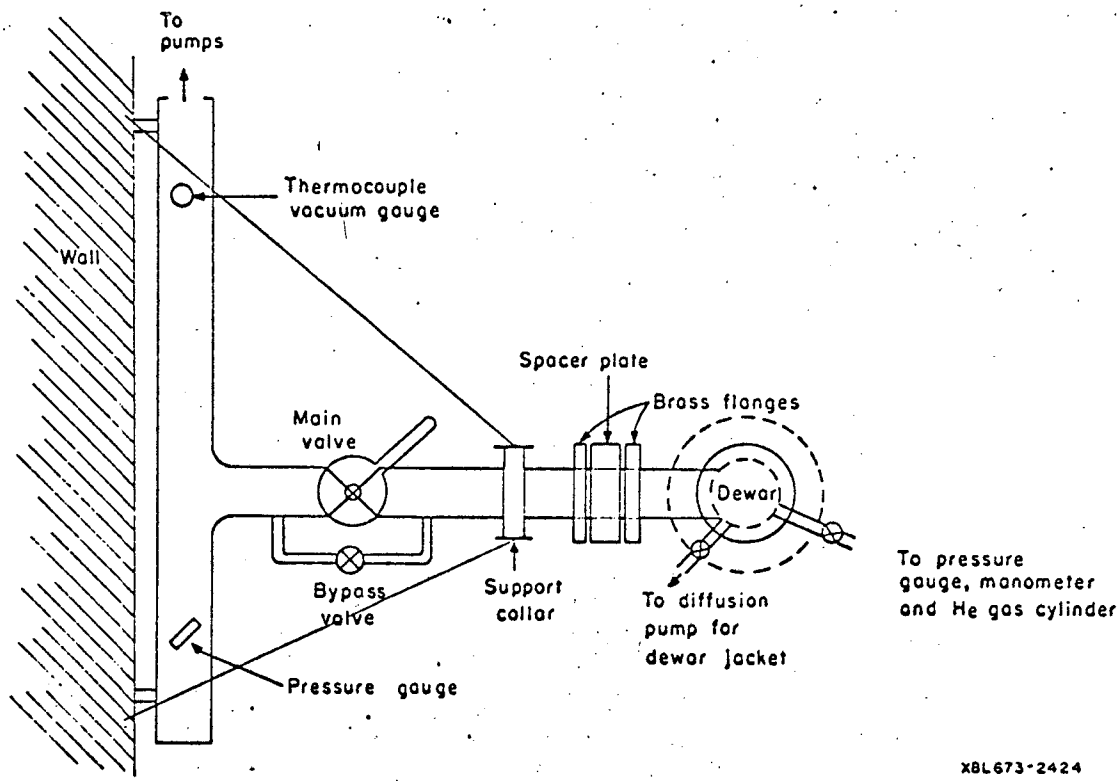

Fig. 11. Top view of the cryostat and vacuum system.

placing the sample and styrofoam in the cavity, the lower part of the waveguide assembly was immersed into liquid nitrogen to quick freeze the sample. Then the blank flange was removed from the tee and a positive pressure of helium gas was applied to the dewar. The waveguide assembly was then inserted into the cryostat and bolted into place and the system was flushed with gaseous helium several times. After purging the transfer line (Johns & Frame Model HTL), it was inserted into the cryostat through a fitting in the top flange and into the liquid helium storage dewar. The transfer line was withdrawn after filling and, after securing the fittings, the manometer valve was opened. Pumping on the liquid helium was started by opening the small bypass valve (Fig. 11) and, when the pressure in the dewar was reduced to about -28 psi, the main valve was opened slowly. The λ-point (2.17°K) was reached about 15-20 minutes after filling with helium and the lowest temperature (~ 1.3°K = 1.2 mm Hg) was obtained in about ten more minutes. The liquid helium usually lasted for periods of up to twelve hours.

For estimating temperatures in the range 1.3 to 4.2°K, the vapor pressure of the liquid helium was measured by reading the mercury manometer and converting the pressure readings to temperature using the 1958 ^{4}He temperature scale.[5] Since the liquid helium was in direct contact with the sample, the only error in these readings was due to the fact that the manometer inlet was not directly above the helium level. It was assumed that the temperatures so obtained were accurate to ±0.01°K. Temperatures above the boiling point of liquid helium were estimated by employing a thermocouple which was soldered to the outside wall of the cavity with Wood's metal. The thermocouple leads consisted of two #30 wires; one had a composition of 99.4 atomic % gold and 0.6 atomic %

cobalt[6] and the other was pure copper. The wires were insulated with teflon sleeving and connected to a 0°C reference bath and potentiometer through the metal to ceramic seal on the upper flange. This thermocouple was calibrated at liquid helium and liquid nitrogen temperatures prior to each run. Representative readings were 10.502 mv at 4.2°K and 8.631 mv at 77°K. A sensitivity of 10 μv per °K was assumed for the 4-20°K range based on earlier results with this thermocouple.[7] The temperature measurements were thought to be accurate to ±2°K in the range 4-20°K and ±8°K in the range 20-60°K.

4. Sample Preparation

a. Sample Tubes and Procedures

The sample tubes used in the liquid helium ESR experiments were sealed pyrex glass ampules. These were prepared from a section of glass tubing (4 mm and 9 mm O.D. for the K- and X-band experiments, respectively) so that the ampule was suspended from the tubing by a narrow neck. This assembly was then attached to a vacuum manifold and dried carefully by flaming with a torch. All joints were greased with Kel-F. For most experiments, the solvent and solute were vacuum distilled into the ampule by cooling the latter with liquid nitrogen. When enough sample was obtained, the ampule was warmed to room temperature and wrapped with wet asbestos tape, leaving the narrow neck exposed. The ampule was then cooled to liquid nitrogen temperature and sealed at the neck with a hot needle-point flame. The length of the ampule was such that it could be placed transversely in the cavity as shown in Fig. 8.

The samples of pure VCl_4 and $V(CO)_6$ were prepared in the same way. For the matrix experiments using mineral oil as a solvent, the ampule was filled with mineral oil prior to attaching to the vacuum line. The

mineral oil was then degassed at room temperature on the vacuum line. The solid samples - e.g. VF_4 and $V(CO)_6/Cr(CO)_6$ - were prepared by filling the ampule in a dry bag flushed with dry nitrogen. Some samples of VCl_4 in $TiCl_4$ were prepared with a known concentration of VCl_4; two calibrated glass bulbs were used for measuring the gas-phase volumes at room temperature and these were converted to molar concentrations using available vapor pressure data.

b. Chemicals

The $V(CO)_6$ was prepared in collaboration with G. V. Nelson according to the method of Werner and Podall.[8] In this method, bis-diglyme sodium hexacarbonyl vanadate, $Na(C_6H_{14}O_3)_2V(CO)_6$ (diglyme = diethyleneglycoldimethylether), is treated with 100% phosphoric acid at 25°C followed by sublimation of the resulting hexacarbonyl vanadium at 45-50°C under vacuum. For our experiments, the sodium diglyme salt was obtained from Alfa Inorganics (Beverly, Massachusetts). The reaction flask was filled with the salt and sufficient H_3PO_4 in a dry box and then attached to a vacuum line. The products of the reaction, which is not a rapid one, were trapped out by pumping through a U-tube kept at -42.5°C with a chlorobenzene/dry ice bath. The U-tube contained some P_2O_5 to remove traces of water. The tube was then warmed to 0°C and the diglyme residue was pumped off. The pure $V(CO)_6$ could then be sublimed under vacuum to a storage bulb held at 77°K. It could be stored at dry ice temperatures for 3-4 days but decomposed rapidly at room temperature in the presence of light. Consequently, the ESR experiments were performed as soon after preparation as possible.

Reagent-grade benzene and n-pentane, which were used as solvents for $V(CO)_6$, were dried with sodium and degassed thoroughly on the vacuum

line before use. No effort was made to measure the concentration of the $V(CO)_6$ in these samples but it was thought to be of the order of one mole percent. In some experiments, mixed crystals of $V(CO)_6$ in $Cr(CO)_6$ (Alfa Inorganics, Inc.) were prepared using a specially-constructed variable temperature sublimator. These were transferred to a sample tube in a dry bag and degassed thoroughly on the vacuum line before sealing off the ampule. The ESR spectrum of these mixed crystals showed a strong g=4 signal which disappeared at liquid nitrogen temperatures. This was not investigated further but it should be mentioned here that the pure $Cr(CO)_6$ became discolored during sublimation; in addition, it is highly likely that some $V(CO)_6$ decomposition also occurred during the preparation of the mixed crystals. When $V(CO)_6$ decomposition occurred on the vacuum line, the vanadium metal plate could be removed easily with dilute HNO_3.

The liquid helium ESR experiments on VCl_4 were performed with material obtained from two sources, K and K Laboratories (Plainview, New York) and Gallard-Schlesinger (Carle Place, New York). It was transferred from the container to flasks in a dry bag and, in early experiments, was used without further purification. However, as is described in detail in Section C of this chapter, a 10-15% $VOCl_3$ impurity was found in the VCl_4 from both sources. Subsequent ESR experiments were performed on VCl_4 purified by fractional distillation but this did not seem to affect the ESR spectrum. The solvents used in this work were mineral oil (Parke-Davis, heavy grade), CCl_4, $SiCl_4$, $TiCl_4$, and $SnCl_4$. All were of reagent grade or higher purity. The CCl_4 was dried and degassed before using; the other tetrachlorides were degassed but not dried since they react violently with water.

Some ESR experiments were also run on VF_4 obtained from Ozark Mahoning Co. (Tulsa, Oklahoma). This compound, which is a solid, is difficult to dissolve. Reagent grade chloroform, acetone and glacial acetic acid were found to dissolve VF_4 to varied but limited extents. Unfortunately, these solvents usually contain water which is difficult to remove; consequently, many of the ESR spectra showed considerable interference from VO^{+2}. However, a broad line believed due to VF_4 was observed in some samples of chloroform and acetic acid. This line had a g-value of less than 2 but was not investigated further.

5. ESR Spectra of DPPH at Liquid Helium Temperatures

The free radical 1,1-diphenylpicrylhydrazyl (DPPH) is commonly used in ESR spectroscopy as a standard for g-value measurements. It has a well-defined g-value (2.0036 ± 0.0002)[9] and therefore can serve as a reference for the measurement of either field or frequency. However, as noted in the literature,[10] the ESR spectrum of DPPH depends to some extent on the solvent from which it is recrystallized. In our experiments, polycrystalline DPPH was sometimes attached to the outside of the sample ampule with silicone grease for the purpose of measuring the magnetic field at the sample position accurately. Since, in later experiments, it was necessary to eliminate the DPPH because it interfered with some of the spectra, the Harvey-Wells NMR probe was placed in the field as close to the dewar tail and cavity as possible for field measurements. Then experiments were run to determine the difference in field between the NMR probe and liquid helium cavity positions with DPPH in the cavity. However, the g-value of DPPH at low temperatures is quite anisotropic[11] and further, the several published values for this molecule at temperatures below 77°K are in disagreement. Some of these differences may be

due to the solvent effect mentioned above. Consequently, the g-values of polycrystalline DPPH were redetermined as described below. The DPPH used in these experiments was obtained from Aldrich Chemical Co. (Milwaukee, Wisconsin) and was not recrystallized. However, most DPPH which is available commercially is recrystallized from benzene, and this was assumed to be the case for our samples.

These experiments were performed at K-band. Measuring the field with the Harvey-Wells NMR, the ESR spectrum of polycrystalline DPPH at 77°K was found to be anisotropic with $g_{\parallel} = 2.0024 \pm 0.0002$ and $g_{\perp} = 2.0036 \pm 0.0002$ ($\langle g \rangle = 2.0032$). A representative spectrum at this temperature is shown in Figure 12a which is similar to that obtained by Yodzis and Koski[11] at 24.3 GHz except that in our spectrum, a line belonging to the third g-value is beginning to appear under the $g_{\perp}$ peak. These authors found $g_{\parallel} = 2.0028$ and $g_{\perp} = 2.0039$ with an error of 0.0002 ($\langle g \rangle = 2.0035$). Although their results were obtained at room temperature, the existing evidence[11] suggests that the g-values of DPPH are equal at both room temperature and 77°K. Therefore, the field correction necessary to account for the different positions of cavity and probe is +0.0003 g-units. Since this correction was small compared to other experimental uncertainties (mainly due to the linewidths in VCl_4 and $V(CO)_6$), it was neglected in the results described in Chapter IV. The spectrum in Figure 12b is that of DPPH at 1.37°K; the lines to the high-field side of g_3 are due to an interfering VCl_4 signal. At this temperature, the DPPH molecule no longer possesses axial symmetry. The g-values indicated in Figure 12b were found to be $g_1 = 2.0114$, $g_2 = 2.0095$ and $g_3 = 2.0041$ ($\langle g \rangle = 2.0083$) with an error of 0.0002. At 1.46°K, the anisotropy was slightly less with $g_1 = 2.0106$, $g_2 = 2.0093$ and $g_3 = 2.0040$ ($\langle g \rangle = 2.0080$)

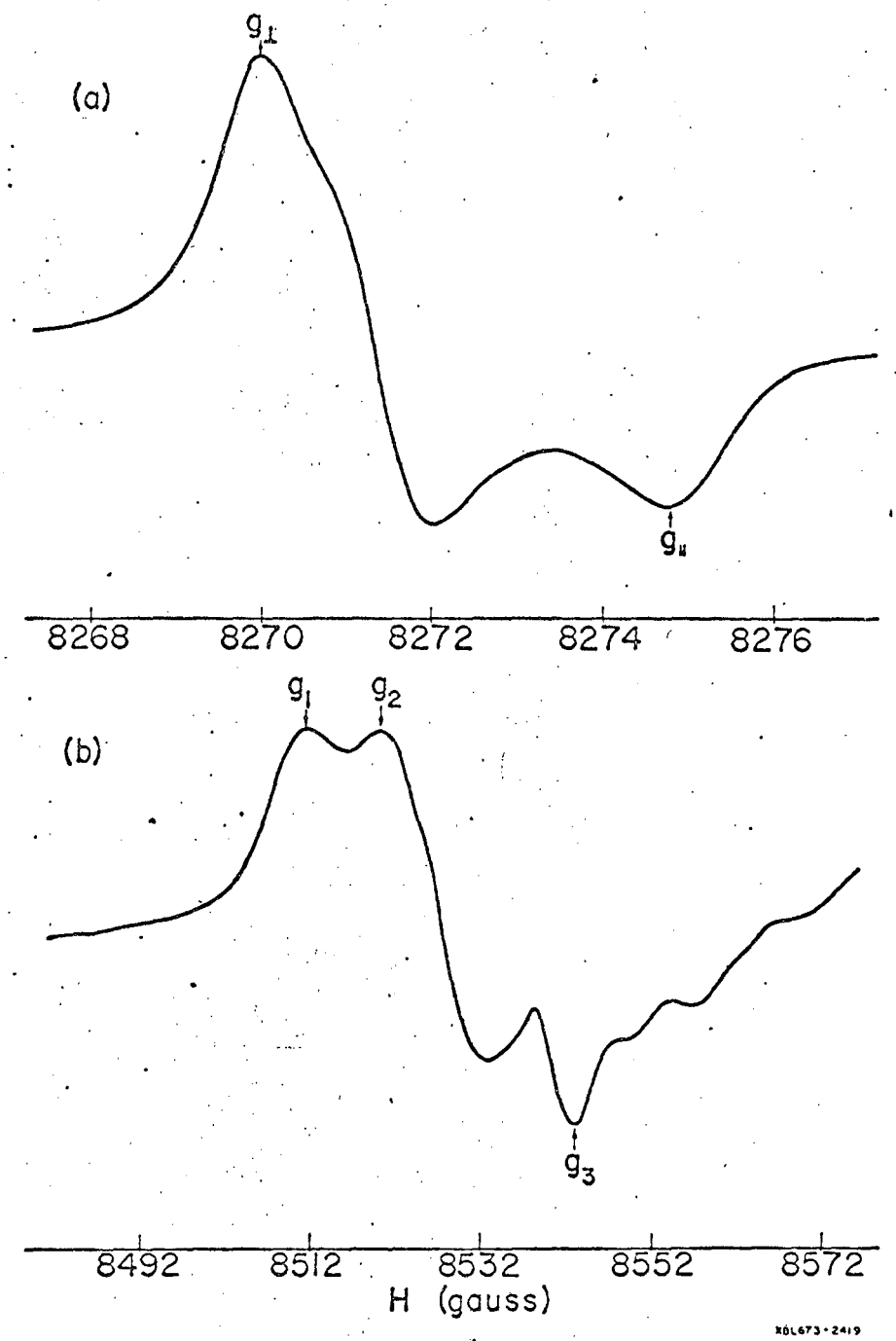

Fig. 12. ESR spectrum of polycrystalline DPPH at K-band. a) 77°K, b) 1.37°K.

with the same error. These values are in reasonable agreement with the single crystal data of Singer and Kikuchi[12] (2.0109, 2.0102, 2.0050; $\langle g \rangle = 2.0087$) which was obtained at 1.6°K at K-band. The only error in our measurements is due to the fact that g_2 should be measured at the baseline since the line belonging to this g-value is a full-derivative.

6. Apparatus for Determining T_1 in VCl_4

A simple microwave pulsing circuit, which is shown in Figure 13, was assembled for the purpose of measuring the electron spin-lattice relaxation time of VCl_4 at liquid helium temperatures. The central components in this network were a solid-state X-band microwave switch (Somerset Radiation Laboratory X405) employing a PIN diode with a response time of 10 nanoseconds and a pulse generator (Datapulse 106C). This switch was inserted into the waveguide line between the manual waveguide switch and the microwave bridge on the helium shelf. The solid state switch was turned on by a +12 volt square wave pulse with a pulse width of about 5 msec from the pulse generator which was triggered manually. During this 5 msec period, the PIN diode was forward-biased and conducted 10-12 ma of current, and the microwave power from the V153 klystron was attenuated only slightly (insertion loss ~ 1.5 DB at 9.3 GHz). Thus, an ESR signal was superimposed on the square wave pulse which appeared at the detector during this period. This was amplified and applied to the Y-axis of the oscilloscope. The X-axis of the scope was triggered with the gate of the pulse generator using a pulse delay (period between gate and pulse) of about 5 msec. The resulting trace was photographed with a Hewlett-Packard 196A oscilloscope camera and high-speed Polaroid film (Type 47, speed 3000) and analyzed to determine T_1.

In the reverse-bias configuration (0 volts), the diode was not

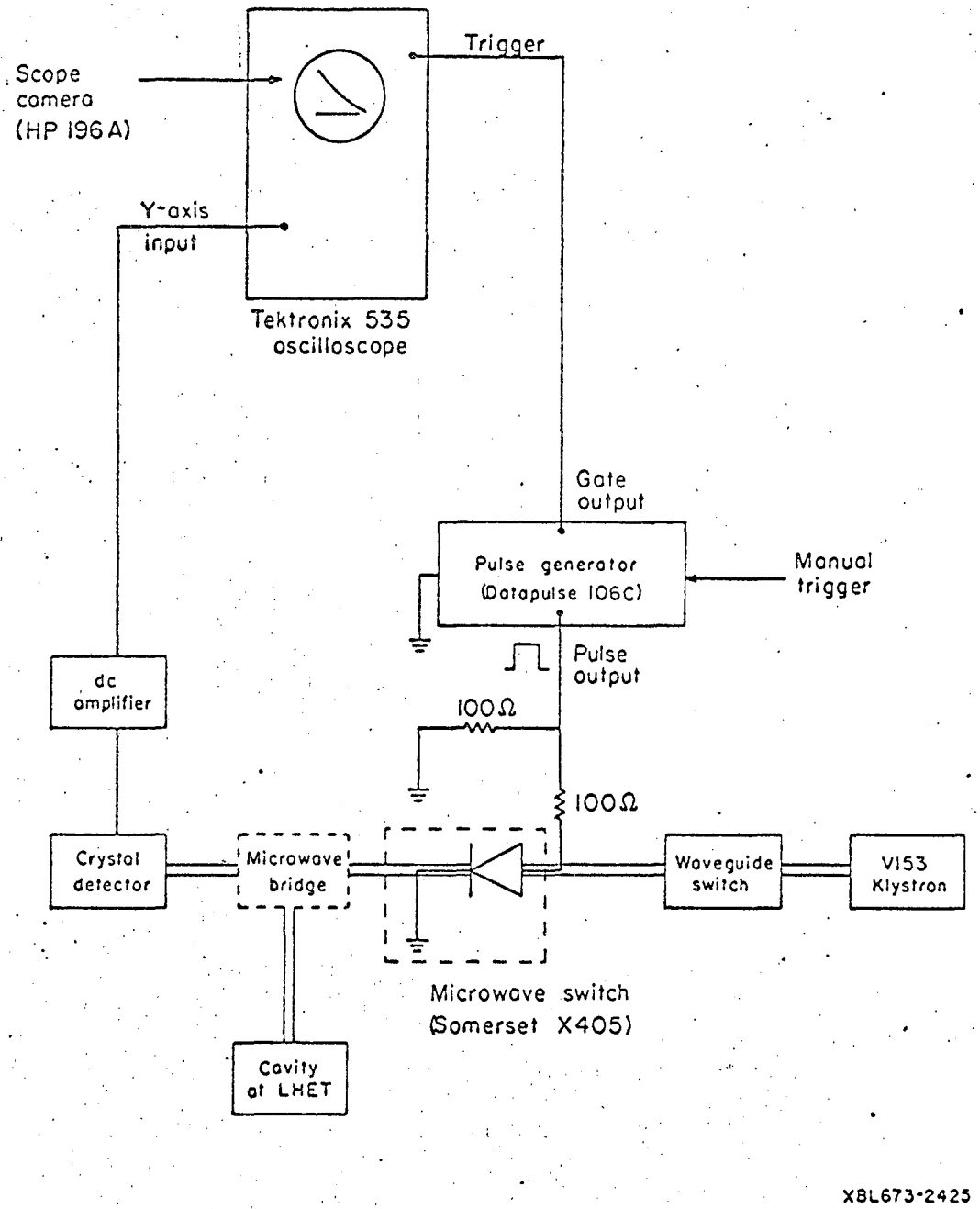

Fig. 13. Block diagram of the circuit used for determining T_1.

conducting and the solid state switch acted as an attenuator (~ -20 DB) of microwave power. For some experiments, the pulse generator was replaced by a manual switch and 25 volt battery. This enabled one to forward-bias the diode for longer periods of time to balance the bridge and observe the entire absorption spectrum of VCl_4 on the XY recorder. In order to record the absorption spectrum, and in the pulse experiments, no magnetic field modulation was employed and the detector output was connected directly to the oscilloscope or recorder. In most cases, DC amplification was not required to observe the absorption spectrum on the recorder. The results of these experiments are described in the next chapter.[13]

C. NMR

1. Experimental Apparatus

The ^{35}Cl and ^{51}V NMR experiments on VCl_4 and related molecules were performed on a Varian V-4200 wide-line spectrometer equipped with a V-4210A variable frequency oscillator. The latter was operated at frequencies of 15.817 MHz(^{51}V) and 5.879 MHz(^{35}Cl) with the appropriate probes. For some experiments the V-4210A was synchronized with a Rhode and Schwartz frequency synthesizer (WIK-BN 4421) which provided a short-term frequency stability of 2 parts in 10^7. However, this was not found to be necessary for the study of the broader ^{35}Cl lines, as the stability of the V-4210A was 1 part in 10^5.

A PAR HR-8 lock-in amplifier was used to provide phase-sensitive detection and magnetic field modulation at 400 and 1000 Hz. The reference output of the HR-8 was amplified with a Bogen CHA-10 audio amplifier and then applied to the modulation coils in the probe. The modulation amplitude was adjusted so as to produce an optimum signal-to-noise ratio without distorting the line shape. All measurements were made under conditions of slow passage and care was taken to prevent saturation of the signal. The static field was swept at a rate compatible with the linewidth and the time constant of the lock-in amplifier. The RF and modulation frequencies were measured with a Hewlett-Packard 5245L electronic counter.

For most of the experiments, the 14.09 KG magnetic field was locked using a V-K3506 superstabilizer and swept by the V-K3507 slow sweep unit. However, in some cases which are described below, it was necessary to sweep over a much wider range of field than provided for by the superstabilizer. Such experiments were performed by unlocking the static field and sweeping with the aid of a V-4280A scanning unit. This provided

a maximum sweep range of about 750 G. It was found useful in these search experiments to measure the magnetic field using an external NMR oscillator and a Harvey-Wells NMR field-control unit (FC-502) was employed for this purpose. The Harvey-Wells probe was placed as close as possible to the Varian probe and provided an NMR reference signal (^{1}H or ^{7}Li) with a 3:1 S/N ratio.

2. Sample Preparation

Figure 14 shows a typical sample tube used in the NMR experiments and its orientation within the probe assembly. The tube was fitted with a stopcock and standard taper joints to facilitate filling on a vacuum line. The VCl_4 (and $TiCl_4$, when required) was distilled into the tube from a sample bulb located elsewhere on the manifold by cooling the sample tube to liquid nitrogen temperature. The inner tube was stoppered to prevent the condensation of water in the tube during the distillation. When enough sample had been collected, the sample assembly was warmed to room temperature and the inner tube was filled with a 3M aqueous NaCl solution using a hypodermic needle. All chemicals were reagent grade; however, the VCl_4 required further purification (vide infra).

a. ^{51}V experiments

The first ^{51}V NMR experiments on pure VCl_4 showed an extremely sharp (width ~50 Hz at room temperature) and intense signal at 15.8167 MHz. The position of this signal with respect to the ^{23}Na signal in the NaCl reference solution was then measured as a function of temperature from 25°C to 100°C. For these runs a wide sweep was necessary in order to observe both the ^{51}V and ^{23}Na signals at the same frequency so the static field was swept with the V-4280A scanning unit. The magnetic field was measured at the position of each of the signals with the

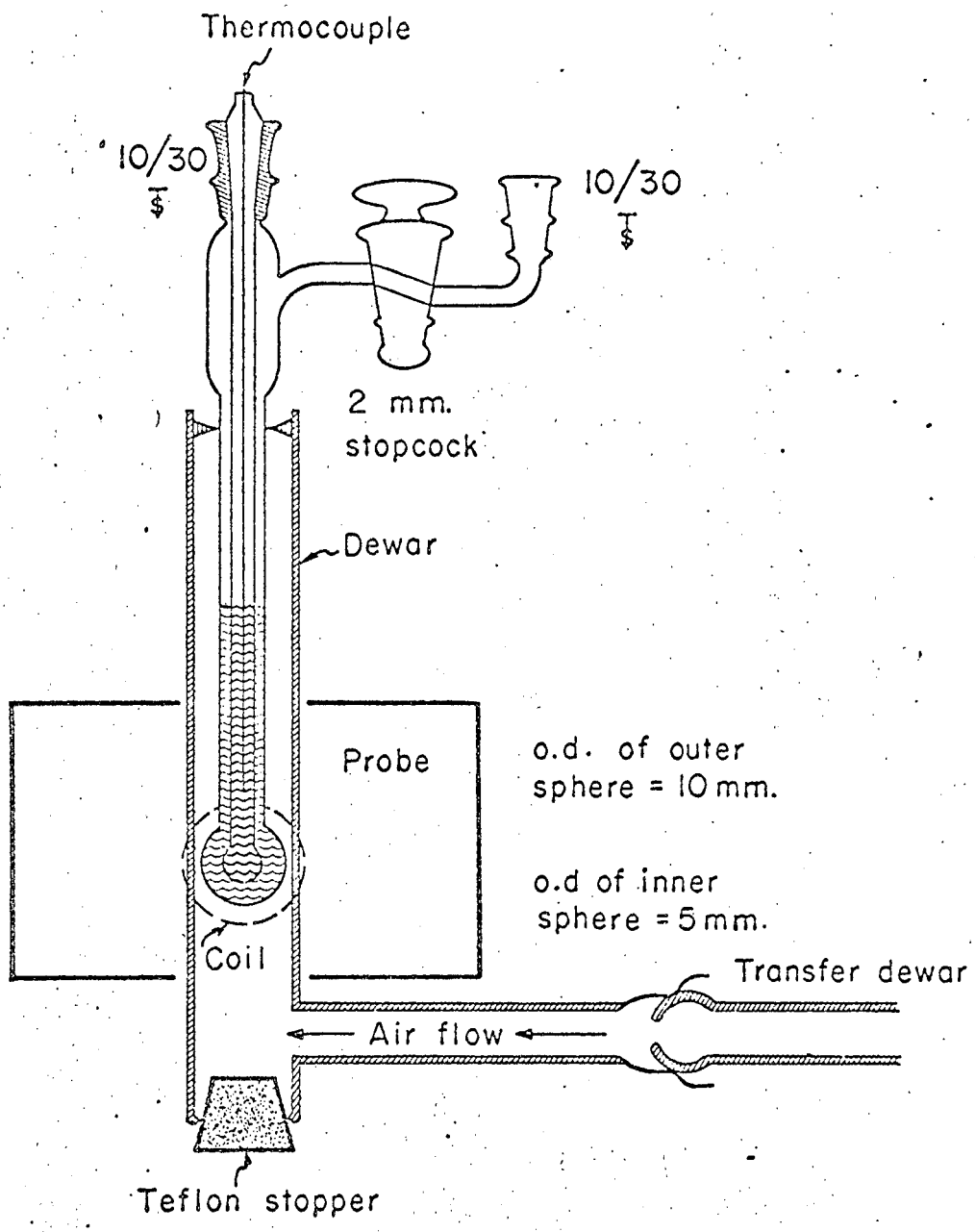

XBL673-2354

Fig. 14. Sample assembly used in the NMR experiments and its orientation within the probe.

Harvey-Wells unit and ^{7}Li probe. These measurements showed that (a) the position of the ^{51}V signal was approximately that expected for ^{51}V in a diamagnetic molecule, unshifted by the large contact interaction observed in the ESR experiments on VCl_4 (vide infra) and (b) the shift of the strong ^{51}V signal from the ^{23}Na signal was essentially temperature-independent, an observation which was also consistent with a diamagnetic ^{51}V.

This information suggested that the observed ^{51}V signal might be due to an impurity in the VCl_4. To estimate the concentration of the supposed impurity, a solution of known concentration in ^{51}V, 0.5M sodium orthovanadate, was prepared by dissolving 5.90 g. $Na_3VO_4 \cdot 16H_2O$ (Fisher Scientific, lot 702319) in 25 cc. of hot NaOH solution such that the final pH was near 14. By comparison with the intensity of the ^{51}V signal in this reference solution, the concentration of the ^{51}V compound producing the signal in VCl_4 was estimated to be 1.4M. Since pure VCl_4 is 9.43M, it was concluded that the sharp line was due to a 10-15% impurity in the VCl_4.

Howarth and Richards[14] have measured the chemical shift of VO_4^{-3} in aqueous solution at pH 14 with respect to $VOCl_3$. This shift is about 535 ppm at a frequency of 14.542 MHz. An approximate measurement of the shift of the ^{51}V signal in VCl_4 with respect to the 0.5M VO_4^{-3} solution yielded 575 ppm. On this basis it was concluded that the impurity in VCl_4 was $VOCl_3$.

To verify this conclusion, several additional experiments were run. In one, a sample of VCl_4 on the vacuum line was divided into two fractions by vacuum distillation and NMR spectra were obtained for each fraction. The intensity of the sharp ^{51}V line for the first fraction was twice that for the second. Since the vapor pressure of $VOCl_3$ is about twice that of VCl_4 (22 mm. vs. 8 mm. at 25°C), this intensity difference is about as

expected if $VOCl_3$ is the source of the signal. Second, some $VOCl_3$ was intentionally added to a sample of VCl_4 and only one line was observed, at the same field position as the line in VCl_4 and considerably more intense. Finally, the VCl_4 was purified by fractional distillation (b.pt. for VCl_4 = ~152°C., for $VOCl_3$ = 126.7°C) under an atmosphere of flowing nitrogen and the last fraction showed no sharp ^{51}V NMR signal. It is also of interest to note that the linewidth of the ^{51}V resonance in $VOCl_3$ at 22°C has been reported to be 52 Hz.[15] in good agreement with the linewidth observed here.

The VCl_4 used for the experiments described here was obtained from two sources. Initial experiments were performed with material obtained from K and K Laboratories, purity 95-99%; whereas later experiments were done with VCl_4 purchased from Gallard-Schlesinger (99+%). Both lots of VCl_4 gave the strong NMR signals described above even though handling procedures were devised to prevent contact with air or water. Therefore, all subsequent experiments were performed on VCl_4 which had been purified by fractional distillation and subsequently stored at dry ice temperature. The $VOCl_3$ concentration in the purified VCl_4 was estimated by the above methods to be no greater than 2-3%.

b. ^{35}Cl experiments

The chemical shift and linewidth measurements on VCl_4 and $VCl_4/TiCl_4$ solutions were performed using the VCl_4 purified by fractional distillation. The Cl^- signal in the 3M NaCl solution in the inner tube was used as a reference point for shift measurements. Some of this data was obtained with cylindrical sample tubes rather than the concentric "spherical" tubes shown in Figure 14; a correction for the bulk-susceptibility shift[16] of the Cl^- signal was made for each temperature using the

equations of Dickinson.[17] Since the ratio of length to diameter of the cylindrical tubes was about three, the correction factor of $2\pi/3$ was used. In order to calculate the correction to the observed shift, it was necessary to know the diamagnetic susceptibility of the reference solution. This was determined using $\chi_M(NaCl) = -30.3\times10^{-6}$ cgs/mole[18] and $\chi_V(H_2O) = -0.721\times10^{-6}$ cgs/cc[19] and assuming Wiedemann's additivity law for susceptibilities, i.e.,

$$\chi_{M,mixt} = x_1\chi_{M,1} + x_2\chi_{M,2}$$

where x_1 and x_2 are the mole fractions of solute and solvent. For 3M NaCl, this relationship gives $\chi_{M,mixt} = -13.9\times10^{-6}$ cgs/mole. The resulting correction was never more than 5% of the observed shift at any one temperature.

3. Temperature Control and Measurement

The temperature dependence of the shifts and linewidths was measured with the aid of a Varian variable-temperature unit modified for use with the V-4200 spectrometer. The temperature range covered in these experiments was from -5 to 100°C. Temperatures below ambient were obtained by flowing dry nitrogen through a brine-ice bath at -15°C at varying rates and through a transfer dewar which was connected to the probe dewar as shown in Figure 14. For the room temperature runs dry nitrogen was passed over the sample without precooling to prevent heating of the sample. Temperatures above ambient were produced by an adjustable flow rate of preheated air. Previous experiments with this apparatus[20] have demonstrated that the maximum temperature gradient across the sample with a low flow rate of air is 2°C.

Temperatures were measured with a calibrated copper-constantan thermocouple which was immersed in the NaCl reference solution in the inner tube (Fig. 14) so that the junction was just above the transmitter coil. The reference junction was kept at 0°C. The maximum standard deviation of thermocouple readings never exceeded 30 μv and was usually much less, so the temperature readings were accurate to better than a degree Kelvin since the flow rates employed were quite high.

4. Signal Display and Measurement

The linewidths of the ^{35}Cl signals in VCl_4 and $TiCl_4$ were of the order to 1-2KHz, whereas those for the reference signals were significantly smaller (20 Hz for Cl^-, 25 Hz for Na^+). Since the modulation frequency employed (usually 400 Hz) was much greater than the reference linewidths, the Cl^- and Na^+ signals appeared as sidebands[21] which were separated by $2\nu_m$,[20] where ν_m is the modulation frequency. The unknown signal, on the other hand, was displayed as a first derivative. Furthermore, because of this large difference in widths, it was necessary to adjust the RF power and modulation amplitude during the course of an experiment so that an optimum S/N ratio was obtained for both the reference and VCl_4 (or $TiCl_4$) signal. For the chemical shift measurements, this adjustment was made as the field was being swept from one signal to the other. Only the RF power, modulation amplitude and time constant settings were changed so the relative position of the two signals was not affected.

The position of the sidebanded signal was defined as the average field position of the two first sidebands. The experimental linewidth is the full width at half height. The linewidth of the derivative is defined for this work as being the peak to peak field difference, which, on the corresponding absorption curve, is equal to the full width between points

of maximum and minimum slope.

Since the first sidebands of the reference signal are separated by $2\nu_m$, each spectrum was conveniently calibrated in Hz/division. As the chart speed varied slightly from day to day, each sweep through the spectrum was calibrated and the shift and linewidth measurements converted to Hz or ppm. The field was swept up and down a number of times at each temperature and the results reported in Chapter IV are an average of at least three runs in each direction. The standard deviation of the shift and linewidth measurements was 0.06KHz for all temperatures. Field inhomogeneity did not contribute to the linewidth even for the narrow reference lines.

III. REFERENCES

1. E. R. Cohen and J. W. M. DuMond, Rev. Mod. Phys. 37, 537 (1965).
2. W. L. Jolly, K. D. Maguire and D. Rabinovich, Inorg. Chem. 2, 1304 (1963); W. L. Jolly, Synthetic Inorganic Chemistry (Prentice-Hall, Inc., Englewood Cliffs, New Jersey, 1960), p. 166.
3. D. H. Levy, The Electron Spin Resonance Spectra of Radical Anions in Liquid Ammonia (Ph.D. Thesis), University of California, Berkeley, UCRL-11864, Jan. 1965.
4. D. C. McCain, The Measurement of Electron Spin Relaxation Times of Ions in Aqueous Solution (Ph.D. Thesis), University of California, Berkeley, UCRL-17064, Aug. 1966.
5. F. G. Brickwedde, Proc. K. Onnes Conf. on Low Temperature Physics (Leiden, 23 June 1958), Physica 24, S128 (1958).
6. We thank Prof. G. C. Pimentel for providing this thermocouple wire. According to J. Brock, gold thermocouple wire with 0.07 atomic % iron has a higher sensitivity at these temperatures when used in conjunction with Chromel P wire. The gold wire can be purchased from Englehard Industries, San Francisco.
7. G. Ewing, unpublished results.
8. R. P. M. Werner and H. E. Podall, Chem. and Ind. 1961, 144.
9. H. Fischer, Magnetic Properties of Free Radicals, Vol. 1 of Landolt-Börnstein (New Series) (Springer-Verlag, New York, 1965), Ed. K.-H. Hellwege.
10. J. P. Goldsborough, M. Mandel and G. E. Pake, Phys. Rev. Letters 4, 13 (1960).
11. See, for example, P. P. Yodzis and W. S. Koski, J. Chem. Phys. 38, 2313 (1963).

12. L. S. Singer and C. Kikuchi, J. Chem. Phys. 23, 1738 (1955).

13. We thank the following people for the loan of some of the instrumentation used in these experiments: M. P. Klein and A. Luntz (microwave switches), C. B. Moore (pulse generator), B. H. Mahan (oscilloscope camera).

14. O. W. Howarth and R. E. Richards, J. Chem. Soc. 1965, 157.

15. O. W. Howarth and R. E. Richards, Proc. Phys. Soc. (London) 84, 326 (1964).

16. J. A. Pople, W. G. Schneider and H. J. Bernstein, High-Resolution Nuclear Magnetic Resonance (McGraw-Hill Book Co., Inc., New York, 1959), p. 80.

17. W. C. Dickinson, Phys. Rev. 81, 717 (1951).

18. W. R. Myers, Rev. Mod. Phys. 24, 15 (1952).

19. See Reference 16, Appendix C.

20. R. S. Marianelli, Nuclear Magnetic Resonance Study of Water Exchange from the First Coordination Sphere of Gd(III) Ion (Ph.D. Thesis), University of California, Berkeley, UCRL-17069, Sept. 1966.

21. J. V. Acrivos, J. Chem. Phys. 36, 1097 (1962) and references contained therein.

IV. RESULTS AND DISCUSSION

A. ESR of $V(CO)_6$ at Liquid Helium Temperatures

1. Assignment of the Spectra

a. Pure $V(CO)_6$.

At 1.3°K, the ESR spectrum of pure polycrystalline $V(CO)_6$ consisted of a single, slightly asymmetric line which is reproduced in Fig. 15. Some additional structure was observed on the high-field side of the spectrum but this was assigned to an unknown decomposition product. This will be discussed in more detail later. Every effort was made to eliminate the asymmetry of the line but so far as could be determined, this asymmetry was real and not due to instrumental causes. The microwave bridge was carefully balanced and the signal was not overwhelmingly strong, so dispersion was not thought to be important. (With very strong signals, the AFC will occasionally unlock, producing a frequency shift and mixing in some dispersion.) The peak to peak width of the major line was measured carefully and found to be 132.8±0.2 gauss.

Based on the isotropic Hamiltonian

$$\mathcal{H} = g\beta H_z S_z,$$

which gives rise to a single transition at a field

$$H_z = \frac{h\nu}{g\beta},$$

the isotropic g-value can be determined from the spectrum by measuring the frequency and the center field of the signal. The result for a number of such measurements was g = 2.0603±0.0003. Experimentally, the "center" field used for this calculation was determined by averaging the field positions of the maximum positive and negative derivatives. If the line were symmetric, this would be equivalent to taking the field

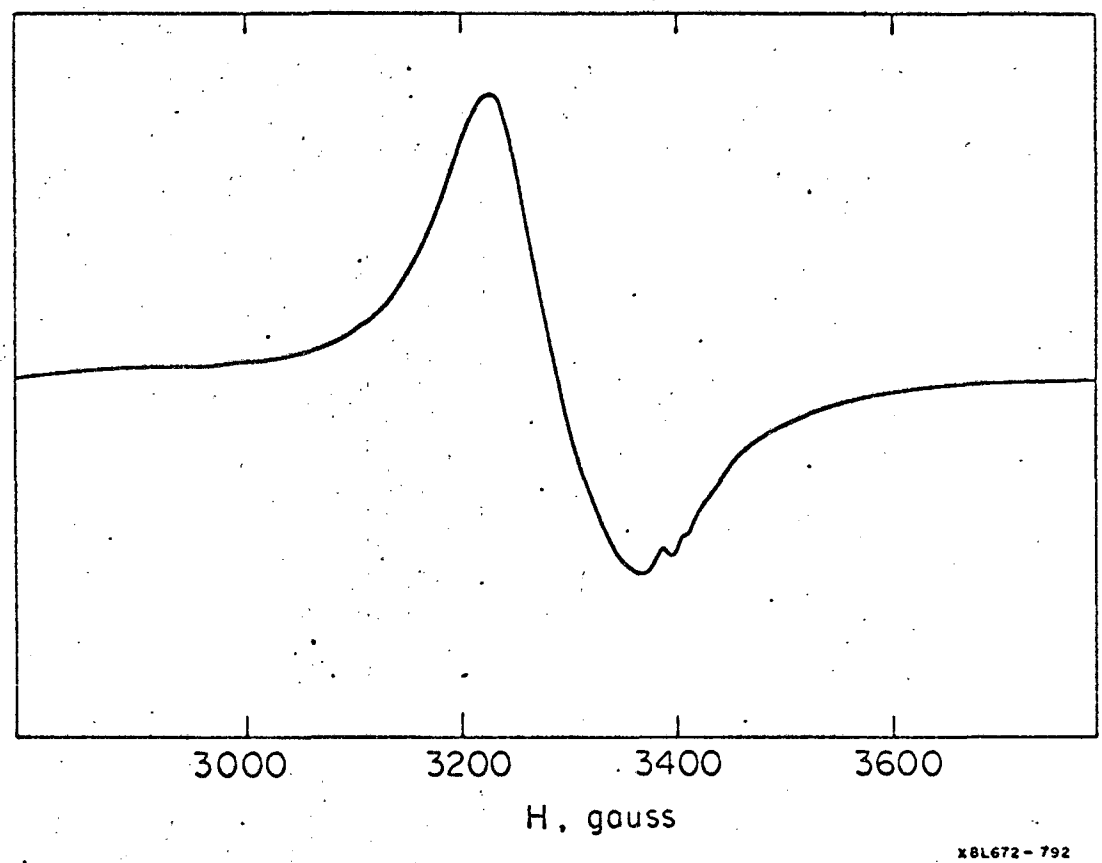

Fig. 15. ESR spectrum of pure $V(CO)_6$ at 1.3°K.

for the g-value to be where the signal crossed the baseline between the two peaks. However, since the derivative is clearly not symmetric, the g-value calculated by the latter method would be different and in this case was found to be 2.063±0.002. This value is quoted to four significant figures only because (a) the point at which the signal crossed the baseline was more difficult to determine and (b) fewer measurements were made in this way.

The spectrum shown in Fig. 15 was obtained at a power level of about 0.5 mw. (-6 DB on the main attenuator) and was essentially unchanged at lower power levels. However, if the incident power was maintained at -6 DB or higher, the intensity of the main absorption gradually decreased as the field was swept back and forth across the spectrum. Further, the line could not be restored to its original intensity at lower power levels even after complete attenuation of the power for periods of up to an hour. Only after the sample was warmed to ~77°K and then re-cooled to liquid helium temperatures was the intensity again "normal". This behavior was reproducible and, during the decrease in signal intensity, no appreciable change in width or g-value was observed. As the samples used for these experiments consisted of a few small grains of polycrystalline $V(CO)_6$ in a pyrex glass ampule, it is possible that the above behavior was due to the poor thermal contact between the $V(CO)_6$ and the walls of the ampule, i.e., the liquid helium bath. No other reason for this behavior could be determined.

The structure on the high-field side of the main line in Fig. 15 did not show the above behavior and so became relatively more intense as the $V(CO)_6$ absorption was saturated. For this reason, it was concluded that this structure was due to another species. As decomposition

of some of the $V(CO)_6$ was fairly common during the preparation of these samples (vide infra), it seemed reasonable to assume that this species was a product of this process. The approximate g-value of this line, assuming it to be a full derivative, was 2.008±0.004.[1]

When the spectrometer gain was increased, some hyperfine structure was detected in the samples which gave spectra analogous to Fig. 15, particularly on the low-field side of the broad $V(CO)_6$ absorption. Only three or four lines, which had the appearance of half-derivatives, were observed, and they were spaced about 50 gauss apart. As the only nuclear spin likely to be present in sufficient amount was ^{51}V with I = 7/2, no assignment of these could be made. The g-value of this structure was close to 2. Again, it was likely that this structure was due to an impurity or decomposition product, since the lines did not exhibit the power dependence shown by the $V(CO)_6$ signal.

In some cases, when the ampule containing the $V(CO)_6$ sample was sealed off, decomposition was evident in the form of a vanadium mirror which plated out on the walls of the ampule. The ESR spectra of these samples were invariably more complicated. Generally, they consisted of eight or more fairly strong hyperfine lines superimposed on a broad line. The g- and A-values of this structure were also about 2 and 50 gauss, respectively. No detailed analysis of these spectra was carried out. One possible origin of the eight hyperfine components was vanadium metal although even in a monolayer the atoms should be subject to a strong exchange interaction (vide infra). In the samples for which spectra similar to Fig. 15 were obtained, no decomposition was observed.

b. $V(CO)_6$ in dilute glasses.

The analysis of polycrystalline or glass ESR spectra to obtain the spin Hamiltonian parameters was first introduced by Sands.[2] Although

single crystal studies are potentially more accurate, spectra of randomly-oriented molecules are usually more readily obtained, especially for unstable species. Such was the case for $V(CO)_6$. The theory of glass spectra has been treated by many authors[3] and is briefly reviewed in Chapter I.

The line shapes which arise in polycrystalline or glass samples are due to the random orientation of the paramagnetic molecules in the local electrostatic fields of the surrounding environment. Thus, as discussed earlier, the g-value for a given molecule will depend on the orientation of the spins, which are quantized along the external field axis, with respect to the axes of the local crystal fields. The resulting line shapes can then be viewed as the integration of g-values over all possible orientations. If the local field of the surrounding environment has cylindrical symmetry, the dependence of g on orientation is given by

$$g^2(\theta) = g_{\parallel}^2 \cos^2\theta + g_{\perp}^2 \sin^2\theta$$

where θ is the angle between the principal axis of the crystal field and the axis defined by the external magnetic field.

The ESR spectrum of $V(CO)_6$ in a benzene glass at 1.29°K is shown in Fig 16. The positive band edge at the low-field side of the spectrum is assigned to $g_{\perp}$ and represents the onset of absorption for those molecules whose principal axis is aligned perpendicular to the magnetic axis. Similarly, the negative peak on the high-field side represents the onset of absorption for the parallel molecules and is assigned to $g_{\parallel}$. This lineshape is a very good example of that expected for a glass sample whose spin Hamiltonian possesses axial symmetry with $g_{\perp} > g_{\parallel}$.[4]

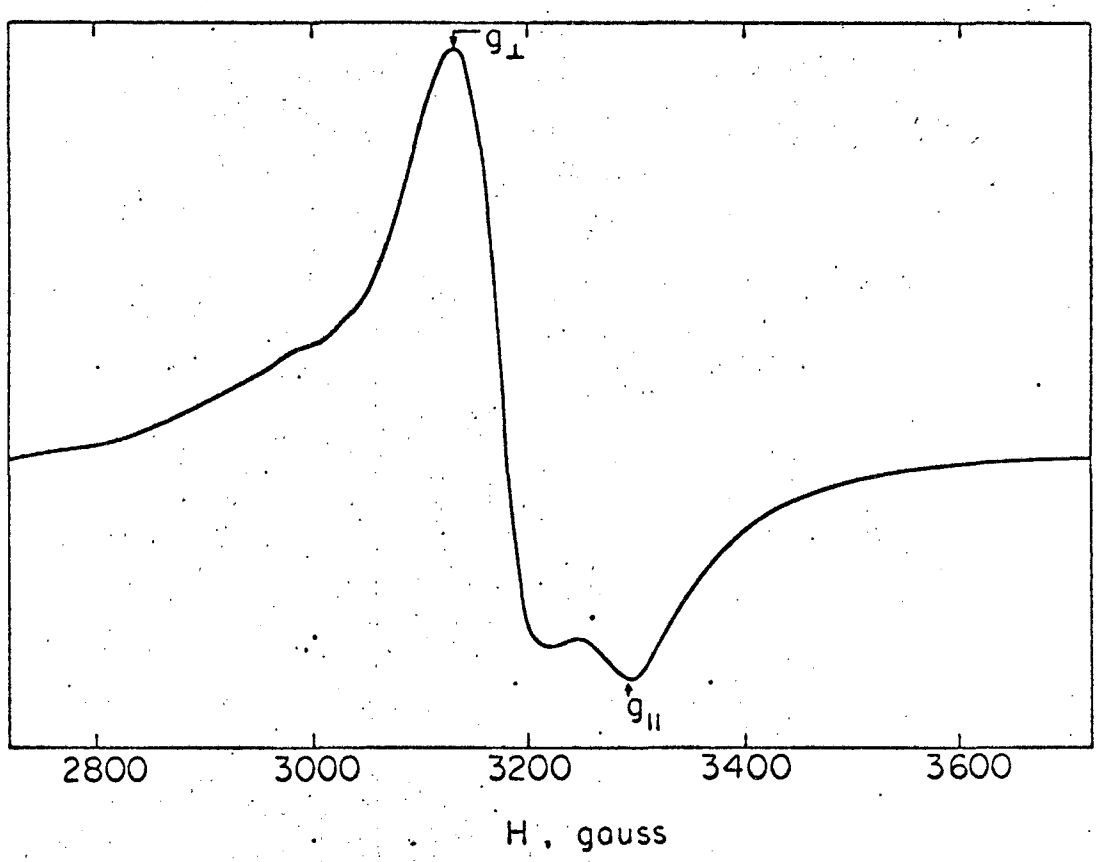

XBL672-793

Fig. 16. ESR spectrum of $V(CO)_6$ in benzene at 1.29°K.

As has been discussed by Kneubühl,[3a] the values of $g_{\parallel}$ and $g_{\perp}$ can be obtained directly from the spectrum. These positions have been labeled in Fig. 16. The g-values for $V(CO)_6$ in benzene were calculated from the relationships

$$g_{\parallel} = \frac{h\nu}{\beta H_{\parallel}} \quad \text{and} \quad g_{\perp} = \frac{h\nu}{\beta H_{\perp}}$$

and found to be 2.0228±0.0015 and 2.1260±0.0010 for $g_{\parallel}$ and $g_{\perp}$, respectively. The isotropic g-value obtained by averaging these principal values, i.e.,

$$\langle g \rangle_{calc} = \frac{2g_{\perp} + g_{\parallel}}{3} ,$$

was 2.0916±0.0012.

For use in later discussion, the behavior of the $V(CO)_6$/benzene glass spectrum under conditions of power saturation will now be described. The field splitting between $H_{\perp}$ and $H_{\parallel}$ in Fig. 16 was about 160 gauss. When the microwave power was increased to the point where a distortion of the line was observed, the tail of the $g_{\perp}$ band and the $g_{\parallel}$ band began to merge until, as the incident power was increased further, the spectrum had the appearance of a single asymmetric line with a peak-to-peak width of about 130 gauss. Thus, the effect of power saturation was to reduce the apparent line width and, as expected, the resolution. Except for a slight flattening of the peaks, the power-saturated lineshape was quite similar to that observed for pure $V(CO)_6$ (see Fig. 15). However, unlike the pure $V(CO)_6$ spectrum, the normal $V(CO)_6$/benzene spectrum was reproduced immediately on reducing the power.

The assignment of the spectrum of $V(CO)_6$ in an n-pentane glass at liquid helium temperatures was not as unambiguous. Figure 17 shows a series of spectra of the $V(CO)_6$/n-pentane sample at 1.34°K. under various power conditions. The gain on the spectrometer was adjusted between each spectrum so as to present the entire absorption on the recorder for, as the power was increased, the signal-to-noise ratio improved noticeably. However, what is of interest here was the obvious dependence of lineshape on power, and further, under high power conditions, that the g-value anisotropy was apparently completely resolved.

First, we discuss the low-power (- 30 DB) spectrum shown in Fig. 17a in which the saturation effects should have been minimal. The points marked with arrows have the g-values (in order of increasing field) $g_1 = 2.162$, $g_2 = 2.123$, and $g_3 = 2.024$. In addition, the g-value defined by the point at which the signal crossed the baseline was $g_c = 2.079$. There were a number of possibilities for the assignment of this spectrum and some of these have been listed in Table IV together with the method of calculation based on an assumed symmetry of the Hamiltonian. Discussion of these will be deferred until the other n-pentane spectra are presented.

Table IV. Possible g-values for the low-power spectrum of $V(CO)_6$ in n-pentane (Fig. 17), calculated from the observed values $g_1 = 2.162$, $g_2 = 2.123$, $g_3 = 2.024$ and $g_c = 2.079$.

	Symmetry Assumed	Isotropic value calculated from	$\langle g \rangle_{calc}$
A	spherical	g_c	2.079
B	spherical	$\frac{1}{2}(g_1 + g_3)$	2.093
C	spherical	$\frac{1}{2}(g_2 + g_3)$	2.074
D	axial	$\frac{1}{3}(2g_1 + g_3)$	2.116
E	axial	$\frac{1}{3}(2g_2 + g_3)$	2.090
F	rhombic	$\frac{1}{3}(g_1 + g_2 + g_3)$	2.103

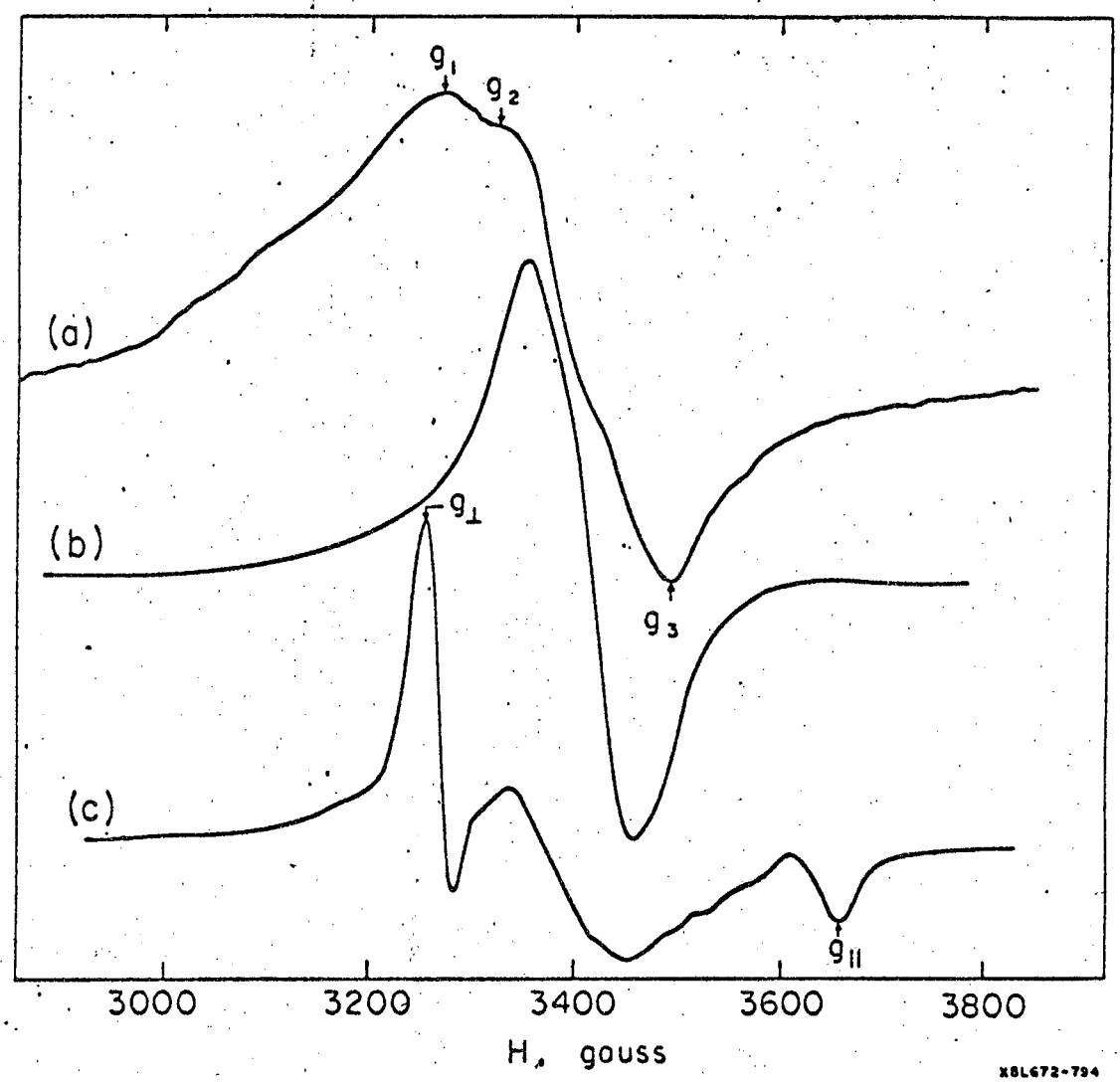

Fig. 17. ESR spectra of $V(CO)_6$ in n-pentane at 1.34°K; (a) -30 DB, (b) -16 DB, (c) -6 DB.

The medium-power (-16 DB) spectrum of the pentane glass sample shown in Fig. 17b exhibited the same narrowing phenomenon as was observed for the benzene glass sample. Thus, the derivative of the medium-power absorption line was nearly symmetric and had lost some of the detail of the spectrum obtained at lower incident power. The width of the former spectrum was 100 gauss compared to an overall width (H_3-H_1) of 215 gauss for the latter. The -16 DB spectrum was apparently isotropic, with a "baseline" g-value of 2.0609±0.0008 (when the positive and negative derivatives were averaged to obtain the center field, the g-value was 2.0702).

At still high power (e.g., - 6 DB), the change in the spectrum was even more pronounced as is indicated in Fig. 17c. In this case, the transition was abrupt, i.e., either the spectrum in Fig. 17b or 17c was observed, there was no intermediate lineshape. In fact, a spectrum similar to Fig. 17c could be produced by sweeping through slowly at lower power (e.g., - 16 DB) with no appreciable change in signal-to-noise ratio. This observation suggested that more than just power saturation was occurring and this possibility is discussed below.

The assignment of the high-power spectrum was facilitated by noting that the relatively sharp feature on the low-field side had the characteristic shape of a perpendicular band. Further, the negative half-derivative on the high-field end appeared to be a well-resolved parallel band. These two bands would then correspond to the lineshape expected for an axial Hamiltonian with $g_\perp > g_\parallel$. Based on this assignment, with $g_\perp$ = 2.1034 ±0.0003 and $g_\parallel$ = 1.9814±0.0010, the isotropic g-value was calculated to be 2.0627±0.0006. This value was in reasonable agreement with the value obtained from the isotropic (medium-power) spectrum of 2.0609. The field position of the broad feature which comprises the remainder of the spectrum

in Fig. 17c corresponds approximately to that of the isotropic line in Fig. 17b.

The g-values obtained for $V(CO)_6$ in the experiments described in this section are listed in Table V together with the results for pure $V(CO)_6$.

By inspection of Table V, it can be seen that there is reasonably good agreement between the isotropic g-values of pure $V(CO)_6$ and those found in the medium- and high-power spectra of $V(CO)_6$ in n-pentane. An average of the entries G, L and N yields $g = 2.062 \pm 0.001$. If the values determined by averaging the field positions of the maximum positive and negative derivatives are included, this average becomes $g = 2.063$. These values therefore support the assignment of the high-power pentane spectrum. Further, they suggest that in the case of our asymmetric lines, the g-values obtained by measuring the field at the point where the signal crosses the baseline are more reliable.

However, none of the isotropic values calculated from the low-power spectrum in n-pentane (see Table IV) are in agreement with those in Table V. Only the entries A (2.079) and C (2.074) of Table IV are close to the average value (2.062) and these two were calculated assuming an isotropic Hamiltonian which the low-power lineshape does not support. One possible interpretation would suggest that there is a g-value shift when the spectrum becomes power-saturated. Indeed, the g-value for the benzene glass, which was measured in the absence of noticeable saturation, was 2.092, which agrees with entries B (2.093) and E (2.090) of Table IV. On the other hand, a change of the g-value in going from the pentane glass to the benzene glass would not be unexpected (<u>vide infra</u>), so a comparison of g-values in different matrices is subject to qualification. Consequently, a definite assignment of the low-power spectrum in n-pentane could not be made at this time.

Table V. $V(CO)_6$ g-values.

Medium	Isotropic	Anisotropic $g_1 = g_\perp$	g_2	$g_3 = g_\parallel$	Comments
G Pure $V(CO)_6$	2.063±0.002[a]				
H Pure $V(CO)_6$	2.0603±0.0003[b]				
J Benzene Glass	2.0916±0.0012[c]	2.1260±0.0010		2.0228±0.0015	
K Pentane Glass		2.162±0.001	2.123±0.001	2.024±0.001	Low Power
L Pentane Glass	2.0609±0.0008[a]				Medium Power
M Pentane Glass	2.0702±0.0008[b]				Medium Power
N Pentane Glass	2.0627±0.0006[c]	2.1034±0.0003		1.9814±0.0010	High Power

a. Center field determined by point at which signal crossed the baseline.

b. Center field determined by averaging field positions of positive and negative derivatives.

c. Calculated from anisotropic components.

A survey of the literature on the effects of different matrices on the g-value suggests that the shift of the isotropic g-value of $V(CO)_6$ from 2.062 in n-pentane to 2.092 in benzene is more than one would expect in non-polar matrices. Jen et al.[5] have reported that the g-value shifts observed for radicals like H, N, and CH_3 in matrices such as H_2, Ar, N_2, and CH_4 are of the order of 0.1-0.2%. In contrast, the shift observed here is about 1.5%. Shifts of this order or larger are of course observed for polar matrices where the local environment is much more ordered. Thus, the large shift in the $V(CO)_6$ glasses could be taken to indicate that these samples have a higher degree of local order than is usually observed for hydrocarbon glasses. Such ordering would presumably be more pronounced in the benzene glass where the possibility of π-bonded charge transfer complexes exists.

Calderazzo[6] has reported a number of reactions of $V(CO)_6$ with aromatic hydrocarbons. With benzene, the red crystalline compound $[V(CO)_4(C_6H_6)][V(CO)_6]$ is found. However, this reaction is very slow and did not affect early magnetic susceptibility results[7] so it was assumed not to be important in the ESR experiments reported here. The time elapsed between preparation of the sample and quick-freezing was never more than thirty minutes (see experimental section). Further, the ionic compound $[V(CO)_4(C_6H_6)][V(CO)_6]$ is insoluble in hydrocarbons[6] and in no case was solid formation noted during the sample preparation. No magnetic susceptibility data on this compound is available.

In addition to the shift of the isotropic g-values in going from pentane to benzene glasses, there was a corresponding shift of the anisotropic components ($g_\perp$ from 2.103 to 2.126 and $g_\parallel$ from 1.981 to 2.023). These shifts have interesting implications for the mechanism of the Jahn-Teller distortion in $V(CO)_6$, which will be discussed following the g-value calculations later in this section.

2. Lineshapes and the Exchange Interaction

Most ESR spectra of paramagnetic ^{51}V compounds show a characteristic hyperfine structure of eight lines (or multiples thereof) owing to the interaction of the unpaired electron(s) with the nuclear spin of ^{51}V (I=7/2). For example, the solution spectrum of the $3d^5$ complex $V(dipyridyl)_3$ consists of eight lines with a coupling constant A = 83.5 gauss.[8] The magnitude of this A-value is typical of those observed for other vanadium compounds. If such hyperfine structure existed in the $V(CO)_6$ spectra, it was unresolved. Therefore, an upper limit for the A-value would be about one-seventh of the linewidth, or 30 gauss or less for the widest lines observed.

A more reasonable explanation for the absence of hyperfine structure in these spectra is provided by postulating the existence of a strong exchange interaction. An interaction of the form $-2J\ \underline{S}_1 \cdot \underline{S}_2$ was first suggested by Gorter and Van Vleck[9] to explain the linewidths observed in concentrated paramagnetic salts. In these systems, the linewidth was much less than predicted on the basis of dipolar broadening, and Van Vleck showed that the smaller width was a consequence of electron exchange between the orbitals of different molecules. This has the effect of averaging out some of the dipolar width and led to the use of the term "exchange narrowing" to describe this phenomenon.

Further work on the theory of the exchange interaction[10] in ESR spectra has shown that if exchange is between similar ions or molecules, it will narrow a single absorption line in the center and broaden it in the wings. As a Gaussian lineshape is obtained from the dipolar interaction alone, the change of an absorption line from Gaussian to Lorentzian shape can be taken as very good evidence of exchange narrowing.[11] In the

presence of hyperfine structure, Kivelson[12] found that as J approached A in magnitude, the hyperfine structure first broadened and then coalesced into a single broad line when $J \sim A$. For $J > A$, the line narrows further as described above. Thus the absence of observable hyperfine structure can be taken as evidence for strong exchange.

In order to explain the unusual lineshape variations observed in the $V(CO)_6$ spectra, the effect of exchange on the g-value anisotropy must also be considered. The basic idea of the theory for the linewidth with exchange narrowing first suggested by Gorter and Van Vleck[9] is that the dipolar interaction is randomly modulated by the exchange interaction. This occurs in much the same way as the dipolar interaction is modulated by tumbling in liquids,[13] except in the latter case the radius vector connecting a pair of dipoles varies in a random fashion. In the exchange case, the interaction modulates the spin orientation rather than the spatial coordinates. Nonetheless, the effect should be the same as in tumbling, i.e. the exchange interaction should average the g-value anisotropies and cause the line to become more isotropic, in addition to narrowing its apparent width.

Figure 18a shows the spectrum of pure $V(CO)_6$ which was obtained at 1.34°K (cf. Fig. 15). In addition, the lineshapes expected for both Gaussian and Lorentzian lines have been superimposed on the low-field side. These curves were plotted using the lineshape functions

$$f(x) = (8/3)\,\frac{a}{1 - x^2/3a^2} \qquad \text{(Lorentzian)}$$

$$f(x) = 1.65\, a\, e^{-\left(\frac{x^2}{2a^2}\right)} \qquad \text{(Gaussian)}$$

as described in the Varian V-4502 Spectrometer Manual[14] where a is half

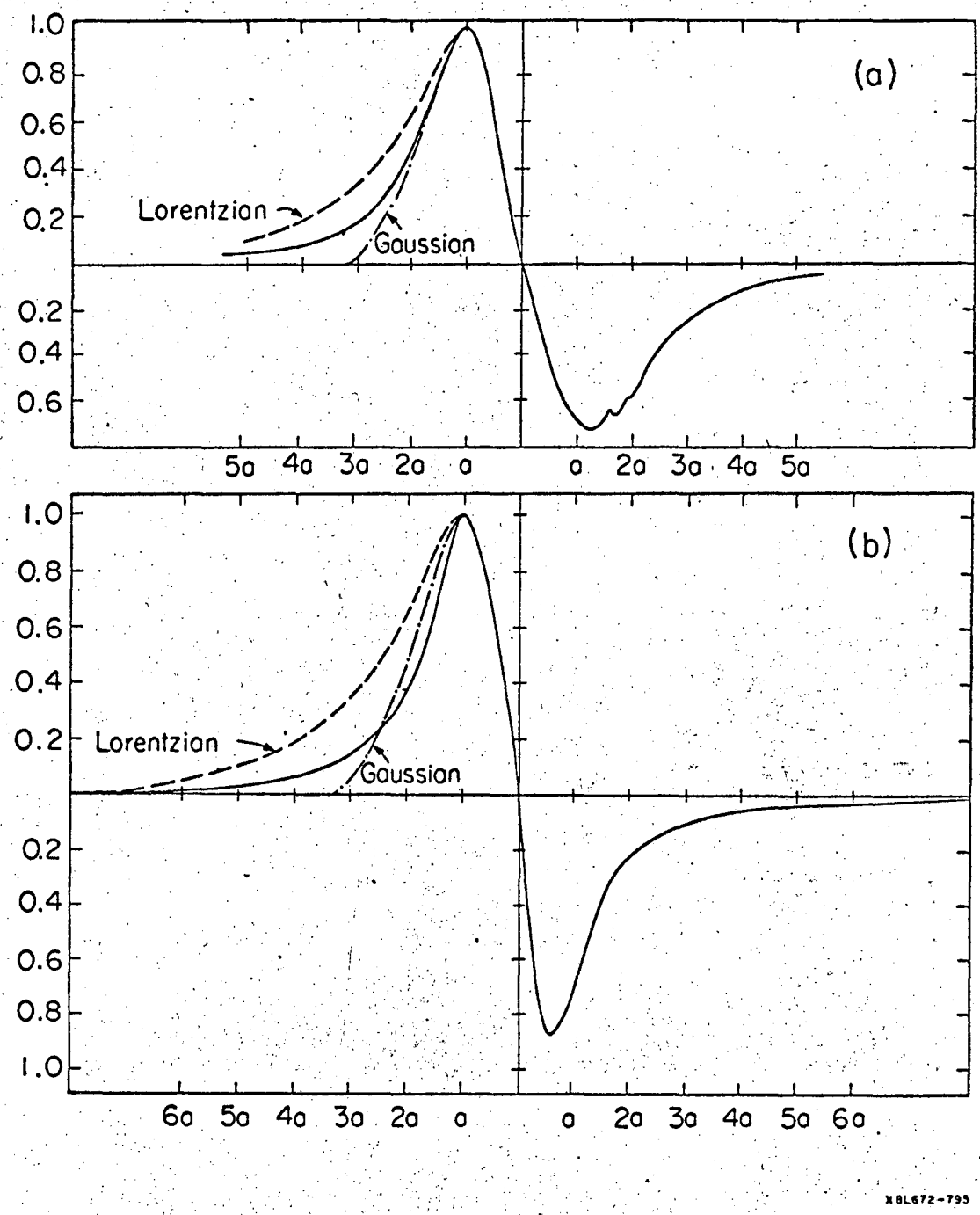

Fig. 18. A comparison of the experimental lineshape observed for $V(CO)_6$ and theoretical Gaussian and Lorentzian lineshapes; (a) pure $V(CO)_6$; (b) $V(CO)_6$ in n-pentane (-16 DB).

the width from peak to peak along the x-axis. This plot shows clearly that the line does not have the Gaussian lineshape expected for the concentrated $V(CO)_6$ sample, especially in the wings. Further, the approach in the wings toward the broader Lorentzian curve, coupled with the absence of the expected hyperfine structure, provides strong evidence for the existence of an exchange interaction in this system.

That a strong exchange interaction existed in the pure $V(CO)_6$ samples is not surprising but, as Fig. 18b shows, there was good evidence for the presence of exchange in the glass samples as well. This plot shows the medium-power spectrum of $V(CO)_6$ in n-pentane (cf. Fig. 17b) on which the predicted lineshapes for both Lorentzian and Gaussian lines of the same width have again been superimposed. In this case, it can be seen that, in addition to the broadening in the wings, there was a pronounced narrowing near the center of the line from the predicted Gaussian lineshape. These effects were less noticeable for the benzene sample. Yet, no hyperfine structure was observed in any of the glass spectra.

In a qualitative way, it is easy to see why the exchange process is more effective for averaging hyperfine structure than for averaging g-value anisotropy. The disappearance of hyperfine structure requires only that the exchange occur between any $V(CO)_6$ molecules, regardless of their relative orientation. However, to average the g-value anisotropy, the exchange must occur between $V(CO)_6$ molecules having different orientations. These arguments would then suggest on a purely statistical basis that the g-value anisotropy would be more effectively averaged in a more concentrated sample where the probability of having nearest neighbors with a different spin orientation is higher. (This dependence of J on the relative orientations of the molecules has led to the use of the term

'anisotropic exchange' and has been discussed briefly by Kivelson.[12]) The observation that the pure $V(CO)_6$ spectra are, in general, more isotropic than those in glass samples is consistent with the above interpretation and we therefore conclude that the exchange is less effective in the glass samples.

Since the paramagnetic molecules in glass samples are assumed to be rather far apart, the presence of any exchange (albeit weak) in these systems must be explained. One likely possibility is that the exchange interaction is effective over a much longer range than is normally observed in dilute paramagnetic systems. The reason for this could be that the $V(CO)_6$ molecule does not formally contain any charged ions. For example, in contrast to the pure $V(CO)_6$ spectra, the anisotropies in $\underset{\sim}{g}$ are still present in the ESR spectra of pure polycrystalline samples of $CuSO_4$ and $CuCl_2$,[3a] both of which are highly ionic. As these anisotropies are of about the same order as in $V(CO)_6$, it can be concluded that exchange in the covalent hexacarbonyl samples is much stronger and fairly long-range.[15] Thus it could be present even in dilute glasses.

A second explanation for the presence of an exchange term in the Hamiltonian of the glass samples is that there could have been a coagulation process which occurred when the samples were frozen. Similar effects have been observed in the preparation of frozen aqueous solutions.[16] This would give rise to paramagnetic sites composed of a single $V(CO)_6$ surrounded by a few other $V(CO)_6$ molecules rather than being completely surrounded by the inert matrix, and would result in some exchange. Table VI gives the linewidths measured for the various $V(CO)_6$ samples. The width in the medium-power spectrum in n-pentane was ~ 30% less than that of the pure $V(CO)_6$ sample. This suggests that the dipolar width was less for the

Table VI. Linewidths measured for $V(CO)_6$

Medium	Width, gauss	How measured
pure $V(CO)_6$	132.8	peak-to-peak
benzene glass	159.7	$H_{\parallel} - H_{\perp}$
pentane glass, low power	215.3	$H_3 - H_1$
pentane glass, medium power	100.1	peak-to-peak
pentane glass, high power	200.1	$H_{\parallel} - H_{\perp}$

glass sample but does not favor one of the above explanations over the other. The remaining widths in Table VI were taken from anisotropic spectra where a 'linewidth' was more difficult to estimate.

Benzene was selected as a matrix for this work because it was felt that the coagulation effects, if they occurred at all, would be less pronounced than in the pentane glass, which freezes at a much lower temperature. No meaningful comparison between the widths in benzene and pentane could be made but, as noted above, the lineshape in benzene was much less affected by exchange. These effects could be studied in more detail with the aid of a computer program to estimate the linewidths in the anisotropic spectra.

3. Effect of Power Saturation in Exchanged Systems

Goldsborough, et al.[17] have observed that in pure crystalline free radical systems such as DPPH, a pronounced narrowing of the resonance line

occurs as the microwave power is increased to the point of saturation. This effect was more noticeable in samples with higher exchange interaction. Their results were interpreted using the three-reservoir model of Bloembergen and Wang.[18] As similar, but not entirely analogous, effects were observed in the $V(CO)_6$ spectra, the Bloembergen model will be introduced here and will be followed by an interpretation of the $V(CO)_6$ results in terms of this model.

The three-reservoir model, which has also been discussed by Van Vleck,[19] assumed the existence of two different temperatures within the spin system; (1) θ_Z, which describes the temperature of the Zeeman system with the Hamiltonian $\mathcal{H}_Z = g\beta HS_Z$ and (2) θ_E, which describes the distribution of energy in the exchange system with $\mathcal{H}_E = -2J\ \underline{S}_1 \cdot \underline{S}_2$. Neither temperature need necessarily be the same as that of the lattice vibrations θ_L, whose Hamiltonian is denoted by $\mathcal{H}_L$. The three-reservoir model, in which the reservoirs are assigned the temperatures θ_Z, θ_E, and θ_L, are shown in Fig. 19 which is taken from the paper of Goldsborough, et al.[17] Each pair of reservoirs is coupled by a relaxation time which describes the rate of energy transfer from one system to the other. Energy transfer occurs between the Z and E systems because of dipolar interaction, between the E and L systems because of the modulation of exchange or dipolar energy by lattice vibrations, and between the Z and L systems because of the modulation of dipolar energy by lattice vibrations. In a strongly-exchanged system at liquid helium temperatures, the transfer of energy via the direct Zeeman-lattice process ('normal' spin-lattice relaxation) is assumed to be negligible compared to the indirect route T_{1a} followed by T_{1b}. This is because lattice vibrations are a small perturbation compared to the exchange interaction at these temperatures and T_{1a} can result from dipolar interaction

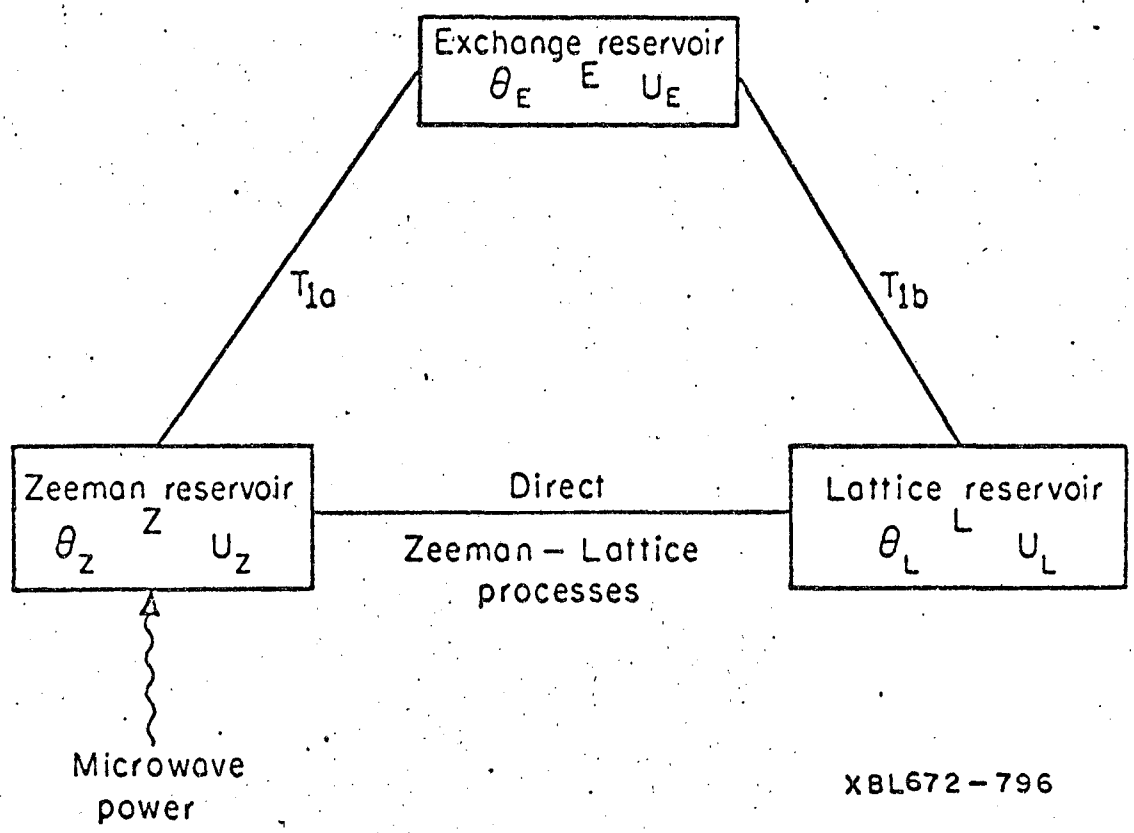

Fig. 19. The three-reservoir model of Bloembergen and Wang.[17,18]

without invoking lattice vibrations. Consequently, the relaxation times for such a system are determined by the rate at which energy exchange occurs via the exchange reservoir.

Following Goldsborough, et al.,[17] the internal energies U_Z and U_E of the Zeeman and exchange reservoirs are defined by

$$U_Z = -K_Z/\theta_Z \; ; \qquad U_E = -K_E/\theta_E \tag{1}$$

Then, ignoring direct processes, the steady-state energy flow from left to right in Fig. 19 is given by the equations

$$\frac{dU_Z}{dt} = 0 = -\gamma^2 H_1^2 T_2 U_Z(\theta_Z) - \frac{1}{T_{1a}} [U_Z(\theta_Z) - U_Z(\theta_E)] \tag{2}$$

$$\frac{1}{T_{1a}} [U_Z(\theta_Z) - U_Z(\theta_E)] = \frac{1}{T_{1b}} [U_E(\theta_E) - U_E(\theta_L)] \tag{3}$$

where, in general, T_1 is defined as the inverse decay rate of internal energy and the other symbols have their usual meaning. The observed ratio of Zeeman and lattice temperatures is interpreted as the usual saturation factor,

$$\theta_Z/\theta_L = 1 + \gamma^2 H_1{}^2 T_2 (T_1)_{eff} \tag{4}$$

Equations (2), (3), and (4) yield

$$\theta_E/\theta_L = \frac{1 + \gamma^2 H_1{}^2 T_2 (T_1)_{eff}}{1 + \gamma^2 H_1{}^2 T_2 T_{1a}} \tag{5}$$

where

$$(T_1)_{eff} = T_{1a} + (K_Z/K_E)\, T_{1b} \tag{6}$$

and T_{1a} is given by the approximate relationship

$$\frac{1}{T_{1a}} \approx \frac{1}{T_2} \exp\left(-\omega_Z^2/\omega_E^2\right). \tag{7}$$

This model can now be used to interpret the behavior of the $V(CO)_6$ n-pentane spectrum. For strong exchange, $\omega_E \gg \omega_Z$ (where $\omega_E = U_E/\hbar$, etc.) and, from Eq. (7), $1/T_{1a} \approx 1/T_2$. Thus the linewidth is determined by T_{1a}. This is assumed to be the case in $V(CO)_6$ at normal power levels. Now, if there is good thermal contact between the lattice and the surrounding bath of liquid helium, the effect of saturation will be to make $\theta_E \gg \theta_L$. Then, from Eq. (5),

$$(T_1)_{eff} >> T_{1a}. \tag{8}$$

With this condition, Eq. (6) becomes

$$(T_1)_{eff} = (K_Z/K_E)\, T_{1b}. \tag{9}$$

If it is assumed that the Zeeman and exchange energies are about the same order of magnitude, $K_Z/K_E \approx 1$ and

$$(T_1)_{eff} = T_{1b}. \tag{10}$$

Therefore, since $T_{1b} >> T_{1a}$, the effect of saturation will be a narrowing of the lines, in agreement with the observations of Goldsborough, et al.[17] Bloembergen and Wang[18] also give convincing arguments that $T_{1a} < T_{1b}$ in general. However, because the heat capacity of the exchange system is much larger than that of the Zeeman system, under normal conditions (low power) the bottleneck in the relaxation process arises from T_{1a} rather than T_{1b}. Thus θ_E is much closer to θ_L than θ_Z in systems with large exchange energy. Only in cases where θ_E becomes large compared to θ_L will the relaxation time $(T_1)_{eff}$ be determined by T_{1b}. This is accomplished by saturation.

Thus, one possible interpretation of the appearance of the sharp parallel and perpendicular bands when the $V(CO)_6$/n-pentane sample is saturated (cf. Fig. 17c) is that the inherent linewidth is decreased. This reveals the g-value anisotropy directly. An important point to note is that the exchange is not any more effective when the line is saturated, i.e., the g-value anisotropy is still present. The effect of saturation is rather to create a bottleneck in the exchange-lattice process and this narrows the line.

A second interpretation of this behavior which cannot be ruled out on the basis of these experiments is that there were two "kinds" of paramagnetic molecules in the $V(CO)_6$/n-pentane samples, those which were exchanged and those which were not. Effectively this means that the g-value anistropy was averaged out for some molecules and not for others. Then, when the microwave power was increased, the signal due to the exchanged molecules was saturated and diminished in intensity whereas that for the unexchanged ones, for some reason, was not. The net signal would then be due mostly to the latter molecules and the anisotropic components would be relatively strong. It is also possible that some of the m_I states could be saturated more readily than others, thus producing a spectrum consisting of transitions for only one or two m_I values. This would reduce the overall width but might also shift the spectrum.

4. Calculation of g-values.

The previous discussion of the ESR properties of $V(CO)_6$ has revealed that an anisotropic g-tensor has been assigned to this molecule. Because of the role of exchange in these systems, this anisotropy was not always apparent from the observed lineshapes. However, experiments at high incident power levels in some of these samples have yielded spectra from which the g-value anisotropy could be obtained explicitly. These values were found to be $g_{\parallel} = 1.981$, $g_{\perp} = 2.103$ for the pentane glass samples and $g_{\parallel} = 2.023$, $g_{\perp} = 2.126$ for the benzene glass samples.

The observed anisotropy in g indicates that the crystal field possesses a symmetry lower than octahedral. The existence of such a distortion in $V(CO)_6$ is in apparent agreement with the theorem of Jahn and Teller[20] which has been discussed earlier. When a molecule is in a crystal lattice, it may not be possible to decide whether the actual distortion is due mainly to its environment, ot its bonding, or whether it is a manifestation of the Jahn-Teller effect. However, knowing that a free molecule will distort, it is of great interest to consider this distortion to see whether it is similar to that observed. Since the g-value reflects not only spin but also orbital contributions to the magnetic moment, and because the orbital contribution is modified by the crystal field, a calculation of the g-value can reveal much about the nature of the Jahn-Teller distortion in the free molecule. In $V(CO)_6$, with two principal g-values, the symmetry of the crystal field must be axial. This can arise from either a trigonal or tetragonal distortion of the octahedral field, and the g-value calculation can, in favorable cases, allow one to decide which distortion is present in $V(CO)_6$ and to assign a magnitude to this effect.

The methods available for calculating g-values have been discussed by many authors.[21] The perturbation-theory approach which will be employed here is originally due to Pryce[22] and has been discussed in detail by Carrington and Longuet-Higgins.[23] The method of Pryce, as outlined by Ballhausen,[24] does not require the determination of first-order wavefunctions but instead uses zero-order wavefunctions obtained from crystal-field theory; consequently, the g-values which result are correct only to first-order in the spin-orbit and crystal-field parameters. Although this approximation was found to be adequate for the tetragonal case, the g-value calculation for the trigonal distortion required a second-order treatment (vide infra). For this reason, the latter method[23] will be outlined here and then used for both the tetragonal and trigonal cases.

The Hamiltonian for a paramagnetic ion under the influence of the crystalline electric field, the spin-orbit coupling, and the external magnetic field is written as follows

$$\mathcal{H} = \mathcal{H}_o + \mathcal{H}' \tag{11}$$

where the unperturbed system $\mathcal{H}_o$ is characterized by energy levels which are obtained from strong crystal field theory. To each of these levels is assigned a zero-order wavefunction which is some linear combination of the 3d wavefunctions. Following Pryce,[22] we assume that the lowest orbital level is non-degenerate apart from the (Kramers) spin degeneracy; in a broad sense, this is a consequence of the Jahn-Teller theorem.

The perturbation Hamiltonian for electron is taken to be

$$\mathcal{H}' = \xi\, \underline{L} \cdot \underline{S} + \beta \underline{H} \cdot (\underline{L} + g_e\, \underline{S}) \tag{12}$$

where ξ is the one-electron spin-orbit parameter which is always positive and g_e is the free-electron g-value, 2.0023. All other terms in Eq. (12)

have their usual meaning. If the unperturbed level is non-degenerate, then the contribution of the spin-orbit coupling vanishes in first order,[22] leaving only the contribution from the external field. The matrix elements of the field-dependent term can then be evaluated in general using the zero-order wavefunctions and g-value expressions correct to first-order in ξ and the crystal-field parameters are obtained.[22] However, we desire to carry this calculation to second-order in these parameters.

The effect of the spin-orbit term in second-order is non-vanishing and gives rise to a mixing of some of the zero-order wavefunctions and a splitting of the corresponding levels. This effect can be treated using first-order perturbation theory,[25] according to which the perturbation $\xi\, \underline{L} \cdot \underline{S}$ changes the state ψ_o into

$$\psi_o' = a\,\psi_o + \Sigma_i\, c_i\, \psi_i \tag{13}$$

with

$$a^2 + \Sigma_i\, c_i^2 = 1 \tag{14}$$

The mixing coefficients c_i are then given by

$$c_i = \frac{\langle i \mid \xi\, \underline{L} \cdot \underline{S} \mid o \rangle}{E_o - E_i} \tag{15}$$

The first order wavefunctions constructed in this way are then used to obtain the matrix elements of the Zeeman interaction, $\underset{\sim}{E} = \beta \underline{H} \cdot (\underline{L} + g_e \underline{S})$. To do this, the Zeeman term is re-written as (taking $g_e \sim 2$)

$$\beta(\underline{L} + 2\underline{S}) \cdot \underline{H} = \beta[\Sigma_i\, (L_i + 2S_i)\, H_i] \quad i = x,y,z \tag{16}$$

$$\beta(\underline{L} + 2\underline{S}) \cdot \underline{H} = \beta\,[g_{zz}(H_z S_z) + g_{xx}(H_x S_x) + g_{yy}(H_y S_y)] \qquad (17)$$

The matrix elements of Eq. (16) are then calculated and from Eq. (17) it is easy to see that

$$g_{zz} = g_{\parallel} = \frac{\beta\langle 0_{,}^{'} + \frac{1}{2}|H_z(L_z + 2S_z)|0_{,}^{'} + \frac{1}{2}\rangle - \beta\langle 0_{,}^{'} - \frac{1}{2}|H_z(L_z + 2S_z)|0_{,}^{'} - \frac{1}{2}\rangle}{\beta H_z} \qquad (18)$$

where $\langle 0_{,}^{'} + 1/2\,|$, etc. are the first-order wavefunctions of the ground-state doublet with $m_s = +1/2$, etc. The $g_{xx} = g_{\perp}$ value is obtained in a similar manner. This approach is valid only if the crystal-field splittings $(E_o - E_i)$ are large compared to the perturbation $\xi\,\underline{L} \cdot \underline{S}$, which for $V^{(0)}$ is about 100 cm^{-1} (<u>vide infra</u>).

As described in Chapter II, the five degenerate d-orbitals of a transition metal ion or molecule such as $V(CO)_6$ are split into groups of three and two orbitals by a strong crystal field of octahedral symmetry. The orbital triplet lies below the orbital doublet by an energy 10 Dq as shown in Fig. 20. This diagram also illustrates how a small tetragonal distortion further splits the doublet and triplet manifolds. With five unpaired electrons in the strong-field approximation, the lower levels are filled first and the configuration is $(e_g)^4(b_{2g})^1$. The splitting of the lower t_{2g} triplet in this way corresponds to an elongation along the C_4 axis of the octahedron and leaves an orbital singlet, $^2B_{2g}$, as the ground state. If the tetragonal distortion were a compression along the C_4 axis, the splitting Δ_2 would be inverted and the electronic configuration would be $(b_{2g})^2(e_g)^3$, leaving a degenerate ground state. As this would be further distorted according to the Jahn-Teller theorem, and would therefore result in three principal g-values, the tetragonal elongation is preferred. In order to be able to treat the $(e_g)^4(b_{2g})^1$ con-

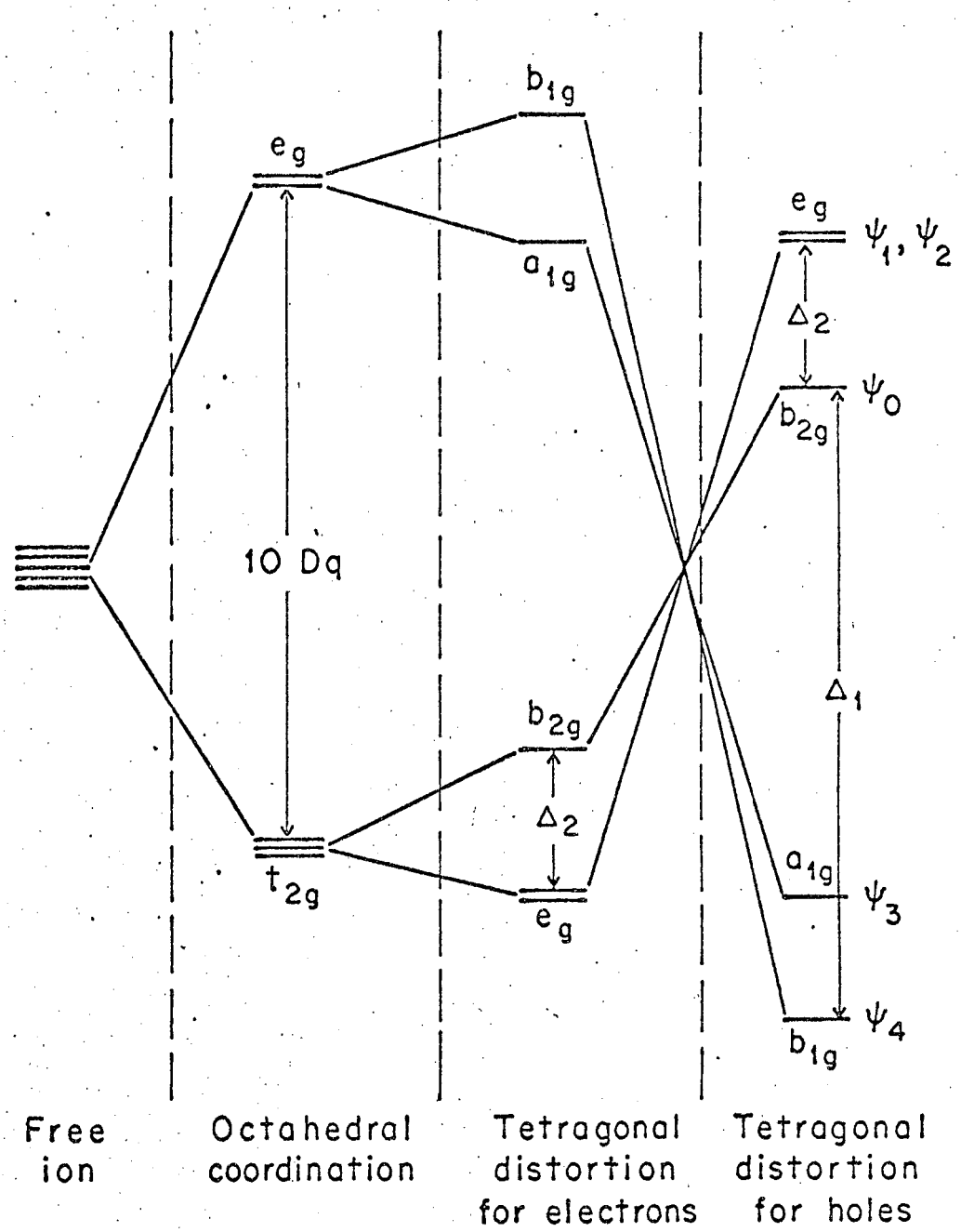

XBL672-892

Fig. 20. Crystal field energy level diagram for $V(CO)_6$ showing the effect of a tetragonal distortion.

figuration as a single electron problem, the whole diagram is inverted about its center of gravity. This configuration can then be considered as a single hole in the t_{2g} shell, i.e., $(b_{2g})^1$, by reversing the sign of the spin-orbit coupling constant.[26] This is indicated on the extreme right of Fig. 20, where the levels are labeled with their respective zero-order wavefunctions and the transformation properties of the wavefunctions under the symmetry operations of the tetragonal group, D_{4h}.

The zero-order wavefunctions for the tetragonal distortion are taken to be the real d-wavefunctions[27]

$$\begin{aligned}
\psi_o &= d_{xy} = \frac{1}{i\sqrt{2}}(|2> - |-2>) \\
\psi_1 &= d_{yz} = -\frac{1}{i\sqrt{2}}(|1> + |-1>) \\
\psi_2 &= d_{xz} = -\frac{1}{\sqrt{2}}(|1> - |-1>) \\
\psi_3 &= d_{z^2} = |0> \\
\psi_4 &= d_{x^2-y^2} = \frac{1}{\sqrt{2}}(|2> + |-2>)
\end{aligned} \tag{19}$$

where $|m_\ell> = R(r)\, Y_2^{m_\ell}$ and the axis of quantization is the C_4 axis along which the octahedron is elongated. Ignoring the spin-orbit interaction for the moment, the ground state may be represented by the pair of symbols

$$\begin{aligned}
|0, 1/2> &= \psi_o \\
|0, -1/2> &= \bar{\psi}_o
\end{aligned} \tag{20}$$

where the pair of numbers in each ket represent the values of m_ℓ and m_s, respectively. When spin-orbit coupling is taken into account these expressions are modified slightly by the admixture of small amounts of states with different values of m_ℓ and m_s.

To see which states mix with the ground state doublet, the expression Eq. (15) is used to determine which of the matrix elements $\langle i|\xi\, \underline{L} \cdot \underline{S}|0\rangle$ and $\langle i|\xi\, \underline{L} \cdot \underline{S}|\bar{0}\rangle$ are non-zero. This can be done using group theoretical arguments, for only if the direct-product representation $\Gamma_i \times \Gamma(\xi\, \underline{L}\cdot\underline{S}) \times \Gamma_o$ contains the totally-symmetric representation A_1 will the matrix element be non-zero. A more tedious way is just to calculate the matrix elements using the expansion

$$\xi\, \underline{L} \cdot \underline{S} = \xi/2\, (L_+S_- + L_-S_+) + \xi\, L_zS_z \tag{21}$$

and the well-known formulae[28]

$$\begin{aligned} L_+|m_\ell\rangle &= \sqrt{L(L+1) - m_\ell(m_\ell+1)}\;\; |m_\ell + 1\rangle \\ L_-|m_\ell\rangle &= \sqrt{L(L+1) - m_\ell(m_\ell-1)}\;\; |m_\ell - 1\rangle \\ L_z|m_\ell\rangle &= m_\ell|m_\ell\rangle \end{aligned} \tag{22}$$

and the analogous ones for S_+, S_- and S_z. The resulting first-order (real) wavefunctions are

$$\begin{aligned} \psi_o' &= a\psi_o + b\bar{\psi}_1 + c\bar{\psi}_2 + d\psi_4 \equiv |\alpha\rangle = \langle\alpha| \\ \bar{\psi}_o' &= e\bar{\psi}_o + f\psi_1 + g\psi_2 + h\bar{\psi}_4 \equiv |\beta\rangle = \langle\beta| \end{aligned} \tag{23}$$

where a, b, c, etc., are the yet-to-be determined mixing coefficients. Thus the ground state mixes with the states $|1\rangle$, $|2\rangle$ and $|4\rangle$ as

predicted by group theory since $\Gamma(\xi\, \underline{L} \cdot \underline{S}) = (A_2 + E)$[29] in D_{4h} and the direct products

$$B_2 \times (A_2 + E) \times E$$

$$B_2 \times (A_2 + E) \times B_2$$

each contain the totally symmetric representation A_1.

To calculate the g-values with these first-order wavefunctions, the matrix elements of $\underset{\sim}{E}'_z = \beta(L_z + 2S_z)H_z$ and $\underset{\sim}{E}'_x = \beta(L_x + 2S_x)H_x$ (cf. Eq. (16)) are calculated using Eqs. (22). The results for the z-component of the Zeeman term are given in Table VIIa and those for the

Table VIIa. Matrix elements of $\underset{\sim}{E}'_z/\beta H_z = (L_z + 2S_z)$; D_{4h}

	$\lvert\beta\rangle$	$\lvert\alpha\rangle$
$\langle\beta\rvert$	$[(-1 + 2f^2 + 2g^2)$ $-2i(2eh + fg)]$	0
$\langle\alpha\rvert$	0	$[(1 - 2b^2 - 2c^2)$ $- 2i(2ad + bc)]$

x-component in Table VIIb, where the equalities (cf. Eq. (14))

Table VIIb. Matrix elements of $\underset{\sim}{E}'_x/\beta H_x = (L_x + 2S_x)$; D_{4h}.

	$\lvert\beta\rangle$	$\lvert\alpha\rangle$
$\langle\beta\rvert$	0	$[(cg + dh - ae - bf)$ $+ i(ag + bh + ce + df)]$
$\langle\alpha\rvert$	$[(cg + dh - ae - bf)$ $+ i(ag + bh + ce + df)]$	0

$$a^2 = 1 - b^2 - c^2 - d^2$$
$$e^2 = 1 - f^2 - g^2 - h^2 \qquad (24)$$

have been used to simplify the matrix elements. Of course, $\underset{\sim}{E}'_x = \underset{\sim}{E}'_y$, as it must for an axial Hamiltonian. The coefficients b, c, d and f, g, h are found using the expression Eq. (15) and are tabulated in Table VIII. The coefficients a and e are as given in Eqs. (24).

Table VIII. Mixing Coefficients for the Ground-State Wave-functions in a Tetragonal Field. (cf. Eq. (23)).

$b = \frac{\xi}{2\Delta_2}$	$f = -\frac{\xi}{2\Delta_2}$
$c = -\frac{i\xi}{2\Delta_2}$	$g = -\frac{i\xi}{1\Delta}$
$d = +\frac{i\xi}{\Delta_1}$	$h = -\frac{i\xi}{\Delta_1}$

The parallel g-value is obtained from Eq. (18) and the matrix elements listed in Table VIIa. Thus,

$$g_{\parallel} = [(1 - 2b^2 - 2c^2) - 2i(2ad + bc)]$$
$$- [(-1 + 2f^2 + 2g^2) - 2i(2eh + fg)]$$

Substituting the appropriate coefficients from Table VIII, this becomes

$$g_{\parallel} = 2 - \frac{\xi^2}{\Delta_2^{\,2}} + 4a\left(\frac{\xi}{\Delta_1}\right) + 4e\left(\frac{\xi}{\Delta_1}\right)$$

Further, since (from Table VIII and Eq. (24))

$$a = |e| = \sqrt{1 - \xi^2/\Delta_1^2} \approx 1$$

this becomes

$$g_{\parallel} = 2 + 8\,(\xi/\Delta_1) - (\xi^2/\Delta_2^2)$$

or, in terms of the shift from the free electron value

$$\Delta g_{\parallel} = g_{\parallel} - g_e = 8\,(\xi/\Delta_1) - (\xi^2/\Delta_2^2) \qquad (25)$$

From Table VIIb, the matrix $\underset{\sim}{E}'_x$ is seen to be off-diagonal with zeroes along the diagonal. Therefore, the ground Kramers doublet splits into the sum and difference of the off-diagonal elements with a separation of $g_{\perp}\beta H_x$. This leads to

$$\Delta g_{\perp} = g_{\perp} - g_e = -2(\xi/\Delta_2) - 2(\xi^2/\Delta_1\Delta_2) + 2(\xi^2/\Delta_1^2) \qquad (26)$$

To first-order, the expressions, Eqs. (25) and (26) agree with those for $g_{\parallel}$ and $g_{\perp}$ in a tetragonal field recently published[30] in a paper on the $3d^5$ systems $Mn(CN)_5NO^{-2}$ and $Cr(CN)_5NO^{-3}$.

The crystal-field splitting scheme for the case of a trigonal distortion is shown in Fig. 21. As in the tetragonal case, the distortion along a C_3 axis of the octahedron leaves an orbital singlet as the ground state. Here, the configuration for holes is $(a_{1g})^1$ and the ground state is $^2A_{1g}$. The levels on the extreme right are labeled with their respective zero-order wavefunctions and their transformation properties under the symmetry operations of the trigonal group, D_{3d}.

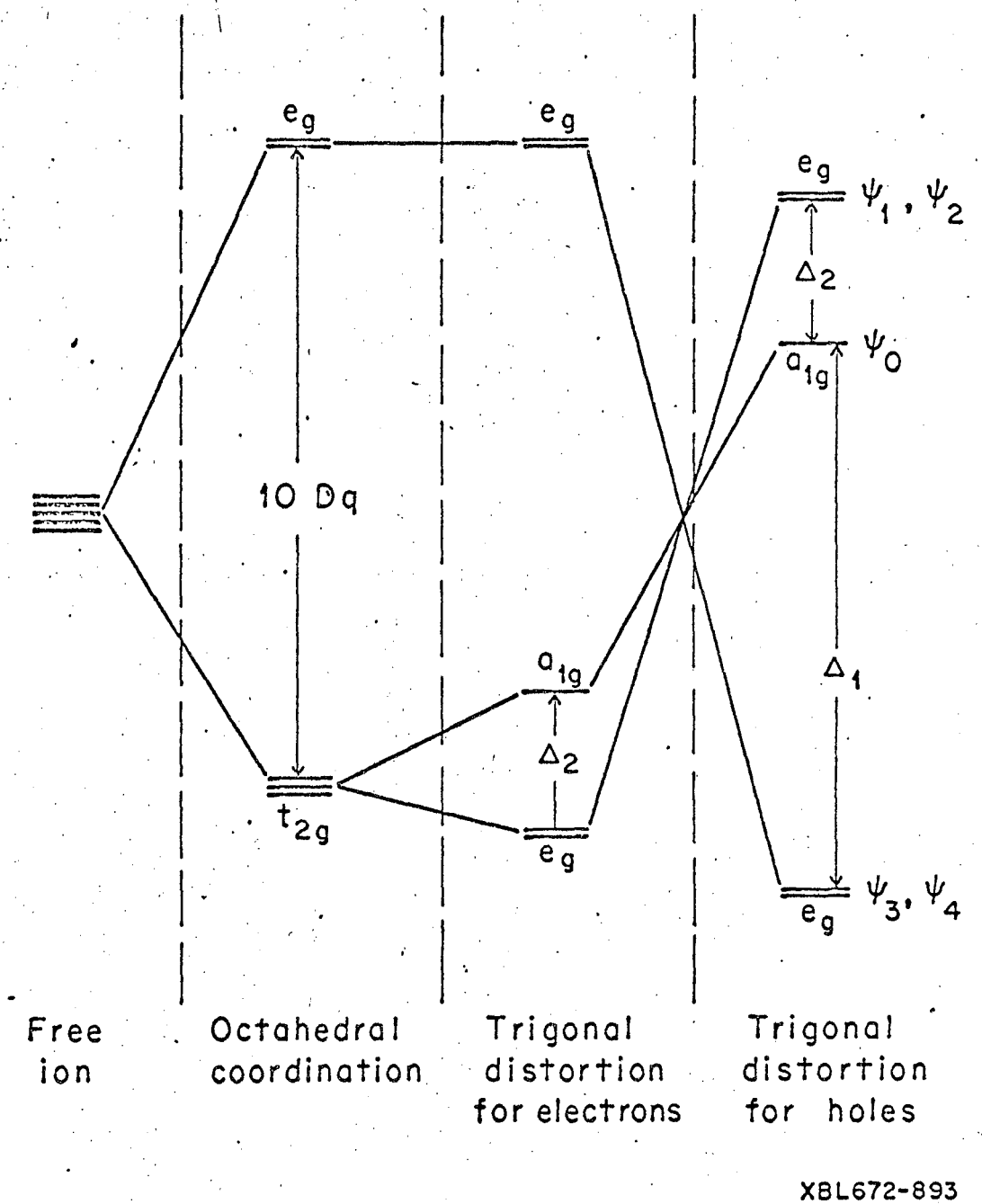

XBL672-893

Fig. 21. Crystal field energy level diagram for $V(CO)_6$ showing the effect of a trigonal distortion.

The trigonal wavefunctions are obtained using a C_3 axis as the axis of quantization and are given by Ballhausen.[31] They are

$$\psi_o = \psi_o^* = |0\rangle$$

$$\psi_1 = \psi_2^* = \frac{1}{\sqrt{3}} \left(\sqrt{2}|2\rangle - |-1\rangle \right)$$

$$\psi_2 = \psi_1^* = \frac{1}{\sqrt{3}} \left(\sqrt{2}|-2\rangle + |1\rangle \right) \qquad (27)$$

$$\psi_3 = \psi_4^* = \frac{1}{\sqrt{3}} \left(|2\rangle + \sqrt{2}\,|-1\rangle \right)$$

$$\psi_4 = \psi_3^* = \frac{1}{\sqrt{3}} \left(|-2\rangle - \sqrt{2}\,|1\rangle \right)$$

where $|m_\ell\rangle = R(r)\, Y_2^{m_\ell}$ as before. The relations between the wavefunctions and their complex conjugates have also been indicated in Eq. (27) since they are in general not real.

Using the methods employed earlier, the first-order wavefunctions are found to be the linear combinations

$$\psi_o' = a\psi_o + b\,\bar{\psi}_1 + c\psi_3 = |\alpha\rangle$$

$$\bar{\psi}_o' = d\bar{\psi}_o + e\psi_2 + f\psi_4 = |\beta\rangle \qquad (28)$$

$$(\psi_o')^* = a\psi_o + b\bar{\psi}_2 + c\bar{\psi}_4 = \langle\alpha|$$

$$(\bar{\psi}_o')^* = d\bar{\psi}_o + e\psi_1 + f\psi_3 = \langle\beta|$$

where the coefficients a, b, etc., are assumed to be real. The set of wavefunctions, Eq. (28) are then used to calculate the matrix elements of the Zeeman interaction. Tables IXa and IXb give the results for

Table IXa. Matrix elements of $\underset{\sim}{E}'_z/\beta H_z = (L_z + 2S_z)$; D_{3d}.

	$\lvert\beta\rangle$	$\lvert\alpha\rangle$
$\langle\beta\rvert$	$-d^2$	0
$\langle\alpha\rvert$	0	a^2

Table IXb. Matrix elements of $\underset{\sim}{E}'_x/\beta H_x = (L_x + 2S_x)$; D_{3d}.

	$\lvert\beta\rangle$	$\lvert\alpha\rangle$
$\langle\beta\rvert$	0	$[ad + be + cf + cd + af - (1/\sqrt{2})(bd + ae)]$
$\langle\alpha\rvert$	$[ad + be + cf + cd + af - (1/\sqrt{2})(bd + ae)]$	0

$\underset{\sim}{E}'_z = \beta(L_z + 2S_z)H_z$ and $\underset{\sim}{E}'_x = \beta(L_x + 2S_x)H_x$ in the trigonal representation. Again,

$$a^2 = 1 - b^2 - c^2$$
$$d^2 = 1 - e^2 - f^2 \tag{29}$$

and $\underset{\sim}{E}'_x = \underset{\sim}{E}'_y$. The mixing coefficients a,b,c and d,e,f are found using Eqs. (15) and (29) and are listed in Table X.

Table X. Mixing Coefficients for the Ground-State Wave-functions in a Trigonal Field. (cf. Eq. (28)).

$a = \sqrt{1 - \frac{\xi^2}{2\Delta_2^2} - \frac{\xi^2}{\Delta_1^2}}$	$d = \sqrt{1 - \frac{\xi^2}{2\Delta_2^2} - \frac{\xi^2}{\Delta_1^2}}$
$b = -\frac{\xi}{\sqrt{2}\Delta_2}$	$e = \frac{\xi}{\sqrt{2}\Delta_2}$
$c = +\frac{\xi}{\Delta_1}$	$f = -\frac{\xi}{\Delta_1}$

The g-values which result are

$$\Delta g_{\parallel} = g_{\parallel} - g_e = -\left(\frac{\xi^2}{\Delta_2^2}\right) - \left(\frac{2\xi^2}{\Delta_1^2}\right) \tag{30}$$

$$\Delta g_{\perp} = g_{\perp} - g_e = -\left(\frac{2\xi^2}{\Delta_2^2}\right) - \left(\frac{4\xi^2}{\Delta_1^2}\right) \tag{31}$$

5. Discussion of g-values.

As the optical spectrum of $V(CO)_6$ has not been assigned (see Chapter II), the expressions for $g_{\parallel}$ and $g_{\perp}$ obtained in the previous section cannot be used to calculate the g-values explicitly. However, by equating these expressions with the observed values, an estimate for the crystal field splitting parameters can be obtained and discussed.

With $\xi < 0$, as assumed in the g-value calculation, the tetragonal expressions become, to first-order

$$\Delta g_{\parallel} = g_{\parallel} - g_e = -8(|\xi|/\Delta_1) \tag{32}$$

$$\Delta g_{\perp} = g_{\perp} - g_e = 2(|\xi|/\Delta_2) \tag{33}$$

The trigonal expressions to second-order are

$$\Delta g_{\parallel} = -(\xi^2/\Delta_2^{\,2}) - 2(\xi^2/\Delta_1^{\,2}) \tag{34}$$

$$\Delta g_{\perp} = -2(\xi^2/\Delta_2^{\,2}) - 4(\xi^2/\Delta_1^{\,2}) \tag{35}$$

A comparison of these equations reveals that, in D_{4h} symmetry, $g_{\parallel} < g_e$ and $g_{\perp} > g_e$, whereas in the trigonal case, both $g_{\perp}$ and $g_{\parallel}$ are less than the free electron value. By inspection of the experimentally-observed g-values in Table XI. it seen that only the n-pentane results are

Table XI. The observed g-values for $V(CO)_6$ in n-pentane and benzene glasses.

Glass	$g_{\parallel}$	$g_{\perp}$
n-pentane	1.981	2.103
benzene	2.023	2.126

consistent with either of these predictions and that the distortion in this case is tetragonal. Because of the agreement between the isotropic g-value observed in the pure $V(CO)_6$ sample (2.063) and that calculated from the anisotropic components in the n-pentane spectrum (2.0627), it

will be assumed here that there is an equivalent distortion in pure $V(CO)_6$. The absence of the anisotropic lineshape in the pure $V(CO)_6$ spectra can be explained by invoking strong exchange effects (vide supra). We shall now estimate the parameters Δ_1 and Δ_2 to see whether the assumption of a tetragonal distortion is reasonable.

Dunn[32] has tabulated the one-electron spin-orbit coupling parameters of the 3d and 4d transition series for the configurations d^x, $d^{x-1}s$, and $d^{x-2}s^2$. His values for $V^{(0)}$ are given in Table XII. These have been

Table XII Values of ξ for $V^{(0)}$ in Various Configurations.[32]

	d^5	d^4s	d^3s^2
ξ, free ion, cm^{-1}	95	130	160

obtained, for the most part, by an interpolation of existing atomic spectral data and are valid only when the field in which the electron moves has spherical symmetry. Further, Owen[33] and others have observed that the spin-orbit parameter ξ appears to be smaller for ions in complexes than for the free ion. Finally, as can be seen from Table XII, the effective value of ξ depends on the extent of admixture of excited states into the ground-state wavefunction. Thus, when accurate crystal-field data are available, ξ is usually treated as an adjustable parameter and the g-value calculation can be used to determine the relative importance of the above effects. However, the data for $V(CO)_6$ will be treated here using the free ion values for $3d^5$.

Taking $|\xi| = 95\ cm^{-1}$ and the following equations

$$g_{\parallel} = 1.981 = 2.002 \left[1 - 4(|\xi|/\Delta_1)\right] \tag{36}$$

$$g_{\perp} = 2.103 = 2.002 \left[1 + (|\xi|/\Delta_2)\right] , \tag{37}$$

we find for the $V(CO)_6$/n-pentane samples (cf. Fig. 20)

$$\Delta_1 = E(b_{1g}) - E(b_{2g}) \leq 36{,}200 \text{ cm}^{-1} \ (2760 \text{ Å})$$

$$\Delta_2 = E(b_{2g}) - E(e_g) \leq 1{,}880 \text{ cm}^{-1}$$

(If the value $\xi = 80$ cm^{-1} is used, these splittings are 30,500 and 1590 cm^{-1}, respectively.) The value of Δ_1 found in this way is in good agreement with values of 10 Dq ($\sim\Delta_1$) observed for other low-spin, strong-field complexes. For example, 10 Dq ~35,000 cm^{-1} in the $3d^5$ $Mn(CN)_6^{-4}$ ion,[34] whereas the analogous splitting in $Fe(CN)_6^{-3}$ is also about 35,000 cm^{-1}.[35] Further, this value of Δ_1 is not inconsistent with the only published optical spectrum of $V(CO)_6$.[36] The value of Δ_1 obtained in this way therefore supports the assumption of a tetragonal distortion.

Of greater interest is the value one obtains for Δ_2, the tetragonal distortion parameter. Thus far, the discussion has neglected the presence of spin-orbit forces, except as they affect the g-value calculations. It was shown in the previous section that the spin-orbit interaction $\xi\, \underline{L} \cdot \underline{S}$, acting alone, mixes some of the t_{2g} wavefunctions in first-order. Thus, it would be expected that some of the degeneracy of the octahedral t_{2g} levels would be lifted by this perturbation in the absence of any further distortion (e.g., tetragonal) of the crystal field. For $\xi << 10$ Dq, Ballhausen[37] shows that the t_{2g} levels are split into an upper singlet and lower doublet with energies

$$E(b_{2g}) = -4\,Dq + \xi$$

$$(\xi > 0) \qquad (38)$$

$$E(e_g) = -4\,Dq - \frac{1}{2}\,\xi$$

Thus the ground state is $^2B_{2g}$ and the splitting between the e_g and b_{2g} levels is $3\xi/2$, or ~150 cm^{-1} for $V(CO)_6$. Two conclusions can be made on the basis of this calculation. First, although the splitting due to spin-orbit terms is in the same direction as that assumed for a tetragonal field in the g-value derivation, it provides only about 10% of the observed splitting, Δ_2. It can also be concluded that, in a narrow sense, $V(CO)_6$ cannot undergo a Jahn-Teller distortion because the ground state is an orbital singlet due to spin-orbit effects.

That the Jahn-Teller effect was subject to the inclusion of spin-orbit effects was discussed in an early paper by Jahn.[38] He showed that, in cases where the $\xi\,\underline{L}\cdot\underline{S}$ term lifted the orbital degeneracy, a symmetrical configuration of the molecule is unstable only if there is a spin degeneracy higher than the twofold Kramers degeneracy. In such cases, the distortion is expected to be extremely small[39] and since the ground state of $V(CO)_6$ is $^2B_{2g}$, it should not occur in this molecule.

One should also remark here that, because the Jahn-Teller theorem is a purely group-theoretical result, very little is known about the mechanism or mechanisms by which Jahn-Teller distortions occur. Consequently, there is some disagreement in the literature as to what constitutes a Jahn-Teller distortion. For example, a situation analogous to $V(CO)_6$ is found in the tetrahedral $CuCl_4^{-2}$ ion ($3d^9$), which is observed to be distorted in the crystalline compound Cs_2CuCl_4.[40] The crystal field splitting scheme for "holes" in a tetrahedral environment is the same as

that for electrons in an octahedral field; i.e., the t_{2g} levels are lower than the e_g levels, providing the sign of ξ is reversed. Therefore, the t_{2g} levels in $CuCl_4^{-2}$ which are split by the term $\xi\ \underline{L} \cdot \underline{S}$ are inverted (i.e., $E(b_{2g}) < E(e_g)$ since $\xi < 0$), and the single hole goes into the b_{2g} level which is an orbital singlet. Thus, one interpretation, which is favored by Ballhausen,[41] is that the distortion is not a result of the Jahn-Teller effect and is probably due to the Coulombic repulsion of the chloride ions.[42]

On the other hand, Sharnoff and Reiman[43] have studied the optical and ESR spectra of $CuCl_4^{-2}$ in different lattices and, in spite of the spin-orbit effects, interpreted their results in terms of the Jahn-Teller effect. (As in the case of $V(CO)_6$, the spin-orbit splitting of the b_{2g} and e_g levels in $CuCl_4^{-2}$ is small (~500 cm^{-1}) compared to the derived tetragonal distortion parameter, Δ_2 (~5000 cm^{-1})). They observed that the g-tensor changed considerably in going from Cs_2CuCl_4 to Cs_2ZnCl_4 as a host lattice even though the lattice constants of the two host crystals are quite similar. The authors concluded from this that the dominant mechanism of the distortion was not intermolecular but rather an intrinsic Jahn-Teller effect. They suggest that the reason for these differences is probably that changes in the amount of ligand character in the e_g (primarily 3d) orbitals occur in going from one lattice to another. A LCAO/MO treatment in their paper is consistent with this interpretation. This approach to the $CuCl_4^{-2}$ problem illustrates the other point of view which exists in the literature; this is, that any distortion which is produced by intramolecular effects can be termed a Jahn-Teller distortion. Thus, in $V(CO)_6$ as in $CuCl_4^{-2}$, the additional splitting ($\Delta_2 - 3\xi/2$) is, in this broader sense, a Jahn-Teller distortion if it results from intramolecular forces even though the t_{2g} degeneracy is lifted by the spin-

In $V(CO)_6$, the possibility of a "pseudo" Jahn-Teller effect must also be considered. This is essentially a dynamic effect in which an additional splitting is produced by the interaction of an excited state with the ground state. This interaction occurs through a vibrational mode of the ground state, and is therefore thought to be important only in cases where the splitting of the ground and excited states is small compared to the zero-point energy of the vibration.[44] Since a tetragonal distortion has been assumed here for $V(CO)_6$, the vibrational mode most likely to produce this effect is the degenerate $\nu_4(e_g)$ mode, whose normal coordinates correspond approximately to an elongation of the z-axis and a compression of the x- and y-axes.[45] Although the M-C vibrational frequencies for $V(CO)_6$ are not known, the value of ν_4 in the corresponding chromium hexacarbonyl is about 375 cm^{-1}.[45] The first excited electronic state of $V(CO)_6$ is assumed to have the configuration $(e_g)^3(b_{2g})^2$. If the only splitting of the t_{2g} levels is due to the spin-orbit terms, then this excited state configuration would be above the ground state configuration $(e_g)^4(b_{2g})$ by about $3|\xi|/2$. Since $1/2\ h\nu_4 \sim 3|\xi|/2$, a "pseudo" Jahn-Teller effect is possible. However, it seems unlikely that this effect could produce the additional splitting of some 1500 cm^{-1} observed here for $V(CO)_6$.

It is therefore concluded that, although $V(CO)_6$ appears to be tetragonally distorted in both the pure crystal and in an n-pentane glass at liquid helium temperatures, the value of Δ_2, the distortion parameter, is much greater than predicted by the inclusion of either spin-orbit or "pseudo" Jahn-Teller terms in the spin Hamiltonian. This discrepancy can be resolved only by postulating the existence of other forces which contribute to the distortion; whether these forces are

Jahn-Teller in their origin is basically a question of semantics, as noted above. Such forces would include Coulombic repulsion of the ligands, perturbations introduced by the surrounding lattice, and electronic effects peculiar to $V(CO)_6$.

Although these effects can only be discussed qualitatively, some interesting comments can be made. First, we suggest that Coulombic repulsion of the ligands and external lattice perturbations can only be important in samples where the lattice is composed of a regular array of molecules in which these forces are quite specific. In a glass sample, where the surroundings are random and there is no local order, the distortion of $V(CO)_6$ would be expected to be an intrinsic property of the molecule rather than a result of intermolecular forces.

A more reasonable explanation, and the one which is preferred here, is that there are electronic effects peculiar to $V(CO)_6$ which produce the distortion. To be more specific, it will be recalled that it is generally believed that "back donation" is an important factor in the M-C band in the carbonyls. This is achieved by the utilization of the t_{2g} orbitals of the metal ion in π-bonding with the π-orbitals of the ligand. These effects can be included in a molecular orbital description of the bonding as was indicated in Chapter II (cf. Figs. 1 and 2). Now, as noted by Orgel,[46] most of the mononuclear metal carbonyls conform to the rule that the total number of electrons available to the metal, if each CO ligand contributes two electrons, is equal to the number required to complete the next inert gas shell. Thus $Cr(CO)_6$, with a strong field configuration...$(t_{2g})^6$, has 18 electrons and an octahedral structure (d^2sp^3 hybridization). In a molecular orbital description with π-bonding, the electronic configuration is therefore ...

$\left\{ t_{2g}(\pi)[d_{xz}, d_{yz}, d_{xy}] \right\}^6$ (cf. Fig. 2). Since the d_{xz}, d_{yz}, and d_{xy} orbitals are completely filled, the π-bonding which occurs in $Cr(CO)_6$ strengthens all M-C bonds equally and the octahedral symmetry of the molecule is maintained.

In $V(CO)_6$, the situation is slightly different because there are now only 17 electrons available to the metal. Referring to Fig. 2, we see that this results in the configuration ... $\left\{ t_{2g}(\pi)\ [d_{xz}, d_{yz}, d_{xy}] \right\}^5$. In addition, from our ESR results we assume that the hole in this shell occurs in the d_{xy} orbital which is primarily of metal ion character (see Fig. 2 and Eq. (19)). Qualitatively, it would seem reasonable that this would disturb the balance between π-bonding and σ-bonding in the M-C bonds in the xy plane of the molecule. Thus a change in the ligand character of the equatorial M-C bonds could produce a distortion of the molecule such as is thought to occur in the $CuCl_4^{-2}$ ion.[43] Further, the removal of an electron from the d_{xy} orbital could result in less "back donation" in the xy-plane and stronger σ-donation from the equatorial carbonyl groups. This interpretation, though somewhat tenuous, would then predict a contraction of the CO groups in the xy-plane. Since this effect is equivalent to an elongation of the z-axis of the molecule, and indistinguishable in our experiments, it is consistent with the ESR results.

Finally, it is interesting to note that, as reported by Haas and Sheline,[36] the C-O stretching band in $V(CO)_6$ is much broader than in $Cr(CO)_6$. Since a strengthening of the equatorial M-C bonds in $V(CO)_6$ would be accompanied by a weakening of the C-O bonds along the x- and y-axis, this would have the effect of splitting (or broadening) the infrared band since the axial C-O bonds would presumably not be affected

by this mechanism. Thus, although this description of the origin of the tetragonal distortion in $V(CO)_6$ is highly conjectural, it is consistent with the spectroscopic results presently available. If this interpretation is correct, it provides strong evidence for the concept of "back donation" in metal carbonyls.

The g-tensor observed for the benzene glass samples of $V(CO)_6$ is also axial but the tensor components are not in accord with those predicted on the basis of either trigonal or tetragonal models.[47] This difference cannot be ascribed to exchange effects because the anisotropy in g ($\Delta g = g_{\perp} - g_{\parallel}$) is about the same in both glasses. This observation lends some support to the suggestion that intermolecular forces are important in these samples. However, in the benzene case it is possible that the ESR spectra observed here are of an intermediate in the reaction of benzene with $V(CO)_6$ which was described in Section 1. A comparison of the UV spectrum of pure $V(CO)_6$ with those of the solutions of $V(CO)_6$ in benzene and n-pentane would help to clarify this situation. Even if there is no evidence for intermediate formation, one would still expect the influence of the lattice to be quite different for benzene and n-pentane glasses, for the local surroundings of the $V(CO)_6$ molecule in benzene are likely to be far more regular.

In order to make a more detailed study of the effects of the surrounding medium on the spectral properties of $V(CO)_6$, it will be necessary to attempt to obtain the ESR spectrum of this molecule in a more regular environment. For example, if dilute single crystals of $V(CO)_6$ in an isomorphous, diamagnetic host carbonyl could be obtained, these effects can be studied in more detail. Some efforts in this direction have been made (see Chapter III) and are being continued by others in this laboratory. If they prove to be fruitful, then an experiment with a ^{13}C enriched

sample might provide additional information on the mechanism for the tetragonal distortion.

B. ESR of VCl_4 at Liquid Helium Temperatures

1. Assignment of the Spectra

a. "Isotropic" spectra.

The ESR spectrum of pure VCl_4 consists of a single broad line which shows no hyperfine structure. Figure 22 shows an example of a spectrum which was obtained at 4.2°K., the boiling point of liquid helium. This line is slightly asymmetric and has a peak-to-peak width of about 200 G. A similar line, of smaller width, was observed with a sample of VCl_4 in n-heptane in which the VCl_4 concentration was of the order of 0.5 - 1.0 mole %. A representative spectrum in the n-heptane glass is illustrated in Fig. 23; here the width was about 140 G. at 1.46°K. These spectra were obtained using the X-band TE012 rectangular cavity for which the resonant frequency was in the range 9.4-9.7 GHz.

The assignment of these spectra on the basis of the isotropic Hamiltonian

$$\mathcal{H} = g\beta H_z S_z$$

is straightforward. The calculation of the isotropic g-value requires the knowledge of both the frequency and the field, both of which could be measured easily. As the Hall device was not found to be reliable for absolute field measurements, it was necessary to include in the cavity a reference material for which the g-value was known accurately. 1,1-diphenylpicrylhydrazyl (DPPH) is commonly used for this purpose; it has an isotropic g-value of 2.0036 ± 0.0002 at liquid nitrogen temperatures and above. However, at low temperatures g becomes anisotropic and this anisotropy is quite temperature dependent. This fact has been discussed in Chapter III in which a representative spectrum of DPPH at these temperatures is shown (see Fig. 12).

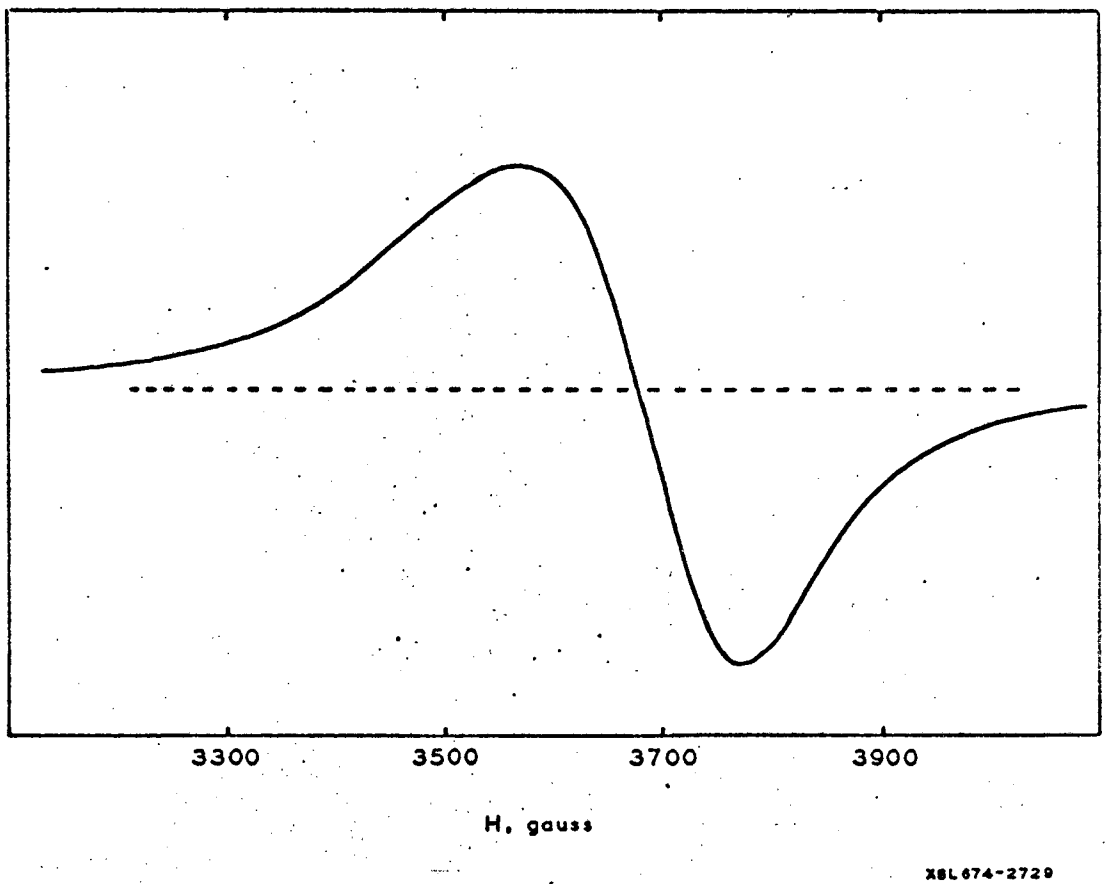

Fig. 22. ESR spectrum of pure VCl_4 at 4.2°K; ν = 9.6399 GHz.

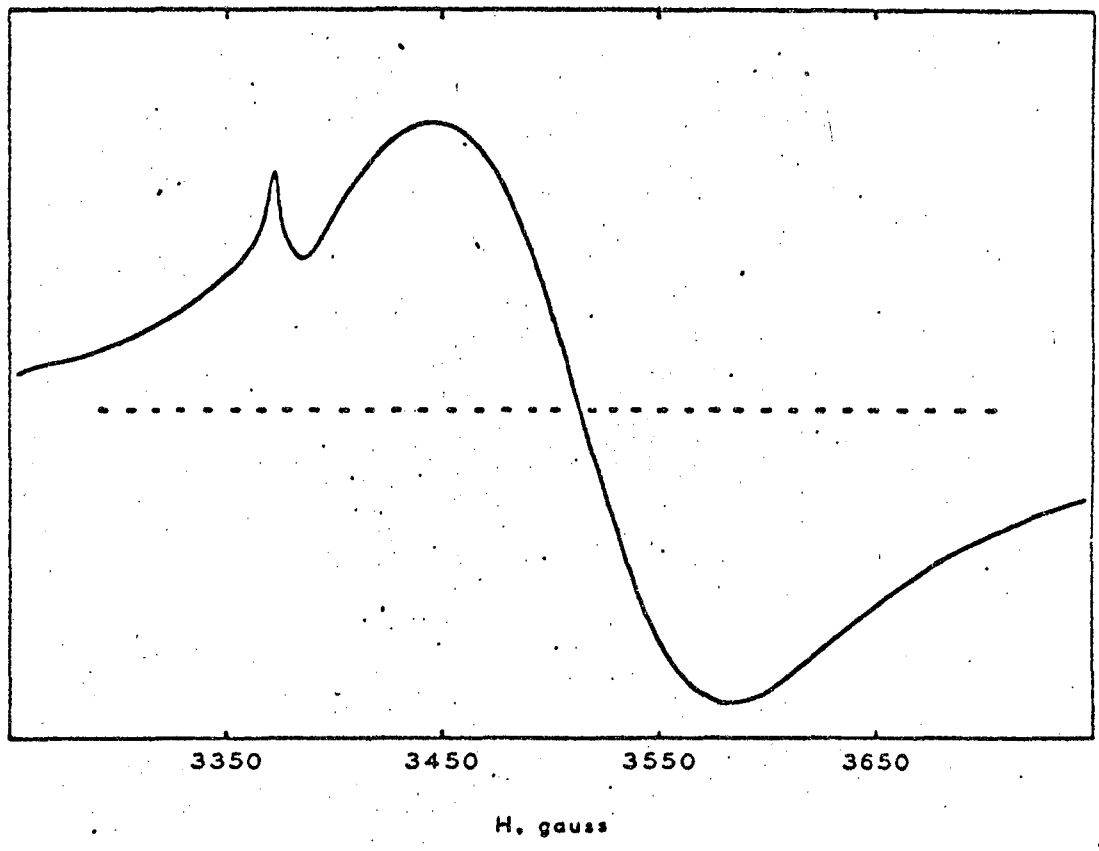

Fig. 23. ESR spectrum of VCl_4 in n-heptane at 1.4°K; ν = 9.4946 GHz. The sharp line is due to DPPH.

The sharp signal on the low-field side of the spectrum in Fig. 23 is due to a sample of DPPH which was located on the bottom of the cavity. Taking the g-value of the positive peak to be 2.010 at 1.46°K [$\frac{1}{2}(g_1 + g_2)$, see Chapter III], the g-value of VCl_4 in n-heptane (defined by the base-line crossover point) was found to be 1.931 ± 0.001. No appreciable shift from this value was observed in the pure VCl_4 spectra.

The absence of noticeable hyperfine structure and g-value anisotropy in these spectra is attributed to the presence of a strong exchange interaction between the unpaired electrons on neighboring molecules. These effects were also observed in the $V(CO)_6$ experiments and are discussed in detail in a previous section (IV.A2). As in the case of dilute $V(CO)_6$ glasses, the existence of such exchange forces in the n-heptane/VCl_4 samples was a bit surprising. However, in the latter case the exchange term is presumably not long range but rather was due to precipitation of VCl_4 which occurred during the freezing process. This explanation was suggested by the following experiments. The samples of VCl_4 in n-heptane which gave spectra similar to Fig. 23 were at room temperature when they were placed into the cryostat and they cooled rather slowly by radiation between the cavity and the outer dewar of liquid nitrogen. On the other hand, when the samples were quick-frozen by immersing the cavity in liquid nitrogen before inserting in the cryostat, the VCl_4 spectrum contained a considerable amount of structure (vide infra). This effect was even more pronounced when solvents with a higher freezing point were used. For example, a sample of VCl_4 in CCl_4 which was not quick-frozen gave a single broad line; when the same sample was removed from the cryostat, warmed to room temperature, and quick-frozen, the resulting spectrum showed considerable hyperfine structure. Finally, only the latter type

of spectrum could be observed in samples of VCl_4 in mineral oil even when they were not quick-frozen. Thus it was concluded that the spectra presented here resulted from paramagnetic sites which consisted of a number of closely packed VCl_4 molecules. The slight asymmetry of these "isotropic" lines is probably due to a lack of complete averaging by this exchange interaction.

In order to observe the hyperfine structure in complete detail, all subsequent samples were quick-frozen prior to placing in the dewar. These spectra were quite anisotropic and are described below.

b. "Anisotropic" spectra.

1. VCl_4 in mineral oil.

Most of the ESR experiments on VCl_4 at liquid helium temperatures were performed using solvents with higher melting points. These included mineral oil, CCl_4, $SiCl_4$, $TiCl_4$ and $SnCl_4$. A representative X-band spectrum of VCl_4 in mineral oil at 1.32°K is shown in Fig. 24. Except for the strong central line, the lineshapes in this spectrum are clearly due to an anisotropic spin Hamiltonian. In addition, the decrease in intensity on the high field side suggests a functional dependence of the linewidth on m_I, m_I^2, etc. These general features are common to all of the spectra to be discussed in this section (b).

The spin Hamiltonian for VCl_4 can be written in the following form

$$\mathcal{H} = \beta \underset{\sim}{S} \cdot \underset{\sim}{g} \cdot \underset{\sim}{H} + \hbar \underset{\sim}{I} \cdot \underset{\sim}{A} \cdot \underset{\sim}{S}. \qquad (39)$$

In cases where $\underset{\sim}{g}$ and/or $\underset{\sim}{A}$ are anisotropic, it is convenient to choose an axis system so that the elements in S_x, S_y, I_x, I_y do not occur in the reduced Hamiltonian. Here it is also assumed that the principal axes for the $\underset{\sim}{g}$ and $\underset{\sim}{A}$ tensors are the same. This is the so-called strong field approximation and is equivalent to taking the axis about which the spin precesses as

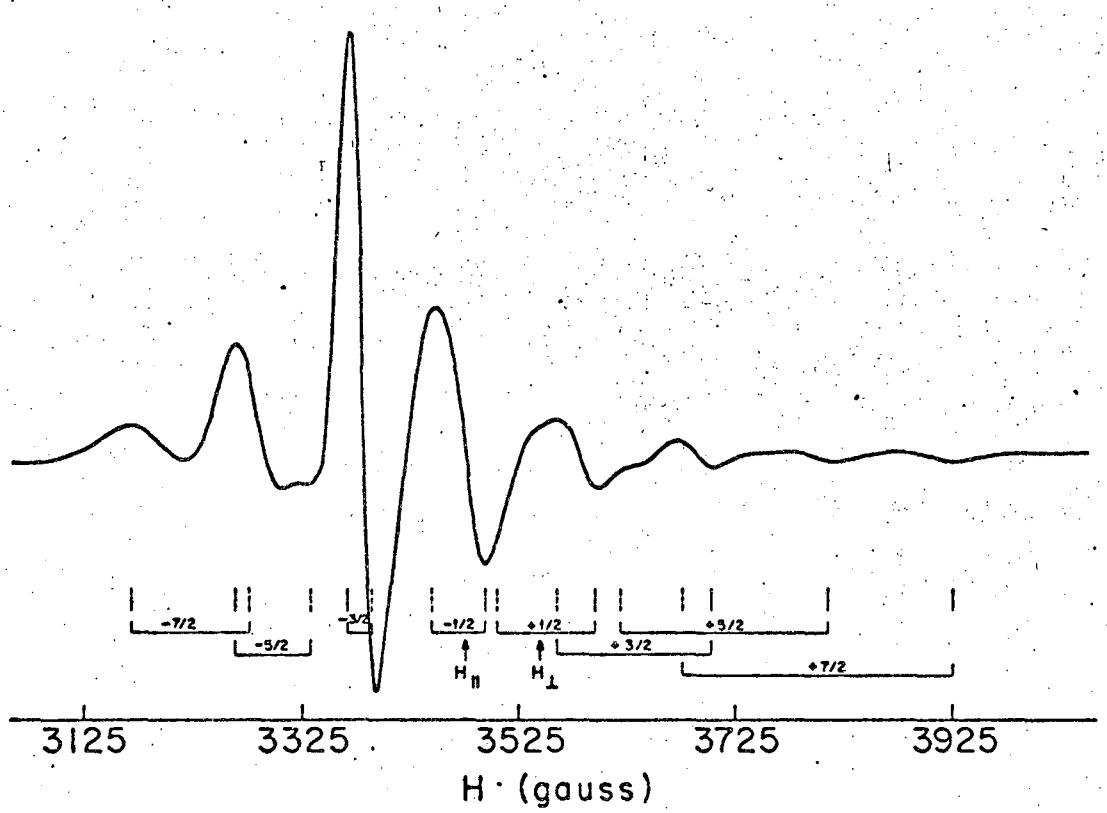

XBL674-2703

Fig. 24. ESR spectrum of VCl_4 in mineral oil at 1.32°K. ν = 9.5012 GHz. The assignment indicated is discussed in the text. The solid lines indicate the positions of the perpendicular signals; the parallel signals are indicated by the dotted lines.

the new z-axis. Then, if the external field is applied at angles θ and ϕ to the principal axis of molecular symmetry, Bleaney[48] and others[49] have shown that the condition for resonance is

$$\omega_o = \frac{g\beta H(m_I)}{\hbar} + Am_I + \frac{(A_x^2 + A_y^2)(A_z^2 + A^2)}{8A^2} \frac{[I(I+1) - m_I^2]}{g\beta H(m_I)/\hbar} \tag{40}$$

where

$$g^2 = g_z^2 \cos^2\theta + g_x^2 \sin^2\theta \cos^2\phi + g_y^2 \sin^2\theta \sin^2\phi$$

$$(gA)^2 = A_z^2 g_z^2 \cos^2\theta + A_x^2 g_x^2 \sin^2\theta \cos^2\phi + A_y^2 g_y^2 \sin^2\theta \sin^2\phi \tag{41}$$

The expression (40) neglects second-order terms in $\sin^2\theta \cos^2\theta$ which do not contribute for $\theta = 0, \pi/2$, the two cases of primary interest in glass spectra. Further, Bleaney's term containing $(2m_S-1)m_I$ is zero for $S = 1/2$. Now, for crystal fields of axial symmetry, $A_x = A_y = A_\perp$ and $g_x = g_y = g_\perp$, so the expression for ω_o becomes

$$\omega_o = \frac{g\beta H(m_I)}{\hbar} + Am_I + \frac{A_\perp^2(A_\parallel^2 + A^2)}{4A^2 g\beta H(m_I)/\hbar} [I(I+1) - m_I^2] \tag{42}$$

with

$$g^2 = g_\parallel^2 \cos^2\theta + g_\perp^2 \sin^2\theta$$

$$(gA)^2 = A_\parallel^2 g_\parallel^2 \cos^2\theta + A_\perp^2 g_\perp^2 \sin^2\theta \tag{43}$$

This expression is equivalent to that used for the assignment of the $V(CO)_6$ spectra except that here the first- and second-order hyperfine terms have been included.

Several papers in the literature have discussed the assignment of glass spectra;[2,50-52] the work of Wilson and Kivelson[49] on VO^{+2} is particularly helpful. The complexity of the spectrum of VCl_4 in mineral oil shown in Fig. 24 is the result of a combination of g- and A-value anisotropies. The hyperfine interaction produces a set of eight (I = 7/2) overlapping lines; however, because of the anisotropy in $\underset{\sim}{g}$, each line is similar to the lines observed for the glass samples of $V(CO)_6$ described in the previous section (A) of this chapter. In the case of VCl_4, the lineshape varies from one hyperfine component to the next because of the anisotropy in $\underset{\sim}{A}$. Therefore, the field splitting from $g_{\parallel}$ to $g_{\perp}$ is not constant for all m_I values and further, the relative signs of the parallel and perpendicular signals can be inverted. Consequently, the only regularities present in such a spectrum are the splittings $A_{\perp}$ and $A_{\parallel}$, modified by the second-order term in Eq. (42).

Values for $A_{\perp}$ and $g_{\perp}$ are easily obtained, for the perpendicular bands are the stronger features of an axial powder or glass spectrum. To do this, we assume the axial Hamiltonian

$$\mathcal{H} = \hbar\omega_o = g\beta H(m_I) + \hbar A m_I + \hbar^2 \left(A_{\parallel}^2 + A^2\right) \frac{A_{\perp}^2}{4A^2} \left(\frac{I(I+1) - m_I^2}{g\beta H(m_I)} \right) \quad (44)$$

with g and A given by Eq. (43). Now, for the perpendicular signals, $\theta = \pi/2$ and Eq. (44) becomes

$$\hbar\omega_o = g_\perp \beta H(m_I) + \hbar A_\perp m + \hbar^2 \left(\frac{A_\parallel^2 + A_\perp^2}{4}\right)\left(\frac{I(I+1) - m_I^2}{g_\perp \beta H(m_I)}\right) \qquad (45)$$

In order to keep track of the lines in the spectrum, we assume for the moment that $A < 0$ (this is consistent with theoretical predictions)[53] and therefore the low field line belongs to $m_I = -7/2$, etc. Then, from Eq. (45), the splitting $H(-5/2) - H(-7/2)$ is given by

$$\Delta_1 = H(-5/2) - H(-7/2) = \frac{-\hbar A_\perp}{g_\perp \beta} + \frac{\hbar^2 Q}{g_\perp \beta}\left\{\frac{3.5 g_\perp \beta H(-5/2) - 9.5 g_\perp \beta H(-7/2)}{(g_\perp \beta)^2 H(-7/2)\, H(-5/2)}\right\} \qquad (46)$$

and similarly, for the splitting between the two highest field lines

$$\Delta_2 = H(7/2) - H(5/2) = -\frac{\hbar A_\perp}{g_\perp \beta} + \frac{\hbar^2 Q}{g_\perp \beta}\left\{\frac{9.5 g_\perp \beta H(7/2) - 3.5 g_\perp \beta H(5/2)}{(g_\perp \beta)^2 H(5/2)\, H(7/2)}\right\} \qquad (47)$$

where

$$Q = \frac{A_\parallel^2 + A_\perp^2}{4}$$

By inspection of these two relations, it can be seen that it is a good approximation to write

$$A_\perp = \frac{\Delta_1 + \Delta_2}{2} .$$

Using the NMR probe (see Chapter III), the positions of all the lines in the VCl_4/mineral oil spectrum were measured carefully. From the positive peaks of the perpendicular lineshapes, marked with the solid lines in Fig. 24, and the above relations, a value for $\hbar A_\perp / g_\perp \beta$ of 103.3 ± 1.0

gauss was obtained for VCl_4 in mineral oil. Defining $H_\perp$ as being the field position

$$H_\perp = \frac{H(-1/2) + H(1/2)}{2}, \tag{48}$$

$g_\perp$ is given by

$$g_\perp = \frac{\hbar\omega_o}{\beta H_\perp}$$

and the value of $g_\perp$ so obtained is 1.915 ± 0.001.

Although similar relations can be developed for the parallel signals of the spectrum, it is clear from Fig. 24 that, because of poor resolution, the assignment of the parallel structure is much more difficult in the mineral oil spectrum. However, as is indicated in the figure by dotted lines, an assignment of the parallel signals has been made. This was done in the following manner. First, it can be seen that the first three perpendicular signals (m_I = -7/2, -5/2, -3/2) are positive whereas the last five are negative. Consequently, the three low-field parallel signals must be negative half-derivatives, with the third one (m_I = -3/2) lying very close to the corresponding perpendicular signal, since this line is nearly isotropic. Further, the remaining five parallel signals are expected to be positive half-derivatives. This information, together with the hints of structure at the parallel positions marked +3/2 and +5/2 in Fig. 24, suggested a possible assignment.

The approximate values of $g_\parallel$ and $A_\parallel$ obtained in this way, together with the more accurate perpendicular parameters, were then used in a computer program developed by Vänngård and Aasa.[54,55] This program is well suited for this particular problem because it includes anisotropies

in $\underset{\sim}{g}$ and $\underset{\sim}{A}$ (to second-order) as well as an (adjustable) single center linewidth for the case $S' = 1/2$. In addition, the variation of transition probability with $\underset{\sim}{g}$[56] is included but the program is restricted to cases of axial symmetry. The results of the computer calculation were plotted on a digital x-y plotter (California Computer Co.) and compared with the experimental spectrum. After several attempts, a reasonable fit was obtained which is shown in Fig. 25. This was obtained using the perpendicular parameters quoted above and $\hbar A_{\parallel}/g_{\parallel}\beta = 56.4 \pm 1.0$ gauss, $g_{\parallel} = 1.941 \pm 0.002$ with a single-center linewidth of 15 gauss. The approximate positions of the parallel lines based on these parameters are the dotted lines in Fig. 24.

Several comments regarding this assignment are in order. First, since the $\pm 7/2$ parallel signals do not show up explicitly in the experimental spectrum, it is possible that the whole parallel pattern could be shifted up or downfield by a multiple of $A_{\parallel}$. However, because of the change in sign of the parallel peak from $m_I = -3/2$ to $m_I = -1/2$ and the satisfactory reproduction of the lineshape in this region in the computed spectrum, the interpretation given here is preferred. Second, the relatively wide lines may obscure slight deviations from axial symmetry which could be present in this matrix. In addition, if the assignment proposed here is correct, then the fact that $A_{\parallel} < A_{\perp}$ suggests that $A_{\perp} < 0$ since the isotropic and anisotropic values are related by the equation

$$\langle A \rangle = \frac{2A_{\perp} + A_{\parallel}}{3} \tag{49}$$

and $\langle A \rangle$ is assumed to be less than zero.[53] No conclusion can be made regarding the sign of $A_{\parallel}$. Finally, we note that the rather strong

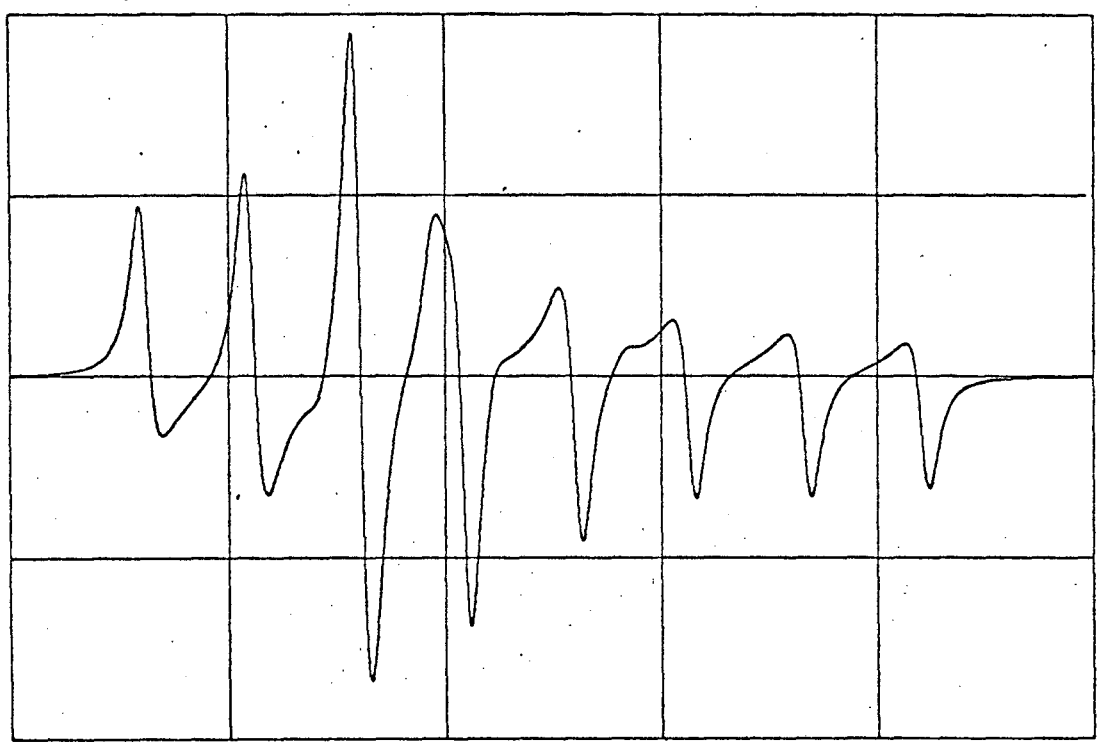

XBL674-2731

Fig. 25. Computed spectrum of VCl_4 in mineral oil using a constant single center linewidth. The horizontal scale is the same as in Figure 24.

dependence of the linewidths on m_I values is apparently the major cause of the difference between the experimental and computed spectra. In order to test this idea, several attempts were made to empirically adjust the linewidths for each m_I value in the computed spectrum. Figure 26 is an example of such a plot. In this plot, the linewidth for the $m_I = -3/2$ line was taken as 15 gauss and increased arbitrarily by 5 gauss per line for the lines to either side of the "isotropic" line (i.e., the single center width for $m_I = 7/2$ was 40 gauss). The g- and A-values assumed for this plot were the same as in Fig. 25, where the single center width was taken as 15 gauss. Qualitatively, it can be said that this plot approximates the experimental lineshapes but the quantitative agreement is still unsatisfactory. Further work on this aspect of the problem is still in progress.

The interesting feature of the linewidth variation in the mineral oil (and other, see later) spectra is that it is quite similar to that observed for VO^{+2} solutions at room temperature.[49,57] In these truly isotropic spectra, the $m_I = -3/2$ line is the narrowest and the reduction in intensity is more pronounced at the high field side of the spectrum. McConnell had shown that the linewidth variation for solutions has the functional dependence

$$\Delta H(m_I) \propto (\Delta g \beta H + \Delta A m_I)^2 \tag{50}$$

where

$$\Delta g = g_{\parallel} - g_{\perp}$$
$$\Delta A = A_{\parallel} - A_{\perp}. \tag{51}$$

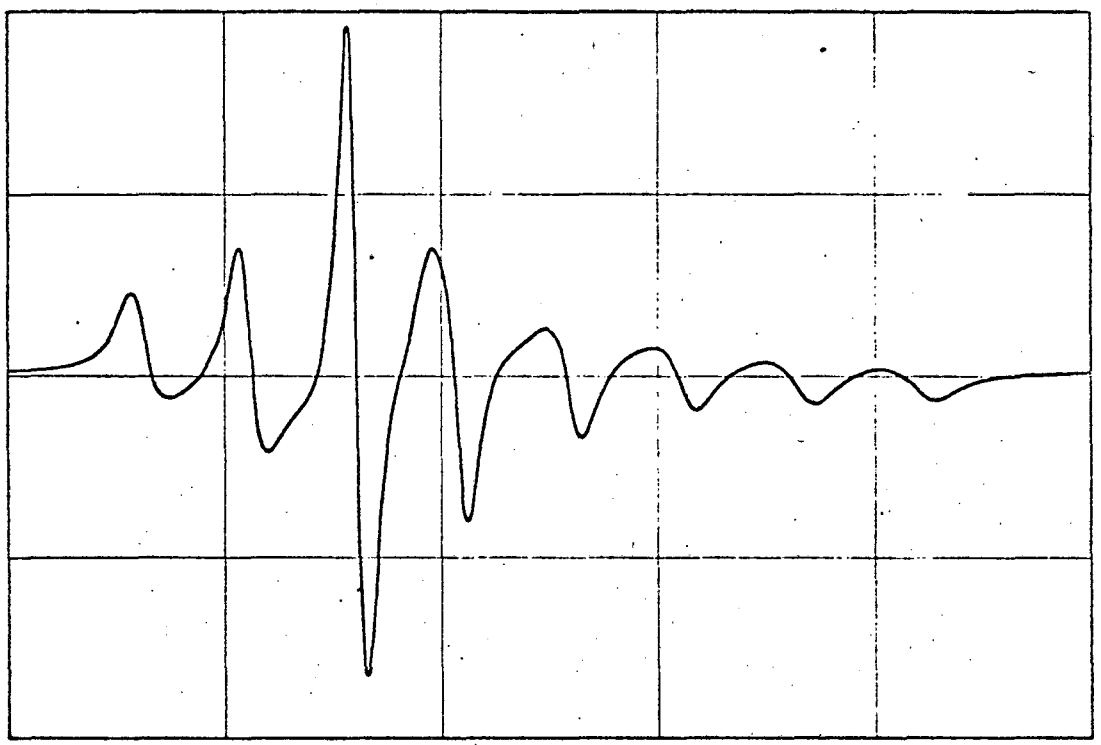

XBL674-2700

Fig. 26. Computed spectrum of VCl_4 in mineral oil using a variable single-center width (see text). The horizontal scale is the same as in Figure 24.

In VO^{+2}, Δg and ΔA are both negative[49] and so the expression

$$\Delta H(m_I) \propto (\Delta g\beta\ H)^2 + (\Delta g\Delta A\beta H)m_I + (\Delta A)^2 m_I^{\ 2} \qquad (52)$$

predicts that the widths at high field ($m_I > 0$) will be greater than at low field and that the narrowest lines of the spectrum will be located in the middle. The relaxation mechanisms giving rise to this dependence are discussed by Kivelson[49] who shows that a model based on rotational averaging of g- and A-value anisotropies with a single correlation time gives theoretical predictions in accord with experiment.

In VCl_4 at low temperatures, the T_2 mechanism must, of course, be quite different. In a paper which will be discussed in more detail later, O'Brien[58] has shown that linewidth effects similar to those resulting from motional narrowing can be produced at low temperatures by a Jahn-Teller effect. In this case, a broadening is produced by vibronic transitions between the various Jahn-Teller states of the complex. This changes the Larmor frequency of the electron but does not flip the electron spin and is consequently a T_2 process. The result is a functional dependence of ΔH on m_I, etc., entirely analogous to the tumbling case, i.e.,

$$\Delta H \propto \tau[(\Delta g\beta H)^2 + (\Delta g\Delta A\beta H)m_I + (\Delta A)^2 m_I^{\ 2}] \qquad (53)$$

where τ is the characteristic time for the dynamic Jahn-Teller effect. Since, from our results, Δg and ΔA are both positive (we assume here that $A_\perp$, $A_\parallel < 0$ as in VO^{+2}), the linewidth variation predicted by this model is in agreement with the observed spectra. Further evidence regarding the presence of a Jahn-Teller effect in VCl_4 will be presented later in this section.

2. VCl_4 in CCl_4 and $SiCl_4$.

A few experiments were run on samples consisting of dilute glasses of VCl_4 in CCl_4 or $SiCl_4$. Although no accurate field measurements were made for these spectra, they are discussed here because they are somewhat more complex than the mineral oil spectra discussed above and provide a good introduction to other spectra to be presented later.

Figure 27 shows an X-band spectrum of VCl_4 in CCl_4 at 4.2°K. Although this is at the boiling point of liquid helium, a good S/N ratio was obtained for these experiments and this is partly due to the narrower lines observed here. Qualitatively, this spectrum has the same overall appearance as the mineral oil spectrum but, because of the sharper lines, is more complex. A possible assignment of the spectrum is shown by the stick diagram at the bottom of Fig. 27. The perpendicular structure, consisting of three positive peaks at the low field end and five negative peaks on the high field side, is denoted by the perpendicular symbols. An approximate analysis of these splittings yields $A_\perp \sim 113$ gauss. As in the case of the mineral oil spectrum, the parallel structure is less well defined so the assignment indicated by the shorter solid lines is only tentative. This gives $A_\parallel \sim 97$ gauss.

The lineshapes for $m_I = +5/2$ and $+7/2$ are more complicated; but, on close analysis, they seem to be describable by a slight deviation from axial symmetry. Thus, the normal perpendicular lineshape splits into a half-derivative and a full-derivative and the positions of these half-derivatives are marked with dotted lines. Further downfield, the transitions belonging to $g_\perp$ merge and the normal perpendicular lineshape is observed. Similar effects are found in the $TiCl_4$ and $SnCl_4$ spectra (<u>vide infra</u>) to a much larger extent. In the CCl_4 spectra, the

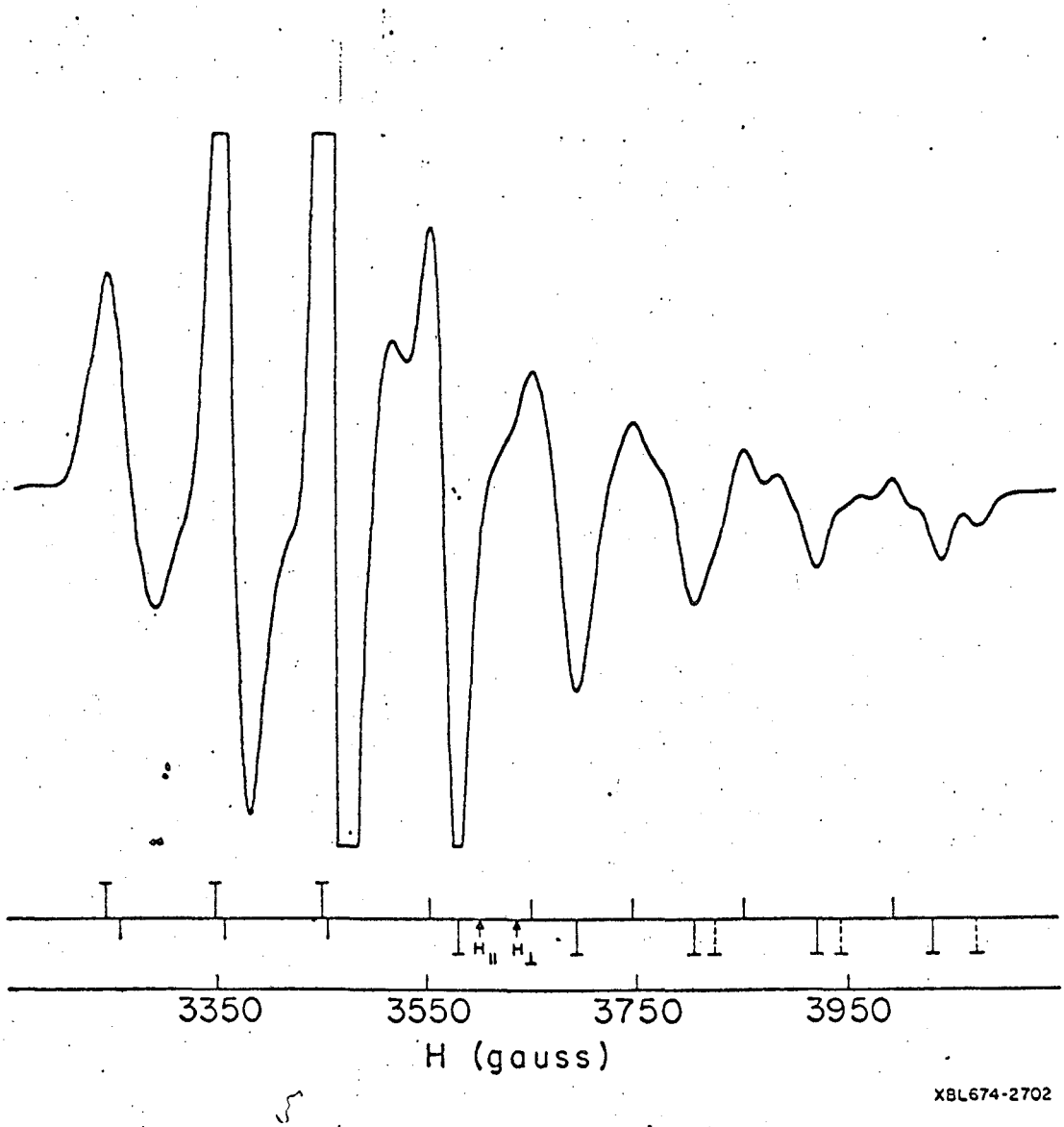

Fig. 27. X-band ESR spectrum of VCl_4 in CCl_4 at 4.2°K.

g-values were not measured but from Fig. 27 we see that $g_{\parallel} > g_{\perp}$ and that the anisotropy in $\underset{\sim}{g}$ is approximately the same as for the VCl_4 spectrum in mineral oil. The spectrum in $SiCl_4$ was quite similar to that described here for the VCl_4/CCl_4 samples. So far as was determined, these results were reproducible for a number of different samples.

3. VCl_4 in $TiCl_4$.

Several experiments on samples of VCl_4 in $TiCl_4$ were performed at both X-band and K-band. The ESR spectra of these samples at liquid helium temperatures are similar to the VCl_4/CCl_4 spectra, but, as can be seen from Fig. 28, are considerably more complex. This particular spectrum was obtained at 9.5659 GHz. at a temperature of 1.33°K. Using the method of assignment described earlier, the eight strong hyperfine components (identified by arrows in Fig. 28) can be assigned an A-value of 121.4 gauss ($=A_1$) and a g-value of 1.8998 ($=g_1$). Although the concentration of VCl_4 in this sample was not measured, it was thought to be of the order of 1 mole %.

As has been indicated on the bottom of Fig. 28, there are some additional regularities in this spectrum. However, a satisfactory assignment of these could not be made on the basis of experiments at a single frequency. For this reason, samples of VCl_4 in $TiCl_4$ were studied at K-band using the spectrometer described in Chapter III. Figure 29 shows an example of a spectrum of VCl_4 in $TiCl_4$ at 23.968 GHz. and 1.52°K. which again consists of eight equally spaced lines and many weaker components. The ESR parameters for the lines marked with arrows in this spectrum are A_1 = 122.0 gauss and g_1 = 1.8966, in very good agreement with the values obtained in the X-band experiments.

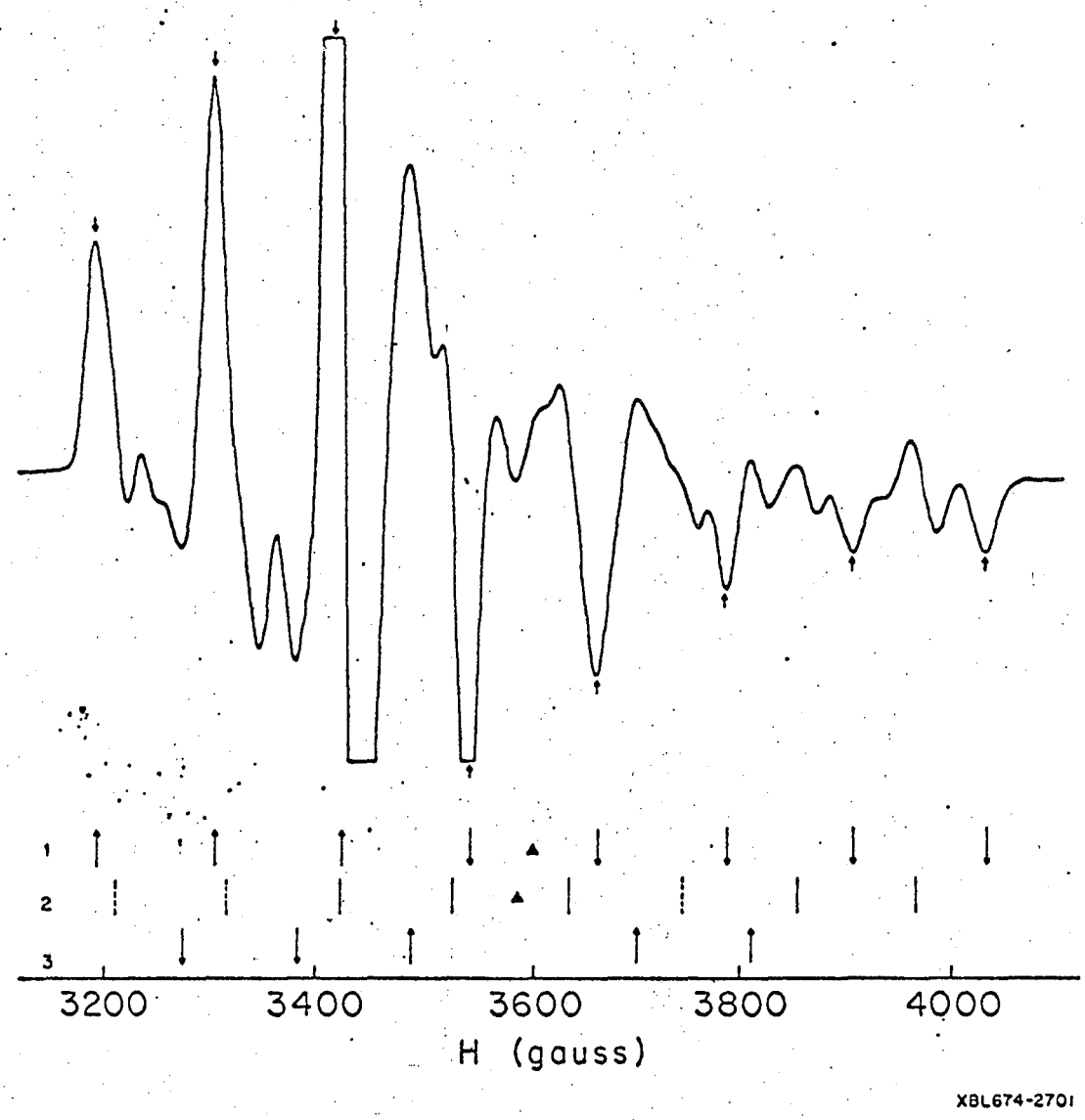

Fig. 28. ESR spectrum of VCl_4 in $TiCl_4$ at 1.33°K, ν = 9.5659 GHz. The assignment indicated is discussed in the text.

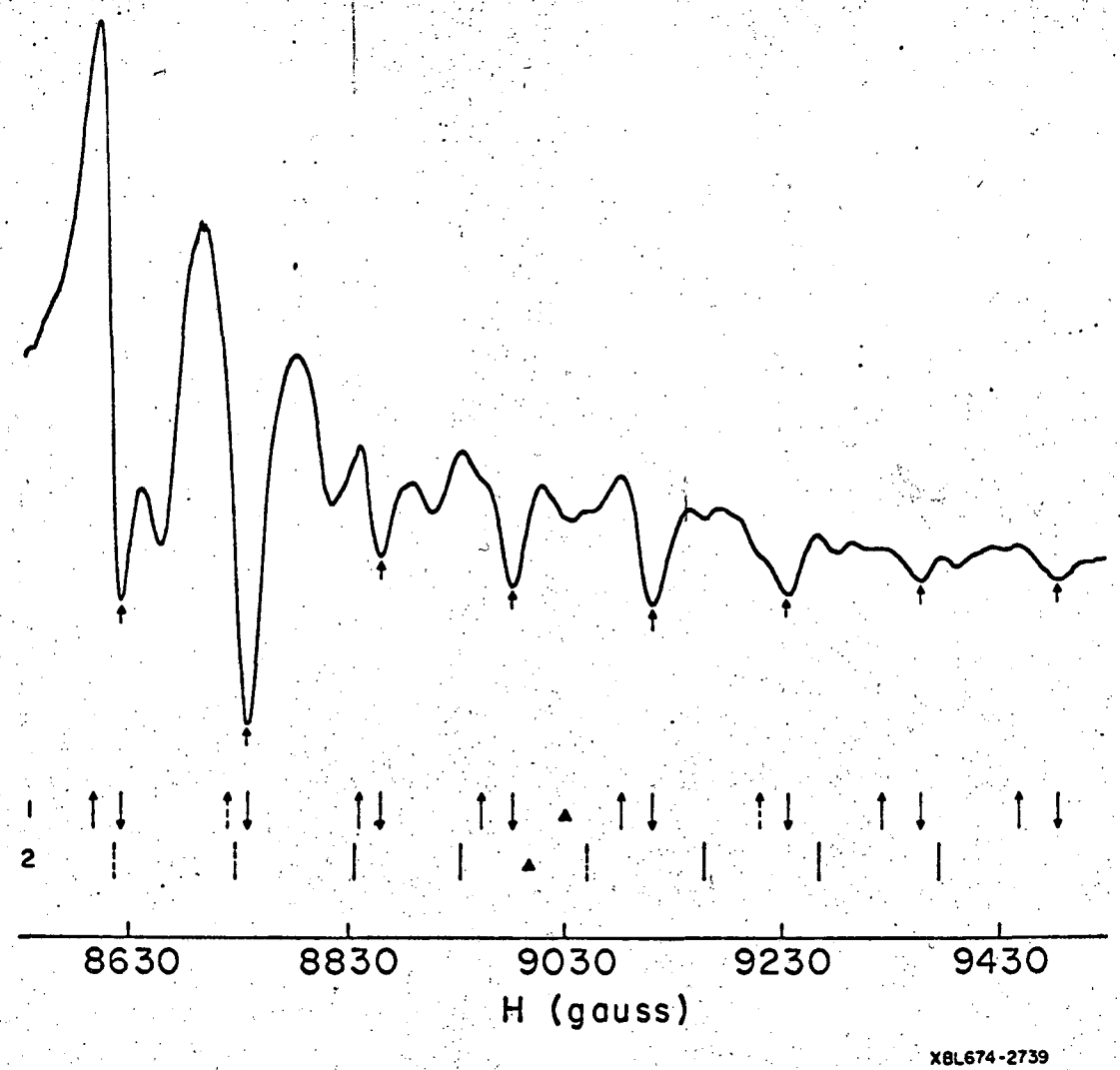

Fig. 29. ESR spectrum of VCl_4 in $TiCl_4$ at 1.52°K. ν = 23.968 GHz.

Because of the fact that the Zeeman term in the spin Hamiltonian is field dependent whereas, to first order, the hyperfine term is not, ESR experiments on an anisotropic spectrum at two different frequencies should produce a shift of one hyperfine pattern with respect to another. This shift should be of the order of the ratio of the two frequencies, or 24/9.6 = 2.5 in our experiments. Thus, if at X-band the difference between the field positions of two g-values is denoted by ΔH_{12}, then the field difference at K-band should be 2.5 (ΔH_{12}). Using this fact as a guide, considerable effort was made to obtain a consistent assignment of the spectra at both frequencies. This approach was only partially successful. For example, the second set of lines in the stick diagram of Fig. 28 shows the observed (solid lines) and predicted (dotted lines) field positions of eight components having $g_2 = 1.907$ and $A_2 \sim 109$ gauss. (The g-values are indicated in the stick diagrams by solid triangles.) Multiplying the field difference between g_1 and g_2 by 2.5, one predicts for K-band a second set of lines which is indicated in Fig. 29. The agreement with experiment is only moderately good.

By careful inspection of the lineshapes in both spectra, it seems clear that the spin Hamiltonian for VCl_4 in $TiCl_4$ possesses a symmetry less than axial. For example, the first set of lines in the X-band spectrum appears to be made up of half derivatives, whereas in the K-band spectrum, each line in this set seems to be a full derivative. Further, this pattern is reversed for set 2; i.e., in the X-band spectrum, the lines belonging to this set are full derivatives. If this is so, then there should be another set of eight lines in each spectrum with different values of g and A. This latter group of lines should be half derivatives, having a sign opposite to that of the other group of half derivatives for

each m_I value. However, no satisfactory assignment of this third group of lines could be made using the observed spectra (see the bottom set of lines in the stick diagrams). This work could be greatly facilitated by using a computer program suitable for rhombic symmetry and work on such a program is in progress. Several attempts to fit the $VCl_4/TiCl_4$ spectrum with the axial program used for the mineral oil spectra were unsuccessful.

Some other aspects of this investigation were interesting and worthy of note. In the first place, the spectrum of VCl_4 in $TiCl_4$ was not completely reproducible. Figure 30 shows two of several variations of the X-band spectrum of 0.05M VCl_4 in $TiCl_4$. Although the spectrum has the same overall appearance, the positions of many of the lines are shifted considerably as can be seen by comparison of these traces with each other and with Fig. 28. Not only was the spectrum not reproducible from sample to sample, but it also showed similar changes for a given sample over periods of up to one month. For example, the upper trace in Fig. 30 is a spectrum obtained from a freshly-prepared sample. During the course of several experiments, the sample was cooled to liquid helium temperatures repeatedly after warming overnight. The lower trace in Fig. 30 is a spectrum of the same sample after two weeks of these experiments. The temperature during warmup (liquid nitrogen was kept in the outer dewar) was estimated to be 110°K. or lower based on thermocouple readings, so it is possible that some "annealing" of the matrix occurred during this time. No changes in the spectrum were observed during any one run at liquid helium temperatures.

However, the changes in the ESR parameters were thought to be small. Table XIII shows the results of several measurements of A_1 and g_1 for

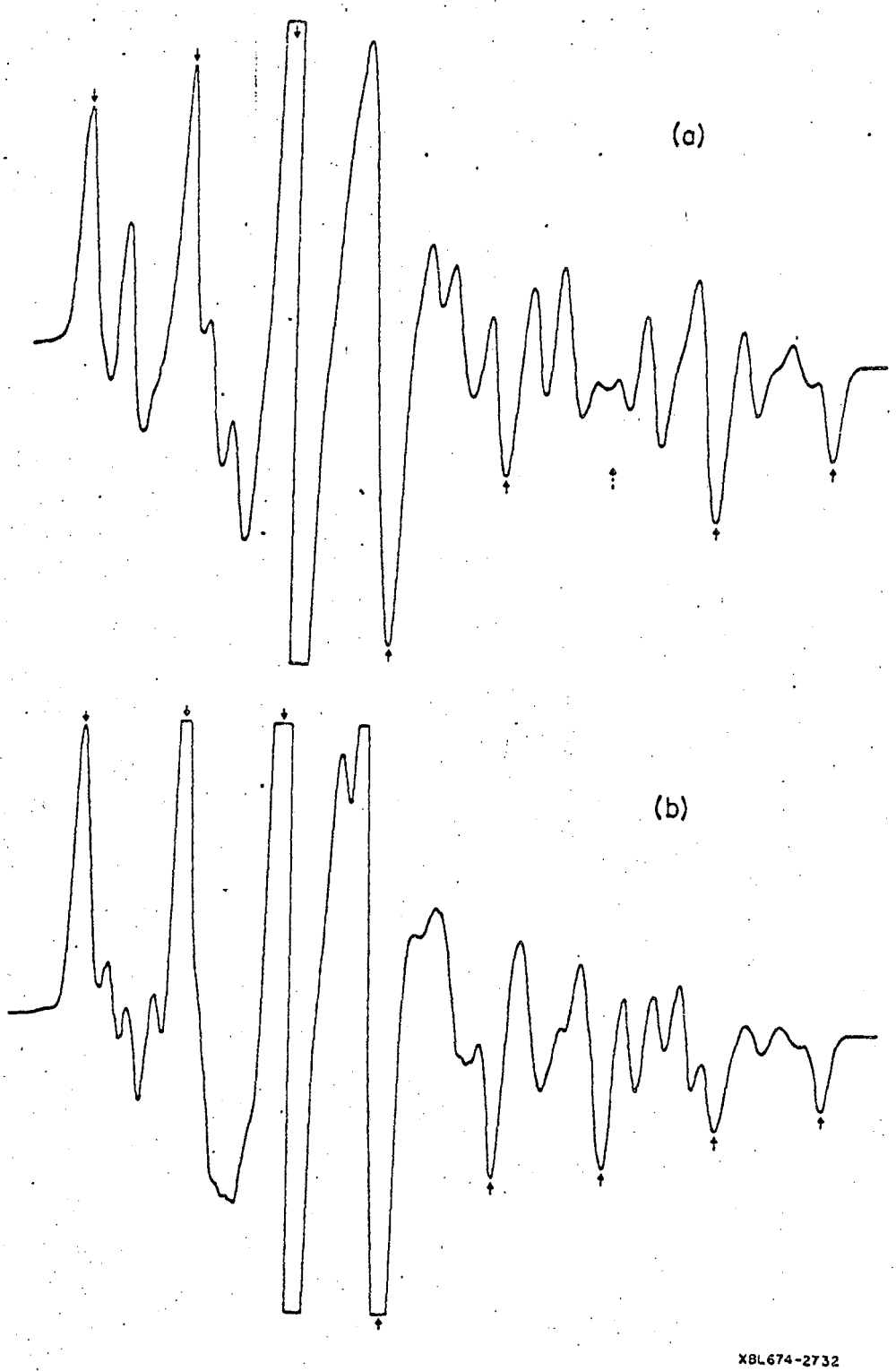

Fig. 30. X-band ESR spectra of VCl_4 in $TiCl_4$. These traces show the non-reproducibility of the spectrum.

Table XIII. A comparison of values of g_1 and A_1 obtained from the ESR spectra of several different samples of VCl_4 in $TiCl_4$.

	Sample No.	g_1	A_1
X-band	1		120.75
	2		121.72
	3	1.9026	117.73
		1.8998	121.35
	4		120.68
		1.8997	121.03
		1.9002	117.85
		1.8996	121.86
		1.9004	119.69
K-band	1	1.8966	121.96
	2	1.8987	

some of these experiments; these include different samples as well as repeated measurements on a single sample. For example, the data reported for sample 4 was obtained over a period of a month. It can be seen from this data that A_1 and g_1 varied very little; because the values for the remaining parameters are not known accurately, it is possible that variations in these were larger. From this data - and some not included in the table - average values of g_1 and A_1 were found to be 1.9004 ± 0.0010 and 120.3 ± 1.0 gauss, respectively.

Several experiments were performed in which the VCl_4 concentration in $TiCl_4$ was varied by factors of two or three in either direction (see Chapter III). So far as could be determined, there was no correlation

between the changes in the spectrum and concentration. Although sample decomposition did occur frequently either during preparation or the experiment, the measurements reported here are for samples in which no decomposition was noted.

One other interesting observation in these experiments was that quite frequently, no ESR signal was initially detected in a sample which had been warmed to room temperature prior to insertion in the cryostat. Yet, after 2-3 hours at liquid helium temperatures, a spectrum began to appear which was at first quite broad and similar to the mineral oil spectrum. The resolution of the spectrum continued to improve with time and, after periods of up to 6 hours, the linewidth was reduced to that normally observed. It is possible that this behavior was due to instrumental difficulties, but it could also be explained by assuming that the VCl_4 molecules undergo some sort of reorientation following the quick-freezing of the sample.

The one consistent interpretation of the experiments on $VCl_4/TiCl_4$ samples described here is that whatever the nature of the distortion in VCl_4, it is quite subject to intermolecular effects from the surrounding matrix. Thus the fact that the spectrum was not reproducible and sometimes not observable initially can be interpreted as indicating the presence of molecular motion in the solid at high temperatures (e.g., above 20°K). Pimentel[59] has suggested that molecular diffusion is possible in low-temperature matrices when the temperature reaches one-half the melting point of the host (T_M = 243°K. for $TiCl_4$); it seems reasonable to assume that reorientation processes not involving translation, e.g., "annealing", can occur at even lower temperatures. Another explanation for these effects could be that there is a low temperature phase transition in these solids;

an attempt using X-ray diffraction to determine whether or not the structure of $TiCl_4$ was cubic at 77°K. yielded inconclusive results.[60] Nonetheless, because exactly analogous behavior was observed for samples of VCl_4 in $SnCl_4$ (vide infra), we conclude that the reason for these effects in the ESR spectra of VCl_4 in $TiCl_4$ and $SnCl_4$ is due to a kind of annealing process involving molecular reorientation. The fact that such changes were not observed in the VCl_4/CCl_4 samples (vide supra) is additional evidence for such motion; the C-Cl bond distance is smaller than the V-Cl distance, whereas the bond distances Sn-Cl and Ti-Cl are larger (see Chapter II). Thus the "cage" in which the VCl_4 is located is probably larger in solid $TiCl_4$ and $SnCl_4$.

The fact that the ESR spectrum of VCl_4 in $TiCl_4$ is not reproducible makes a unique assignment impossible, but it does not explain why a single spectrum is so difficult to assign. The presence of impurities and/or multiple sites[61] in the matrix is always a possibility and, as is usually the case, such factors cannot be ruled out in these experiments. A more interesting suggestion is that there are forbidden lines in the spectrum which complicate the already complex hyperfine patterns. Such transitions could be of the type $\Delta m_S = \pm 1$, $\Delta m_I = \pm 1$ produced either by a large quadrupole interaction[48,62] ($\underset{\sim}{I} \cdot \underset{\sim}{P} \cdot \underset{\sim}{I}$) or by off-diagonal hyperfine terms. Taking q for a pure 3d electron to be -1.20×10^{-15} esu.,[63] one calculates for $P \sim eQq/2I(2I-1) \sim 1$ gauss. Since the intensity of these forbidden lines will be of the order of $(P/A)^2$, quadrupole effects are not thought to be important, especially since the coupling constant P is probably much less than 1G for the (more or less) symmetrical VCl_4. The role of off-diagonal hyperfine terms, such as might arise if the axes of the $\underset{\sim}{g}$ and $\underset{\sim}{A}$ tensors do not coincide,[64] is much more difficult to

assess and will not be discussed further. Other "forbidden" lines could result from a Jahn-Teller effect;[58] also, extra transitions arising because of certain peculiar properties of the analytic function describing the distribution of magnetic axes in glass samples are possible.[51]

4. VCl_4 in $SnCl_4$.

A few experiments on samples of VCl_4 in $SnCl_4$ were performed at X-band. Figure 31 shows two representative spectra and by comparison with the $TiCl_4$ results described above, it is seen that the spectra in $SnCl_4$ are quite similar. The two traces in Fig. 31 were obtained at 1.35°K on the same sample; it was kept at liquid nitrogen temperatures for the period between the two experiments (~ 3 days). Thus the behavior of this sample was exactly analogous to that observed in $TiCl_4$ and will not be described further. The values for g_1 and A_1 in $SnCl_4$ are 1.915 ± 0.003 and 113.6 ± 3.0 gauss, respectively.

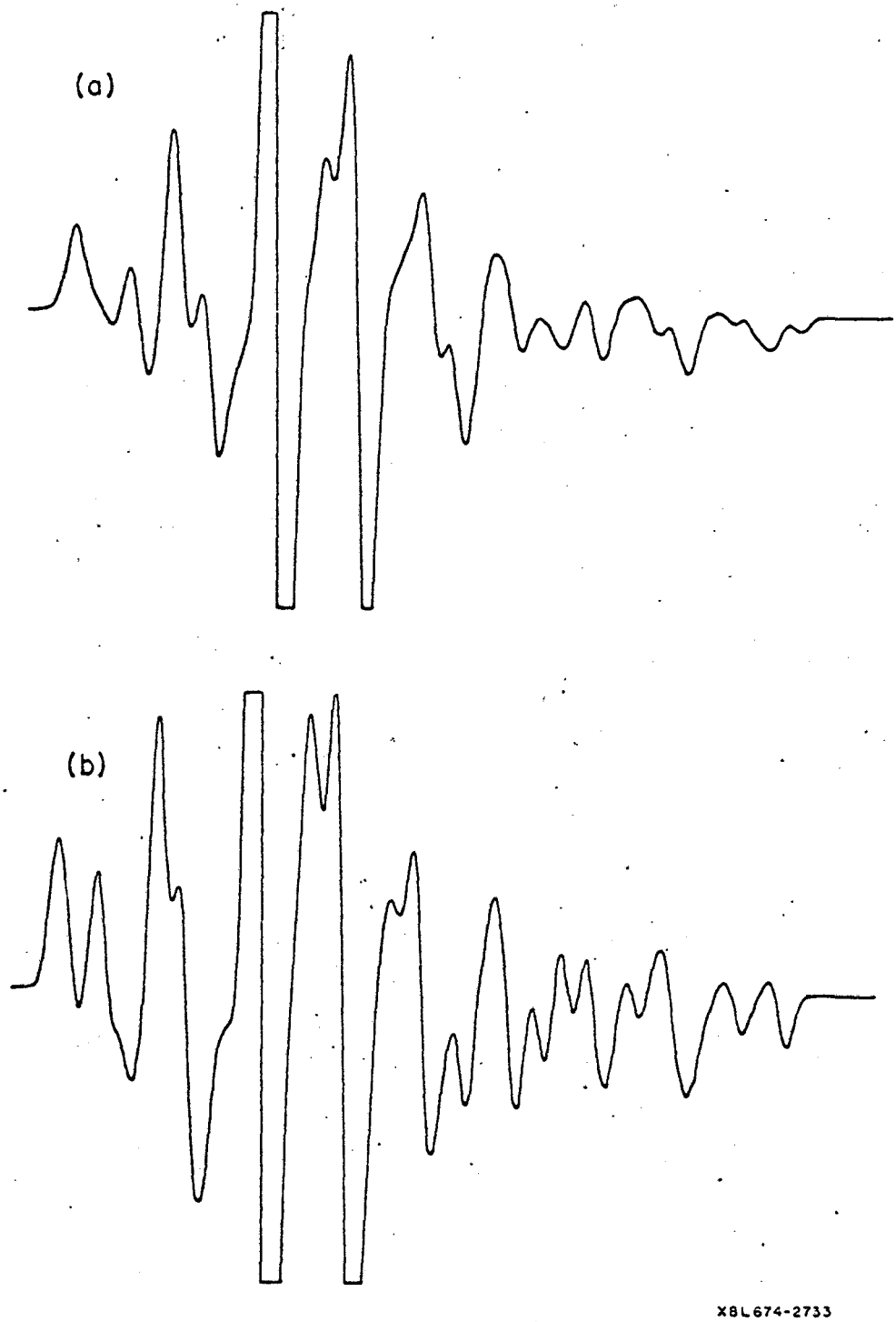

Fig. 31. X-band ESR spectra of VCl_4 in $SnCl_4$ at 1.35°K.

2. Temperature Dependence of the Spectra

In agreement with the reported results of earlier experiments,[65] no ESR spectrum of VCl_4 could be observed at liquid nitrogen temperature or above in any of the solvents used in this work. Further, as can be seen by inspection of the spectra in the previous section, there was no appreciable change in the ESR linewidths between 1.3 and 4.2°K in any single solvent. Because of a general interest in relaxation processes and their possible connection with the supposed Jahn-Teller effect in this molecule, several experiments were tried in which the VCl_4 signal was monitored as the sample warmed from liquid helium temperatures. In these experiments, an Au/Co//Cu thermocouple attached to the outside of the cavity with Wood's metal was used to follow the temperature as described in the experimental section. Because of the poor thermal contact between the cavity and the sample in the absence of liquid helium and the rapid warmup time, accurate temperature measurements were not possible with existing apparatus, but the data reported here serve to provide a qualitative description of the behavior of the spectrum in the range 4-60°K.

Figure 32 shows a series of spectra obtained from a $VCl_4/TiCl_4$ sample as it warmed from liquid helium temperatures. The top trace is that of a center portion of the spectrum in which the strong feature is the prominent line in Fig. 28. The subsequent traces, in which the center of the sweep and the spectrometer gain were adjusted to keep the strong line on the chart paper, show that as the sample warmed the individual hyperfine lines broadened and finally merged into a single line of nearly 1 KG width at about 50°K. This broad line completely disappeared at about 60°K. The sharp line which appears in the middle trace is due to DPPH and serves to locate the approximate position of the strong hyperfine

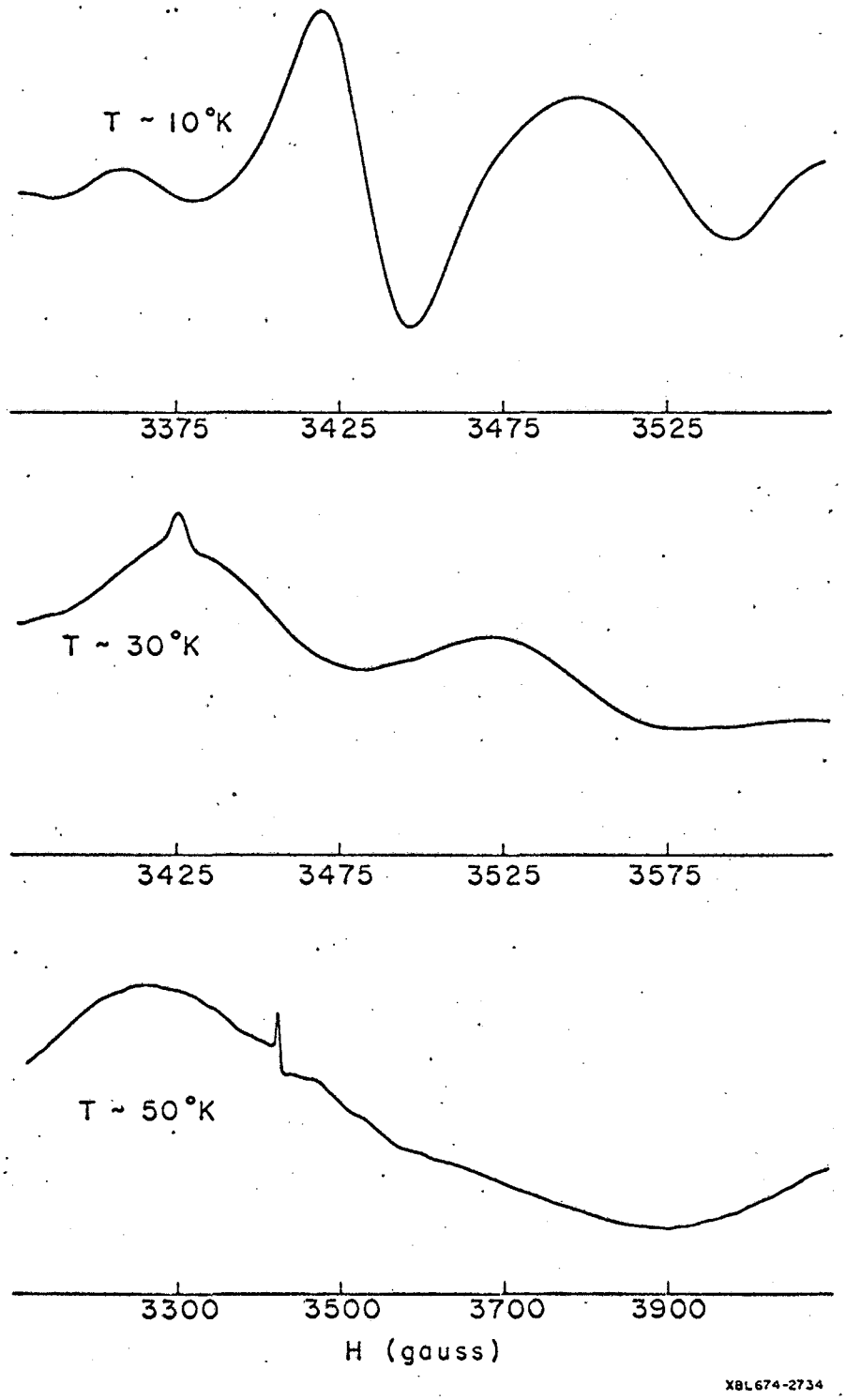

Fig. 32. Temperature dependence of the linewidth of the $m_I = -3/2$ line in the ESR spectrum of VCl_4 in $TiCl_4$.

component in the last spectrum. The elapsed time between the first and last of these spectra was about thirty minutes and no g-value measurements were possible in this period because of the rapid drift of the cavity frequency.

A plot of the peak-to-peak linewidth of the strong hyperfine component versus temperature is shown in Fig. 33. As can be seen by the dotted line in this graph, the data at temperatures below 20°K show a very good linear dependence on temperature with a slope approximately equal to one. Above this temperature, the linewidth increase with temperature is more rapid, although this may be due to thermocouple error (see Chapter III). This temperature dependence may then be used to discuss the mechanisms by which the transfer of energy from the spin system to the lattice system occurs.

In a very dilute paramagnetic crystal at low temperatures, there are three basic mechanisms for relaxing an ion in an excited spin state by a spin-phonon interaction.[66] These are the direct, Raman (indirect), and Orbach processes. The direct process describes the mechanism by which the downward transition in the spin system is accompanied by the creation of a single phonon of equal energy in the lattice. The Raman, or indirect process, involves inelastic scattering of a higher energy phonon with the production of a new phonon, the energy difference between the initial and final phonons being equal to the spin energy. The Orbach process is analogous to the indirect mechanism except that the absorption of a phonon by the lattice raises the system into a real (rather than virtual) excited state from which it decays by the emission of a new phonon. The temperature dependence of each process is quite different.[66] Van Vleck[67] originally showed that the spin-lattice relaxation time for the direct

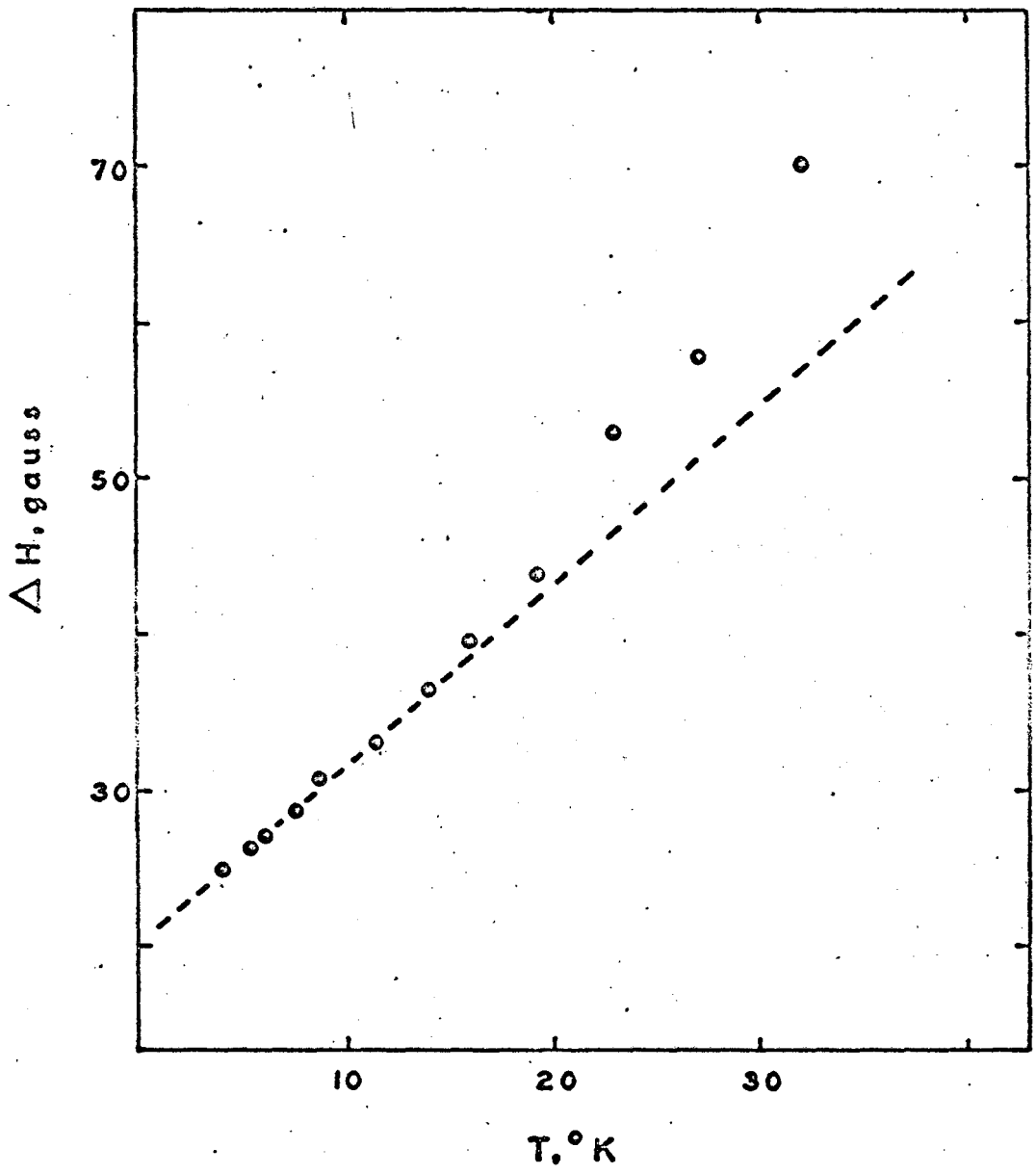

XBL 674-2728

Fig. 33. ESR linewidth versus temperature for the m_I = 3/2 line in VCl_4.

process varied inversely with the absolute temperature, whereas the Raman process showed a stronger temperature dependence, either T^{-7} or T^{-9} depending on the type of spin system. Since the Orbach process occurs via a real excited state, the relaxation rate is proportional to $\exp(-\Delta/kT)$, where Δ is the splitting of the excited state from the ground state. There are several examples in the literature[68] of low temperature electron spin systems which follow the temperature dependences predicted by these theories. In fact, rather good agreement is found in many cases between these theories for T_1 and those found by experiment.

In most solids, it is found that the width of the ESR transitions bears little relation to the true spin-spin relaxation time (T_2). This is because these transitions are inhomogeneously broadened[69] due to unresolved hyperfine interaction, imperfections in the solid state, g-value anisotropy, or other factors. Under some circumstances, most of the transitions for VCl_4 in $TiCl_4$ may be inhomogeneously broadened, but the strong central line appears to be a single isotropic transition that is homogeneously broadened at most temperatures and power levels. With this assumption, we can use the observed width to determine T_2 for this state of VCl_4 in $TiCl_4$.

If above 4°K we assume that $T_1 = T_2$, then our data are consistent with spin relaxation by a direct process. The data also predict that, if such a linear relation still holds up to a relatively high temperature, $T_1 \sim 1 \times 10^{-10}$ sec at 300°K. This is more or less in agreement with the NMR data on pure VCl_4 (<u>vide infra</u>) and with the fact that no ESR spectrum can be observed above about 60°K even in the pure solid.

However, the conclusion that the principal mechanism for electron spin-lattice relaxation in the temperature range 4-20°K is a direct

process is not consistent with most observations in low-temperature solids.[68] At temperatures of the order of 10°K, the Raman process should be very important because of the large number of higher energy phonons available above 1 or 2°K.[70] The sharp temperature dependence of these inelastic processes should then dominate the functional dependence of T_1 on temperature, and a linear relationship between T_1 and T^{-1} is not expected.

The fact that, if $T_1=T_2$, the ESR linewidth of the strong line in the VCl_4 spectrum is considerably larger than normally observed at these temperatures suggests the possibility of additional relaxation mechanisms. (A width of 30 gauss corresponds to a T_2 of the order of nanoseconds, whereas at these low temperatures relaxation times of the order of milliseconds or longer are usually observed.) This possibility was investigated, and it was found that the linewidth data for VCl_4 could be fit by an expression of the form

$$\Delta H' \propto (e^{\Delta/kT} - 1)^{-1} \qquad (54)$$

where $\Delta H'$ is an excess linewidth defined as the difference between the experimental width and the width at T=0°K, i.e.,

$$\Delta H' = \Delta H - \Delta H^{\circ} \qquad (55)$$

Taking ΔH° to be 20 gauss (see Fig. 33), Table XIV shows that the product $\Delta H'[\exp(\Delta/kT)-1]$ is reasonably constant if a value of Δ/k in the range 5-10°K is assumed. Not only does this reproduce the linearity of the linewidth data in the range 4-20°K, but it also predicts the rapid increase in width at higher temperatures.

A temperature dependence of this form has been observed in several systems described in the literature,[68] for example, Cr^{+3} in cadmium

Table XIV. Values of $\Delta H'[e^{\Delta/kT}-1]$ calculated from the VCl_4 linewidth data. See text.

T, °K	$\Delta H'$	$\Delta H'[e^{\Delta/kT}-1]$ for $\Delta/k = 5°K$	$\Delta H'[e^{\Delta/kT}-1]$ for $\Delta/k = 10°K$
4.2	5.0	11.6	50
8.7	10.8	7.9	22
16.0	19.7	7.5	17
22.9	32.5	8.1	18
32.2	50.2	8.5	18

tungstate.[71] Manenkov and Prokhorov[72] have shown that this result is to be expected when the splittings of the spin system energy levels involved in relaxation are larger than kT. Thus the behavior observed in Cr^{3+} was interpreted[71] as indicating that direct relaxation between the investigated lower levels $m_S = \pm 1/2$ is forbidden and that relaxation takes place through the upper level $m_S = 3/2$. This was confirmed by measuring the splitting between the $m_S = 1/2$ and 3/2 states spectroscopically and comparing this value with that calculated from T_1 data. The possible existence of such upper states in VCl_4 through which relaxation could occur will be discussed later.

3. Enhancement Phenomena and T_1 Measurements

During the investigation of the X-band ESR spectrum of VCl_4 at liquid helium temperatures, an unusual behavior of the spectrum was observed in CCl_4, $TiCl_4$ and $SnCl_4$ solvents. This is illustrated in Fig. 34, which shows a portion of the derivative spectrum of ~0.1M VCl_4 in $SnCl_4$ at 1.3°K. In this figure, the upper trace is that of a spectrum obtained by sweeping from low to high field (A to B). Then the y-axis of the recorder was offset slightly and the field was swept in the opposite direction, yielding the lower trace (C to D). Of interest here is the fact that the first lines observed in the upper trace appear to be power saturated, yet when the field is swept in the reverse direction, a normal spectrum is observed. A similar behavior was observed for the high-field end of the spectrum when the field was swept first downfield and then upfield. Further, subsequent experiments on both derivative and absorption spectra showed that the power saturated lines could be enhanced; i.e., returned to their normal intensity, by setting the field on top of the line in question and waiting for periods of the order of a minute. Since power saturation usually results in a 'permanent' dimunition of intensity, until the field is turned off resonance, this self-enhancement behavior was unexpected and consequently was investigated further. These experiments were usually performed by detecting the absorption spectrum, rather than the first derivative one, and a representative example of a VCl_4 ESR absorption spectrum in $TiCl_4$ at 1.3°K is shown in Fig. 35. Although similar behavior was observed for samples of VCl_4 in CCl_4 and $SnCl_4$, the results reported here are for $TiCl_4$ samples.

Several qualitative experiments were run in order to obtain more information on this effect. Some of the results were as follows:

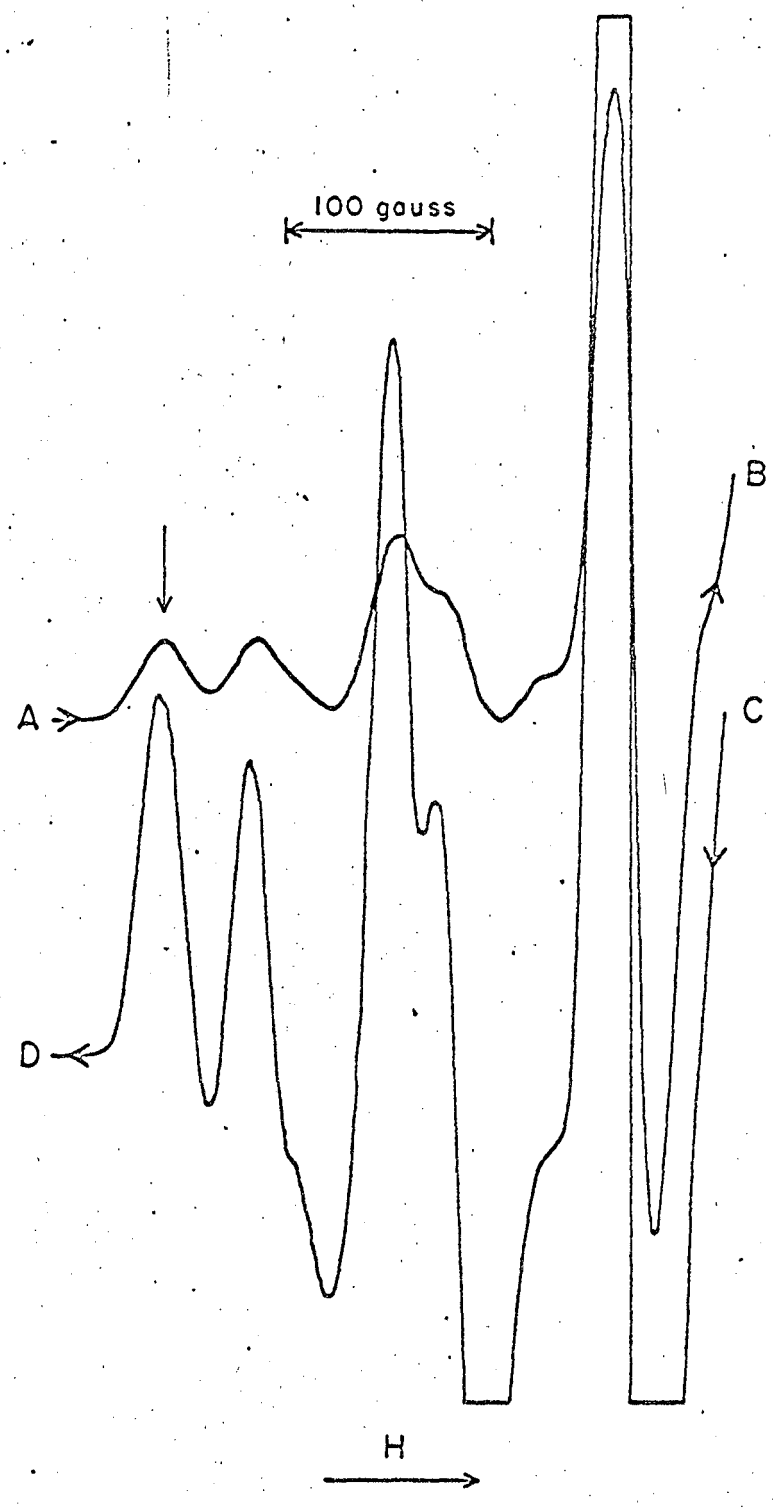

XBL673-986

Fig. 34. Anomalous spin relaxation in VCl_4. The spectrum was first swept from A to B and then immediately returned to the starting field by sweeping from C to D. The recorder was adjusted from B to C to displace the two records. Sweep time was about one minute each direction. Arrows along curves indicate direction of sweep. Vertical arrow marks position of line A.

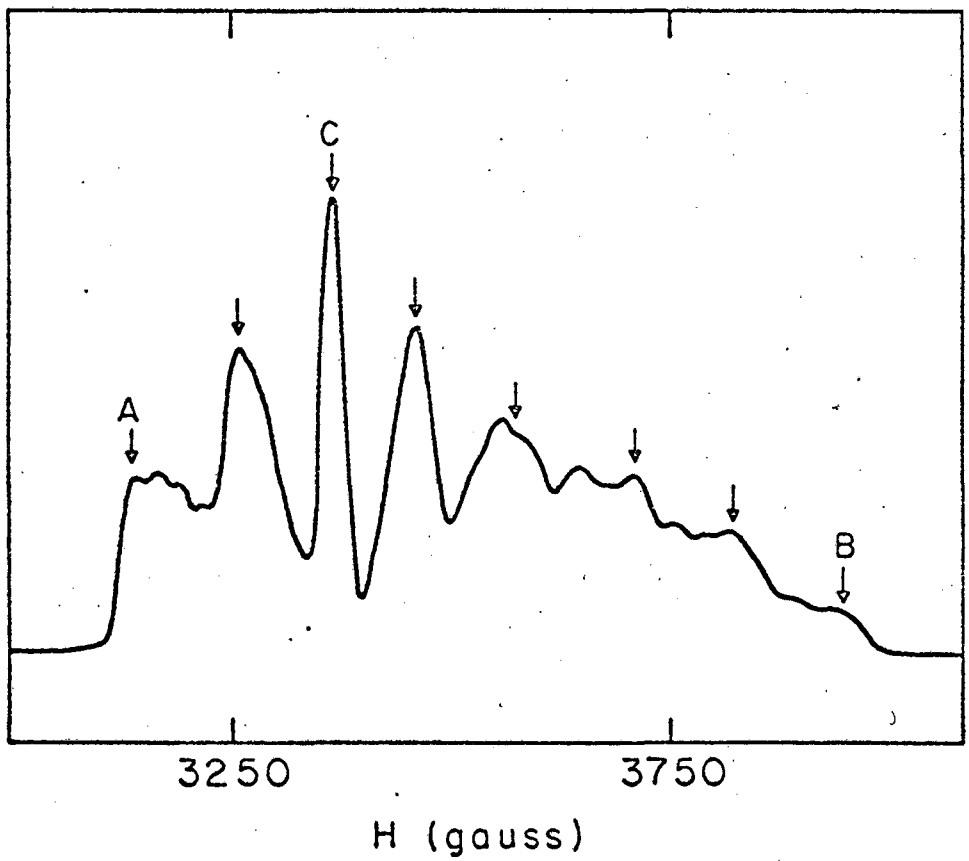

XBL674-2735

Fig. 35. X-band ESR absorption spectrum of VCl_4 in $TiCl_4$ at 1.3°K.

(a) The extent of saturation, i.e., how many lines of the spectrum could be saturated during a given sweep, was dependent on sweep speed and power level. More lines could be saturated with a more rapid sweep and/or higher power levels; however, the entire spectrum could not be saturated at the fastest sweep rates (0.5 sec., 10 KG sweep) and highest power levels. No effect was observed at -30 DB and below; there was only a small effect at -20 DB.

(b) After sitting for 2-3 minutes on a line in the middle of the spectrum with the microwave power on, the field was tuned quickly by hand to an outside line. The outside line could not be saturated at even the highest power levels.

(c) Starting with the microwave power off (using the manual wave-guide switch), the field was swept slowly and, at the field position of one of the weaker lines (A or B in Fig. 35), the power was turned on. This line was of normal intensity, the next two or three lines were saturated, and all remaining lines were normal. However, the strongest two or three lines of the spectrum could not be saturated and the effect was most pronounced at the edges of the absorption envelope.

(d) Once the lines were enhanced, two or three minutes completely off resonance were required before any part of the spectrum could be saturated and subsequently enhanced.

(e) At very slow sweep rates and medium power, no saturation was observed.

These effects were completely reproducible, even for a number of different samples, and the spectrometer was checked carefully to make sure that instrumental difficulties were not the source of this behavior. Because of the possibility that this anomalous relaxation phenomenon might be

related to processes connected with the Jahn-Teller effect in VCl_4, the enhancement of some of the lines was studied as a function of power and temperature. These results are described below.

a. Measurement of enhancement times.

Figure 36 shows an enhancement spectrum of one of the lines (A in Fig. 35) in the ESR spectrum of VCl_4 in $TiCl_4$ at 1.34°K. This was obtained in the following way. The derivative spectrum was recorded on an XY plotter and the field was tuned to the peak position of the line. Then the microwave power was turned off for a period of 2-3 minutes. Using a second plotter with time base, the sweep was started (2 sec/in in Fig. 36) and, after a delay of a few seconds, the microwave power was turned on with the manual waveguide switch. In this spectrum, the power level was -20 DB (0.72 MW) so the line was not completely saturated. Thus the plot of signal intensity vs. time in Fig. 36 shows the small intensity of the saturated signal which, after a period of about 20 seconds, was enhanced to its normal level. The slight decrease in intensity at $t > 20$ sec was thought to be due to a small saturation of the enhanced signal but could also result from spectrometer drift. The enhancement time (τ_e) is defined as the time required for the signal to reach its maximum intensity and in this spectrum is 20 seconds.

The enhancement times of lines A and B (Fig. 35) were measured as a function of incident power level and temperature. The power level was measured using a power meter (HP 431A) equipped with a thermistor mount (HP X486A) which was attached to one arm of the crossguide coupler in the cavity arm (cf. Fig. 7, Chapter III). Since the actual power absorbed by the sample was a function of the coupling of the cavity, the power measurements reported here are only relative. Table XV summarizes some of the data for enhancement times obtained in this way.

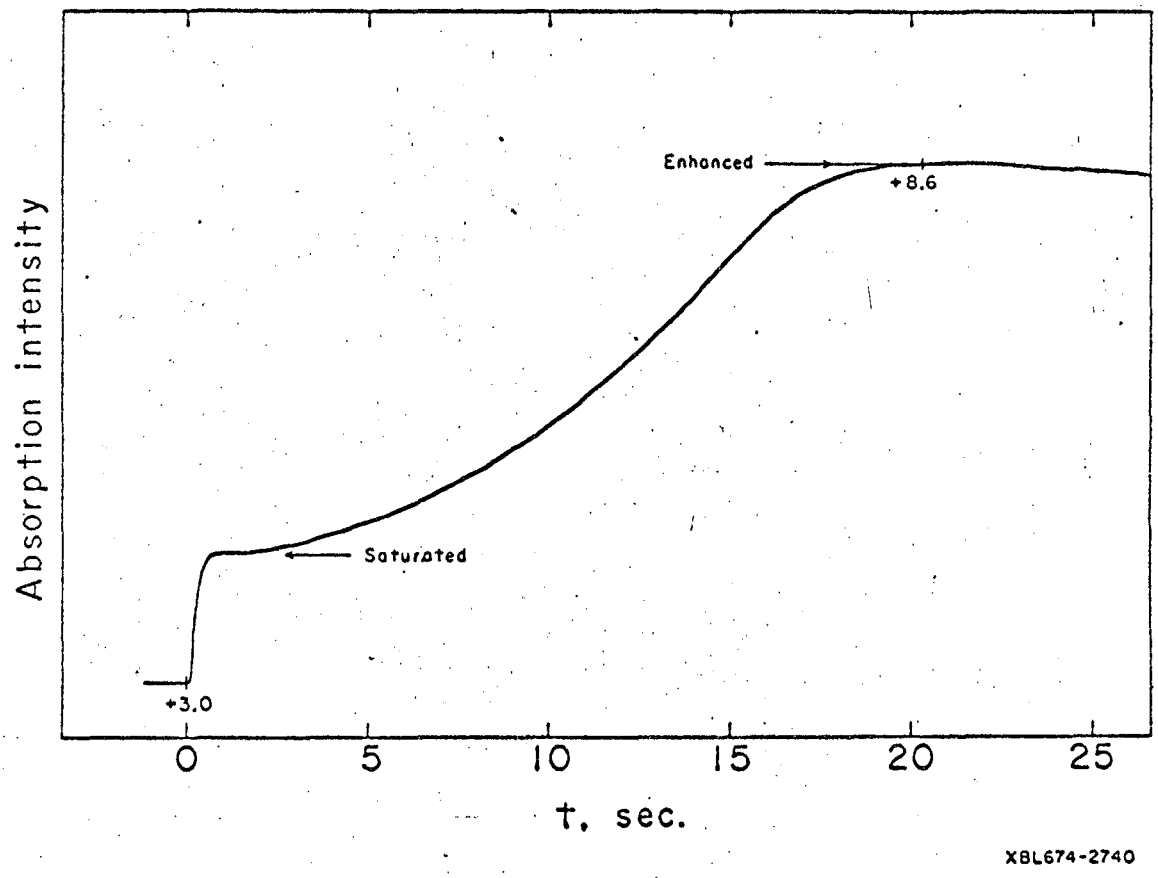

Fig. 36. X-band ESR enhancement spectrum of VCl_4 in $TiCl_4$ at 1.34°K. See text.

Table XV. Enhancement times as a function of incident power and temperature for lines A and B.

	T, °K	Power level, MW [a]	τ_e, sec [b]	Heat
A	1.34	78	4.2	79×10^{-3}
		34	5.9	48
		8.6	9.1	19
		0.72	20	3.3
	2.02	51	1.83	22×10^{-3}
		28	1.98	13
		6.4	2.7	4.1
		0.60	5.7	0.72
	4.2	18	0.43	1.9×10^{-3}
		9.9	0.48	1.2
		2.0	0.59	0.24
		0.16	1.70	0.07
B	1.34	48	13	148×10^{-3}
		8.3	26	53
		2.9	44	31
		0.78	140	26
	2.02	51	3.6	43×10^{-3}
		6.4	8.9	14
		2.3	14	7.7
		0.60	19	2.6
	4.2	15	0.53	1.9×10^{-3}
		1.6	0.86	0.24
		0.43	1.67	0.17
		0.10	2.46	0.05

a. Determined with HP 431A power meter, adding 20 DB to correct for directional coupler.
b. Corrected for rise time of recorder.

Qualitatively, it can be seen that, for a given line, the time required to produce enhancement decreases with an increasing power level and/or temperature. Further, at a given temperature and power, τ_e for line B is much longer than τ_e for line A. A graph of the power dependence of τ_e for line A at 1.34°K. is shown in Fig. 37. This sharp power dependence and the fact that τ_e decreases markedly with temperature increase suggests that the phenomenon of enhancement depends on the amount of heat absorbed by the sample. That this might be so is indicated by the last column in Table XV, where the relative heat dissipated in the cavity during the period of enhancement has been calculated. These numbers are the products of τ_e and the incident power level, converted to calories (1 calorie = 4.18×10^3 MW.-sec.). Obviously, the heats involved are very small.

The fact that the calculated heats are not constant is not unexpected, for we have neglected so far the presence of the bath of liquid helium which completely surrounds the ampule containing the sample. At the long enhancement times, and to a lesser extent the shorter ones, the heat produced by the microwave power is dissipated not only in the sample but also in the liquid helium. Further, since line B is weaker than line A, the sample absorbs less power when the field is tuned to B and the liquid helium proportionately more, so the enhancement times for line B are much longer.

The actual heat absorbed by the VCl_4, i.e., the heats calculated above corrected for that which is absorbed by the surrounding lattice and liquid helium, could be estimated by measuring the absorption coefficients of the lines. This was done for lines A and B in the following manner. The power incident on the cavity (at -6 DB) was measured with the power

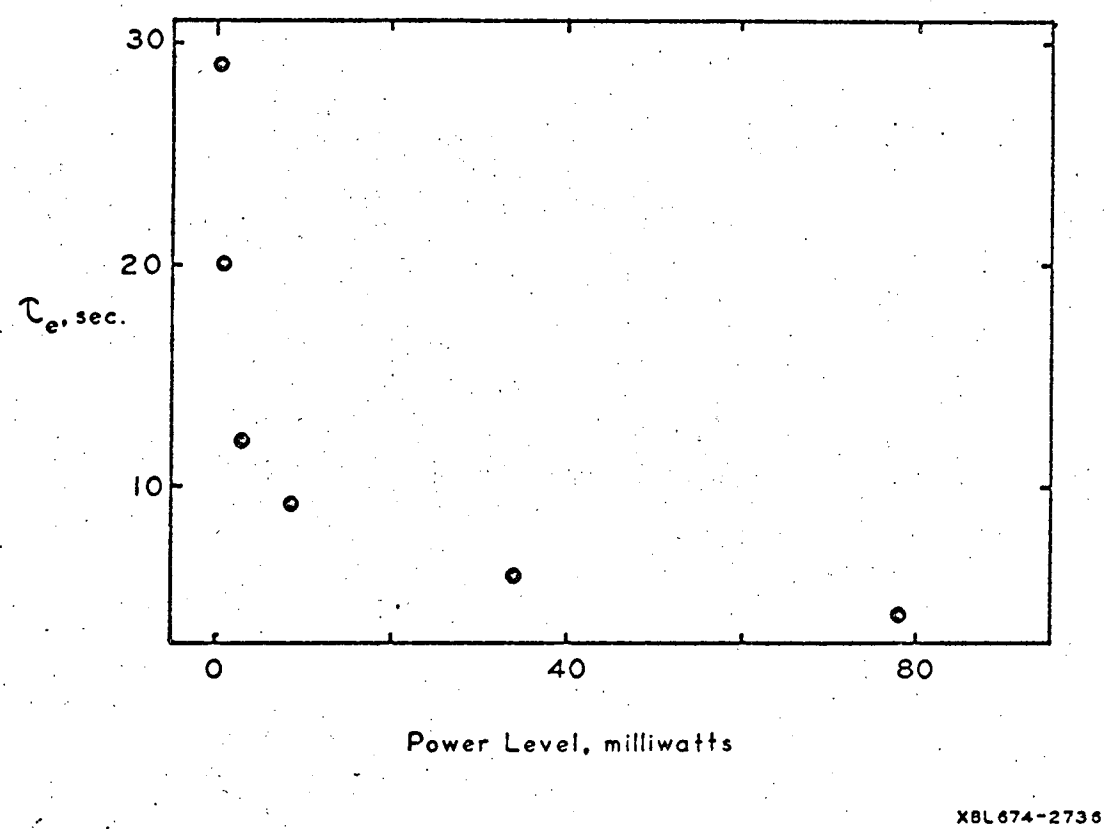

Fig. 37. Enhancement time vs incident power, line A, T = 1.34°K.

meter and was found to be 19.6 MW. Since the cavity was only one-half coupled, the actual power coupled into the cavity was about 10 MW. Then the absorption spectrum was recorded under conditions of no saturation. The power meter was moved to the detector arm of the bridge and the power level at the detector was measured when the field was tuned to the strong line (C) in Fig. 35. Then the field was tuned completely off resonance and the power measured again. The absorption coefficient for the strong line can then be estimated using the relationship

$$\epsilon \sim \frac{\text{(Power at detector, off res)} - \text{(Power at detector, on res)}}{\text{Incident power}} \qquad (56)$$

For line C,

$$\epsilon_C \sim \frac{0.45}{10} \sim 5 \times 10^{-2}.$$

Then the absorption coefficients of lines A and B can be obtained by multiplying ϵ_C by the ratio of the line A or B intensity to the line C intensity; this gives

$$\epsilon_A \sim 2 \times 10^{-2}$$

$$\epsilon_B \sim 3 \times 10^{-3}.$$

Thus the heat absorbed by the VCl_4 during the period of enhancement is very small indeed, being of the order of 10^{-5} calories or less, whereas the remainder of the heat ($\sim 10^{-3}$ cal.) is dissipated in the surrounding material and liquid helium bath.

b. Discussion of the enhancement behavior.

The lattice heat capacity of the $VCl_4/TiCl_4$ sample is presumably quite small at these temperatures. For example, if one assumes a Debye θ of 300°K. for $TiCl_4$, the heat capacity is less than 10^{-3} cal/deg

mole.[73] Thus the absorption of even 10^{-5} calories of heat by one millimole of sample would produce a temperature increase of at least 10°K. (the volume of these samples was about 0.5 cc.; this corresponds to about 5 millimoles of $TiCl_4$). Interestingly enough, taking the heat capacity of liquid helium at this temperature to be 0.6 cal/deg mole,[74] the absorption of 10^{-3} calories by a millimole of helium would produce an increase in temperature of about 1.7°K. Therefore, if the solid sample was not in good thermal contact with the walls of the ampule and thus with the liquid helium, the absorption of even 10^{-5} calories of heat by the sample could be significant. For, if saturation is viewed as being the result of a phonon bottleneck,[75] then a slight heating of the $VCl_4/TiCl_4$ matrix might break the bottleneck by populating higher vibrational modes of the lattice. This might reduce the T_1T_2 product (the saturation factor is $1 + \gamma^2 H_1^2 T_1 T_2$) and produce an "enhancement" because the line can no longer be saturated. Evidence of crystal heating at high power levels has been observed in some systems,[76] even at these temperatures, and has been discussed by Faughnan and Strandberg.[77] The decrease in the T_1T_2 product would presumably have no effect on the linewidth because it is probably determined by T_2 processes at this temperature (<u>vide infra</u>).

Unfortunately, whether or not there was good thermal contact between the sample and the liquid helium bath could not be determined. However, because the effect was observed to various extents for many different samples, it is worthwhile to consider other explanations. One suggestion, which is quite interesting, is based on the assumption that the heat absorbed by the VCl_4 spins during the enhancement period is not transferred to the surrounding $TiCl_4$ lattice, but rather is converted to

energy of internal motion in the VCl_4 molecules. Since the VCl_4 concentration in these samples was of the order of 0.01M, the absorption of a small amount of heat could produce a Boltzmann distribution in VCl_4 corresponding to a temperature considerably higher than 10°K. This could be so even with good thermal contact between the sample and the liquid helium, for the transfer of energy from the VCl_4 vibrational modes to the modes of the surrounding $TiCl_4$ lattice might be very slow.

It is interesting to speculate on the nature of this "melted" lattice. Certainly, in order to be of any effect in reducing T_1T_2, the modes excited by this increase in temperature would have to be fairly low frequency ones. Since the lowest vibrational mode in VCl_4 is thought to be in the region of 100 cm^{-1} (see Table III), an increase of 10-100°K. in the vibrational temperature of VCl_4 could produce an appreciable change in the population of excited vibrational states. On the other hand, it is thought[78] that dynamic Jahn-Teller motions in VCl_4 are much lower in energy, and so it is also possible that the melted lattice corresponds to VCl_4 molecules undergoing dynamic Jahn-Teller motion. Once this motion is excited, the lines would again be more difficult to saturate.

Figure 38 is a schematic representation of the sequence of events that might occur if such a transition from the frozen to the melted state did occur by the absorption of microwave power. In this diagram, the existence of two sublattices, in addition to the $TiCl_4$/liquid helium lattice, has been assumed. One sublattice is composed of VCl_4 molecules which are statically distorted and in thermal equilibrium with the $TiCl_4$ lattice. These VCl_4 molecules are represented by open circles, where the levels represent the splitting of the S = 1/2 state in the magnetic field. The second lattice consists of VCl_4 molecules undergoing dynamic

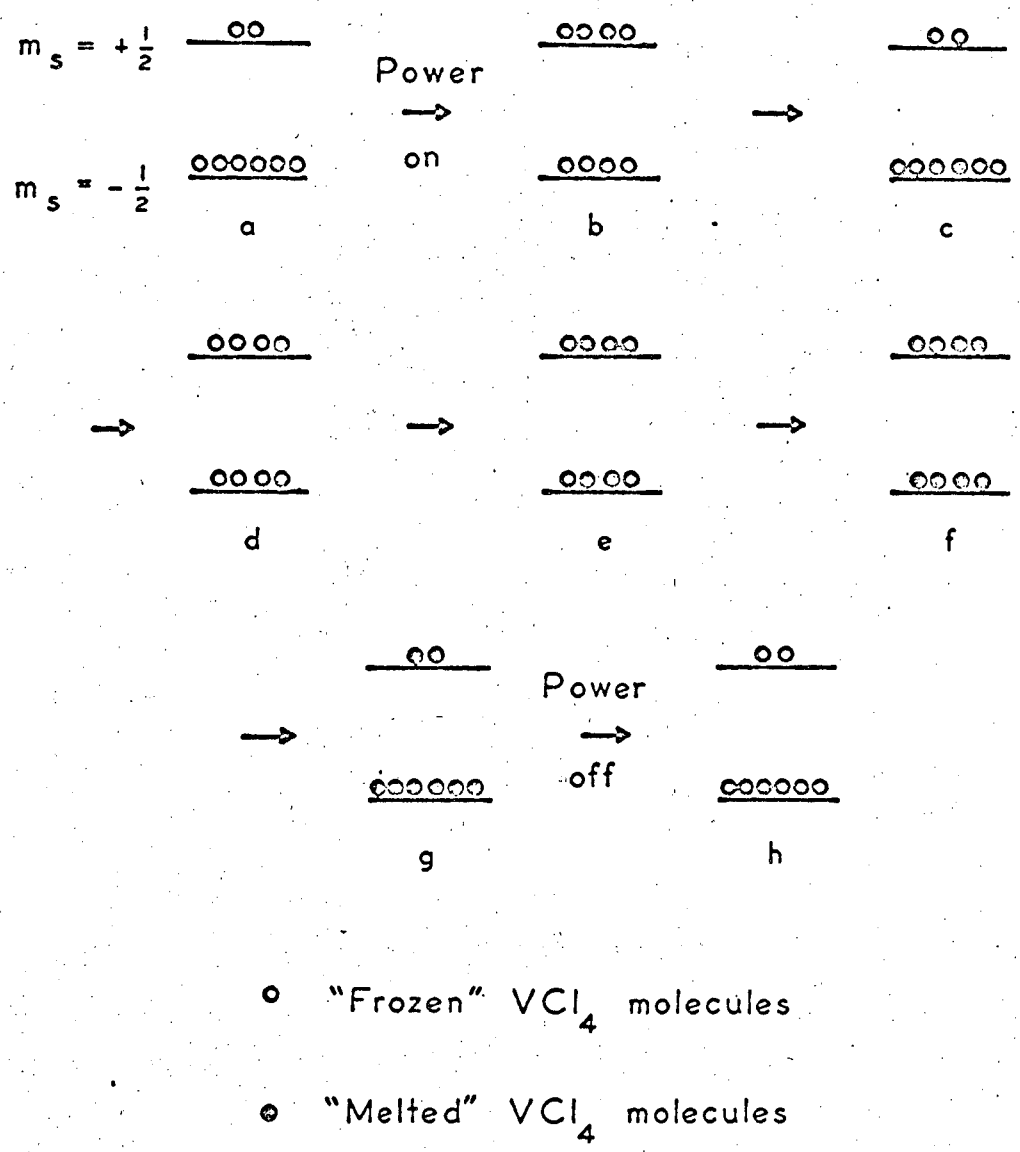

XBL674-2737

Fig. 38. Proposed model for the sequence of events occurring during enhancement. See text.

Jahn-Teller motion and are indicated in Fig. 38 by the filled circles. When the microwave power is turned on, the normal Boltzmann distribution (a in Fig. 38) is disturbed and the levels are saturated (b). As more heat is absorbed by the spins, the energy is transferred to the Jahn-Teller modes and more of the molecules are melted, (c) through (e). When the VCl_4 sublattice has absorbed enough heat to melt all the molecules (f), the T_1T_2 product is reduced and the levels can be described by a new Boltzmann distribution which is characterized by a slightly higher temperature (g). Then the lines are enhanced and, when the power is turned off, the molecules revert to the frozen state in a period of 2-3 minutes (h).

If the preceding is an accurate description of the behavior of the VCl_4 molecule when it is irradiated with a relatively high microwave power at very low temperatures, then one might expect to see evidence of this effect in the ESR spectrum. This is because the $\underset{\sim}{g}$ and $\underset{\sim}{A}$ tensors might be slightly different in the "frozen" and "melted" states. Indeed, by comparing the positions of some of the lines at low power with those at high power, some small differences which appear to be real are observed. For example, Table XVI compares the splitting of the first two "perpendicular" bands under enhanced conditions with that observed at very low power where the line could not be saturated. The latter values were measured by sweeping over the line very quickly at -30 DB, so the field was swept in both directions to prevent errors due to time constant asymmetry. However, although a difference in $\underset{\sim}{A}$ and/or $\underset{\sim}{g}$ between a statically- and dynamically-distorted molecule could explain these observations, there are other causes which might produce this effect.

Table XVI. A comparison of the splitting of the first two perpendicular bands (m_I = -7/2, -5/2) of the ESR spectrum of $VCl_4/TiCl_4$ under enhanced and normal conditions. T = 1.3°K.

H(-5/2) - H(-7/2), Enhanced. (MHz).	H(-5/2 - H(-7/2), Normal. (MHz).	
	Up	Down
0.50490	0.49168	0.50166
0.50567	0.49134	0.50151
0.50514	0.49084	0.50099
0.50691		

A full analysis of these results must be deferred until the VCl_4 spectrum in $TiCl_4$ is more completely understood. The spectra described earlier in this chapter are assumed to be for the melted state.

c. Measurement of T_1 using pulse techniques.

The observation that some of the ESR lines in the spectrum of VCl_4 could be saturated suggested that it might be possible to measure an electron spin relaxation time (T_1, T_2 or a product of these) for this molecule. Since such experiments would have to be done on a time scale short compared to the enhancement times discussed above, a microwave pulse network was assembled. This circuitry is described in detail in Chapter III. Basically, the circuit consisted of a fast solid-state microwave switch which was placed in the waveguide line between the klystron and the microwave bridge, and a pulse generator which was used to turn the switch on and off. With the switch on, the power level was

set to -20 DB; the power level when the switch was off was about -35 DB. Figure 39a is a schematic representation of the detector signal when the switch was turned on (pulse width ~5 msec.) and the field was tuned off resonance. Actually, the leading and trailing edges of the square wave pulse were rounded slightly because of a slower response time of the detector crystal (1N23E) and/or the associated circuitry, but these effects were small compared to the information contained in the detector signal when the field was on resonance. The detector signal when the field was tuned to an absorption line of the VCl_4 spectrum is shown in Fig. 39b; here, the differences between the detector signal on and off resonance have been magnified considerably for ease of visualization. When the field is on resonance and the microwave power is off (i.e., at the -35 DB level), the power at the detector is slightly less (or more, depending on bridge balance) than with the field off resonance because of the small ESR absorption which exists even at this power level.

Following the microwave switch, the detector signal rises sharply to a peak level when the power is turned on (-20 DB) but, since the field is tuned to a line, the DC voltage at the detector drops (1), Fig. 39b) because of ESR absorption. The line is then saturated and the detector level rises again exponentially to a value which is greater than the DC voltage at -35 DB. (2). The fact that the DC level is greater is due to the saturation of the spin levels, the spins absorb even less power than at -35 DB. When the incident power is reduced from -20 to -35 DB, the detector continues to see more power (3), but, as the spins begin to assume a normal Boltzmann distribution, the DC level at the detector approaches its original (-35 DB) value.

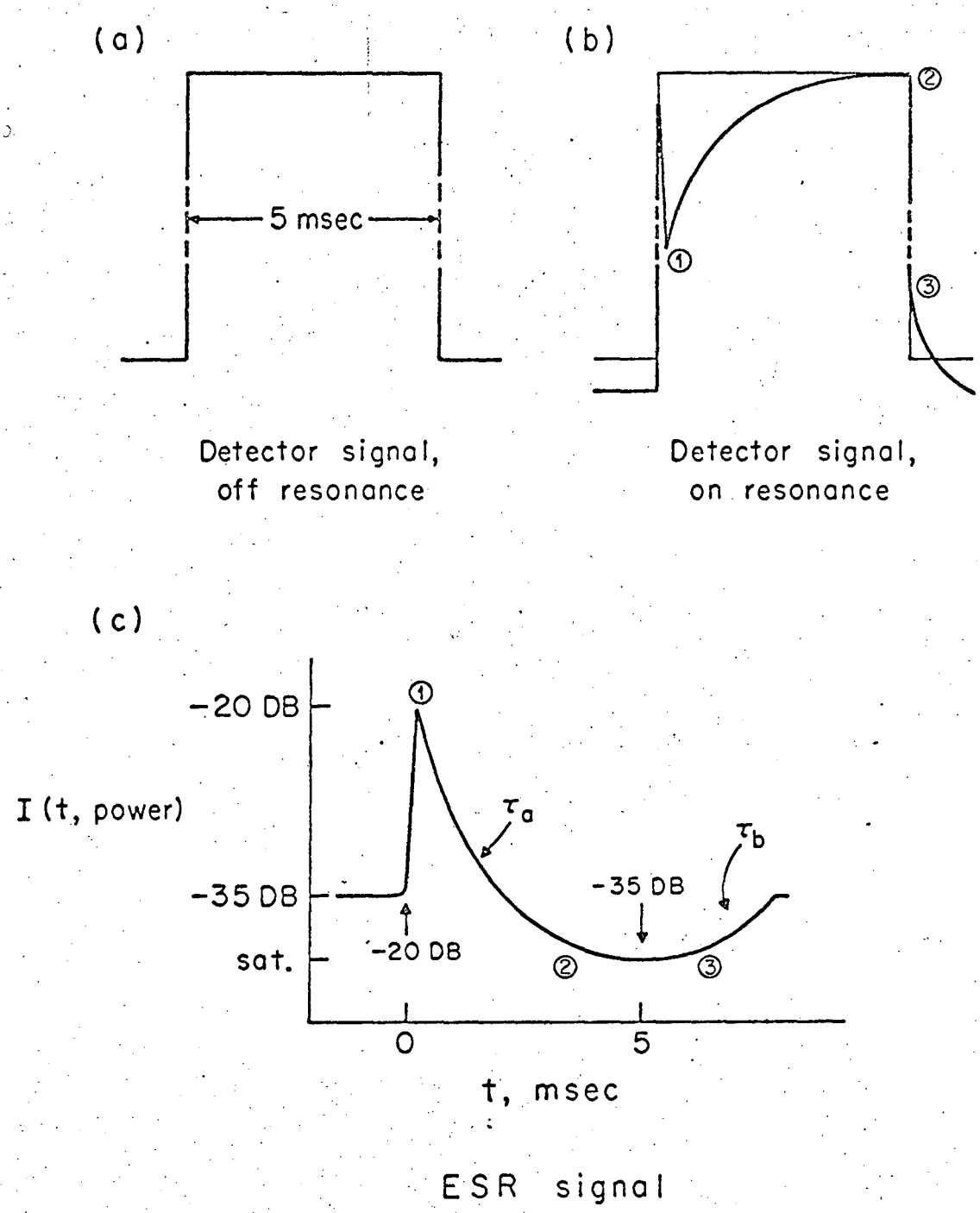

XBL674-2738

Fig. 39. Time development of detector and ESR signals during pulse experiment.

Thus, the time-dependence of the corresponding ESR signal after its initial increase from the -35 DB to the -20 DB intensity is describable by two exponentials. The first expresses the onset of saturation and has a time constant which we denote by τ_a. The second, with time constant τ_b, describes the approach of the spin system to Boltzmann equilibrium. This is illustrated in Fig. 39c. These two exponentials were photographed with an oscilloscope camera by suitable adjustment of the pulse delay and width and some representative results are shown in Figs. 40 and 41. The shapes of these curves correspond to portions of the detector signal on resonance (Fig. 39b). The photograph in Fig. 40 is that of the onset of saturation of the perpendicular component of the $m_I = 7/2$ line in VCl_4. The sinusoidal signal which is superimposed is due to the 10 KHz. AFC modulation of the klystron reflector voltage and the upper horizontal trace is the scope retrace. The other photograph (Fig. 41) shows the recovery of the $m_I = -1/2$ line (perpendicular signal) from saturation where the baseline (i.e., the signal at -35 DB) appears to the left of the trace.

A rigorous analysis of the data obtained from experiments of this type would be extremely complicated and does not appear to have been attempted. Instead, the usual approach[79,80] in the study of transient effects in magnetic resonance spectroscopy is based on the Bloch equations which, although only semi-quantitative in nature, are relatively easy to work with. The use of pulse techniques to study the time dependence of the magnetization has been limited mainly to the field of NMR, and early experiments by Torrey[81] and Hahn[82] showed that it was possible to obtain values for T_1 and T_2 in this way. The Torrey method,[81] called transient nutation, is concerned with the transient behavior of the spins during

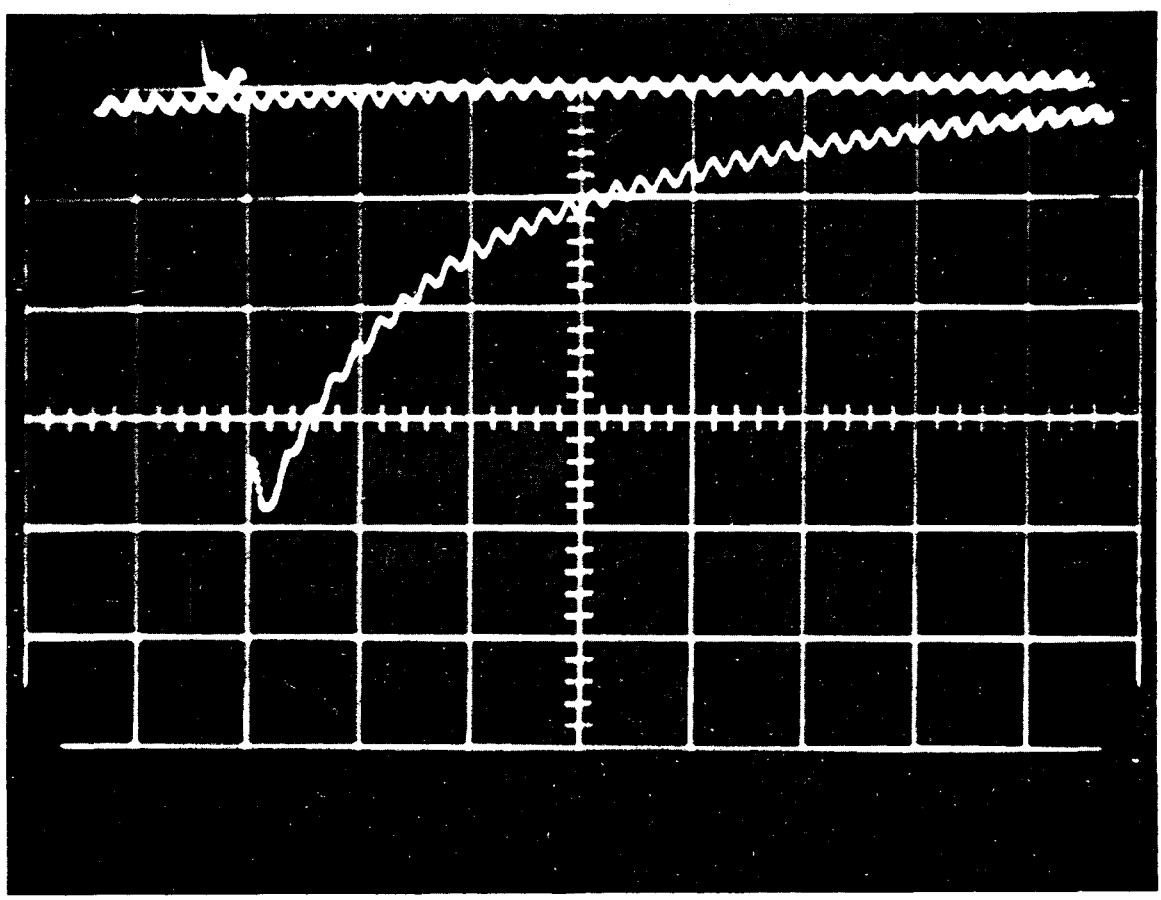

XBB673-1639

Fig. 40. Onset of saturation of the perpendicular component of the $m_I = 7/2$ line in VCl_4. Horizontal scale is 0.5 msec/cm. Pulse width = 5 msec, pulse delay = 1 msec. Decay time = τ_a.

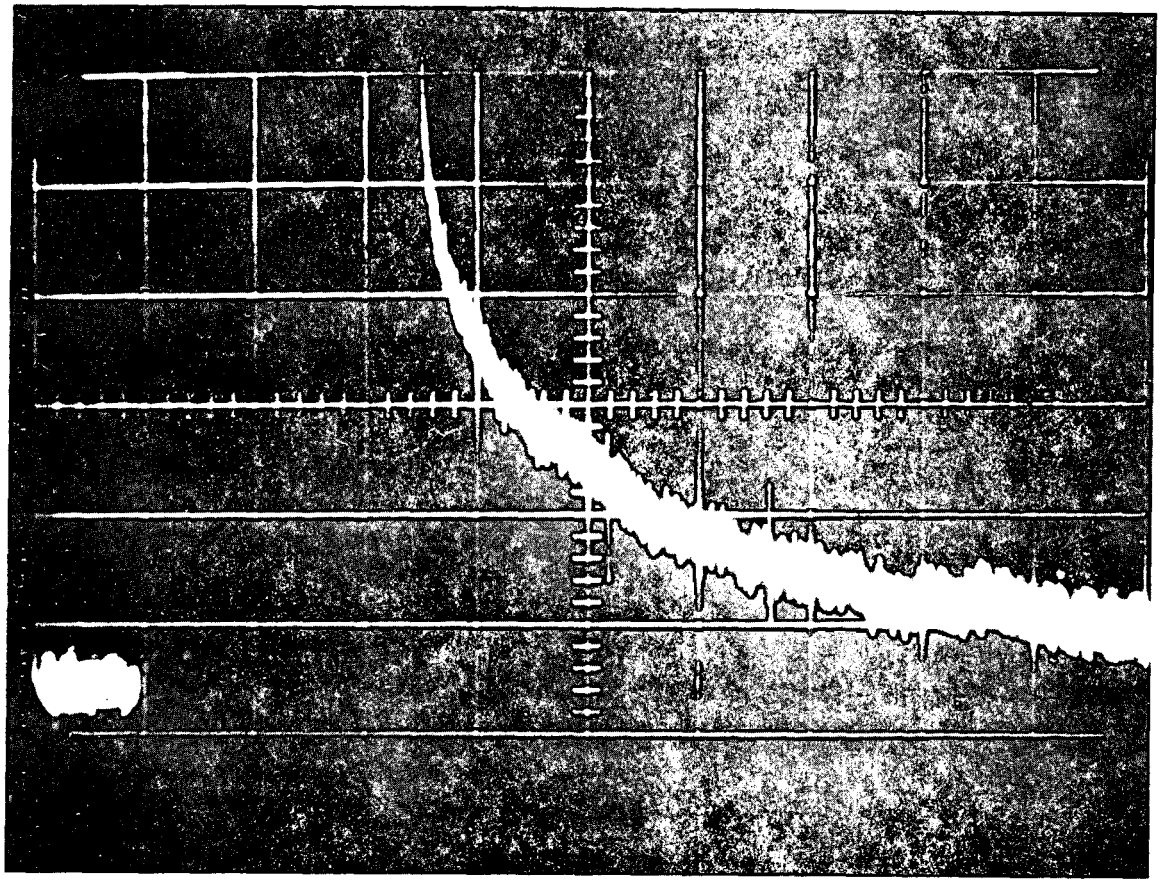

XBB673-1637

Fig. 41. Recovery from saturation of the perpendicular $m_I = +1/2$ line in VCl_4. Horizontal scale = 2 msec/cm. Pulse width = 5 msec, pulse delay = 2 msec. Decay time = τ_b (= T_1).

the time the radiofrequency pulses are applied. The experiments are done in a way which is quite similar to ours; namely, the approach to resonance is very rapid and takes place in a time which is short compared with the times T_1, T_2 and $(g\beta H_1/h)^{-1}$, and neither H_o nor H_1 are modulated. Making the following assumptions

$$(g\beta H_1/h)^{-1} << T_1,\ T_2 \tag{57}$$

and taking the initial conditions at t = 0 to be

$$M_x = M_y = 0, \quad M_z = M_0; \tag{58}$$

Torrey solved the Bloch equations for the time dependence of the magnetization during the period when the pulse is applied. In the usual rotating coordinate system, he found that the equation of motion for M_y, the absorption component of $\underline{M}$, described a damped precession of M_y around H_1 with a time constant which is given by

$$\frac{1}{2}\left(\frac{1}{T_1} + \frac{1}{T_2}\right) .$$

Consequently, the decay time of the exponential approach to saturation is

$$2\left(\frac{1}{T_1} + \frac{1}{T_2}\right)^{-1} .$$

The values of τ_a observed for various lines in the VCl_4 spectrum were of the order of 1-3 milliseconds. These are considerably longer, in view of the linewidths in our experiments and the values of T_1 (<u>vide infra</u>), than predicted by the above expression based on Torrey's model. Thus it must be concluded that this model is not a valid one for our experiments because of his assumption that $(g\beta H_1/h) << T_2$. The proper interpretation of our results therefore requires that solutions to the Bloch equations

be obtained without this assumption, and such an analysis is tedious.

The second decay time observed in our experiments, τ_b, is more easily treated. It is a direct measure of the return to Boltzmann equilibrium by the saturated spin system. This recovery of the magnetic moment during the "off" period is just T_1, the spin lattice relaxation time. Thus the method we have used is the so-called direct method,[83] which was first described by Bloembergen, et al.[13] Recent applications of this method in ESR experiments at liquid helium temperatures have been described.[66] In this case, the observed recovery of the signal follows the exponential law

$$1 - e^{-t/T_1}.$$

It is easy to see that when $t = T_1$, the signal intensity has reached 0.63 of its maximum value. Thus, the traces similar to Fig. 41 were used to measure the time elapsed between the time when the power was turned off and the point where the signal had reached 0.63 of its maximum intensity. The value of T_1 so obtained was measured for seven of the eight strongest absorption lines (perpendicular bands) in VCl_4 and the results are listed in Table XVII. The arrows in Fig. 35 indicate the approximate field positions of these measurements.

Several comments regarding these results should be made. In the first place, it is interesting to note that T_1 does not seem to differ much from one line to the next and that the overall variation in T_1 is only a factor of two. This suggests that the T_1 mechanism(s) which exists at this temperature is not very m_I-dependent. The values quoted here are thought to be accurate to only ±20% because there is a large measuring error and also because some of the lines (see Table XVII)

Table XVII. Values of T_1 for the perpendicular bands in the ESR spectrum of VCl_4 in $TiCl_4$ at 1.36°K.

m_I	T_1, milliseconds
*-7/2	5.6
*-5/2	6.0
-3/2	5.6
-1/2	2.8
* 1/2	2.8
3/2	3.8
* 5/2	3.4
7/2	---

* Decay appears to be slightly non-exponential.

appeared to be non-exponential. However, since a T_1 of 3 milliseconds would produce a linewidth (taking $T_1 = T_2$) of less than a milligauss, from our results we can conclude that $T_2 < T_1$ for VCl_4 at these temperatures. Attempts were also made to measure T_1 at higher temperatures (e.g., 2.0°K.) but these were unsuccessful. At higher temperatures, the transition to the "melted" state is more rapid and further, T_1 may be sharply dependent on temperature in this region.

The values of T_1 obtained above were measured by pulsing the microwave power at 2-3 minute intervals and for this reason they are thought to be characteristic of the "frozen" state. Figure 42 shows a sequence of traces which demonstrate that T_1 is much shorter in the melted state. In this experiment, the power was first turned on by the switch to -20 DB and the upper trace resulted. Then the power was set manually to about

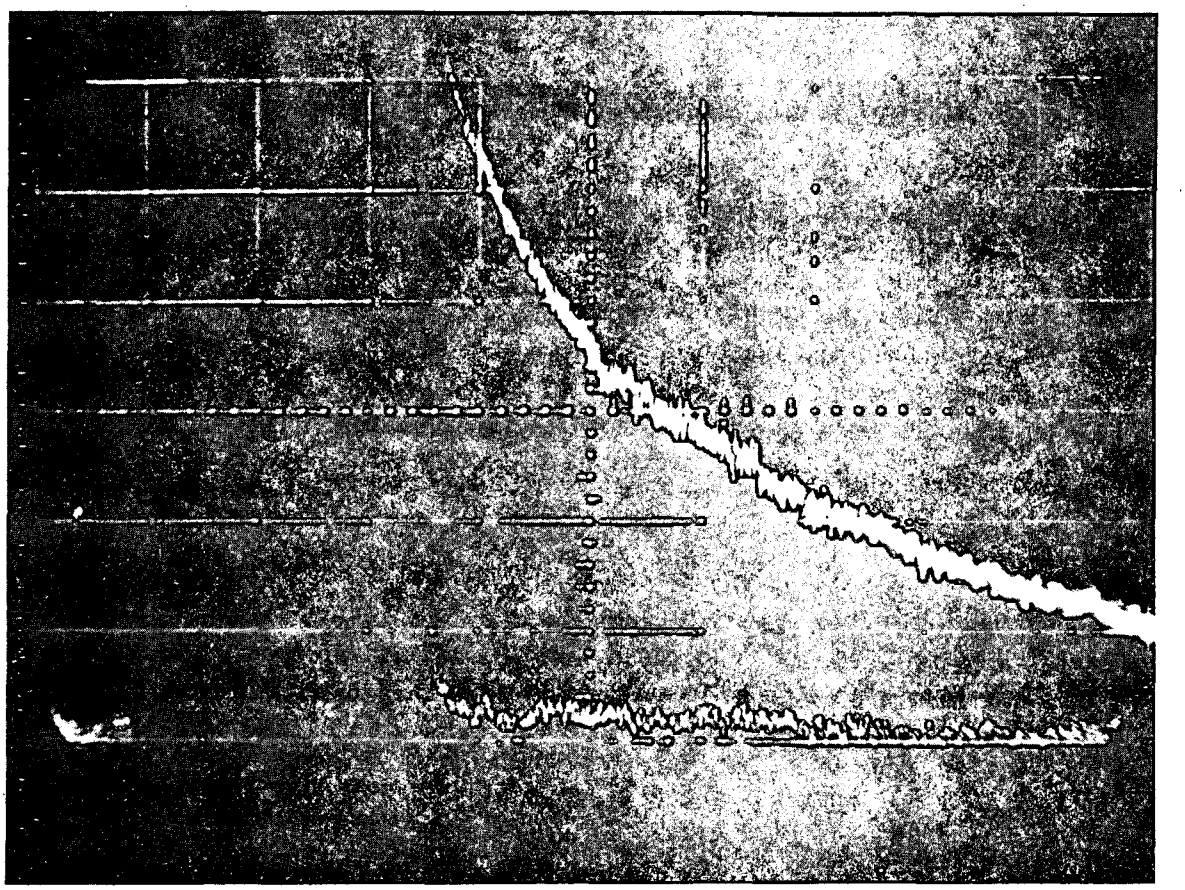

XBB673-1638

Fig. 42. Pulse experiments showing that T_1 (melted) $\ll$ T_1 (frozen). Scale and experimental conditions are the same as in Figure 41.

-16 DB for 30 seconds, returned to the -35 DB level and pulsed again. The lower trace shows that, after irradiating with a relatively high power for this period, no saturation occurred during the second pulse. This is consistent with the interpretation that, when the spectrum is enhanced, T_1 is considerably reduced.

4. Discussion

The data which have been obtained from the ESR spectra of VCl_4 in various hosts at liquid helium temperatures have been collected in Table XVIII. In this section we shall present an interpretation of these results, particularly as they relate to the structure of VCl_4 and the possible existence of a Jahn-Teller effect in this molecule. It will be recalled that such a discussion was fruitful in the case of $V(CO)_6$, and our approach here will be similar to that of Section A of this chapter. However, for VCl_4, the optical properties are relatively well understood and thus the theoretical g-values should be more quantitative. From Table XVIII, it is also apparent that considerable shifts in the ESR parameters are produced in going from one matrix to another. Although these shifts can be due to various factors, they are more or less predictable on the basis of a Jahn-Teller model which will be presented here. Finally, some comments regarding the observed relaxation effects in VCl_4 will be made.

a. g-Values and the Jahn-Teller effect in VCl_4

The crystal field energy level diagram for tetrahedral VCl_4 shown in Figure 6 (Chapter II) is exactly analogous to that for octahedrally-coordinated divalent copper ($3d^9$). Consequently, providing that the

Table XVIII. Observed g- and A-values for VCl_4 in various matrices at liquid helium temperatures.[a]

Host	g	$A/g\beta$ (gauss)
n-heptane	$\langle g \rangle = 1.931$	
mineral oil	$g_\perp = 1.915$ $g_\parallel = 1.941$ $\langle g \rangle = 1.924$	$A_\perp = 103.3$ $A_\parallel = 56.4$ $\langle A \rangle = 87.7$
CCl_4	$g_\parallel > g_\perp$	$(A_\perp = 113)$ $(A_\parallel = 97)$
$TiCl_4$	$g_1 = 1.900$ $(g_2 = 1.907)$	$A_1 = 120.3$ $(A_2 = 109)$
$SnCl_4$	$g_1 = 1.915$	$A_1 = 113$

[a] The values shown in parentheses are based on a tentative assignment. See text.

sign of the one-electron spin orbit parameter ξ is taken as positive, the g-value calculations in the literature for octahedral Cu^{+2} [21,84] are also appropriate for tetrahedral V^{+4}. The lowest electronic levels in tetrahedral VCl_4 (and octahedral Cu^{+2}) belong to the E representation of the group T_d (O_h for Cu^{+2}) and it is convenient to choose as wave-functions for these levels the pure orbitals

$$\psi_0(e) = d_{z^2} = |0\rangle \quad (= d_{3z^2-r^2}) \tag{59}$$

$$\psi_1(e) = d_{x^2-y^2} = \frac{1}{\sqrt{2}} (|2\rangle + |-2\rangle) \ . \tag{60}$$

where one of the S_4 axes of the molecule is taken as the axis of quantization. Using methods similar to those described previously, Ballhausen[21] has shown that, with this choice of basis functions, the g-values for each of these levels are approximately ($g_e = 2$)

$$\psi_o: \quad g_{\parallel} = 2, \; g_{\perp} = 2(1 - 3\xi/\Delta) \tag{61}$$

$$\psi_1: \quad g_{\parallel} = 2(1 - 4\xi/\Delta), \quad g_{\perp} = 2(1 - \xi/\Delta) \tag{62}$$

where Δ (= 10 Dq in Fig. 6) is the splitting between the e levels and the three t_2 levels. The wavefunctions for the latter in the coordinate system defined by the choice of the e wavefunctions are

$$\begin{aligned} \psi_2(t_2) &= d_{yz} = -\frac{1}{i\sqrt{2}}\left(|1\rangle + |-1\rangle\right) \\ \psi_3(t_2) &= d_{xz} = -\frac{1}{\sqrt{2}}\left(|1\rangle - |-1\rangle\right) \\ \psi_4(t_2) &= d_{xy} = \frac{1}{i\sqrt{2}}\left(|2\rangle - |-2\rangle\right) \end{aligned} \tag{63}$$

Any specific choice of basis functions for a tetrahedral VCl_4 will result in an anisotropic g-tensor; this is because the electronic wavefunction is really a linear combination of many orbitals, of which d_{z^2} and $d_{x^2-y^2}$ are only two. Thus the fact that (61) and (62) predicts an axial g-tensor is a natural result of selecting only one of these orbitals; if we took the full linear combination, $\underset{\sim}{g}$ would be isotropic.

Although the values of $g_{\parallel}$ and $g_{\perp}$ given in (61) and (62) have no physical significance in a tetrahedral molecule, they can be used to calculate an isotropic g-value for each of the e levels. The values of $\langle g \rangle$ so obtained are meaningful because they are the appropriate parameters in a classical energy expression and the energy of a molecule

is independent of the choice of a representation. The value of Δ for VCl_4 is known from spectroscopic measurements to be 9000 cm^{-1};[85] for ξ we take the reduced value 150 cm^{-1}[86] (the value 248 cm^{-1} is found from atomic spectroscopy for the free V^{+4} ion[87]). From (61) and (62), this choice of parameters gives for the predicted g-values of the states d_{z^2} and $d_{x^2-y^2}$,

$$\begin{aligned} d_{z^2}: \quad g_{\parallel} &= 2.002, \quad g_{\perp} = 1.900 \\ d_{x^2-y^2}: \quad g_{\parallel} &= 1.867, \quad g_{\perp} = 1.967 \end{aligned} \tag{64}$$

The isotropic g-values calculated from these components are equal for the two states, i.e.

$$d_{z^2},\ d_{x^2-y^2}: \quad \langle g \rangle = 1.934 ,$$

as they should be since the levels are degenerate in tetrahedral symmetry.

From Table XVIII we see that the predicted isotropic g-value of 1.934 agrees quite well with the value measured for VCl_4 in n-heptane, 1.931. Further, the value of $\langle g \rangle$ calculated from the anisotropic components observed in the VCl_4/mineral oil spectrum (1.924) is close to that predicted from this simple calculation. However, neither of the measured parameters allow one to conclude which of the two states is the true ground state of the molecule. This can only be determined by a consideration of the theoretical expressions for the anisotropic components of g.

As has been discussed in Chapter II, the only axial field which will break the two-fold orbital degeneracy of the e levels in VCl_4 is

of tetragonal symmetry. This distortion, which is assumed to be a consequence of the Jahn-Teller theorem, can be either a compression or an elongation of the tetrahedron. The splitting of the crystal field levels in both cases was shown in Figure 6. Taking the basis set used in the preceding discussion, the wavefunctions for the levels in a tetragonal field are

$$\psi_o(a_1) = d_{z^2} \qquad \psi_1(b_1) = d_{x^2-y^2}$$

$$\psi_2(e) = d_{yz} \qquad \psi_3(e) = d_{xz} \tag{65}$$

$$\psi_4(b_2) = d_{xy}$$

Thus an elongation produces a molecule of D_{2d} symmetry with a b_1 ground state (ψ_1), whereas the ground state in the compressed molecule (also D_{2d}) is $\psi_o(a_1)$. To first-order, the g-value expressions for each of the two possibilities are[21]

$$\psi_o(a_1) = d_{z^2}:$$

$$g_{\parallel} = 2$$

$$g_{\perp} = 2(1 - 3\xi/\Delta_1) \tag{66}$$

$$\psi_1(b_1) = d_{x^2-y^2}:$$

$$g_{\parallel} = 2(1 - 4\xi/\Delta_2)$$

$$g_{\perp} = 2(1 - \xi/\Delta_3) \tag{67}$$

where (cf. Figure 6)

$$\Delta_1 = E(e) - E(a_1)$$

$$\Delta_2 = E(b_2) - E(b_1) \qquad (68)$$

$$\Delta_3 = E(e) - E(b_1)$$

(Note that Δ_2 as defined here is different from that shown in Figure 6.) The second-order terms obtained by Abragam and Pryce[84] are assumed to be negligible.

The values of Δ_1, Δ_2 and Δ_3 can in principle be obtained from the optical data on VCl_4. However, for our purposes we shall first make the approximation that

$$\Delta_1 \sim \Delta_2 \sim \Delta_3 = 10\ Dq \qquad (69)$$

which seems reasonable. Then the g-values for the two possible ground states are the same as given in (64), i.e.

$$d_{z^2}: \quad g_{\parallel} = 2.002, \quad g_{\perp} = 1.900$$

$$d_{x^2-y^2}: \quad g_{\parallel} = 1.867, \quad g_{\perp} = 1.967$$

The values observed for VCl_4 in mineral oil are (Table XVIII) $g_{\parallel} = 1.941$ and $g_{\perp} = 1.915$ and thus the agreement with the predicted values for either state is very poor. For example, if one takes the experimental values and the expressions for the $d_{x^2-y^2}$ ground state, the calculated values for Δ_2 and Δ_3 are 19670 and 3448 cm^{-1}, respectively. Since these values are considerably different from the spectroscopic value of 10 Dq (9000 cm^{-1}), it is concluded that the static tetragonal model assumed for this calculation is incorrect for VCl_4 at low temperatures.

However, if we assume that the true wavefunction for the unpaired electron in the ground state of VCl_4 is a linear combination of the d_{x^2} and $d_{x^2-y^2}$ orbitals, e.g.,

$$\Psi_o = \cos\alpha \ \psi_o + \sin\alpha \ \psi_1 \tag{70}$$

then the true g-values are also linear combinations of the form

$$g(\text{obs}) = (\cos\alpha)^2 \ g(\psi_o) + (\sin\alpha)^2 \ g(\psi_1) \tag{71}$$

Now, since the observed isotropic g-value for the mineral oil spectrum is in good agreement with that predicted earlier, we know that the true wavefunction must be a linear combination of the form (70). Hence, Eq. (71) and the required trigonometric identity

$$\cos^2\alpha + \sin^2\alpha = 1 \tag{72}$$

can be used to calculate the mixing coefficients. As will be shown later, if a dynamic Jahn-Teller model is assumed, $g_{\parallel}$ will correspond to the g-value for distortions along each of the three principal axes of the molecule. Hence the observed $g_{\parallel}$ is an average of these three values, and in each of these distortions the ground state is either $d_{x^2-y^2}$ or d_{z^2}. Although a similar average for $g_{\perp}$ is in agreement with this calculation, the meaning of the observed $g_{\perp}$ value is not as clearly defined. Thus, Eq. (71) for $g_{\parallel}$ and (72) give for the mixing coefficients

$$\cos\alpha = 0.740 \qquad \sin\alpha = 0.672 \tag{73}$$

and the ground state is d_{z^2} with a large contribution from $d_{x^2-y^2}$. Whatever the nature of the interaction which produces this mixing, the "averaged" structure of VCl_4 at about 1°K is a compressed tetrahedron. This is in disagreement with the theoretical work of Liehr and Ballhausen,[78] who predicted that the ground state of VCl_4 was an elongated tetrahedron,

i.e., that the unpaired electron was in the $d_{x^2-y^2}$ orbital.

A possible explanation for the origin of this mixing is a dynamic Jahn-Teller effect. As was discussed in some detail in Chapter II, Abragam and Pryce[88] were the first to show that the g-values observed for $CuSiF_6$ were explicable by this effect. The theoretical aspects of this problem, particularly as they apply to Cu^{+2} have been investigated in detail by Avvakumov, et al.[89] and in a later paper by O'Brien.[58] In our brief discussion of this effect, we shall follow the nomenclature of O'Brien. An excellent discussion of the Jahn-Teller effect can be found in Herzberg.[90] The reader is also referred to Ballhausen[21] for a general description and to a review article by Liehr.[91]

Formally, the mixing of the electronic wavefunctions produced by the Jahn-Teller effect can be represented by the addition of potential energy terms in Q_i, Q_i^2, etc. to the Hamiltonian, where the Q_i are the normal coordinates of the non-totally symmetric vibrations. In VCl_4, these "vibronic" terms must be of symmetry class e^{90} (ν_{2a} and ν_{2b}) and they produce a splitting of the potential functions of the states d_{z^2} and $d_{x^2-y^2}$. O'Brien[58] has shown that the electronic eignefunctions for the resulting potentials, when terms linear in the Q_i are retained and all other terms are neglected, are of the form

$$\begin{aligned} &\cos\theta/2\ |z^2\rangle + \sin\theta/2\ |x^2-y^2\rangle \\ &\sin\theta/2\ |z^2\rangle - \cos\theta/2\ |x^2-y^2\rangle \end{aligned} \tag{74}$$

In these expressions, the polar coordinates ρ, θ in the space of the coordinates Q_i defined by

$$Q_{2a} = \rho \cos\theta$$
$$Q_{2b} = \rho \sin\theta \qquad (75)$$

have been substituted for the Q_i. The angle $\theta/2$ therefore corresponds exactly to the angle α of the previous discussion. Rather than describe the resulting potential surfaces in detail here, the reader is referred to Herzberg.[90] The situation which is thought to exist in VCl_4 at this level of approximation is shown in Fig. 16 of this reference.

The inclusion of higher order vibronic terms in the Hamiltonian produces a lower potential energy surface consisting of three "bowls" separated by saddle points, all of which are joined together in the center by a conical peak (see Figs. 17 and 18 of Herzberg[90]). Thus there are two barriers to consider. One is a single barrier at $Q_{2a}=Q_{2b}=0$ which is the result of first-order vibronic terms. The second is a threefold barrier in the trough, the position of the molecule in the trough being defined by the angle θ. Whether or not the center peak actually touches the upper surface at $Q_{2a}=Q_{2b}=0$ (i.e., whether the ^2E state is split for zero displacement) depends on the magnitude of the spin-orbit interaction connecting the two states and is not relevant to our discussion here.

If we assume that the height of the center barrier is large compared to (a) kT at liquid helium temperatures and (b) the zero-point energy of the Jahn-Teller motion, then the situation is as follows. The molecule is confined to the trough in the lower potential surface which surrounds the center peak. If the zero-point energy of the motion is sufficiently high compared to the threefold barrier, the nuclei may tunnel through or surmount the saddle points in going from one potential minimum to another.

It is clear that the degree of freedom θ, but not ρ, is more or less cyclic, corresponding to a slightly hindered internal rotation or inversion. This continuous interconversion from one distorted form to another produces a variation in the charge density $|\Psi_o|^2$ with time; it is therefore impossible to specify which of the original wavefunctions the system is in.

Now, we know from symmetry considerations that the motion which breaks the degeneracy of the ^2E state in VCl_4 must have e symmetry. With this fact as a guide, Ballahusen and Liehr[78] have shown, using a point charge model, that the motion of a VCl_4 molecule undergoing a dynamic Jahn-Teller distortion is a sort of pseudo rotation. In their model, each chlorine atom is displaced from the normal tetrahedral position and rotates around the tetrahedral bond axis with a radius of 0.11 Å. This motion generates a cone with an apex angle of 6°. The angle θ (Ballhausen and Liehr use ϕ) defines the position of a chlorine atom on the circle traced out by its rotation. From our ESR results, we know that the lowest energy configuration corresponds to a compressed tetrahedron; hence the positions of minimum energy ($\theta = 0, 2\pi/3, 4\pi/3$)[78] occur when each chlorine atom touches an edge (and not a face, as in reference 78) of a cube enclosing the tetrahedron.

Although this model seems to agree with the ESR data on VCl_4 in mineral oil, on closer examination there are some inconsistencies. In the first place, regardless of the nature of the Jahn-Teller motion, the fact that there is such severe mixing of the d_{z^2} and $d_{x^2-y^2}$ orbitals ($\cos^2\theta/2 = 0.548$, $\sin^2\theta/2 = 0.452$) means that there must be nearly free rotation of the molecule in the trough. This is because, with a three-

fold barrier of approximately zero height, the values of the mixing coefficients are just their time averages, i.e., $\cos^2\theta/2 = \sin^2\theta/2 = 0.50$. If this is the case, then the g-tensor should be essentially isotropic, rather than the clearly anisotropic one which we have observed. These comments can be put on a more quantitative basis by assuming a specific model for the Jahn-Teller motion. For example, with a pseudo rotation of the type described above, one gets an effective rotational constant B of the order of 10 cm^{-1}. This would correspond roughly to the splitting between the vibronic levels E and A[58] in the threefold barrier. The Jahn-Teller frequency, classically, is of the order of the inverse of this splitting. Since the ESR frequency (or more correctly, the difference between $g_{\parallel}$ and $g_{\perp}$ expressed in frequency units) is much less than this inverse splitting, an isotropic Hamiltonian is predicted.

There is a brief report in the literature[92] of a $3d^1$ system (CaF_2: Sc^{+2}) in which the splitting of the vibronic levels E and A is 10 cm^{-1}. In this case, the authors observe an anisotropic Hamiltonian below 40°K and an isotropic one above this temperature. However, their values of the mixing parameters are about $\cos^2\theta/2 \sim 1$ and $\sin^2\theta/2 \sim 0$, so the mixing is very slight. Thus the anisotropic spectrum "belongs" to the lower E state and becomes isotropic when the A state is populated; the barrier is therefore about 50 cm^{-1}. It is still possible, in the case of VCl_4, that the motion in the trough is such that an anisotropic Hamiltonian results. This will depend very sensitively on the barrier height and the vibronic spacings and calculations of this height using the model of Ballhausen[78] and the observed values of $\cos^2\theta/2$ and $\sin^2\theta/2$ are in progress.

There is one other explanation of the observed g-values which is, at the moment, more satisfactory. This is that there exists in VCl_4/

mineral oil samples a static distortion having a value of θ which corresponds to the observed mixing coefficients (i.e., $\theta \sim 84°$). The nature of this distortion cannot be described, but it is clearly not tetragonal. If the cage in mineral oil is small compared to the size of a VCl_4 molecule, then such a distortion, necessarily axial, is possible.

However, we can conclude from our results that the two e-wavefunctions are mixed and that the ground state of VCl_4 in mineral oil has

$$\Psi_o = 0.74\ \psi_o(d_z{}^2) + 0.67\ \psi_1(d_{x^2-y^2}). \qquad (76)$$

Because of the agreement between the observed g-values and those calculated using this Ψ_o, it is clear that this distortion is produced by a Jahn-Teller effect. Whether this is static or dynamic in nature remains to be determined. Although we cannot discuss the spectra of VCl_4 in solvents other than mineral oil as quantitatively, our interpretation of these spectra is consistent with a Jahn-Teller model. As has been pointed out above, the symmetry of the spin Hamiltonian is a sensitive function of the size of the threefold barrier. O'Brien[58] has shown, for octahedral Cu^{+2} compounds, that as the height of this barrier decreases, the g-tensor becomes more anisotropic and eventually has three principal values (so-called rhombic symmetry) for vibronic states below the barrier. Similar considerations apply to the A-tensor and it seems reasonable to assume that these predictions are also valid for VCl_4. Consequently, our observations (a) that the spectrum of VCl_4 in CCl_4 is describable by a spin Hamiltonian with a symmetry slightly less than axial and (b) that the g- and A-tensors of VCl_4 in $TiCl_4$ and $SnCl_4$ are rhombic are consistent with a lowering of the barrier in the order mineral oil, CCl_4 and $TiCl_4$.

This decrease in the barrier height must of course be such that even in $TiCl_4$, the ground vibronic level of VCl_4 is still considerably below the barrier. Such an interpretation is consistent with the usual considerations of "cage" size in matrices of this type. It is interesting to note also that the accurately-known g-value in $TiCl_4$ is 1.90; this is just what is predicted for a pure d_{z^2} ground state. O'Brien also shows that when a rhombic Hamiltonian exists, there are additional transitions not at g_1, g_2, or g_3 which are the result of the mixing of higher vibronic levels with the ground state. Transitions of this type may be causing part of the difficulty in making the assignment of the $VCl_4/TiCl_4$ ESR spectra. Moreover, the annealing process suggested as an explanation for the non-reproduciblity of these spectra could produce small changes in the barrier height.

b. Relaxation effects.

We have already discussed the fact that the m_I-dependence of the linewidths in the VCl_4/mineral oil spectrum is explicable using the model proposed by O'Brien.[58] In this case, transitions between the vibronic energy levels produces a broadening of the ESR lines which is proportional to

$$\tau\,[(\Delta g\beta H) + (\Delta A m_I)]^2 .$$

The author also shows that, as the temperature increases, τ becomes shorter. Then, when the relaxation rate becomes fast compared to the frequency difference between the resonance lines from the different vibronic states, the g- and A-value anisotropies are averaged out and the spectrum becomes a single line with an average g-value. Thus the value of $\Delta \sim 10°K$. obtained by fitting the temperature dependence of the

linewidths to the expression (see Section 2)

$$\Delta H' \propto (e^{\Delta/kT} - 1)^{-1}$$

probably corresponds to the splitting between neighboring vibronic levels. A confirmation of this may be provided by the barrier calculations mentioned earlier.

The enhancement behavior described in Section 3 is more difficult to analyze. However, we would suggest that this phenomenon can be explained by assuming that the heating of the VCl_4 molecules produced by (relatively) high microwave power results in the excitation of at least some molecules to excited vibronic states. These would have a shorter T_1T_2 product because of the higher probability of relaxing via other vibronic levels, including those in adjacent potential minima. It is clear that these excited states must also be considerably below the barrier since the spectrum is still anisotropic. O'Brien[58] suggests that the expectation value of cos $\theta/2$ may be different for different vibronic states and this could produce slight changes in g and A such as were observed in going from the normal to the enhanced spectrum.

C. NMR of VCl_4 and $TiCl_4$

1. Assignment of the Spectra

a. Pure VCl_4.

The ^{35}Cl NMR spectrum of VCl_4 consists of a single, broad line whose peak-to-peak width at room temperature is approximately 2.25 KHz. (5.40 gauss). A representative spectrum, which was obtained at 5.8785 MHz. in a field of 14.09 KG., is shown in Fig. 43. With an external 3M NaCl reference solution, the position of the VCl_4 signal with respect to the Cl^- signal was determined employing the methods described in the experimental section. At 23°C., the VCl_4 line was shifted downfield from the Cl^- line by about -619 ppm. (=3.64 KHz. = 8.73 G.). This shift was found to be temperature-dependent and this behavior was used for the measurement of the chlorine hyperfine coupling constant in VCl_4 (vide infra).

b. Pure $TiCl_4$.

A somewhat narrower (0.871 KHz. = 2.09 G. at 23.2°C.) ^{35}Cl NMR line was observed for the pure $TiCl_4$ liquid. Figure 44 illustrates a spectrum which resulted when the field was swept at a low enough RF power to observe the Cl^- sidebands on the same record. The two first sidebands are split by twice the modulation frequency (ν_m = 400 Hz.); consequently, the position of the $TiCl_4$ signal with respect to Cl^- could be obtained directly. (The same was true for the VCl_4 spectra). The shift measured in this way was -864 ppm. (=5.08 KHz. = 12.2 G.). This value compares favorably with that given in the literature[93] (-820 ppm.) and, so far as could be determined, was independent of temperature. At higher RF power, the S/N ratio of the $TiCl_4$ signal was considerably improved (see insert, Fig. 44) but the Cl^- sidebands were power saturated. Thus, during a given sweep of the type shown in Fig. 44 , the RF power and

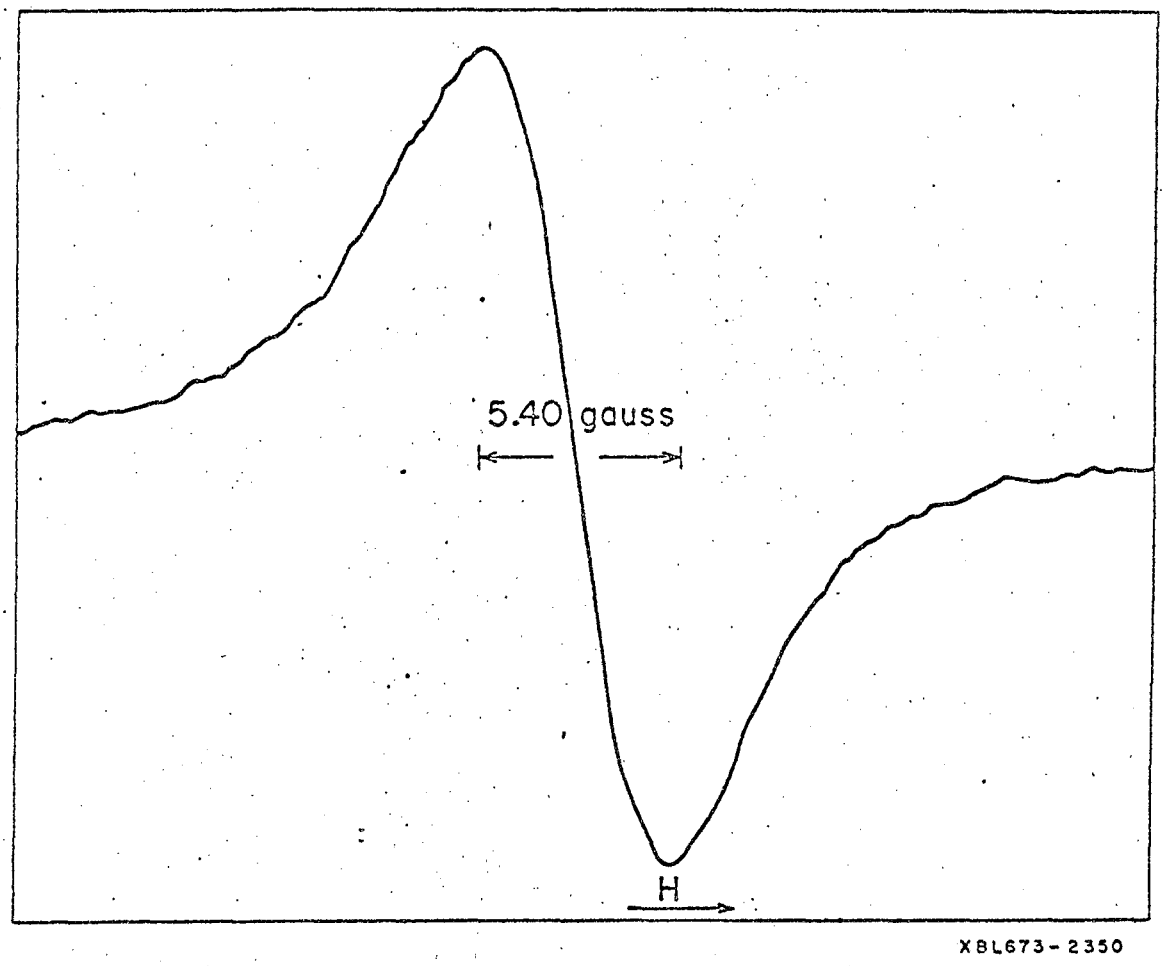

Fig. 43 Room-temperature ^{35}Cl NMR spectrum of pure VCl_4 at ν = 5.8785 MHz.

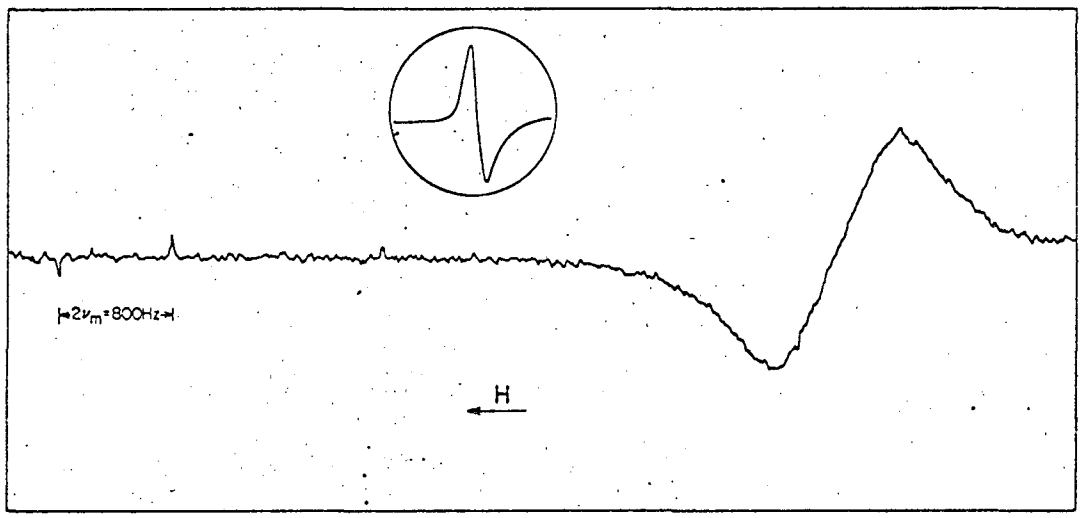

XBL673-2349

Fig. 44 Room temperature ^{35}Cl NMR spectrum of pure $TiCl_4$ showing the Cl^- sidebands of the 3M NaCl reference solution. Insert shows the $TiCl_4$ signal at higher power.

modulation amplitude were adjusted in order to obtain optimum S/N ratios for both signals. All measurements of shifts and linewidths reported here were performed in this way. Further, the "spherical" sample tubes shown in Fig. 14 (Chapter III) were used unless otherwise indicated.

c. $TiCl_4/VCl_4$ solutions.

Because VCl_4 and $TiCl_4$ are completely miscible, $TiCl_4$ would serve as a good internal reference for obtaining the temperature-dependent shift of the VCl_4 ^{35}Cl NMR signal. With such an internal reference, bulk susceptibility corrections[83] would be unnecessary even with cylindrical sample tubes. However, experiments with $TiCl_4/VCl_4$ solutions showed only one ^{35}Cl line to be present. Further, the position of this signal was dependent on the $TiCl_4/VCl_4$ ratio and was characterized by a chemical shift whose value was in between those for the pure liquids. For example, with a 4:1 $TiCl_4/VCl_4$ ratio, the shift at room temperature was 11.3 gauss. If one assumes that the presence of a single line indicates that $TiCl_4$ and VCl_4 exchange chlorines rapidly, then one would predict that the line would be shifted downfield from Cl^- by

$$4/5\ (12.2) + 1/5\ (8.73) = 11.5 \text{ gauss}$$

where 12.2 and 8.73 are the chemical shifts of $TiCl_4$ and VCl_4 at room temperature, expressed in gauss.[94] Because of the agreement between the predicted and observed field positions, and also because the observed line showed no structure, it was concluded that there is rapid exchange of chlorines in the $TiCl_4/VCl_4$ solutions. If two lines were present, they would be nearly resolved in view of the difference in chemical shifts in pure VCl_4 and $TiCl_4$ and the width of the observed signal in solution (1.31 KHz = 3.15 G. in the 4:1 mixture).

The effect of chemical exchange between two magnetically-inequivalent

sites on the experimental lineshape has been considered by many authors.[83,95] In the limit of very rapid exchange, there is only one signal in an appropriately averaged position with a linewidth which is given by

$$\frac{1}{T_2'} = \frac{x_a}{T_{2a}'} + \frac{x_b}{T_{2b}'} \qquad (77)$$

where x_a, x_b; $(T_{2a}')^{-1}$ and $(T_{2b}')^{-1}$ are the mole fractions and linewidths of $TiCl_4$ and VCl_4, respectively. This equation gives a predicted width of 1.15 KHz for a 4:1 $TiCl_4/VCl_4$ mixture, compared to the experimentally observed width of 1.31 KHz. This excess width can be explained as arising from an exchange which is not quite rapid enough to produce a complete collapse of the two signals and it can be used in the following way to estimate an exchange frequency for this process. The rate required for the averaging of the different environments is determined by the magnitude of the chemical shift difference; therefore, the time for exchange will be of the order of the inverse of this difference. Thus, Eq. (77) should be modified by the addition of the term[83]

$$4\pi^2 x_a^2 x_b^2 (\nu_a - \nu_b)^2 (\tau_a + \tau_b) \qquad (78)$$

where ν_a, ν_b; τ_a, τ_b are the Larmor frequencies (Hz) and mean lifetimes for a chlorine in the two environments, respectively. Setting the above expression equal to the excess linewidth (160 Hz) and assuming $\tau_a = \tau_b = \bar{\tau}$, one obtains an average mean lifetime $\bar{\tau} = 7.5\times10^{-6}$ sec. for a chlorine on either VCl_4 or $TiCl_4$. Thus the exchange frequency, $(\bar{\tau})^{-1}$, is estimated to be 1.3×10^5 sec^{-1}.

2. <u>^{35}Cl A-value in VCl_4</u>

The primary purpose of the NMR experiments was to determine the ^{35}Cl

hyperfine coupling constant in VCl_4. This was accomplished by measuring the shift of the VCl_4 signal from the external Cl^- reference signal as a function of temperature. This shift can be attributed to three factors:

(a) the difference between the bulk diamagnetic susceptibilities of VCl_4 and the Cl^- reference compound, denoted by δ_d,

(b) the shift resulting from the paramagnetic susceptibility of VCl_4, δ_p, and

(c) the shift of the VCl_4 signal due to the presence of a contact interaction between the unpaired electron and the chlorine nucleus, δ_c. Factor (a) is temperature-independent and can be obtained from the intercept in a plot of the observed shift as a function of temperature. The second contribution, δ_p, should exhibit a Curie-law dependence on temperature and, if the susceptibility of the sample is known, it can be corrected for by using equations in the literature.[83] However, such corrections are only necessary if non-spherical sample tubes are used; if the reference solution is contained within a sphere which is located inside of and concentric with the VCl_4 sample sphere, the magnetic field will be constant over the reference volume and equal to the field present in the VCl_4 sample. Factor (c) is temperature-dependent and will be related to the slope of an Arrhenius-type plot of the shift.

a. Derivation of the expression for the contact shift.

The explicit form of the relation between the observed contact shift and the hyperfine coupling constant can be obtained by considering the spin Hamiltonian appropriate to the problem. For a single nucleus with $I = 1/2$ in a paramagnetic molecule with $S = 1/2$, the spin Hamiltonian may be written as

$$\underline{\mathcal{H}} = \underline{\mathcal{H}}_E + \underline{\mathcal{H}}_N + \underline{\mathcal{H}}_1 \tag{79}$$

where

$$\underline{\mathcal{H}}_E = g\beta\, \underline{H} \cdot \underline{S} \tag{80}$$

$$\underline{\mathcal{H}}_N = -g_I\, \mu_N\, \underline{H} \cdot \underline{I} \tag{81}$$

and

$$\underline{\mathcal{H}}_1 = \underline{I} \cdot \underset{\sim}{A} \cdot \underline{S} \tag{82}$$

For liquids with short tumbling times ($\tau_c \sim 10^{-11}$ sec.), only the isotropic part of $\underline{\mathcal{H}}_1$ is important and so we can use

$$\underline{\mathcal{H}}_1 = A\, \underline{I} \cdot \underline{S} \tag{83}$$

Following Abragam,[96] for the situation in VCl_4 where the electron spin relaxation time T_{2e} is very short, the four levels predicted by the complete Hamiltonian are reduced to a two-level system. The nuclear part of the Hamiltonian can then be replaced by $\langle \underline{\mathcal{H}}_N \rangle$, where

$$\langle \underline{\mathcal{H}}_N \rangle \doteq -g_I \mu_N\, I_z\, [H + \langle H_e \rangle] \tag{84}$$

and $\langle H_e \rangle$ is the contribution to the magnetic field at the nucleus due to $\langle \underline{\mathcal{H}}_1 \rangle$. This is given by

$$\langle H_e \rangle = -\frac{A}{g_I \mu_N} \langle S_z \rangle, \tag{85}$$

and because of thermal equilibrium,

$$\langle S_z \rangle = S_0 = -\frac{g\beta H}{4kT} \tag{86}$$

The negative sign is due to the fact that the $m_s = -1/2$ state has a greater population than does $m_s = +1/2$.

In the two-level representation, the short electron spin relaxation time also provides a mechanism for nuclear spin relaxation. This falls under the class of what Abragam calls "scalar relaxation of the second kind." The nuclear resonance linewidth is proportional to $1/T_{2n}$ and

$$\frac{1}{T_{2n}} = \frac{A^2}{4\hbar^2}\left[\frac{T_{2e}}{1+\omega_e^2 T_{2e}^2} + T_{1e}\right] . \qquad (87)$$

For the ^{35}Cl nuclear resonance in VCl_4 there are two other possible sources for the linewidth. The ^{35}Cl nucleus has $I = 3/2$ and a quadrupole moment. Consequently, quadrupolar relaxation through molecular tumbling is probably the primary source of linewidth in $TiCl_4$ and it must therefore be important for VCl_4. In addition, the possible dynamic Jahn-Teller effect in VCl_4 can serve as a source of modulation for A and hence falls under Abragam's class of scalar relaxation of the first kind. Its contribution to $1/T_{2n}$ in VCl_4 is quite similar to electron spin relaxation except that the "A-value" must be of the order of the average difference between the A values in the Jahn-Teller states; the lifetime of these states must also be substituted for T_{2e} and T_{1e} in Eq. (87).

In the absence of scalar coupling, or at infinite temperature, the resonance condition for nuclei is

$$h\nu_0 = g_I \mu_N \; H_0 \qquad (88)$$

while, with ν_0 constant, in the presence of scalar coupling it becomes

$$g_I \mu_N H_0 = h\nu_0 = g_I \mu_N \; [H + \langle H_e \rangle] \qquad (89)$$

Therefore, the field for resonance in the latter case is

$$H = H_0 - \langle H_e \rangle$$

$$H = H_0 - \frac{A}{g_I \mu_N} \langle S_z \rangle$$

$$H = H_0 - \frac{g\beta HA}{4kTg_I \mu_N} \qquad (90)$$

and, since H is very close to H_0, it is a good approximation to write

$$\delta H = H - H_0 = - \frac{g\beta H_0 A}{4kTg_I \mu_N} \qquad (91)$$

Thus, a plot of the observed shift versus 1/T will give a straight line with a slope of $-g\beta H_0 A/4kg_I \mu_N$ and an intercept which corresponds to the field position in the absence of a contact interaction, H_0. Further, since the sign of μ_N for ^{35}Cl is known (positive),[97] the sign of A can be determined directly from the slope of the line. The expression (91) is identical to those given in the literature for $S = 1/2$.[98]

b. Measurement of the ^{35}Cl A-value in VCl_4.

The determination of the shift of the VCl_4 ^{35}Cl NMR signal as a function of temperature was performed using concentric spherical sample tubes. With such tubes it is not necessary to make the bulk susceptibility corrections mentioned in the preceding section. The temperature range covered in these experiments was -4.2 to 97.0°C.

Table XIX summarizes the data which were obtained in these experiments. An inspection of the shifts, which are defined as negative because the VCl_4 signal occurs at lower field than the Cl^- signal, reveals that they are consistently higher for those runs in which the magnetic field was swept from the Cl^- signal to the VCl_4 line (i.e., in which the

Table XIX . The shift of the VCl_4 ^{35}Cl NMR line from Cl^- as a function of temperature. ν = 5.879 MHz.

T, °C	$\delta\nu_{up}$, KHz[a]	$\delta\nu_{down}$, KHz[b]	$\overline{\delta\nu}$, KHz
-4.2	-3.37	-3.54	-3.46
11.9	-3.43	-3.57	-3.50
23.3	-3.57	-3.71	-3.64
34.0	-3.59	-3.77	-3.68
48.5	-3.76	-3.92	-3.84
63.9	-3.80	-3.95	-3.88
78.7	-3.92	-3.97	-3.95
97.0	-4.06	-4.17	-4.12

a. Field increasing; i.e., from the VCl_4 signal to the Cl^- signal.

b. Field decreasing.

field was decreasing). This effect, which was small, was due to a time-constant produced asymmetry in the broad VCl_4 line. In order to minimize the effect of this systematic error, the data for both the upfield and downfield runs were averaged for each temperature. A reasonable error estimate, independent of this effect, was $\pm 2\sigma_{max}$, where σ_{max} is the maximum standard deviation of the data for either the up or down sweeps at a single temperature. This was found to be 0.10 KH_z, so the error introduced by the time-constant asymmetry was less than the overall experimental error of ±0.2 KH_z. Each measurement reported in Table XIX is the average over a number of sweeps.

Using a least-squares analysis, the points were fit by a straight line and the slope and intercept at infinite temperature were determined. The results are plotted in Fig. 45 in which the experimental points

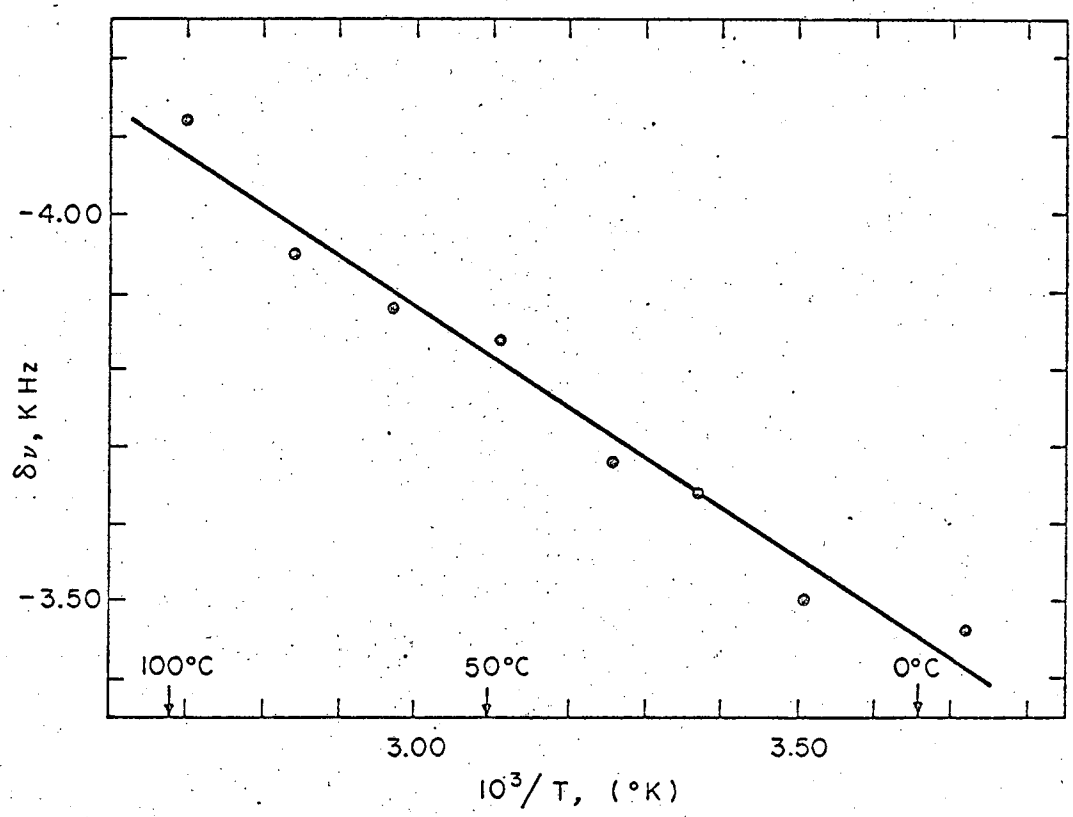

XBL673-2353

Fig. 45 Plot of the ^{35}Cl NMR chemical shift of VCl_4 vs Cl^- ($\delta\nu$) versus reciprocal temperature.

have also been included. The least-squares slope and intercept are

$$\text{slope} = 6.51\times10^2 \text{ KHz } ^\circ\text{K} = (\delta\nu)_c$$

$$\text{intercept} = -5.83 \text{ KHz} = (\delta\nu)^0$$

The maximum difference between the observed data and those predicted by the above parameters was 0.05 KHz. The intercept, -5.83 KHz, leads to a value of the diamagnetic chemical shift of VCl_4 from Cl^- of -990 ppm. This is greater in magnitude by about 10% than the value for $TiCl_4$, -864 ppm. A general increase in the absolute value of this shift has been observed[93] for the series of compounds $SiCl_4$, CrO_2Cl_2, $VOCl_3$ and $TiCl_4$. This behavior has been interpreted as indicating a substantial paramagnetic contribution of hybridized d-orbitals to the M-Cl bond and the fact that $\delta_d(VCl_4) > \delta_d(TiCl_4)$ supports this interpretation.

In order to calculate the coupling constant from the slope of the line in Fig. 45, Eq. (91) of the preceding section must be put in slightly different form. First, because the shifts were measured with respect to a dilute NaCl reference solution, we subtract the absolute field for the Cl^- resonance, H^*, from both sides of (91). This gives

$$(H - H^*) = (H_0 - H^*) - \frac{g\beta H_0 A}{4kTg_I\mu_N} \qquad (92)$$

This equation now expresses the shifts from Cl^- directly in gauss; to convert to frequency units, we multiply (92) by the magnetogyric ratio for a chlorine nucleus ($g_I\mu_N/h$). Introducing some new nomenclature, Eq. (92) becomes

$$(\delta\nu)_{obs} = (\delta\nu)^0 - \frac{g\beta H_0 A}{4kTh} \tag{93}$$

where

$$(\delta\nu)_{obs} = \frac{g_I \mu_N}{h} (H-H^*) \tag{94}$$

$$(\delta\nu)^0 = \frac{g_I \mu_N}{h} (H_0-H^*) \tag{95}$$

Further, the slope is given by

$$(\delta_\nu)_c = -\frac{g\beta H_0 A}{4kh} \tag{96}$$

so the equation for the observed shift can be rewritten as

$$(\delta_\nu)_{obs} = (\delta\nu)^0 + \frac{(\delta\nu)_c}{T} \quad . \tag{97}$$

Taking $g = 1.93$ and $H_0 = 14.09$ KG., Eq. (96) yields for A in ESR gauss (when $(\delta\nu)_c$ is expressed in Hz °K),

$$A/g\beta = -(8.10\times10^{-7})\ (\delta\nu)_c$$

The value of A obtained in this way is

$$A/g\beta = -0.527\pm0.050 \text{ gauss.}$$

The value -0.546 G. was obtained from cylindrical tube data corrected for bulk susceptibility effects and therefore provides a good check on the above number.

c. Interpretation of the A-value

The hyperfine structure of the $^2P_{3/2}$ ground state of the ^{35}Cl atom has been investigated using atomic beam techniques and a coupling constant of 205 MHz was found.[99] This is therefore the A-value for a 'pure' p-electron in a 3p orbital of the chlorine atom. With this value, it is possible to estimate the fraction of 3p chlorine orbital present in the wavefunction for the unpaired electron in VCl_4. Taking the ratio of our observed A-value in VCl_4 and the above value for ^{35}Cl atom, one obtains for this estimate 0.69%. Implicit in this calculation is the assumption that the mechanisms which produce the unpaired electron spin density are the same in both the atom and in VCl_4.

Since the contribution to the hyperfine structure arising from the magnetic dipole-dipole interaction between electron and nucleus averages to zero for a rotating molecule, the A-values measured for both the atom and the ^{35}Cl nucleus in VCl_4 at room temperature must be the result of a Fermi contact interaction. The most reasonable explanation for the presence of such a term in VCl_4 is to suggest that there is a small amount of π-bonding between the mixed d_{z^2}, $d_{x^2-y^2}$ vanadium orbital and a π-symmetry orbital of the chlorine ligand (See Fig. 5). This latter orbital is formed by a linear combination of the $3p_x$ and $3p_y$ chlorine atomic orbitals. Employing the usual arguments of spin polarization, it is possible to show that a positive spin density in either of these two atomic orbitals will produce a negative spin density in either of the two chlorine inner 1s and 2s orbitals. Since the A-value for a hydrogen atom is positive, the ^{35}Cl A-value resulting from the spin polarization mechanism in VCl_4 should be negative, as observed. Molecular orbital calculations using the hyperfine coupling constants for both ^{51}V and ^{35}Cl in VCl_4 are in progress.

3. Temperature Dependence of the Linewidths

a. Pure VCl_4

The temperature dependence of the linewidth of the ^{35}Cl line in VCl_4 was measured over the range -4.2 to 97.0°C. using the spherical sample tubes. The data, which have been collected in Table XX , can be fit by a straight line in a log $\Delta\nu$ vs 1/T plot, where $\Delta\nu$ is the peak-to-peak width of the signal in KHz. Figure 46 shows such a graph for the data in Table XX ; the straight line is the result of a least-squares analysis of this data.

Table XX . ^{35}Cl NMR linewidth in VCl_4 as a function of temperature.

T, °C	$10^3/T$, °K	$\Delta\bar{\nu}$, KHz [a]	σ , KHz [b]
-4.2	3.72	2.72	0.07
11.9	3.51	2.38	0.03
23.3	3.37	2.27	0.05
34.0	3.26	2.14	0.04
48.5	3.11	2.05	0.04
78.7	2.84	1.88	0.05
97.0	2.70	1.79	0.05

a. Average over at least 6 sweeps at each temperature.

b. Standard deviation.

The slope of this line can be used to calculate an activation energy for the narrowing process in VCl_4 using the following relationship:

$$\Delta\nu = \Delta\nu^{o} e^{E\ddagger/RT} \qquad (98)$$

From our least-squares fit, a slope (m) of 0.170×10^{3}°K is obtained. Then,

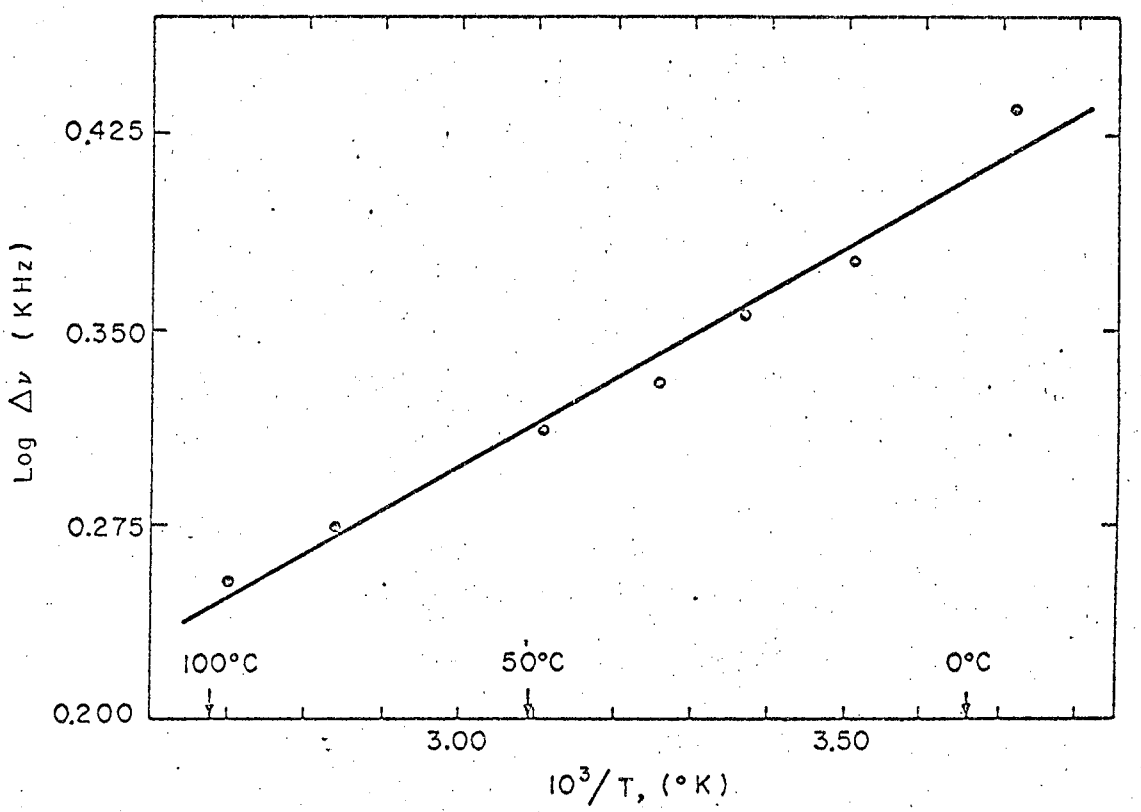

XBL673-2352

Fig. 46 Plot of the ^{35}Cl NMR linewidth (KHz) of VCl_4 as a function of reciprocal temperature.

$E^{\ddagger}$ = 2.303 mR yields an activation energy of 0.776 Kcal/mole. The temperature-independent linewidth, $\Delta\nu^{0}$, is 6.14×10^{2} Hz (1.47 gauss).

b. Pure $TiCl_4$

Similar experiments were performed on $TiCl_4$. Masuda[93] has reported that the peak-to-peak linewidth for this compound is 1.2 G. Although he did not specify the temperature at which this width was measured, earlier experiments by the same author[100] were performed at room temperature in a field of 6227 G so it will be assumed here that his results for $TiCl_4$ were obtained under the same conditions. Our early experiments on $TiCl_4$ indicated that the peak-to-peak width of the ^{35}Cl NMR line in this molecule was about 2 G at ~25°C.; consequently, we have re-investigated the width of the signal and its temperature dependence. Table XXI lists the results of these measurements.

Table XXI . Peak-to-peak width of the ^{35}Cl NMR absorption in $TiCl_4$ as a function of temperature.

T, °C	$\Delta\nu$, Hz	Δ H, gauss
23.2	871	2.09
39.1	848	2.03
63.6	791	1.90

Although the data cover a fairly narrow temperature range, it is clear from Table XXI that the line does narrow with increasing temperature. Before discussing the relaxation mechanisms which would lead to this temperature dependence, some qualitative observations can be made. First, the widths reported here are definitely larger than those measured by Masuda.[93] Because our samples were prepared by vacuum distillation

of the $TiCl_4$, it is unlikely that paramagnetic impurities were the source of the excess width. Since Masuda's experiments were performed at a considerably lower magnetic field (~6 KG vs our ~14 KG), it is possible that the linewidth in $TiCl_4$ is strongly frequency-dependent. Second, if one assumes that the temperature dependence of the linewidth is expressed by Eq. (98), then an activation energy of 0.483 Kcal/mole and a temperature-independent linewidth of 3.86×10^2 Hz (0.93 G) are obtained from a least-squares analysis. However, an Arrhenius plot of the data shows that the linewidth does not follow a straight line but instead increases less rapidly than predicted as the temperature is decreased. Some possible explanations for this behavior will be discussed below.

4. Relaxation Effects in VCl_4 and $TiCl_4$

a. Nuclear relaxation

The various relaxation mechanisms available for nuclei in liquids and gases have been described in detail by several authors.[13,96,101] In most cases, relaxation is produced by the modulation of an intra- or intermolecular interaction by tumbling or chemical exchange. Those interactions which are most appropriate for the ^{35}Cl nucleus in the pure liquids VCl_4 and $TiCl_4$ are (a) nuclear dipole-dipole interactions, (b) scalar coupling between unpaired electrons and nuclei (VCl_4 only), (c) nuclear quadrupole coupling and (d) anisotropic chemical shifts.

As was discussed in Chapter II, a strong correlation has been observed between eqQ values and NMR linewidths for the chlorine nuclei in $TiCl_4$, $VOCl_3$, etc.[93,102] Thus, it is reasonable to assume that the primary mechanism for ^{35}Cl nuclear relaxation in $TiCl_4$ is the coupling between the nuclear quadrupole moment and the electric field gradient

at the nucleus, modulated by tumbling. This mechanism should also contribute to the linewidth in VCl_4. The contribution to $(T_{1n})^{-1}$, the inverse nuclear spin-lattice relaxation time, from quadrupolar coupling is given by [103]

$$\left(\frac{1}{T_{1n}}\right)_{eqQ} = \frac{3}{40}\left\{\frac{2I+3}{I^2(2I-1)}\right\}\left(1+\frac{\eta^2}{3}\right)\left(\frac{eqQ}{\hbar}\right)^2 \frac{\tau_c}{1+\omega^2\tau_c^{\,2}} \qquad (99)$$

where η is the asymmetry parameter, τ_c the correlation time for tumbling and ω the nuclear Larmor frequency. Taking $\eta^2/3 \ll 1$ and $I = 3/2$ for ^{35}Cl, this becomes

$$\left(\frac{1}{T_{1n}}\right)_{eqQ} = \frac{1}{10}\left(\frac{eqQ}{\hbar}\right)^2 \frac{\tau_c}{1+\omega^2\tau_c^{\,2}} \qquad (100)$$

Masuda[93] has shown that, within experimental error, $T_{1n} = T_{2n}$ in these molecular chlorine compounds. For Lorentzian lines, the relation between T_{2n} and the peak-to-peak width expressed in Hz (for derivative lines) is[101]

$$\frac{1}{T_{2n}} = \sqrt{3}\,\pi\,\Delta\nu \qquad (101)$$

Therefore,

$$\Delta\nu_{eqQ} = \frac{1}{10\sqrt{3}(\pi)}\left(\frac{eqQ}{\hbar}\right)^2 \frac{\tau_c}{1+\omega^2\tau_c^{\,2}} \qquad (102)$$

The correlation time for tumbling in liquids can be estimated from Stokes' law [13,104]

$$\tau_c = \frac{4\pi\eta a^3}{3kT} \qquad (103)$$

where a is the radius of the molecule and η is the viscosity of the liquid at the temperature T. For $TiCl_4$, a reasonable estimate for a lies in the range 3.17 Å - 3.99 Å.[93] Taking $\eta(24°C) = 0.794$ cp,[105] $\tau_c(24°C)$ is in the range 2.58 - 5.15×10^{-11} sec. Therefore, for $TiCl_4$, $\omega^2\tau_c^2 \approx 6\times10^{-8}$ at 14 KG, and it is a very good approximation to neglect $\omega^2\tau_c^2$ in the denominator of Eq. (102). Since this is more true at lower fields, this model predicts that $\Delta\nu_d$ should be independent of frequency. It does not explain the discrepancy between the observed and reported linewidths for $TiCl_4$.

Taking $\omega^2\tau_c^2 << 1$ and the expression (103) for τ_c, the quadrupolar model predicts the following temperature dependence of the linewidth:

$$(\Delta\nu)_{eqQ} = \frac{2a^3}{15\sqrt{3}} \left(\frac{eqQ}{\hbar}\right)^2 \frac{\eta}{T} \qquad (104)$$

Luchinskii[105] has measured the viscosity of $TiCl_4$ as a function of temperature in the range -15 - 50°C. The temperature-dependence of his data can be described by the following expression

$$\eta = A_{exp}\,(\Delta E_{vis}/RT), \qquad (105)$$

with $\Delta E_{vis} = 1.58$ Kcal/mole. Although there is no viscosity data available for VCl_4, it would seen reasonable to expect that the activation energy for viscous flow in this liquid would be about the same as in $TiCl_4$. In order to estimate the activation energy for the narrowing due to quadrupolar relaxation in both molecules, the temperature dependence of the linewidth expressed in Eq. (104) is written as

$$\frac{\eta}{T} \doteq \frac{A_{exp}(\Delta E_{vis}/RT)}{T} \qquad (106)$$

A plot of log (η/T) versus 1/T using Luchinskii's viscosity data[105] for $TiCl_4$ yields a straight line with a slope of 2.14. Therefore, if the quadrupolar mechanism is the only source of linewidth in these tetrachlorides, a slope of about 2 should be obtained from a plot of $\Delta\nu$ versus η/T. Further, as predicted from Eq. (104), this plot should go through zero at infinite temperature if this mechanism is the only source of linewidth.

Figure 47 is a graph of some of the VCl_4 and $TiCl_4$ data plotted in this way. The points for VCl_4 were obtained from the least squares fit to the linewidth data in Table XX where it has been assumed that $\eta(VCl_4) = \eta(TiCl_4)$. Those for $TiCl_4$ are the actual experimental data listed in Table XXI and the smooth curve is drawn merely for illustrative purposes. Although the VCl_4 slope is about two, the intercept is clearly finite and suggests the presence of a temperature independent width in the ^{35}Cl NMR spectrum. This will be discussed below. On the other hand, the $TiCl_4$ data is distinctly non-linear. It is entirely possible that additional data will show the predicted temperature dependence and that the "anomalous" behavior observed here for $TiCl_4$ is due to experimental difficulties. However, we would like to point out that there are other possible interpretations of these results which also explain the larger linewidth observed at 14 KG.

For example, if one assumes the existence of two different chlorine environments in $TiCl_4$ (e.g., monomers and dimers) which have slightly different chemical shifts, then the observed ^{35}Cl NMR line would actually consist of two superimposed lines, one for each environment. The width of the combination line would then depend on the rate of exchange of chlorines between the two sites as well as the relaxation processes pertinent to each. As the temperature is decreased, the linewidth would

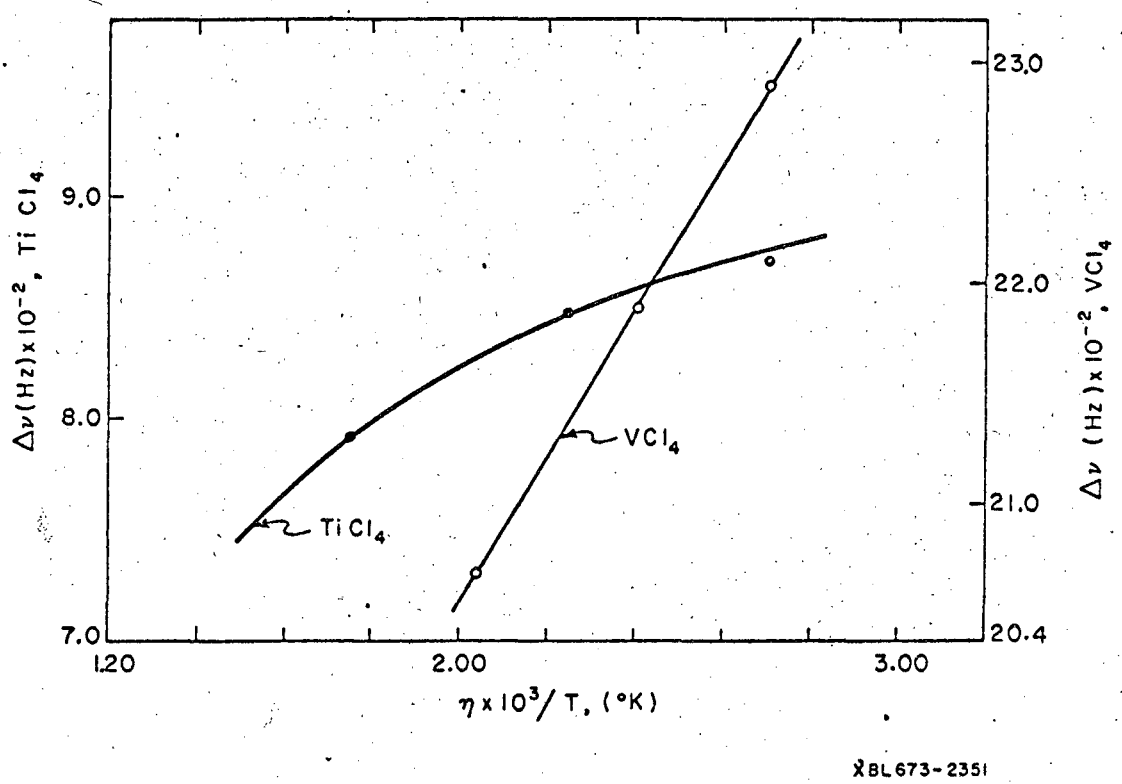

Fig. 47 Plot of the ^{35}Cl NMR linewidths in $TiCl_4$ and VCl_4 as a function of η/T.

increase until the exchange rate decreased to the point where essentially no exchange occurred during the period of a Larmor cycle. At this point, the width might be expected to become independent of further temperature decrease. In addition, since the magnitudes of the shifts are field-dependent, the width at 14 KG should be larger than at 6 KG as has been observed.

A second explanation of the difference in widths of the $TiCl_4$ absorption at the two fields is that the chemical shift in this molecule is anisotropic. Abragam[106] has shown that the contribution to the linewidth due to the modulation of this anisotropy by tumbling is proportional to H_o^2. This model therefore predicts that the width at 14 KG would be larger than at 6 KG but it also suggests that the activation energy for narrowing would be about the same as for viscosity. Thus the first explanation is preferred since it is consistent with both the excess width at 14 KG and the anomalous temperature dependence.

Since our experiments with $TiCl_4/VCl_4$ solutions showed that exchange of chlorines between these two molecules is likely (vide supra), the suggestion that there are species other than monomer $TiCl_4$ in the pure liquid compound is not unreasonable. The existence of "local order" in pure liquids is sometimes indicated by the value of the Trouton's constant, $(\Delta H_{vap}/T_b)$,[107] which for normal liquids is about 21 (e.g., $\Delta H_{vap}/T_b$ $(CCl_4) = 20.4$ [109]). The value for $TiCl_4$ is 23.4,[108] whereas the value for water is 26.0.[109] The increase in water is usually ascribed to the presence of hydrogen-bonding between water molecules, and it is possible that the increase in $TiCl_4$ is due to the existence of dimers in the pure liquid although this small deviation from the normal value cannot be taken as proof of this fact.[107] Clearly, more experimental work is in order and we would suggest that as a first experiment,

the linewidth of $TiCl_4$ be measured at a lower field to see if the widths are actually frequency dependent. Further experiments should include more complete measurements of the linewidth as a function of temperature.

Even though the linewidth data for VCl_4 plotted in Fig. 48 follow the temperature dependence expected for quadrupolar relaxation, the activation energy for the narrowing process is 0.78 Kcal/mole (cf. Section 3a). This is somewhat less than predicted from the viscosity data of Luchinskii[105] and suggests that there are other relaxation processes which contribute to the ^{35}Cl NMR linewidth in VCl_4. This is not surprising, for it might be expected that the scalar coupling which exists between I and S would result in relaxation of the chlorine nucleus. If we assume that there is no time dependence in the coupling constant A (e.g., such as might be produced by chemical exchange), then relaxation of the nucleus I (^{35}Cl) can be produced through scalar coupling by rapid relaxation of the electron spin S. This has been termed "scalar relaxation of the second kind" by Abragam[110] and was discussed earlier. In this case, the contribution to the linewidth is

$$\left(\frac{1}{T_{2n}}\right)_{I\cdot S} = \frac{A^2}{3\hbar^2} S(S+1) \left[\frac{T_{2e}}{1+(\omega_I-\omega_S)^2 T_{2e}^2} + T_{1e}\right] \qquad (107)$$

Taking $(\omega_I-\omega_S)^2 \cong \omega_S^2$, this becomes

$$\left(\frac{1}{T_{2n}}\right)_{I\cdot S} = \frac{A^2}{3\hbar^2} S(S+1) \left[\frac{T_{2e}}{1+\omega_S^2 T_{2e}^2} + T_{1e}\right] \qquad (108)$$

Ignoring for the moment the absolute values of T_{2e} and T_{1e}, this expression can be treated in the two limiting cases $T_{2e} \lesssim T_{1e}$ and $T_{2e} \sim T_{1e}$. In the former,

$$T_{1e} >> \frac{T_{2e}}{1 + \omega_S^2 T_{2e}^2}$$

and Eq. (108) reduces to

$$\left(\frac{1}{T_{2n}}\right)_{I \cdot S} = \frac{A^2}{3\hbar^2} S(S+1) T_{1e} \qquad (109)$$

Then the temperature dependence of this contribution to the linewidth in VCl_4 is just the temperature dependence of T_{1e}. Unfortunately, this is not known but it would seem reasonable to assume that the electron spin-lattice relaxation time in the pure liquid is relatively insensitive to temperature variation in the range covered by our NMR experiments.[111] If this is so, then the plot of linewidth versus temperature should be the sum of two contributions; one with an activation energy of about 2 Kcal/mole which is due to the viscosity-dependent narrowing of the quadrupolar width and a second which is essentially independent of temperature and represents the (smaller) T_{1e} width. This would result in an overall activation energy which is lower than that predicted from viscosity arguments and suggests that as the temperature is increased still further, the width would reach a minimum value which is the T_{1e} width given by Eq. (109). This is presumably the width given by the intercept in Fig. 47.

On the other hand, if $T_{1e} = T_{2e} = T_e$, then Eq. (108) becomes

$$\left(\frac{1}{T_{2n}}\right)_{I \cdot S} = \frac{A^2}{3\hbar^2} S(S+1) \left(\frac{T_e}{1+\omega_S^2 T_e^2} + T_e\right) \qquad (110)$$

The behavior of the scalar contribution to the width in this case with changes in temperature is more difficult to estimate. In addition, this width may be frequency dependent since the available evidence (<u>vide infra</u>)

seems to suggest that the approximation $\omega_S^2 T_e^2 << 1$ might not be valid at high fields. This could be checked by performing NMR experiments on VCl_4 at other fields. In order to see which of the above limits is more reasonable, we shall now discuss the electron relaxation times more quantitatively.

b. Electronic relaxation.

The discussion in the previous section has shown that, in addition to the relaxation mechanism via quadrupolar coupling, there exists a second mechanism for the relaxation of the ^{35}Cl nucleus in VCl_4. It was suggested that this latter mechanism was scalar relaxation of the second kind as described by Abragam.[96] In this case, the modulation of the interaction is provided by the rapid relaxation of the electron spin rather than by chemical exchange. Thus there are two contributions to the linewidth in VCl_4 and, if the quadrupolar width can be estimated independently, the excess width due to the contact interaction can be used to determine the electron spin relaxation time in this molecule.

Because of the correlation which has been observed between the ^{35}Cl NMR linewidth and ^{35}Cl eqQ values in some molecular chlorine compounds,[93] it should be possible to estimate the quadrupolar width in VCl_4 from the width in $TiCl_4$ and the ^{35}Cl eqQ value in VCl_4. However, since the linewidth of $TiCl_4$ appears to be anomalous and may contain contributions from other sources, e.g., chemical exchange, this analysis can only be qualitative in nature. As a first approximation, we will assume that the entire width of the ^{35}Cl line in VCl_4 arises from the scalar mechanism. This width was 2.27×10^3 Hz at about 23°C. Then, assuming for the moment that $T_{1e} << T_{2e}$, T_{1e} can be estimated from Eq. (109). Writing this expression in the form (cf. Eq. (101))

$$(\Delta\nu)_{I\cdot S} = \frac{A^2}{3\sqrt{3}\,\pi\hbar^2}\; S(S+1)\; T_{1e} \qquad (111)$$

and taking $A/g\beta = -0.53$ G, T_{1e} is approximately

$$T_{1e} = \frac{4\sqrt{3}\,\pi\,(\Delta\nu)_{I\cdot S}}{(A/\hbar)^2} \sim 6 \times 10^{-10} \text{ sec.}$$

As it seems unlikely that the entire width in VCl_4 is due to scalar relaxation, a width due to quadrupolar effects can be estimated from the $TiCl_4$ data. It will be recalled that the $TiCl_4$ linewidth at 6 KG is 1.2 gauss and that this width was approximately that expected from the eqQ value in this molecule.[93] Thus, as a second approximation, a width of one gauss for $TiCl_4$ will be assumed as arising from quadrupole relaxation. This must then be corrected to account for the difference in values of eqQ in $TiCl_4$ and VCl_4. The value of eqQ for ^{35}Cl in VCl_4 has not been measured, but on qualitative grounds it should be larger than that for $TiCl_4$ because of the presence of the single d-electron in the former. This increase can be estimated by a comparison of the $eqQ/\hbar$ values in the series of compounds $TiCl_4$, $TiCl_3$, and VCl_3 which are, respectively, 12.1,[112] 14.8,[113] and 18.8 MHz.[113] Thus there is a decrease of about 18% in eqQ in going from $TiCl_3$ $(3d^1)$ to $TiCl_4$ $(3d^0)$. If one assumes that a similar reduction occurs from $(3d^2)$ to $(3d^1)$ in the vanadium chlorides, then from the value of $eqQ/\hbar$ for VCl_3 we obtain 15.4 MHz for VCl_4. Therefore, the linewidth in VCl_4 due to quadrupolar relaxation is, at about 23°C,

$$(\Delta\nu)_{eqQ}(VCl_4) = \left\{\frac{eqQ/\hbar(VCl_4)}{eqQ/\hbar\,(TiCl_4)}\right\}^2 (\Delta\nu)_{eqQ}\,(TiCl_4). \qquad (112)$$

Taking $(\Delta\nu)_{eqQ}(TiCl_4) = 4.2\times10^2$ Hz (1xG), we calculate for $(\Delta\nu)_{eqQ}(VCl_4)$ 6.7×10^2 Hz. Since the observed width at this temperature in VCl_4 was 2.27×10^3 Hz, the excess width due to scalar relaxation is estimated to be 1.6×10^3 Hz. Assuming again that $T_{1e} >> T_{2e}$, this leads to

$$T_{1e} \sim 4 \times 10^{-10} \text{ sec.}$$

A relaxation time for the unpaired electron in VCl_4 of 5×10^{-10} sec would correspond to a peak-to-peak ESR linewidth of

$$\Delta H = \frac{h}{g\beta} (\pi\sqrt{3}\, T_e)^{-1} \qquad (113)$$

$$\Delta H \sim 140 \text{ gauss}$$

if the line is Lorentzian. Since the spectrum of VCl_4 is not observable above about 60°K, the approximation that $T_{1e} >> T_{2e}$ at room temperature would seem to be reasonably good because a signal with a width of 2 KG or less should be detectable in an ESR experiment. Thus the first interpretation of the ^{35}Cl NMR linewidth data for VCl_4 offered in the preceding section is preferred; the decrease in the activation energy for narrowing is due to the addition of a small temperature-independent width which is determined by T_{1e}.

The value of T_{1e} obtained in this way can be used to determine a lower limit (i.e., without quadrupole effects) on the linewidth for the ^{51}V NMR signal in VCl_4. Taking $A/g\beta \sim 100$ G and Eq. (111), we predict that $\Delta\nu \geq 10$ MHz. Therefore, it is not surprising that efforts which were made to observe such a signal were unsuccessful.[114]

D. ESR of Sulfur-Nitrogen Radicals

1. Assignment of the Spectra.

a. Chemical reduction experiments.

In a series of experiments performed with Dr. S. K. Ray, a reducing agent was added to a solution of either S_4N_4 or S_4N_3Cl in THF. The resulting solution exhibited a number of color changes and the radicals produced were followed by ESR. Both sodium naphthalide and sodium-potassium alloy were used as reducing agents; the reaction with the former was slower and so most of the experiments were performed with this compound. Analogous results were obtained using the alloy; further, both S_4N_4 and S_4N_3Cl showed the same behavior. All reactions were reversible.

Upon the addition of a small amount of naphthalide at 0°C or above, the solution became deep red in color and showed a relatively strong five-line spectrum attributable to a species with two equivalent nitrogens (I=1) which we denote as radical A. This solution gradually turned deep blue as more reducing agent was added and a second radical, B, was detected by the presence of three lines indicating a single nitrogen. This signal overlapped the signal from A; this is illustrated in Fig. 48. These two signals gradually disappeared as more sodium naphthalide was added, and, when the total concentration of reducing agent exceeded two equivalents per S_4N_4 (or S_4N_3Cl) the solution turned dark green and yielded a weaker nine-line spectrum. The ESR spectrum of this species, radical C, is shown in Fig. 49.

Relative intensity measurements were performed by comparing the relative signal areas of the S_4N_4 spectra with those of a DPPH/THF

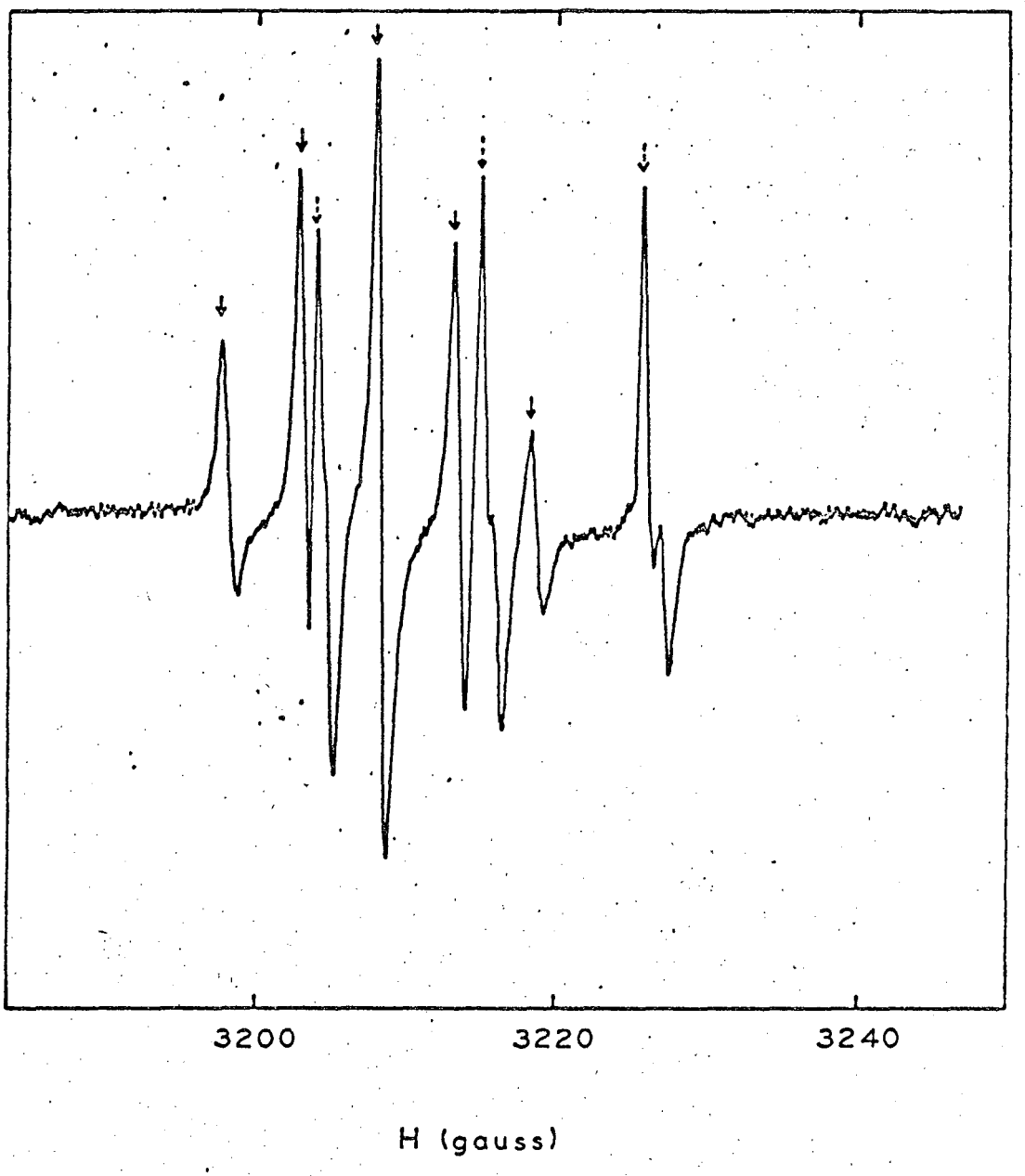

Fig. 48 Room temperature ESR spectrum of reduced S_4N_4. The dotted arrows show the triplet splitting due to radical B in a spectrum dominated by the quintet of radical A (solid arrows).

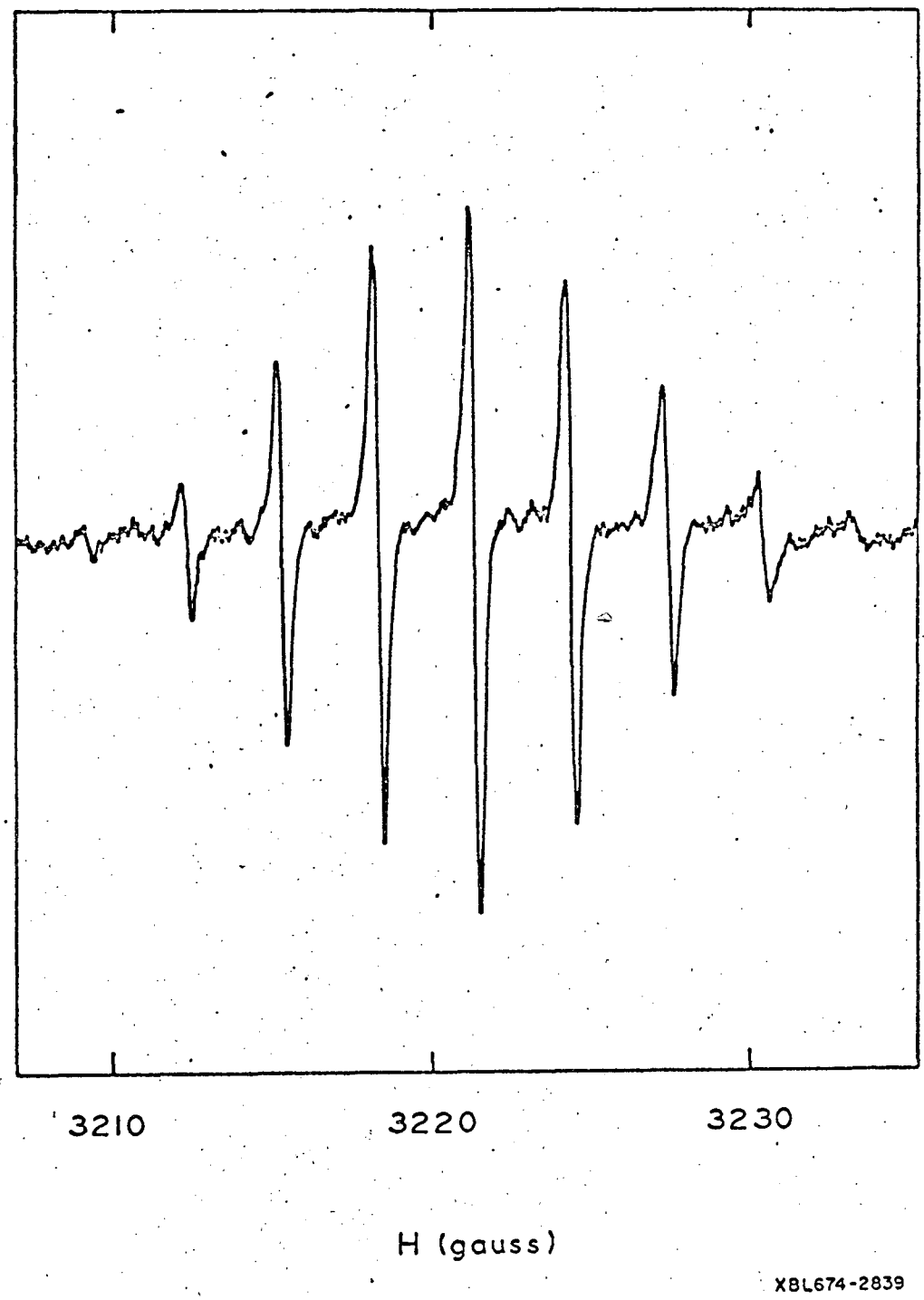

Fig. 49 The ESR spectrum of Radical C at room temperature.

solution and calculating from these data the approximate percentage of the starting material in radical form. These results, together with the g-values and ^{14}N coupling constants for the three radicals, are listed in Table XXII. Also listed in this table are the g- and A-values of radical D; this was produced by the addition of reducing agent to S_4N_3Cl and was observed instead of radical B in solutions of this compound. The ESR parameters of B and D are quite similar.

Table XXII. Parameters measured from the ESR spectra of S_xN_y radicals

Radical	g.	A/gβ (gauss)	Relative % at max. intensity	Number of equivalents of e^- added
A	2.0101±0.0003	5.13±0.02	1.0	1.0
B	2.0053±0.0010	11.2 ±0.1	0.1	0.5
C	2.0065±0.0003	3.13±0.02	0.01	2-3
D	2.0069±0.0003	10.74±0.1	---	---

Attempts were made to detect ^{33}S (0.74% abundant) hyperfine structure in these radicals without much success. The linewidths for radical A were rather large (1.40 G.) and could not be narrowed significantly by decreasing the temperature (1.20 G. at -30°C.). Some structure was observed in the nine-line spectrum (C) but, after those lines probably due to ^{15}N (0.37% abundant) were excluded, there was no regular pattern from which either ^{33}S coupling constants or the number of sulfur atoms could be deduced.

b. Electrolytic reduction experiments.

Similar, but not entirely analogous, results were obtained in electrolytic experiments subsequently performed by the author. In these, the electrolysis cell described by Levy[115] was used to generate the S_xN_y radicals. These experiments were performed on S_4N_4 in THF and are described in Chapter III.

Radicals A and B were also observed in these experiments; the g- and A-values measured for these compared favorable with those given in Table XXII. Radical C was not observed; this was assumed to be the result of poor S/N. The most interesting result of these experiments was the fact that, if the electrolysis was performed at low temperatures - just above the melting point of THF - a new nine-line radical (E) was observed. This signal disappeared quickly on warming but could be regenerated by cooling again. Figure 50 shows the ESR spectrum of this radical; the g- and A-values were measured and found to be 2.0004 ±0.0010 and 1.21±0.05 gauss. The linewidths in this spectrum are quite small (~0.6-7 gauss); the intensities are roughly (because of overlap) 1:4:10:16:19:16:10:4:1, the ratio expected for four equivalent nitrogens. Also shown in Fig. 50 is the broader spectrum of radical A which was also present at low temperatures; the additional structure in this five-line pattern was not analyzed.

2. Discussion

The radicals produced by reduction of S_4N_4 have previously been studied using ESR techniques.[116] In this work, Chapman and Massey observed first a claret-red solution which became green after further reaction. (Reaction with sodium showed the color changes red, blue, green and yellow-green). However, they detected only one ESR signal;

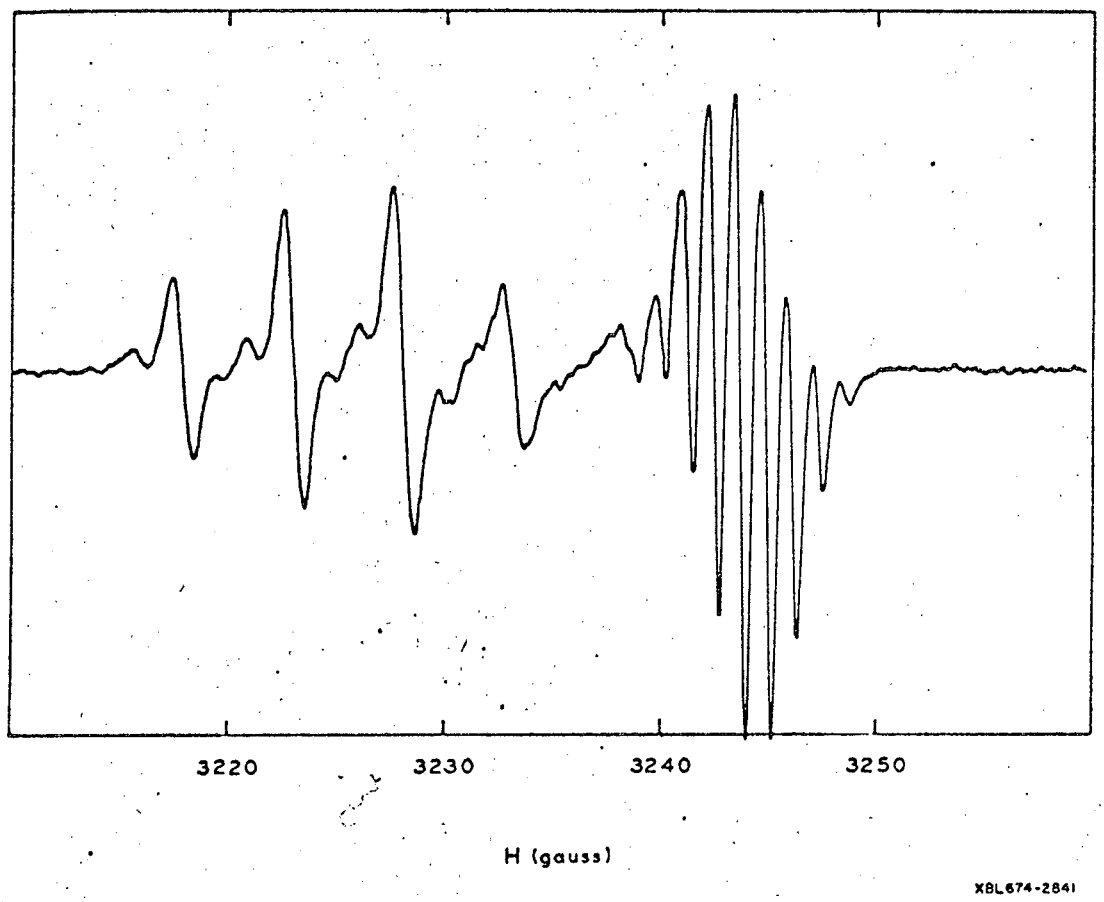

Fig. 50 ESR spectrum of Radicals A and E.

this was a nine-line spectrum with g = 2.006 and A = 3.22 gauss. They assigned this spectrum to $S_4N_4^-$. It is also of interest to note that the g- and A-values for our radical A are similar to those found by Chapman and Massey for a five-line species formed when S_4N_4 is distilled over silver gauze and the product is dissolved in dimethoxyethane and then reacted with potassium. This gave an orange solution which yielded a spectrum of five broad lines with g = 2.008 and A = 5.29 gauss. The authors suggested that this is probably due to the formation of the symmetric SN_2^- radical.

From our results given in Table XXII, it can be seen that the radicals A-C are formed in very small yield, particularly C. Since A and B are formed before C, and C is found only after more than one equivalent of reducing agent, it is highly unlikely that C, which has the same g- and A-values as those reported by Chapman and Massey, is the simple radical anion of the S_4N_4 ring. It is more likely a polymerization product of smaller species which are formed by cleaving the S_4N_4 ring.

Subsequent work by others in this laboratory[117] has shown that our radical E (a nine-line species with g = 2.0004 and A = 1.21 G) has the following properties; a) its ESR spectrum is broadened by the addition of S_4N_4, b) the radical is readily formed in high yields at low temperatures and c) its A and g values are considerably different (e.g., $g < g_e$) from the radicals A-D. On the basis of this evidence, it can be concluded that radical E is probably $S_4N_4^-$. Therefore, it is probable that $S_4N_4^-$ is first produced during the reduction sequence and is stable only at low temperatures. Above 0°C, this radical decomposes to give first the one and two nitrogen radicals and finally the four nitrogen radical of Chapman and Massey. Presumably in

S_4N_3Cl, the initial nine-line spectrum cannot be observed.

No assignments can be made with regard to the number of sulfur atoms present in radicals A-D. Further, because of the largely diamagnetic character of the solutions investigated, one cannot suggest a meaningful reaction mechanism on the basis of these results. Molecular orbital calculations are in progress[118] which will help to justify the assignment of radical E as $S_4N_4^-$.

IV. REFERENCES

1. It could also be argued here that the structure observed was indicative of an axial spin Hamiltonian, in which the $g_{\parallel}$ peak was poorly resolved. This might help to explain some of the line asymmetry. The isotropic g-value based on this assumption, with $g_{\parallel} = 2.006$ and $g_{\perp} = 2.103$ (the g-value of the low-field peak), is 2.071±0.004. However, if this were the case, the line shape would be quite different than that observed and more like that observed for the spectrum of $V(CO)_6$ in benzene which is described later. Hence the interpretation in the text is preferred.
2. R. H. Sands, Phys. Rev. 99, 1222 (1955).
3. See, for example, (a) F. K. Kneubühl, J. Chem. Phys. 33, 1074 (1960) and (b) H. R. Gersmann and J. D. Swalen, J. Chem. Phys. 36, 3221 (1962); also see (c) N. Bloembergen and T. J. Rowland, Acta Met. 1, 731 (1953) for similar effects in NMR spectra.
4. See Fig. 3, reference 3a.
5. C. K. Jen, S. N. Fonce, E. L. Cochran and V. A. Bowers, Phys. Rev. 112, 1169 (1958). See also C. K. Jen in Formation and Trapping of Free Radicals (Academic Press, Inc., New York, 1960), ed. A. M. Bass and H. P. Broida, Chapter 7.
6. F. Calderazzo, Inorg. Chem. 3, 810, 1207 (1964); 4, 223 (1965). Other reactions have been reviewed recently; see T. A. Manuel in Adv. Organometallic Chem. 3, 195 (1965).
7. F. Calderazzo, private communication, 1966.
8. E. König, Proc. VIII Int. Conf. on Coördination Chemistry, Vienna, 1964 (Springer-Verlag, Publishers, New York, 1964). See also E. König, Z. Naturforsch. 19a, 113[illegible] (1964).

9. C. J. Gorter and J. H. Van Vleck, Phys. Rev. 72, 1128 (1947); J. H. Van Vleck, Phys. Rev. 74, 1168 (1948).

10. P. W. Anderson and P. R. Weiss, Rev. Mod. Phys. 25, 269 (1953); P. W. Anderson, J. Phys. Soc. Japan 9, 316 (1954).

11. D. J. E. Ingram, Free Radicals as Studied by Electron Spin Resonance (Butterworths Scientific Publ., London, 1958), Chapter 4.

12. D. Kivelson, J. Chem. Phys. 27, 1087 (1957).

13. N. Bloembergen, E. M. Purcell and R. V. Pound, Phys. Rev. 73, 679 (1948).

14. V-4502 EPR Spectrometer System Manual (Varian Associates, Palo Alto, California), Chapter 5.

15. A molecule more similar to $V(CO)_6$ in these respects is the free radical DPPH. In solutions of DPPH, the hyperfine structure was unobservable at concentrations of 0.01M and greater. (C. A. Hutchison, R. C. Pastor, and A. G. Kowalsky, J. Chem. Phys. 20, 534 (1952)). However, the role of exchange in solution is complicated by molecular diffusion, so that the effective concentration for exchange is probably somewhat higher. See G. E. Pake and T. R. Tuttle, Phys. Rev. Letters 3, 423 (1959).

16. R. T. Ross, J. Chem. Phys. 42, 3919 (1965).

17. J. P. Goldsborough, M. Mandel and G. E. Pake, Phys. Rev. Letters 4, 13 (1960). See also A. M. Prokhorov and V. B. Fedorov, Sov. Phys. (JETP) 46, 1937 (1964); Eng. Trans. 19, 1305 (1964).

18. N. Bloembergen and S. Wang, Phys. Rev. 93, 72 (1954).

19. J. H. Van Vleck, Suppl. Nuovo cimento 6, 1081 (1957).

20. H. A. Jahn and E. Teller, Proc. Roy. Soc. (London) A161, 220 (1937).

21. See, for example, C. J. Ballhausen, Introduction to Ligand Field Theory (McGraw-Hill Book Co., Inc., New York, 1962), Chapter 6.

22. M. H. L. Pryce, Proc. Phys. Soc. (London) A63, 25 (1950); Suppl. Nuovo cimento 6, 817 (1957).

23. A. Carrington and H. C. Longuet-Higgins, Quart. Revs. 14, 427 (1960). See also A. Carrington and A. D. McLachlan, Introduction to Magnetic Resonance (Harper and Row, Publ., New York, 1967) Chapter 10.

24. See Ref. 21, p. 133.

25. L. I. Schiff, Quantum Mechanics, 2nd ed. (McGraw-Hill Book. Co., Inc., New York, 1955), Chapter 7.

26. B. Bleaney and M. C. M. O'Brien, Proc. Phys. Soc., (London) B69, 1216 (1956).

27. See Ref. 21, p. 64.

28. See Ref. 21, p. 13.

29. E. B. Wilson, J. C. Decius and P. C. Cross, Molecular Vibrations (McGraw-Hill Book Co., Inc., New York, 1955), Appendix X.

30. J. J. Fortman and R. G. Hayes, J. Chem. Phys. 43, 15 (1965).

31. See Ref. 21, p. 68.

32. T. M. Dunn, Trans. Far. Soc. 57, 1441 (1961).

33. J. Owen, Proc. Roy. Soc. (London) A227, 183 (1955).

34. B. N. Figgis, Introduction to Ligand Fields (Interscience Publ., John Wiley and Sons, New York, 1966).

35. C. S. Naiman, J. Chem. Phys. 35, 323 (1961).

36. H. Haas and R. K. Sheline, J. Am. Chem. Soc. 88, 3219 (1966).

37. See Ref. 21, p. 119.

38. H. A. Jahn, Proc. Roy. Soc. (London) A164, 117 (1938).

39. U. Öpik and M. H. L. Pryce, Proc. Roy. Soc. A238, 425 (1957).

40. L. Helmholtz and R. F. Kruh, J. Am. Chem. Soc. 74, 1176 (1952).

41. See Ref. 21, p. 206.

42. G. Felsenfeld, Proc. Roy. Soc. (London) A236, 506 (1956).

43. M. Sharnoff and C. W. Reiman, J. Chem. Phys. 43, 2993 (1965).

44. See W. D. Hobey, J. Chem. Phys. 43, 2187 (1965) for a discussion of this effect.

45. N. J. Hawkins, H. C. Mattraw, W. W. Sabol and D. R. Carpenter, J. Chem. Phys. 23, 2422 (1955).

46. L. E. Orgel, An Introduction to Transition Metal Chemistry (Methuen and Co., Ltd., London, 1960), Chapter 9.

47. It is of interest to note that the isotropic g-value of the $3d^5$ complex $V(dipyridyl)_3$ is 1.9831 (see Ref. 8). This is in accord with our g-value expressions for the trigonal case, which predict $\langle g \rangle \langle g_e$; further, a trigonal distortion seems reasonable for this molecule. We thank Dr. A. von Zelewsky for bringing this work to our attention.

48. B. Bleaney, Phil. Mag. 42, 441 (1951).

49. See, for example, R. Wilson andD. Kivelson, J. Chem. Phys. 44, 154 (1966).

50. S. M. Blinder, J. Chem. Phys. 33, 748 (1960).

51. R. Neiman and D. Kivelson, J. Chem. Phys. 35, 149, 156, 162 (1962).

52. H. R. Gersmann and J. D. Swalen, J. Chem. Phys. 36, 3221 (1962). See also S. Lee and P. J. Bray, J. Chem. Phys. 39, 2863 (1963).

53. A. Abragam, J. Horowitz and M. H. L. Pryce, Proc. Roy. Soc. (London) A230, 169 (1955).

54. T. Vänngård and R. Aasa, Proc. 1st Intl. Conf. Paramagnetic Resonance, ed., W. Low (Academic Press, New York, 1963), p. 509.

55. We thank Drs. Vänngård and W. Burton Lewis for providing us with copies of this program. Mr. J. J. Chang of this laboratory adapted the program for the CDC-6600 computer and re-wrote the plotting routine. The variable linewidth feature described later in this section was also included by him.

56. B. Bleaney, Proc. Phys. Soc. (London) A75, 621 (1960).

57. D. C. McCain and R. J. Myers, J. Phys. Chem. 71, 192 (1967).

58. M. C. M. O'Brien, Proc. Roy. Soc. (London) A281, 323 (1964).

59. G. C. Pimentel in Formation and Trapping of Free Radicals (Academic Press, Inc., New York, 1960), ed., A. M. Bass and H. P. Broida, Chapter 4.

60. We thank Dr. T. Hopkins of Prof. Templeton's group for performing these experiments.

61. D. E. O'Reilly and J. H. Anderson, in Physics and Chemistry of the Organic Solid State (Interscience, John Wiley and Sons, New York, 1965), ed., Fox, Labes and Weissberger, p. 209.

62. C. D. Jeffries, Phys. Rev. 117, 1056 (1960).

63. Estimated from C. H. Townes and A. L. Schawlow, Microwave Spectroscopy (McGraw-Hill Book Co., New York, 1955), p. 231.

64. H. Zeldes and R. Livingston, J. Chem. Phys. 35, 563 (1961); W. C. Moseley and W. G. Moulton, J. Chem. Phys. 43, 1207 (1965).

65. J. C. W. Chien and C. R. Boss, J. Am. Chem. Soc. 83, 3767 (1961).

66. R. J. R. Hayward, in Molecular Relaxation Processes (J. Chem. Soc. (London) Special Publication No. 20, Academic Press, Inc., New York, 1966), p. 173.

67. J. H. van Vleck, Phys. Rev. 57, 426 (1940).

68. Spin-lattice Relaxation in Ionic Solids (Harper and Row, Publishers, New York, 1966), ed. by A. A. Manenkov and R. Orbach.

69. A. M. Portis, Phys. Rev. 91, 1071 (1953).

70. R. Orbach, in Fluctuation, Relaxation and Resonance in Magnetic Systems (Plenum Press, New York, 1962), ed. by D. ter Haar, p. 219.

71. E. B. Andreeva, N. V. Karlov, A. A. Manenkov, V. A. Milyaev and A. V. Shirkov, Fix. Tverd. Tela 6, 1649 (1964). [English trans.: Sov. Phys. (Solid State) 6, 1293 (1964).]

72. A. A. Manenkov and A. M. Prokhorov, J. Exptl. Theoret. Phys. (USSR) 42, 1371 (1962). [English trans.: Sov. Phys. (JETP) 15, 951 (1962).]

73. W. A. Stark and R. N. Kortzeborn, University of California, Berkeley, California, UCRL-17225, 1966.

74. F. London, Superfluids, Vol. II (John Wiley and Sons, New York, 1954), p. 3.

75. P. L. Scott and C. D. Jeffries, Phys. Rev. 127, 32 (1962).

76. G. A. Candela, J. Chem. Phys. 42, 113 (1965).

77. B. W. Faughnan and M. W. P. Strandberg, J. Phys. Chem. Solids 19, 155 (1961).

78. C. J. Ballhausen and A. D. Liehr, Acta Chem. Scand. 15, 775 (1961).

79. A. Abragam, The Principles of Nuclear Magnetism (Oxford University Press, London, 1961), Chapter 3.

80. E. R. Andrew, Nuclear Magnetic Resonance (Cambridge University Press, London, 1958), Chapter 5.

81. H. C. Torrey, Phys. Rev. 76, 1059 (1949).

82. E. L. Hahn, Phys. Rev. 80, 580 (1950).

83. J. A. Pople, W. G. Schneider and H. J. Bernstein, High-Resolution Nuclear Magnetic Resonance (McGraw-Hill Book Co., Inc., New York, 1959).

84. A. Abragam and M. H. L. Pryce, Proc. Roy. Soc. (London) A206, 164 (1951).

85. L. E. Orgel, J. Chem. Phys. 23, 1004 (1955).

86. J. Owen, Proc. Roy. Soc. (London) A227, 183 (1955).

87. C. E. Moore, Atomic Energy Levels, Natl. Bur. Standards Circ. 467, Vol. 1, 1949; Vol. 2, 1952; Vol. 3, 1958.

88. A. Abragam and M. H. L. Pryce, Proc. Phys. Soc. (London) A63, 409 (1950).

89. V. I. Avvakumov, J. Expt. Theoret. Phys. (USSR) 37, 1017 (1959) [English trans.: Sov. Phys. (JETP) 37, 723 (1960)]; Vi. I. Avvakumov, N. S. Garif'yanov, B. M. Kozyrev and P. G. Tishkov, ibid. 37, 1564 (1959)[English trans.: ibid. 37, 1110 (1960)].

90. G. Herzberg, Electronic Spectra and Electronic Structure of Polyatomic Molecules, (D. Van Nostrand Co., Inc., Princeton, N. J., 1966).

91. A. D. Liehr, Ann. Rev. Phys. Chem. 13, 41 (1962).

92. U. T. Höchli and T. L. Estle, Bull. Ann. Phys. Soc. 12, 41 (1967).

93. Y. Masuda, J. Phys. Soc. Japan 11, 670 (1956).

94. These experiments were performed in concentric cylindrical sample tubes; therefore, this equation should also contain the shift of the $TiCl_4$ and VCl_4 signals from the external Cl^- reference due to the paramagnetic susceptibility of the solution. However, these corrections are small and their absence should not invalidate the qualitative arguments presented here.

95. J. W. Emsley, J. Feeney and L. H. Sutcliffe, High Resolution Nuclear Magnetic Resonance Spectroscopy, Vol. 1 (Pergamon Press, Inc., New York, 1965), Chapter 9.

96. A. Abragam, The Principles of Nuclear Magnetism (Oxford University Press, London, 1961), Chapters 6 and 8.

97. N. F. Ramsey, Nuclear Moments (John Wiley and Sons, Inc., New York, 1953).

98. N. Bloembergen, J. Chem. Phys. 27, 595 (1957); H. S. Gutowsky, H. Kusumoto, T. H. Brown and D. H. Anderson, J. Chem. Phys. 30, 860 (1959).

99. L. David, B. T. Field, C. W. Zabel, and J. R. Zacharias, Phys. Rev. 76, 1076 (1949).

100. Y. Masuda and T. Kanda, J. Phys. Soc. Japan 9, 82 (1954).

101. R. S. Marianelli (Ph.D. Thesis) University of California, Berkeley California, UCRL-17069, 1966.

102. P. Diehl, Helv. Phys. Acta. 29, 219 (1956).

103. Reference 96, p. 314.

104. P. Debye, Polar Molecules (Dover Publications, New York, 1945) Chapter 5.

105. G. P. Luchinskii, J. Gen. Chem. (USSR) 7, 2116 (1937).

106. Reference 96, p. 316

107. G. N. Lewis and M. Randall, Thermodynamics, 2nd Ed., revised by K. S. Pitzer and L. Brewer (McGraw-Hill Book Co., Inc., New York, 1961).

108. Assuming ΔH_{vap} = 9.6 Kcal/mole and T_o = 409.6°K; data taken from JANAF Thermochemical Data (Dow Chemical Co., Midland, Michigan, 1961).

109. S. H. Maron and C. F. Prutton, Principles of Physical Chemistry, (MacMillan Co., New York, 1958) p. 96.

110. Reference 96, pp. 306-312.

111. Such an assumption is usually made in the treatment of scalar relaxation of the first kind for aqueous solutions of paramagnetic ions. M. Judkins, private communication, 1967.

112. H. G. Dehmelt, J. Chem. Phys. 21, 380 (1954).

113. R. G. Barnes, S. L. Segal, and W. H. Jones, J. Appl. Phys. 33, 296 (1962).

114. In these experiments, the field was swept about 750 gauss above and below the position expected for a diamagnetic ^{51}V nucleus at a frequency of 15.803 MHz., both at room temperature and ~100°C.

115. D. H. Levy (Ph. D. Thesis) University of California, Berkeley, California, UCRL-11864, Jan. 1965.

116. D. Chapman and A. G. Massey, Trans. Fara. Soc. 58, 1291 (1962).

117. R. Meinzer, unpublished results at University of California, Berkeley, 1966.

118. R. J. Myers, private communication, 1967.

ACKNOWLEDGEMENTS

This thesis was prepared under the direction of Prof. R. J. Myers. I would like to express my sincere gratitude to him for counsel and guidance during the course of the experiments reported herein and the preparation of this manuscript. His enthusiastic approach to these problems has been a constant source of encouragement. I am also grateful to Prof. H. L. Strauss for discussions concerning some theoretical aspects of this thesis.

Numerous discussions and experiments with my colleagues have also been invaluable. In particular I would like to thank D. C. McCain for assistance with electronic problems, J. J. Chang for his efforts in preparing computer programs, W. C. Easely and N. M. Edelstein for their suggestions on the design of the cryostat, S. K. Ray and G. V. Nelson for assistance in preparing some of the samples studied in this thesis, and R. S. Marianelli for his help in the NMR experiments. The chemistry department machine shop provided valuable technical assistance. I would also like to thank Mrs. Charlotte Machen and Mrs. Pat Cookson for their efficient work in preparing the final manuscript.

Finally, I would like to acknowledge the unseen but very important contribution made by my wife, JoAnn, without whose support and patience this work would not have been completed.

This work was done under the auspices of the United States Atomic Energy Commission through the Inorganic Materials Research Division of the Lawrence Radiation Laboratory.

APPENDIX I

ESR Linewidth of $Gd(H_2O)_9^{+3}$ as a Function of Temperature

The ESR linewidth of 0.01M aqueous solutions of $Gd(ClO_4)_3$ was measured as a function of temperature in the range 22-262°C. The data are listed in Table XXIII. An Arrhenius plot of this data yields an activation energy of -3.30 Kcal/mole.

Table XXIII. Peak to peak linewidth of $Gd(ClO_4)_3$ as a function of temperature.

T, °C	ΔH, gauss	T, °C	ΔH, gauss
22.2	460.3	131.2	103.6
22.2	462.0	144.2	89.3
33.2	394.3	157.8	80.0
46.4	312.4	167.4	76.8
51.3	290.7	178.5	69.6
63.6	236.5	190.8	66.1
71.8	204.2	196.4	62.5
83.6	177.0	212.4	57.1
96.6	145.1	228.0	53.6
113.2	121.3	247.4	49.8
126.4	108.2	262.4	47.1

This report was prepared as an account of Government sponsored work. Neither the United States, nor the Commission, nor any person acting on behalf of the Commission:

A. Makes any warranty or representation, expressed or implied, with respect to the accuracy, completeness, or usefulness of the information contained in this report, or that the use of any information, apparatus, method, or process disclosed in this report may not infringe privately owned rights; or

B. Assumes any liabilities with respect to the use of, or for damages resulting from the use of any information, apparatus, method, or process disclosed in this report.

As used in the above, "person acting on behalf of the Commission" includes any employee or contractor of the Commission, or employee of such contractor, to the extent that such employee or contractor of the Commission, or employee of such contractor prepares, disseminates, or provides access to, any information pursuant to his employment or contract with the Commission, or his employment with such contractor.